ParH: A Novel Regulator of Septum Site Placement in *Streptomyces coelicolor*

Michael David Gillespie

A thesis submitted for the degree of Doctor of Philosophy

University of East Anglia

School of Biological Sciences

March 2017

Acknowledgements

I would like to start by thanking my supervisor Dr Gabriella Kelemen for originating the project and guiding me throughout the ups and downs of the research. I recognise that I am not the best student and my supervisor put up with a lot more antics than other supervisors probably have the patience for. In addition to my primary supervisor I would also like to thank my secondary supervisors Dr Andrew Hemmings and Prof Andrea Munsterberg. I would especially like to thank Dr Hemmings for his help, support and expertise in determining the structure for one of my proteins. Next I would like to thank the members of the group throughout my time in the lab: Ruchita Desai, Eric Lin, Alan Lau, Elena Tan, Sundeep Kaur, Emily Alcock, Gemma Cassettari, Lucy Burrows, Kavan Bywater-Brenna and Matthew Stephens. Not only did you all create the wonderful atmosphere in which it was a pleasure to work, but contributions to constructs and the functioning of the lab made my PhD possible. I would like to also thank undergraduate project students Naomi Clarke and Pauline Walton, who contributed to my project. I would next like to acknowledge Dr Neil Holmes, who has been my friend through my academic career from undergraduate all the way to the end of my doctorate. You have always cheered me up when I was down and engaged in discussions about my project that helped to further my research. I would like to thank all the postgrads that were forced to share the Pamela Salter room with me and put up with me when I wasn't at my best. In particular I would like to thank Rhiannah Zalm for graciously accommodating the mess on my desk that often spilled onto her desk. I would also like to mention Ethan Drury and John Munnoch for their friendships throughout my PhD. I would like to thank everyone else at UEA who made my PhD that bit better and that bit easier through there help and interactions over the years.

Finally I would like to thank all of my family for their love, support and sacrifices over the years that has culminated in this moment after which I get to make them all call me Doctor for the rest of their lives. In all seriousness it wouldn't have been possible without my parents and grandparents guiding me all these years. I want to especially take this time to remember my gran and grandad who were unable to see this moment come to fruiting but who both did a lot to shape it.

Abstract

Streptomyces coelicolor is a Gram-positive, GC-rich, soil-dwelling, filamentous bacterium with a complex life cycle, which begins from a single uni-genomic spore. The life cycle is completed after the differentiation of multi-genomic aerial hyphae into uni-genomic spores. This process requires the segregation and organisation of many chromosomes of the sporogenic hyphae which are then compartmentalised by the synchronous placement of 20-50 septa, generating a single chromosome in each pre-spore compartment. Chromosome segregation and septum site-placement are two key components of cell division. Throughout the bacterial kingdom, these processes are controlled by the ParA/MinD superfamily of proteins. These proteins can be divided into two categories according to their function: those involved in chromosome segregation and those involved in septum-site placement.

In *S. coelicolor*, the only characterised protein belonging to this superfamily is ParA that has been implicated in chromosome segregation along with its partner protein, ParB. Prior to septation, ParA forms long filaments along the length of the hyphae where they position ParB bound to the chromosomes. This study characterises a novel homologue of the ParA/MinD superfamily encoded by the gene *SCO1772*, which we have designated *parH*. We also characterised the gene (*SCO1771*), which is downstream of *parH* and translationally coupled. Through *in vitro* techniques such as analytical gel filtration, native-PAGE, chemical crosslinking, pelleting assays we have characterised their oligomerisation, determined their protein:protein interactions and present structural data for SCO1771. We show that ParH is involved in the determination of septum site placement during division. We also link ParH to both the chromosome segregation machinery and the tip organising centre (TIPOC), a multi protein assembly that drives growth. This work helps to clarify the link between chromosome segregation and septum site placement.

Table of Contents

1 Introduction

Propagating genetic material to the next generation is, within our understanding, the ultimate purpose for all living organisms. The ability to achieve this in the most effective and efficient manner, and thus outcompete opponents, is the key driver of evolution. This is no different in bacteria, where the ability to successfully produce identical offspring containing all of the genetic code required for form and function has led to varied adaptation for the different environments. This process (the life cycle) consists of three interconnected but distinct processes; growth, chromosome segregation and cell division. In order to complete the cycle, bacteria must coordinate these processes through the use of cytoskeletal proteins. These proteins are classically defined through their ability to form polymers both *in vitro* and *in vivo* from a monomeric subunit and often have dynamic assemblies which assemble and disassemble in response to various signals (Shih and Rothfield, 2006). This definition, imported from eukaryotic systems, originally referred to the three classes of filamentous eukaryotic cytoskeletal proteins; microtubules, actin filaments and intermediate filaments (Desai and Mitchison, 1997; Goodson and Hawse, 2002; Steinert and Roop, 1988). Structural homologues for all of these classes have now been found in bacteria, which laid the groundwork for our current understanding of the bacterial cell cycle. However, this definition does not include the proteins which while play a crucial role in the cycle do not fit the strict cytoskeletal definition.

1.1 Bacterial growth

In order to grow bacteria are required to insert peptidoglycan precursors into the cell wall (Vollmer et al., 2008). There are three established sites of growth in bacteria which are under the control of different proteins (Figure 1). The most common site of growth in bacteria occurs during cell division where peptidoglycan is inserted mid-cell in order to form the septal division ring (Cabeen and Jacobs-Wagner, 2005). This mainly occurs at the mid cell and is the only growth mechanism seen in spherical (cocci) bacteria (Cabeen and Jacobs-Wagner, 2005). Growth at the

site of division is driven by FtsZ, the bacterial homologue of eukaryotic tubulin (Carballido-Lopez and Errington, 2003). The other two mechanisms of growth both contribute in their simplest form to bacteria becoming rod shaped. The most widely studied of these is growth that occurs along the lateral wall, found in *Bacillus subtilis* and *Escherichia coil*, and is driven by MreB, the bacterial homologue of eukaryotic actin. The final mechanism of bacterial growth found mainly in *Actinobacteria*, is polar growth, which occurs, as the name implies, at the poles. This form of growth is driven by DivIVA, a protein that currently is not considered to be a homologue of any class of eukaryotic protein (Flardh, 2003a). DivIVA is a coil-coiled protein which is also the structure that eukaryotic intermediate filaments are formed from, although DivIVA has not been shown to form the same domain architecture that defines the intermediate filament proteins (Steinert and Roop, 1988; Walshaw et al., 2010). After growth in both lateral and polar locations, rod shape bacteria then undergo the same FtsZ driven division event seen in cocci (Cabeen and Jacobs-Wagner, 2005).

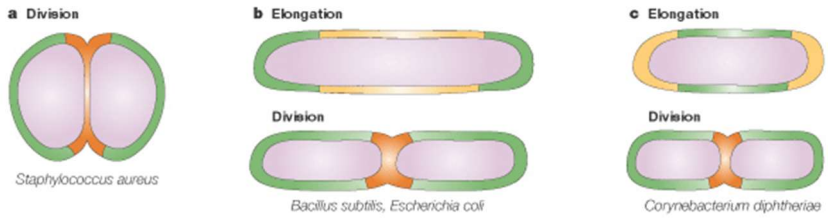

Figure 1: Mechanisms of Bacterial Growth
There are three sites at which precursors of peptidoglycan are inserted into the cell wall during bacterial growth. (A) The most common, found in most bacteria, is at the site of division. In spherical bacteria this is the only site of growth. This mechanism is driven by FtsZ. There are two mechanisms of growth that lead to the elongation of bacteria, MreB dependent lateral wall growth (B) and DivIVA dependent polar growth (C). Taken from Cabeen and Jacobs-Wagner (2005).

1.1.1 Lateral growth – MreB dependent

The majority of bacteria thus far characterised are rod shaped with growth occurring along the lateral walls (Daniel and Errington, 2003). One of the first proteins identified to contribute to this mode of growth are the MreB proteins, which were first described in *E. coli* and *B. subtilis* (Levin et al., 1992; Wachi et al., 1987).

The distribution of these proteins correlates to the shape of the organism, with most rod shape bacteria containing at least one MreB homologue, while the vast majority of spherical bacteria lack homologues of this protein (Cabre et al., 2015; Daniel and Errington, 2003). Across most bacteria containing an MreB homologue, the gene encoding this protein is found in a gene operon containing *mreC* and *mreD,* creating the *mreBCD* operon (Carballido-Lopez and Errington, 2003; Doi et al., 1988; Levin et al., 1992; Varley and Stewart, 1992). The role of these other genes in the operon are yet to be determined although, in *E. coli*, they are required for correct localisation of MreB and are assumed to form a complex with MreB based upon interactions between all three proteins (Kruse et al., 2005). Further searches for homologues of MreB have thus far revealed that some bacteria contain multiple MreB proteins with two, Mbl (MreB-like) and MrebH (MreB homologue), being found in *B. subtilis* in addition to MreB (Jones et al., 2001; Varley and Stewart, 1992). Studies on these proteins have shown that all are required to form a rod shape. However, the effect on shape of the absence of each protein is unique, suggesting that they interact with different components of the cell wall synthesis machinery (Carballido-Lopez et al., 2006; Defeu Soufo and Graumann, 2006; Dominguez-Cuevas et al., 2013; Kawai et al., 2009). Initial localisation of MreB and Mbl, using immunofluorescence of an epitope-tagged MreB and detection of an Mbl-GFP fusion, in *B. subtilis* revealed that they form helical filaments that wrap around the cell wall longitudinally from pole to pole (Jones et al., 2001). This localisation pattern suggested that the proteins had an actin-like function within bacteria, which was confirmed when the structure of MreB was solved and found to be structurally homologous to the eukaryotic actin (van den Ent et al., 2001a; van den Ent et al., 2001b). Localisation of the sites of cell wall insertion in *B. subtilis* showed that this also occurs in a helical pattern suggesting that MreB proteins contribute to the control of location of cell wall synthesis in bacteria (Daniel and Errington, 2003). The initial localisation pattern of these proteins was challenged by data observing MreB filaments using electron cryotomography (ECT),which suggested that in fact MreB localises as discreet disconnected patches that follow a helical path through the cell and are moved through coupling to the cell wall synthetic machinery (Dominguez-Escobar et al., 2011; Garner et al., 2011; Swulius et al., 2011; van Teeffelen et al., 2011). More recently, data observing MreB

in vitro has tilted the model of MreB localisation back towards the initial helical filaments. MreB has been shown to form antiparallel filaments that interact extensively with membranes (Salje et al., 2011; van den Ent et al., 2014). In addition, observations of MreB localisation using high-end microscopy methods such as structured illumination microscopy (3D-Sim) have shown helical filaments once again in actively grown cells (Olshausen et al., 2013; Reimold et al., 2013). All of this data leads to the current suggested model (Figure 2) in which MreB filaments associate to the membrane and elongate upon a uniform and favourable cylindrical shape, where they recruit multiple cell wall synthetic complexes. These complexes create new peptidoglycan strands which are guided by the motion of the MreB helices (Errington, 2015).

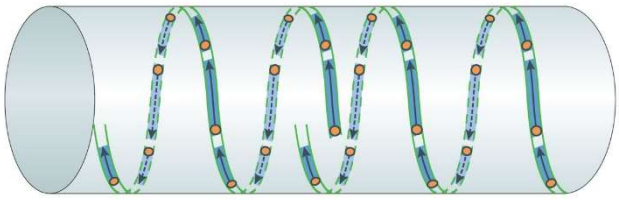

Figure 2: Model for the role of MreB in shape determination

MreB filaments (solid and dashed lines) elongate along the cell wall due to the cylindrical shape of the bacteria. The filaments are able to recruit peptidoglycan synthetic complexes (orange circles) which in turn generate new peptidoglycan strands. Taken from Errington (2015).

1.1.2 Polar Growth – DivIVA Dependent

While lateral growth is the predominant form of growth in the bacteria that have thus far been characterised, a significant number of bacteria exhibit an alternative form of growth – polar growth. This mode of growth is especially prevalent in the Gram-positive Actinobacteria and the Gram-negative *Rhizobium* and *Agrobacterium* genera (Brown et al., 2012; Daniel and Errington, 2003). The first protein implicated in driving polar growth was DivIVA, which was found in both *S. coelicolor* and *Brevibacterium lactofermentum* and is an essential protein (Flardh, 2003a; Ramos et al., 2003). Homologues of DivIVA have since been shown to be essential for growth in other *Actinobacteria*, including the pathogenic

Mycobacterium tuberculosis, where it has the alternative name Wag31 (Kang et al., 2008; Nguyen et al., 2007). The DivIVA protein was originally identified in *B. subtilis*, where it plays a role in division (Cha and Stewart, 1997). In this organism, DivIVA is located to the poles where it recruits MinD via the intermediary protein MinJ (Patrick and Kearns, 2008). As we will discuss later, MinD is part of the septum site determining Min system (Margolin, 2001). As DivIVA in *S. coelicolor* was identified due to its homology with the division associated DivIVA protein from *B. subtilis*, it was named accordingly (Cha and Stewart, 1997; Flardh, 2003a). Although DivIVA has two functions in different bacteria e.g. division in *B. subtilis* and growth in *S. coelicolor*, in all cases the protein is localised to the poles (Flardh, 2003a; Marston et al., 1998). This suggests that DivIVA homologues all share similar characteristics from which bacteria have adapted their function whether in growth or division. In *Actinobacteria*, DivIVA is thought to localise key components of the cell wall synthesis machinery, and it has been shown to make direct contact with penicillin-binding protein 3 (PBP3) in *Mycobacterium* (Mukherjee et al., 2009). Interestingly, while partial complementation of the *divIVA* null mutant in *Corynebacterium glutamicum* by DivIVA homologues from other *Actinobacteria* was possible, DivIVA homologues from the *Firmicutes*, such as *B. subtilis*, failed to sustain viability in *C. glutamicum* suggesting an evolutionary divergence among DivIVA homologues (Letek et al., 2008). More recently the use of super-resolution microscopy has suggested that in *Mycobacterium* growth is not occurring right at the tip, but at a sup-polar location that is just behind the pole (Meniche et al., 2014). It remains to be seen whether sub polar growth is a feature of all bacteria that show polar growth or is specific to *Mycobacteria* and most likely other *Actinobacteria*. While DivIVA has been implicated in numerous *Actinobacteria* in driving growth, there are no homologues of DivIVA found in Gram-negative bacteria (Oliva et al., 2010). Thus far in Gram-negative bacteria that exhibit polar growth, there is no mechanism identified that controls polar growth (Oliva et al., 2010). Across bacteria that have polar growth there is great diversity in how growth at different poles is regulated to produce a variety of shapes and nuances to growth (Figure 3), with the filamentous *Streptomyces*, the bi directional growth of *Corynebacterium*, the asymmetrical bi directional growth of *Mycobacterium* and the uni-directional growth of *Agrobacterium* (Aldridge et al.,

2012; Allan and Pearce, 1983; Brown et al., 2012; Meniche et al., 2014; Sieger et al., 2013).

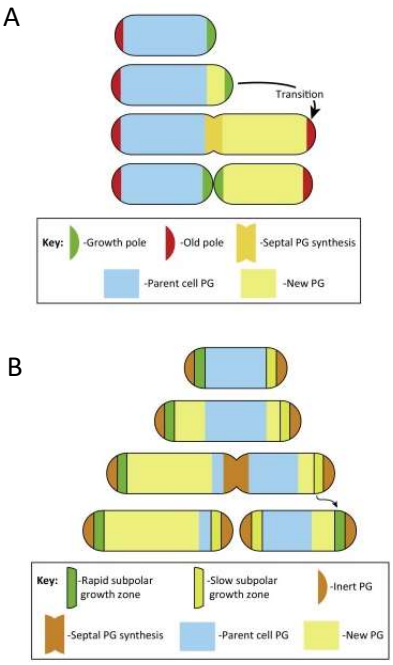

Figure 3: Polar growth in bacteria.

Bacteria that exhibit polar growth do so in a variety of mechanisms such as in (A) *Agrobacterium* where only the newly generated cell pole grows during the next cell cycle (unidirectional growth) and (B) *Mycobacterium*, where there is slower growth at the newly generated cell pole compared to the rate of growth seen at the old pole (bi-directional asymmetric growth). Taken from Cameron et al, (2015).

1.1.3 Cell Division

Bacterial cell division in its simplest form, binary fission, is the process by which bacteria divide to create two identical offsprings containing a single and complete chromosome. Except for cocci, in which the only growth exhibited is at the site of division, all division occurs after bacteria have grown and segregated their replicated chromosome. An efficient division event is thus essential for bacteria to pass on their genetic information as quickly as possible therefore reaching exponential growth.

1.1.3.1 FtsZ – the driver of cell division

As mentioned before, the key protein controlling cell division in bacteria is FtsZ. When the structure of FtsZ was solved, it was found to be remarkably similar to that of the eukaryotic cytoskeletal protein tubulin despite the lack of any sequence homology found between the proteins (Erickson, 1998; Nogales et al., 1998). The FtsZ protein consists of two domains, an N-terminal GTPase domain and a C-terminal tubulin like loop domain, connected by a central connecting helix (Lowe and Amos, 1998). In fact the structural homology between FtsZ and tubulin is most pronounced among residues required for GTP binding and hydrolysis (Erickson, 2007). Before the discovery of FtsZ, it was thought that bacterial cell shape was solely maintained by the cell wall and none of the cytoskeletal elements found in eukaryotes were present in bacteria. This was primarily because the bacterial homologues contain virtually no sequence identity with their eukaryotic counterpart (Wang and Lutkenhaus, 1996).

The most widely studied example of FtsZ driven cell division is in *E. coli* where bacterial cytokinesis can be separated in to three stages (de Boer, 2010). Initiation occurs with the assembly of a polymeric FtsZ structure or 'Z ring' at the future site of cell division (Bi and Lutkenhaus, 1991). Polymerisation of FtsZ is regulated by GTP in which filamentation occurs when FtsZ is in the GTP bound form before the polymers disassemble as GTP is hydrolysed into GDP (Erickson et al., 1996). After a lag, the Z ring undergoes maturation through the recruitment of downstream division proteins, many of which are essential, forming the complete divisome (Figure 4). Finally, the divisome begins to constrict concomitantly with the synthesis and splitting of septal peptidoglycan, resulting in invagination and division of the bacteria into two daughter cells (Gerding et al., 2009; Goley et al., 2011). Interestingly, it has been shown using liposomes that, by the addition of the membrane-targeting sequence (MTS) of MinD, and in the presences of GTP, FtsZ is able to form membrane associated rings and generated clear indentations of the liposome wall. This indicates that FtsZ is able to exert some level of constrictive force, although this was found to be dependent on GTP hydrolysis (Jimenez et al., 2011; Osawa et al., 2008).

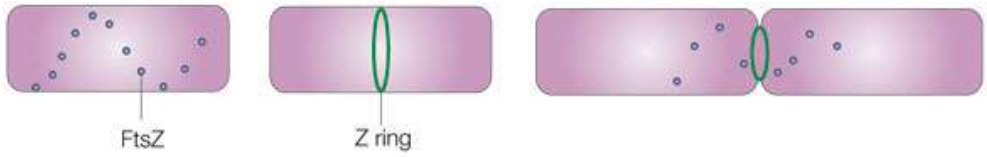

Figure 4: FtsZ ring formation in bacteria.

FtsZ initially forms spiral patterns, which eventually condenses into the FtsZ ring mid cell in a GTP dependent manner during division. The FtsZ ring contracts with the loss of FtsZ subunits from the ring as the cell divides. Taken from Margolin (2005)

1.1.3.2 Stabilising the Z ring

The regulatory factors that act upon the Z ring can be separated into two categories: those proteins that positively regulate Z ring formation helping formation, and the negative regulators, such as Min and NO, that inhibit Z ring formation near the poles or over chromosomes (Huang et al., 2013). Positive regulation of the Z ring is mediated by proteins that actively promote stabilisation of the Z ring and anchor it to the membrane at sites of future cell division. Gram-negative bacteria, such as *E. coli*, achieve this through the presence of one of the two trans-membrane proteins FtsA and ZipA both of which are necessary to complete division (Pichoff and Lutkenhaus, 2002).

While ZipA is only found among Gram-negative bacteria, FtsA homologues are also found among numerous Gram-positive bacteria In fact besides FtsZ, FtsA is the most widely conserved member of the divisome found across bacteria (Haeusser and Margolin, 2016). Like MreB, FtsA is an actin-like protein and able to form actin-like protofilaments (Szwedziak et al., 2012). In *E. coli,* generation of mutants of FtsA which fail to polymerise display a gain of function, creating strains which tolerate the loss of ZipA. This suggests that competition exists between the generation of FtsA polymers, which do not recruit downstream proteins required for division, and its monomeric form, which is driven by interaction with FtsA and do recruit the downstream proteins (Pichoff et al., 2012). In *B.subtilis* however, the same FtsA mutant demonstrates a loss of function, suggesting that polymerisation is required

for the recruitment of downstream proteins involved in the divisome (Szwedziak et al., 2012). This has led to uncertainty as to the exact role of FtsA polymerisation in cytokinesis, particularly surrounding its mechanism for recruiting other proteins to the divisome (Huang et al., 2013).

In *E. coli*, ZipA has some overlapping function with FtsA in tethering the Z ring to the membrane. ZipA interacts with FtsZ at the C-terminus of ZipA, while the N-terminus contains a membrane embedded domain which helps to anchor the Z ring, reinforcing its placement (Ohashi et al., 2002; Pichoff and Lutkenhaus, 2002). However, in mutant strains with depleted ZipA filaments, Z rings, while still being able to assemble, do so less frequently and more variably than in wild-type *E. coli* (Hale and de Boer, 1999).

In Gram-positive bacteria, which lack ZipA homologues, it is suggested that the role of ZipA is, in part, carried out by the protein SepF. Not only has SepF been shown to both self-interact and interact with FtsZ in a yeast two-hybrid assay, but *sepF* mutants show slight cell shape defects and aberrant septa formation (Hamoen et al., 2006). In addition, overexpression of SepF counters division defects seen in *ftsA* mutants, indicating an overlapping of function, while *ftsA-sepF* double mutants are synthetically lethal and are unable to form Z rings (Ishikawa et al., 2006).

SepF localises to the division site in *B. subtilis*, which is dependent upon its interaction with FtsZ (Hamoen et al., 2006; Ishikawa et al., 2006). It is essential for correct septum formation, with *sepF*-depletion strains showing a deformed septum which does not fully close (Hamoen et al., 2006). Recent data suggests that SepF promotes the correct formation of FtsZ polymers required for proper cell division (Gundogdu et al., 2011).

As demonstrated by transmission electron microscopy (TEM), SepF *in vitro* polymerises into very large ringed structures with a diameter of 50 nm (Gundogdu et al., 2011). In the presence of GTP, FtsZ forms protofilaments. However, the addition of SepF caused the formation of long regular tubular structures with a diameter of 48 nm, remarkably close to the diameter of SepF rings (Figure 5). Further incubation of FtsZ with SepF led to the formation of more complex structures, including branches and rings. This suggests that SepF rings act to bundle FtsZ protofilaments probably to aid in the formation of the FtsZ ring (Gundogdu et al., 2011).

A screen for randomly generated mutations in *sepF* alleles found two different mutations, A98V and F124S, which led to *B. subtilis* cells that were unable to grow when over expressed in the presence of a wild-type allele (Gundogdu et al., 2011). Observations of FtsZ-GFP localisation revealed that Z-ring formation was abolished when these *sepF* variants were over expressed in an *ftsA* mutant background (Gundogdu et al., 2011). Characterisation of the two mutant proteins, using TEM, showed that while F124S forms the same ring structure of wild-type SepF, A98V does this less readily suggesting impairment (Gundogdu et al., 2011). More importantly, no FtsZ tubular structures are formed in the presence of the mutant SepF proteins. To determine the effect of SepF ring formation on FtsZ polymerisation a SepF G135N, a mutation in a highly conserved residue, protein variant was characterised. This protein, while interacting with FtsZ *in vitro* and localising to the Z-ring *in vivo*, forms long filamentous structures rather than the rings associated with wild-type SepF (Gundogdu et al., 2011). This mutant also produced a lethal

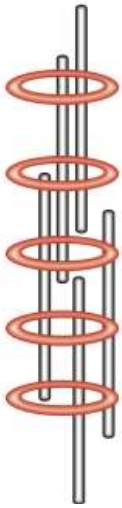

Figure 5: SepF bundling of FtsZ protofilaments.

SepF rings (red) bundle FtsZ protofilaments (grey) in order to help promote FtsZ ring formation. Taken from Gundogdu et al, (2011)

phenotype when over expressed in an *ftsA* mutant background. All of this data suggests that SepF forms a ring structure, which aids the formation of FtsZ polymerisation into a tubular structure. This allows for regulation of the width of the FtsZ superstructure (Gundogdu et al., 2011).

1.1.3.3 Maturation of the Z-Ring

Once the FtsZ ring has been successfully formed and tethered to the membrane, maturation of the ring can begin. In the two most widely studied bacteria, *E. coli* and *B. subtilis*, maturation of the Z ring occurs in a slightly different fashion, although with many of the same proteins being involved. In *E. coli* this is a linear process whereby each protein or protein complex is required to be localised before the next protein can be localised (Figure 6). In *B. subtilis* however, divisome formation could be considered to be a two stage process in which stabilisation of the Z ring occurs, after which the proteins responsible for maturation all localise interdependently forming the divisome (Harry et al., 2006).

In *E. coli* the first protein recruited to the FtsZ ring after it is tethered to the membrane is the DNA translocase protein FtsK, which is conserved across bacteria (Margolin, 2000). The N-terminal region of FtsK is involved in cell division through the recruitment of the next protein required for maturation. At the same time the C-terminal region of the protein has been implicated in the resolution of sister chromosomes into their respective daughter cells thus linking both cell division and chromosome segregation (Aussel et al., 2002; Bigot et al., 2004). The *B. subtilis* homologue of FtsK, SpoIIIE, has thus far only been found to play a role in DNA translocation during sporulation (Sharp and Pogliano, 2003).

Post FtsK localisation in *E. coli* the next proteins involved in Z-ring maturation are FtsQ, FtsL and FtsB, which form a protein complex, and as shown using co-immunoprecipitation of FLAG-tagged proteins, formation of the FtsQLB complex occurs prior to septal localization (Buddelmeijer and Beckwith, 2004). These are represented in *B. subtilis* by the homologues DivIB, FtsL and DivIC respectively. All of these proteins are very similar in structure with a short cytoplasmic region, a single transmembrane segment, and a larger periplasmic domain. Although the function of FtsQ/DivIB is unknown, crystal structure data reveals that it has an α-domain with

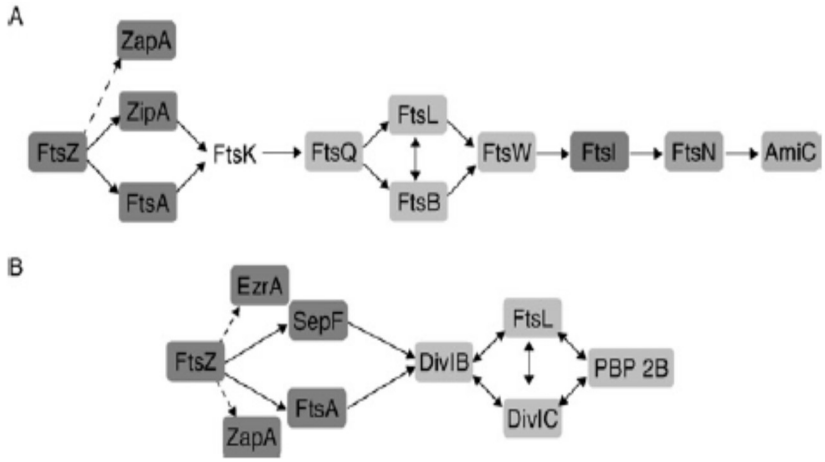

Figure 6: Stabilisation and maturation of the Z ring.

After stabilisation of the Z-ring with the localisation of FtsZ, FtsA, ZipA and SepF, the Z-ring undergoes maturation. (A) In *E. coli* this is a linear process where the recruitment of proteins is sequential and dependent upon localisation of the previous protein. (B) In *B. subtilis* maturation is a single-step process whereby all proteins required for maturation localise concurrently in an interdependent manner. Taken from Harry et al, (2006).

similarity to polypeptide transport-associated domains (van den Ent et al., 2008) and is essential for cell survival in *E. coli* (Storts et al., 1989) but only at high temperatures in *B. subtilis* (Beall and Lutkenhaus, 1992; Katis et al., 2000). Further data on FtsL suggests that it may play a role in regulating Z ring constriction in *B. subtilis* through recruitment regulation of later acting division proteins to allow constriction (Kawai and Ogasawara, 2006). FtsB/DivIC are known to be essential for cell survival in their respective bacteria, although their function is still unknown (Buddelmeijer and Beckwith, 2004; Levin and Losick, 1994).

The next protein recruited to the divisome in *E. coli* is FtsW which is a transporter of lipid-linked precursors for peptidoglycan synthesis, such as lipid II, across the membrane (Mohammadi et al., 2011). FtsI and its homologue PBP2B are both encoded just downstream of *ftsW* in their respective organisms. They are involved in the final stages of PG synthesis and were identified through their ability to bind penicillins, hence their name (Goffin and Ghuysen, 1998). FtsN is not a well-conserved protein and is only found in enteric bacteria and *Haemophilus spp*. (Errington, 2003). In *E. coli*, FtsN localises in a ring pattern at the septum late in the division cycle. It is an essential gene with depletion mutants losing viability after forming long filaments (Dai et al., 1993). More recent data has suggested that it interacts with PBPIB, stimulating its murein synthesis activity (Muller et al., 2007;

Ursinus et al., 2004). The final protein localised to the maturing Z ring in *E. coli* is the amidase AmiC, an enzyme involved in cleaving murein crosslinks, which is required for septal cell wall degradation and hence cell separation (Bernhardt and de Boer, 2003; Weiss, 2004).

1.2 Bacterial division – Chromosomes and Septa

So far we have discussed the importance of FtsZ in the formation of bacterial septa as well as the process that cells use to create a stable Z ring that will allow division to occur. While septum formation is important for generating progeny, it of itself it is not sufficient to generate identical progeny. To achieve identical progeny two events must be coordinated, the segregation of chromosomes and the placement of the septa mid cell such that the chromosomes are not guillotined during division. Given the coordination required between these two processes in order that efficient division can occur, it is not surprising that both of these processes are performed by a single superfamily of proteins; the ParA/MinD superfamily (Lutkenhaus, 2012). Beyond the obvious functional similarity of this family, all ParA/MinD proteins share a deviant walker ATPase motif characterised by the amino acid sequence GXGGXHKTS, which is located within a nucleotide-binding P-loop near the N-terminus of the protein (Koonin, 1993). This superfamily can broadly be assigned to two subgroups based upon the function of the individual protein (Lutkenhaus, 2012), that is, those involved in chromosome segregation, the Par proteins, and those involved in septum positioning, the Min proteins (Lutkenhaus, 2012). Even within these subgroups we find enormous diversity in how mechanistically the proteins carry out their function. This is likely to be due to the unique environmental factors that different bacteria have been exposed to, which has given rise through evolution to adaptations that increase the reproductive fitness of the bacteria. While this is clearly the case, we have very limited understanding of why these different mechanistic processes developed (Lutkenhaus, 2012).

1.2.1 The ParAB system – segregating chromosomes

In order for viable daughter cells to be produced during cell division, correct segregation of the chromosome prior to construction of the Z ring is essential. Originally it was thought that the chromosome was tethered to the cell membrane and segregation driven by cellular elongation, dragging the chromosome into the daughter cell (Jacob and Brenner, 1963). However, with advances in understanding that cell elongation occurs throughout the cell and the inability of cell growth to match the speed at which chromosomes move in the cell, it became clear that a different regulatory system was responsible (Nanninga, 1998; Viollier et al., 2004). The first system of protein driven DNA segregation in bacteria came with the discovery of the Type 1 plasmid partitioning system. This plasmid partitioning system, which has been most widely studied in *E. coli*, generally consists of three components, a cis-acting centromeric DNA site (either *parS* or *parC*), a Walker Box ATPase (ParA or ParA-like protein), and a DNA binding protein (ParB or SopB) (Davis et al., 1992; Ebersbach and Gerdes, 2001; Mori et al., 1989; Viollier et al., 2004; Watanabe et al., 1989). The ParAB system is built upon several characteristics, which appear to be present in all of these systems characterised thus far and define the ParA subfamily of proteins. The ParA protein in these systems is a very weak ATPase whose activity is upregulated through interaction with the ParB protein. This interaction requires the presence of ATP bound form of ParA, with ParA mutants deficient for ATP binding unable to interact with ParB. ParA forms a dimer in the presence of ATP and a monomer after hydrolysis of ATP has occurred. This creates a mechanism by which dimerisation or oligomerisation of ParA is regulated by the presence of ParB. In addition, ParB is a Helix-Turn-Helix (HTH) DNA binding protein that binds to *parS* sites clustered around the origin of replication of either plasmids or chromosomes. Beyond these common characteristics, bacteria are able to vary the action and interplay between these components in order to meet the needs of the organism.

If we were to first consider the original discovery of bacterial partitioning systems in plasmids, we find a system built upon oscillation, with one of the best

understood of these being the ParAB system encoded on the *E. coli* plasmid pB171 (Figure 7). In this system ParB is bound to the *parS* sites on the plasmid (Ringgaard et al., 2007). At the same time ParA binds to the chromosome in an ATP dependent manner, at a position away from the plasmid (Leonard et al., 2005). The ATP bound ParA then begins to polymerise, forming a filament which stretches across the

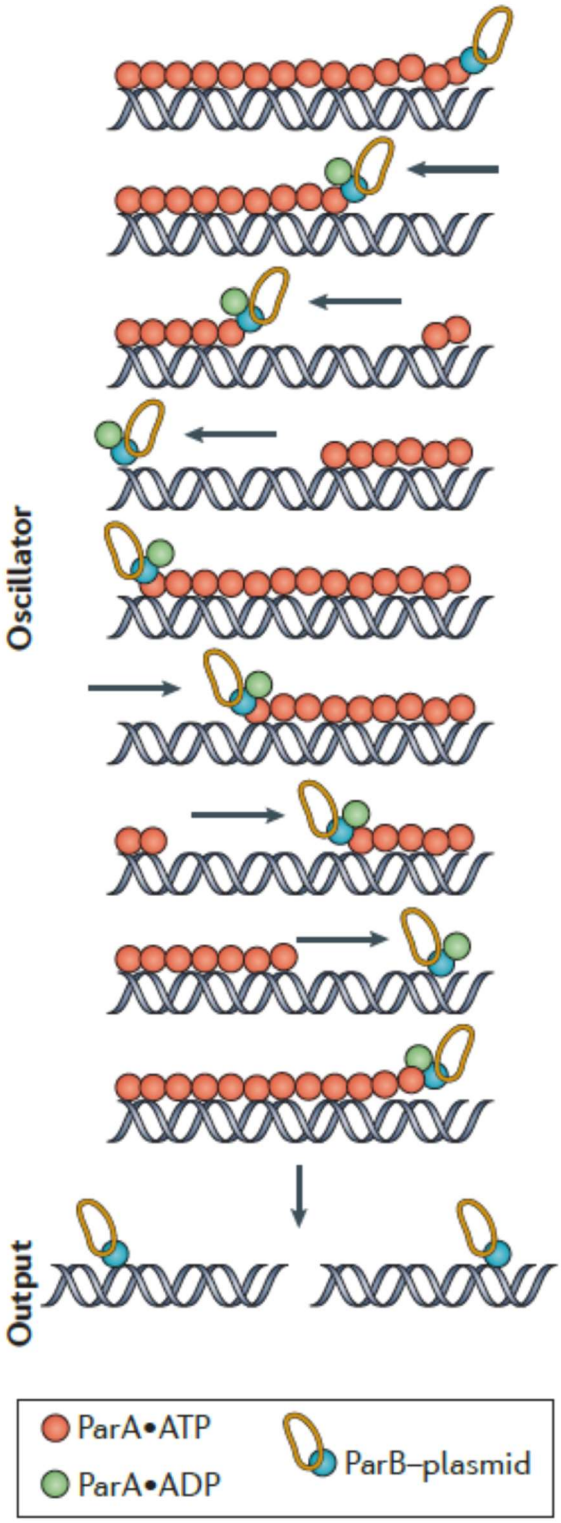

Figure 7: ParA oscillation in the segregation of plasmid pB171 in *E. coli*.

While the ParB bound plasmid is at one end of the chromosome, ParA forms an ATP dependent filament which stretches from a position away from ParB until the two proteins interact. Upon interaction, the ATPase activity of ParA is upregulated by ParB causing hydrolysis of the ATP bound to ParA. This causes the ParA to disassemble from the filament and diffuse away as a monomer. The loss of the ParA monomer leads to retraction of the filament which in turn pulls the ParB bound plasmid across the chromosome. This process continues until the ParA filament is completely disassembled and the plasmid has been pulled the length of the chromosome. As the plasmid is pulled to one end of the chromosome another ParA filament begins to form at the other end of the chromosome ready to pull the plasmid in the other direction. Taken from Lenz and Sogaard-Andersen (2011).

surface of the chromosome until it comes into contact with the ParB-*parS* complex of the plasmid. At the interface of this interaction the ATPase activity of ParA is upregulated causing the hydrolysis of the bound ATP, resulting in its conversion to ADP (Gerdes et al., 2010). This also causes the depolymerisation of ParA from the end of the filament releasing the ParA molecule as a monomer and abolishing its DNA interaction. The filament has then contracted slightly from the plasmid which then is pulled towards the remaining end of the ParA filament by the interaction of the ParB-*parS* complex with the ParA filament. This process continues until the plasmid is pulled the length of the filament to one end of the chromosome. While the plasmid is being pulled towards one end of the chromosome, the free monomeric ParA molecules, which have been liberated from the ParA-ATP filament, begin to assemble from the other end of the chromosome in an ATP dependent manner. Once this filament reaches the plasmid it pulls the plasmid back in the other direction (Ebersbach and Gerdes, 2004; Ebersbach et al., 2006). This cycle continues with the oscillation of ParA from one end of the chromosome to the other creating a reciprocal oscillation in plasmid localisation which was confirmed using high resolution microscopy (Ringgaard et al., 2009). With the addition of more plasmids within this system, an equilibrium between all plasmids starts to form such that they become evenly distributed along the surface of the chromosome. This distribution allows for the efficient retention of the plasmid in both progeny cells after division.

Another ParAB system with a variation that moves away from oscillation can be found in the crescent shaped bacteria *Caulobacter crescentus*. The same underlying biochemical principles seen in plasmid segregation exist in the ParAB mechanism for chromosome segregation in *C. crescentus* (Figure 8). ParA forms a dimer in the presence of ATP which gives it affinity to both ParB and DNA. The interaction between ParB and the ATP associated ParA dimer causes upregulation of the ATPase activity of ParA leading to the hydrolysis of the ATP molecule and the formation of monomeric ParA which has neither affinity to ParB nor DNA. The monomeric ParA is then able to dimerise by finding another ATP molecule away from ParB (Ptacin et al., 2010). However, beyond the biochemical properties the two systems ultimately segregate DNA in different ways. Rather than an oscillation, this system relies on a singular static ParA gradient which pulls the replicated

chromosome from one pole to the other. This static gradient is not generated through any intrinsic properties of the ParA and ParB proteins in the bacterium, but is instead brought about by the effect of other proteins which act upon the system. During growth the chromosome is not located freely in the mid cell but is tethered to the old pole through the immobilisation of the ParB-*parS* segrosome by the pole-organising protein PopZ. *C. crescentus* has two proteins which act as markers of both the old pole (PopZ) and the new pole (TipN). PopZ is a small, acidic protein which forms a polymeric structure at the old pole where it not only anchors the chromosome during division but also localises other proteins such as CckA and DivJ which are involved in morphogenesis and cell cycle signalling (Ebersbach et al., 2008). Deletion of PopZ leads to filamentation of *C. crescentus,* demonstrating that it is essential for correct segregation of chromosomes (Bowman et al., 2008). TipN on the other hand is a large, coiled-coil protein which localises to the new pole where it

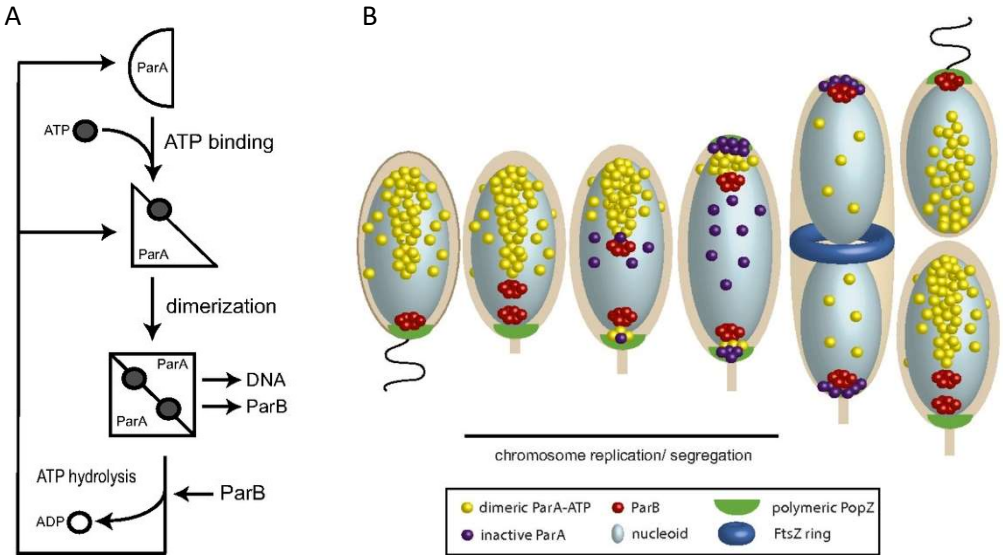

Figure 8: Chromosome segregation in *C. crescentus*.

(A) Dimerisation of ParA monomers occurs through ATP binding. This allows interaction with both DNA and ParB. Upon interaction with ParB the ATPase activity of ParA is upregulated and the ATP hydrolysis occurs. This causes ParA to become monomeric abolishing interaction with ParB and DNA. Monomeric ParA can then begin the cycle over. (B) At the beginning of the life cycle in C. crescentus the chromosome is tethered to the membrane through the ParB segrosome which is bound by the membrane tethered protein PopZ. Upon chromosome replication, the replicated chromosome which also contains the ParB segrosome is pulled to the new pole by the retracting ParA filament. Once the replicated chromosome is pulled to the new pole the ParB-PopZ interaction tethers the chromosome at the new pole. Taken from Ptacin et al, (2014).

recruits proteins involved in the formation of the flagella (Huitema et al., 2006; Lam et al., 2006). Deletion of TipN has a less severe effect on chromosome segregation causing only a mild elongation (Lam et al., 2006).

It was originally thought that during chromosome segregation, after chromosome replication the original chromosome stayed anchored to the old pole by the ParB-*parS* segrosome interaction with PopZ. ParA, which was anchored to the new pole by TipN, then formed an ATP dependent filament from the new pole to the replicated chromosome, which also has a ParB-*parS* segrosome, pulling it to the new pole in the already established mechanism (Ptacin et al., 2010). This model has been superseded (Figure 8) however, with the discovery that during chromosome replication, PopZ releases the ParB-*parS* segrosome and localises to both poles where it recruits ParA to both poles. The replicated centromeres of the chromosomes are initially driven apart either by the force generated by replicating DNA or through natural diffusion. The ParA at the poles then binds ATP and starts to accumulate towards the chromosomes from each pole. Upon encountering the ParB-*parS* complex it begins to pull the chromosomes apart using the established ParA-ParB dynamics (Ptacin et al., 2014).

In *B. subtilis*, the homologues of ParA and ParB are called by the alternative names of Soj and Spo0J respectively (Ireton et al., 1994; Sharpe and Errington, 1996). The difference in naming was due to the role that Spo0J has in sporulation, the null mutant being blocked in this process and Soj being a suppressor of Spo0J (Ireton et al., 1994). Both mutants of these genes show a defect in chromosome segregation during both vegetative division and sporulation with an increased prevalence of anucleate cells, although less pronounced in the Soj mutant, which led to the idea that they operated in a similar manner to other classical ParAB systems (Ireton et al., 1994; Sharpe and Errington, 1996). In fact, biochemically the proteins behave in a same manner as the previous ParA and ParB proteins we have discussed. It has been demonstrated that Soj forms a dimer in the presence of ATP or a monomer either in the presence of ADP or absence of nucleotide (Hester and Lutkenhaus, 2007; Leonard et al., 2005). The oligomeric state of Soj has been shown to be regulated by its interaction with Spo0J which upregulates the ATPase activity of Soj pushing it towards a monomeric state (Scholefield et al., 2011). Like other systems Spo0J has

also been shown to bind to a number of *parS* sites found around the origin of replication from which Spo0J spreads laterally along the chromosome in a non-specific interaction (Breier and Grossman, 2007; Lin and Grossman, 1998). Soj also has been shown to have affinity to DNA, again this is dependent on it being in its ATP bound dimer state, with mutants unable to dimerise also lacking the ability to bind DNA (Scholefield et al., 2011). All of these properties are not surprising given the characterisation of other ParA and ParB protein. Although Spo0J is involved in chromosome segregation, as demonstrated by the incidence of anucleate cells in the *spo0J* null mutant, it is not just through its interaction with Soj that correct segregation is achieved. In addition segregation is enacted through a chromosome organising pathway which consists of SMC (structural maintenance of chromosomes) and its partner proteins ScpA and ScpB (Gruber and Errington, 2009; Sullivan et al., 2009). During chromosome replication, ParB recruits SMC to the origin where SMC is loaded onto the chromosome which aids in segregation (Gruber and Errington, 2009; Sullivan et al., 2009). Interestingly, in *B. subtilis*, the Soj protein also has a role in the initiation of chromosome replication rather than just the established chromosome segregation function seen in other ParA homologues (Figure 9). When in its ATP bound dimer form, Soj binds DNA and promotes overinitiation of DNA replication (Murray and Errington, 2008). While the mechanism for this is unclear, as interaction between dimeric Soj and DnaA, the initiator of replication, has not been shown, it is suggested that Soj perhaps changes the topology of the DNA near *oriC,* allowing more efficient binding of DnaA. When in this dimeric state Soj also blocks sporulation through the so called Sda checkpoint system (Murray and Errington, 2008). When the Soj dimer encounters Spo0J, upregulation of Soj ATPase activity causes it to disassemble and enter its monomeric state in which Soj forms a complex with DnaA, inhibiting chromosome replication (Murray and Errington, 2008). This relationship explains the original phenotype found in the *spo0J* null mutant in which sporulation was blocked. In the absence of Spo0J, Soj remains in its dimeric form and blocks sporulation, sporulation can only occur when Spo0J causes Soj to become monomeric.

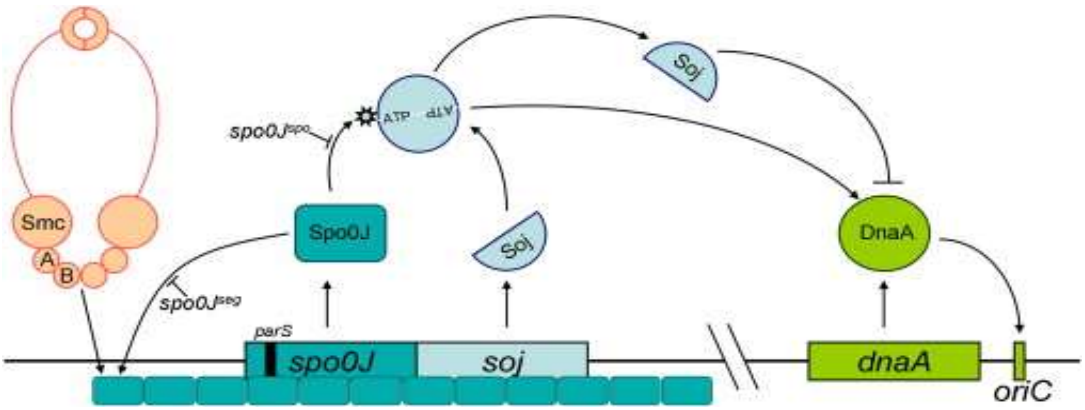

Figure 9: Spo0J binds to *parS* sites around the replication origin of the chromosome where it can trigger SMC/condensing mediated chromosome segregation. Soj regulates the initiation of chromosome replication through the replication initiator DnaA through a mechanism in which monomeric Soj inhibits DnaA while dimeric Soj acts as an activator. The ATPase activity of Soj, and thus is oligomer state, is regulated by Spo0J. Taken from Gruber and Errington (2009).

1.2.2 SMC and DNA organisation

SMC, or MukB in *E. coli*, is a large protein that consists of an N-terminal globular domain containing a Walker A nucleotide binding motif, followed by two coiled-coil domains separated by a small globular hinge domain and rounded off with a final globular domain containing a Walker B motif (Melby et al., 1998; Yamanaka et al., 1994). The SMC protein is found across all eukaryotes where it has been implicated in diverse functions such as chromosome segregation and cohesion as well as DNA recombination and repair, with mutations in SMC responsible for a range of genetic disorders (Ball Jr and Yokomori, 2001; Strunnikov and Jessberger, 1999). In prokaryotes SMC, which is found in all Gram-positive bacteria and archaea but less than half of Gram-negative bacteria, have mainly been implicated in chromosome condensation and partitioning (Jensen and Shapiro, 1999; Lindow et al., 2002; Soppa, 2001). SMC is associated with two proteins, the segregation and condensin proteins ScpA and ScpB. The current understanding of how SMC/ScpAB complexes are loaded onto the DNA is the model proposed for eukaryotic cohesion. When DNA is in the vicinity of the DNA-sensing Lysine residues on the head domain of SMC upregulation of the ATPase activity of the SMC molecule causes hydrolyses of the bound ATP into

ADP. This opens the first interlocking gate allowing the DNA strand to pass through the head domains which are bound by the ScpA. The head domains then dimerise through interaction with another ATP molecule which traps the DNA in the pocket formed by ScpA. At the same time that ATP causes dimerisation the second interlocking gate is opened when ScpA and the hinge domain disengage due to the activity of Wapl (Wings apart-like protein homologue). This allows the DNA strand to pass through and become trapped by SMC. It is thought that loading and unloading of the SMC/ ScpAB from DNA happens by a similar mechanism (Uhlmann, 2016).

As well as the role in packing DNA so that chromosomes are able to fit efficiently within the confines of a cell, SMC has been shown to play a crucial role in orienting chromosomes throughout the bacterial life cycle. Studies using Fluorescent in situ hybridisation (FISH) have determined the spatial arrangement of chromosomes in a range of bacteria. In *C. crescentus* for example, chromosomes align with the origin (*ori*) at one pole and the terminus (*ter*), with the chromosome arms stretching across the cell, the so-called *ori-ter* orientation (Viollier et al., 2004). This pattern is followed through the division event with the replicated chromosome being pulled to the other pole and the terminus regions of the chromosomes ending up at the newly formed division septa. Interestingly *E. coli* exhibits different chromosome organisations depending upon whether they are fast or slow growing. In slow growing *E. coli* cells the origin and terminus are both held mid cell with the two chromosome arms flanking both left and right of the mid cell creating a left-*ori*-right configuration (Nielsen et al., 2006; Wang et al., 2006). Fast growing *E. coli* on the other hand adopt the same configuration as C*. crescentus* exhibiting polarly localised origins during replication (Youngren et al., 2014). *B. subtilis* possess an interesting chromosome organisation which depends upon the developmental phase of the cell. During vegetative growth the chromosome alternates between an *ori-ter* and a left-*ori*-right pattern, while during sporulation the replicated chromosomes or an *ori-ter*/*ter-ori* orientation (Wang et al., 2014; Wang and Rudner, 2014). In the absence of SMC these chromosome orientations are perturbed, indicating SMC is required for the correct organisation of chromosomes in cells (Danilova et al., 2007). It has also been demonstrated, and is especially severe in *B. subtilis*, that the loss of the SMC/ScpAB complex leads to a range of chromosome defects and a rise in the

number of anucleate cells (Britton et al., 1998; Gruber and Errington, 2009; Sullivan et al., 2009). However, so far no direct mechanism has been demonstrated which implicates SMC actively in chromosome segregation, so as of yet it is unclear whether it is the alignment of the chromosomes that is allowing efficient segregation or if SMC is actively contributing towards this process.

Recent developments in technology called high throughput chromosome capture, first exploited in mapping the 3D organisation of eukaryotic chromosomes, have now been applied in some of the bacterial model organisms for the mapping of chromosome organisation such as *C. crescentus*, *E. coli* and *B. subtilis* (Weng and Xiao, 2014). The Hi-C method starts with crosslinking DNA within the chromosomes that are close within the 3D space in live cells. Selectively sequencing fragments that are crosslinked reveals DNA sequences that are in close proximity in the cells. Surprisingly, this method identified proximity between DNA fragments not only located adjacently on the chromosome but fragments that are far apart. This methodology was pivotal to establishing that bacterial chromosomes are organised on multiple levels within the cell (Weng and Xiao, 2014). The first organisation generates micro-domains (10-100 Kbps) which are the result of supercoiling of DNA into plectonomic loops which can be stabilised by nucleoid associated proteins (Hsu et al., 2006; Tadesse and Graumann, 2006). The second level of organisation are the macro-domains of which there are four, the *ori*, *ter*, left and right. Interestingly these macro-domains are further compacted into a compact rod shaped nucleoid and these different macro-domains are positioned at different locations within the cell (Figure 10) (Cagliero et al., 2013). In *C. crescentus* for example the *ori* region is at the flagellated pole while the *ter* is at the other pole with left and right arms juxtaposed (Le et al., 2013). This arrangement means that DNA on the left arm are in close proximity to the appropriate region on the right arm which was identified using the Hi-C method. In *E. coli*, the *ori* and *ter* are held mid-cell with left and right at either pole with no contacts between the two replichores (Nielsen et al., 2006; Wang et al., 2006). The Hi-C technique was used to show that in *C. crescentus* the SMC mutant strain, the chromosomes failed to intertwine. It is thought that SMC is loaded on to the chromosome at the *ori*, where it then migrates along the chromosome in order to facilitate intertwining of the DNA (Le et al., 2013).

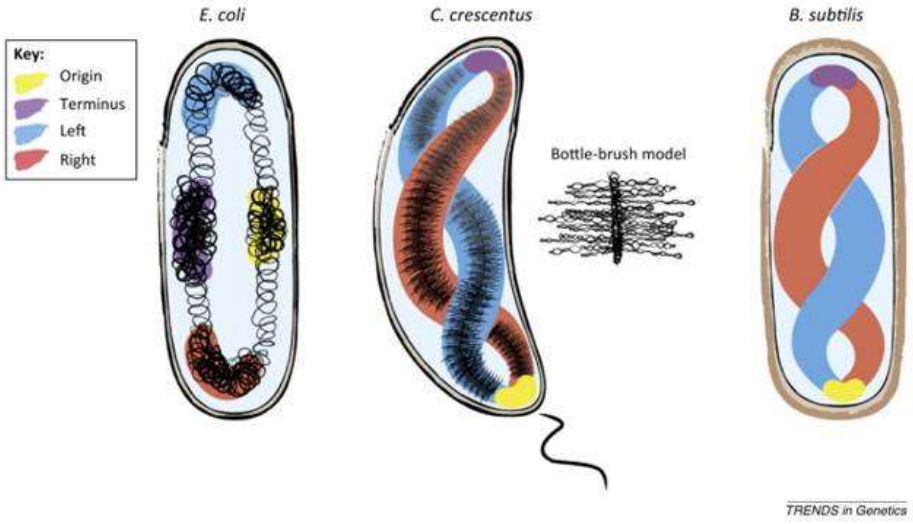

Figure 10: Models for nucleoid organization in *E. coli*, *C. crescentus*, and *B. subtilis*.

In *E. coli*, the chromosome is organised with the *ori* and *ter* mid-cell and the left and right replichores at respective poles. The chromosomes are not intertwined. In *C. crescentus* and *B. subtilis* the chromosomes are organised with the *ori* at one pole and the *ter* at the other. The left and right, which are located mid-cell, are intertwined in these bacteria. Taken from Weng and Xiao (2014).

1.2.3 The MinD system – controlling septum positioning

Having considered the role of ParA proteins and their diversity not only in their role in the cell but also in how bacteria utilise the basic underlying properties of the proteins to produce variations of mechanisms, we can now move on to discuss the other subgroup in the superfamily, the MinD proteins. As described for the ParA proteins, bacteria can use different mechanisms to utilise the basic properties of MinD proteins to carry out a common function that is adapted to meet the environmental challenges. While ParA proteins are primarily involved in the chromosome segregation aspect of division, MinD proteins have generally been characterised as functioning in another aspect of division, septum positioning. As we will discuss, the placement of the septum in the cell is a heavily orchestrated event, which tries to ensure that the shape and size of the organism is maintained through the division process such that, in most organisms, equal sized progeny are produced. The ability of the bacteria to find the mid cell is predicated upon the bacteria utilising

spatial cues within the cell, whether that is the poles of the cell or the position of the chromosome. Before discussing how these cues are utilised in accurate septum placement we must first understand how a division site can be regulated to form at any given position in the cell. Previously, we talked about FtsZ and its role as the marker of future septum positioning (Bi and Lutkenhaus, 1991). FtsZ is a GTPase and it binds to GTP which polymerises FtsZ first into protofilaments and then into the FtsZ ring important for division. This polymerisation can be reversed or inhibited by up regulation of the GTPase activity of FtsZ, which converts the bound GTP into free GDP (Erickson et al., 1996). By spatially regulating this GTPase activity, and FtsZ self-interaction the cell is able to direct the location of the Z-ring in the cell. The MinD system is one of the bacterial systems that regulate septum positioning by regulating FtsZ polymerisation. The MinD protein was first discovered in *E. coli* and named for the mini cell phenotype and subsequent increase in anucleate cells observable in the null mutant (Adler et al., 1967). The *E. coli* the Min system, which consists of the three proteins MinC, MinD and MinE, is the dominate determinate of FtsZ placement (Margolin, 2001). Absence of the Min system in *E. coli* leads to an increase in the frequency of FtsZ ring formation near the cell pole and thus an increase in mini-cells lacking chromosomes results (de Boer et al., 1992). The actual interference of polymerisation of FtsZ occurs through a MinC-MinD ATP complex in which the MinD protein is membrane bound at the cell pole and the C-terminal region of MinC inhibits lateral interaction of FtsZ polymers (Figure 11). In addition, the complex competes with the proteins ZipA and FtsA, responsible for tethering the ring to the membrane and stabilising it, for binding FtsZ polymers (Dajkovic et al., 2008; Shen and Lutkenhaus, 2009). Pole to pole oscillation of MinD ensures that there is an increase in the concentration of the complex at cell poles in a time dependent manner. This results in lower concentrations of the complex mid-cell where cell division takes place (Dajkovic et al., 2008). Oscillation of MinD is an ATP dependent process which begins with the initial localisation of dimeric ATP bound MinD to a single pole. Further dimers of MinD-ATP begin to assemble at the pole from where they stretch along the membrane towards the mid cell (Hu et al., 2002; Hu et al., 2003; Lackner et al., 2003). MinE, which forms a ring structure in response to MinD, assembles at the edge of the MinD-ATP dimer zone where it has two regulatory effects upon MinD. Firstly MinE

competes with MinC for MinD binding causing the disassociation of MinC from the MinD-MinC complex, and secondly it upregulates the ATPase activity of MinD (Hu and Lutkenhaus, 2001). This upregulation results in hydrolysis of the ATP bound to MinD converting it to ADP, and releases MinD-ADP monomers into the cytosol (Hu and Lutkenhaus, 2001). MinE then binds the next MinD-ATP dimer repeating the process until all the MinD-ATP dimers are disassembled from the membrane, after which MinE itself disassembles (Park et al., 2011; Park et al., 2012). The MinD-ADP monomers, after being ejected from the pole, diffuse to the other pole away from the regulation of the MinE ring, where after ATP/ADP nucleotide exchange MinD-ATP dimers begin to assemble again. MinE, after completing the disassembly of the MinD-ATP dimers from the first pole, then diffuse to the new MinD-ATP assemblies to

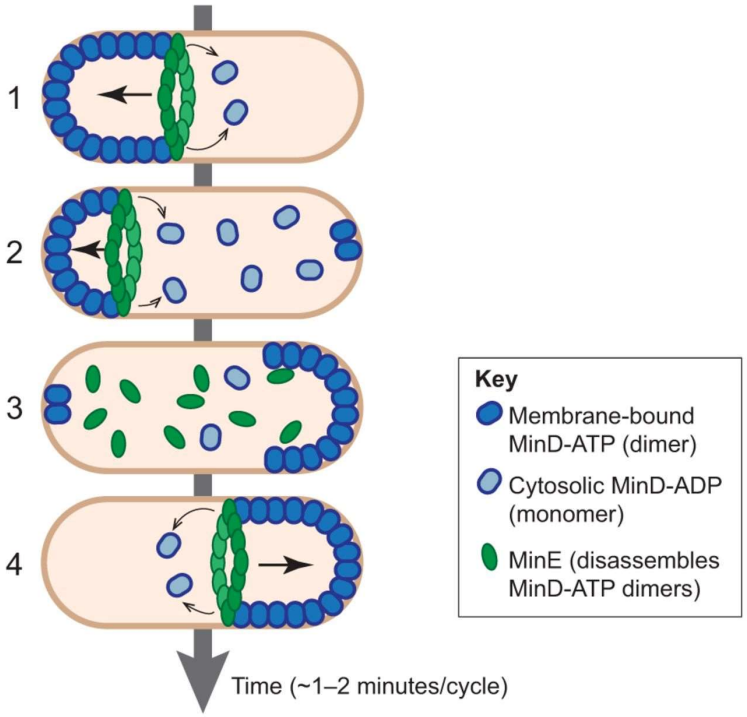

Figure 11: MinD oscillation in *E. coli*.

ATP bound dimers of MinD bind to the membrane at the cell pole accumulating until it reaches near the mid-cell. At the edge of the MinD gradient the MinE ring assembles interacting with MinD. This interaction causes upregulation of the ATPase activity of MinD causing hydrolysis of the bound ATP and forming MinD-ADP monomers. These monomers no longer bind to the membrane or interacts with MinE but diffuses to the other pole where upon nucleotide exchange reform MinD dimers that binds the membrane. As the MinD-ATP gradient retracts it pulls the MinE ring until all MinD-ATP dimers have disassembled. The process then begins at the other pole. Taken from Laloux and Jacobs-Wagner (2014).

repeat the process. Interestingly, while it is unknown exactly why MinD moves to the pole during oscillation, other than this is the furthest point away from the MinE ring, in filamentous cells that grow abnormally long, MinD has been shown to localise in a stripe pattern along the length of the cell (Raskin and de Boer, 1999). The MinD oscillation mechanism is very similar to the oscillation shown for ParA during plasmid segregation, where multiple plasmids can be evenly segregated along the length of the chromosome. It is perhaps possible that the pole-to-pole MinD oscillation observed in *E. coli* is primarily a result of the distance between the poles. When discussing ParA proteins, in *E. coli* we only discussed these proteins in relation to plasmid segregation and not chromosome segregation. This is because *E. coli*, as well as some other related bacteria, such as *Salmonella sp* and *Yersinia sp*, do not contain recognisable ParA proteins, although in *E. coli* the *parS* like sequence *migS* has been found near the *oriC* (Livny et al., 2007; Yamaichi and Niki, 2004). While it has been speculated that the SMC homologue MukB may play a role in chromosome segregation, no specific chromosome segregation mechanism has been found in *E.*

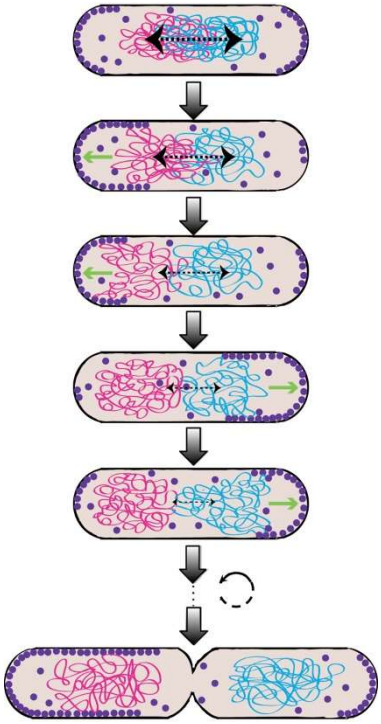

Figure 12: MinD oscillation is involved in chromosome segregation in *E. coli*.

As MinD oscillates from one pole to the other, the DNA binding properties of the protein in its ATP bound dimeric state help to pull the replicated chromosomes to each pole. Taken from Di Ventura et al, (2013).

coli. More recently, it has been suggested that MinD, through its oscillation, is able to help chromosomes segregate in *E. coli* (Figure 12). Like the ParA proteins, *E. coli* MinD has been shown to bind DNA in an ATP-dependent manner, and to tether the replicated chromosome to the pole during division by a process of edging the chromosome towards the pole during the phases of MinD oscillation (Di Ventura et al., 2013).

In *B. subtilis*, MinD localisation is not achieved through oscillation but rather through static localisation to the poles (Figure 13) and newly synthesised division septa through the polar marking protein DivIVA (Cha and Stewart, 1997; Marston and Errington, 1999; Marston et al., 1998). Like in *E. coli*, inhibition of FtsZ polymerisation is carried out in a similar manner by MinC which is localised in an ATP dependent mechanism by MinD (Karoui and Errington, 2001; Marston and Errington, 1999).

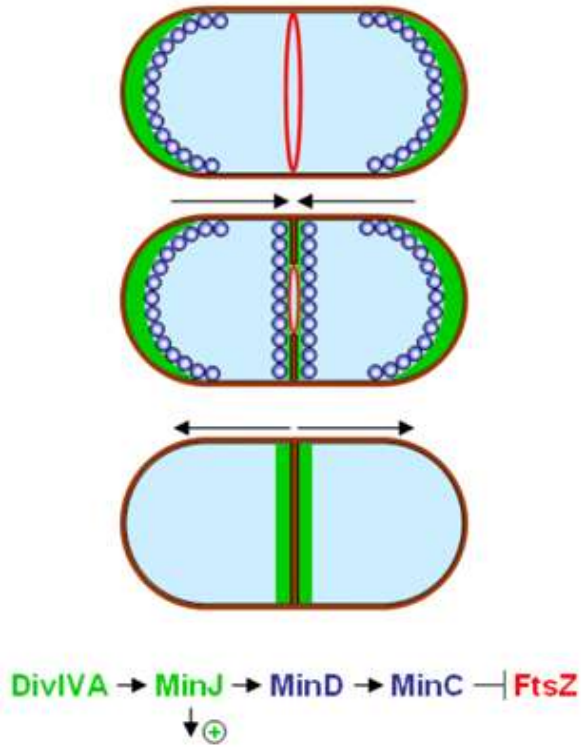

Figure 13: MinD localisation in *B. subtilis*.

In *B. subtilis*, MinD is statically localised to the pole by the polar localising protein DivIVA which recruits the intermediary MinJ. MinD then recruits MinC to the poles which inhibits FtSZ polymerisation at the poles. MinD is also localised to the mid-cell once the division membrane starts to form. This prevents secondary division events from occurring mid-cell. Image curtesy of Dr Marc Bramkamp.

However, while ATP binding is important for MinD activity, no regulatory protein for the ATPase activity of MinD, such as MinE in *E. coli*, has been shown in *B. subtilis*. Localisation of MinD to the pole, while dependent on the preceding localisation of DivIVA, is facilitated by the intermediary protein MinJ, which interacts with both DivIVA and MinD (Patrick and Kearns, 2008). Localisation of DivIVA to the poles has been shown to be a result of the negative curvature of the membrane at these sites (Ramamurthi and Losick, 2009). While it was originally thought that localisation of DivIVA to the site of division was due to an interaction with the maturing divisome complex, it has instead been shown that this localisation is due to the initial constriction of the membrane during septum formation which generates the negative curvature that localises DivIVA (Eswaramoorthy et al., 2011). Localisation of MinDC to the site of septum formation prevents any aberrant secondary FtsZ rings from forming close to the mid cell during or after division.

MipZ – *C. crescentus*

Interestingly, *C. crescentus* does not contain a classical Min system as seen in *E. coli* and *B. subtilis*. Instead, regulation of septum positioning is achieved through the MipZ pathway (Thanbichler and Shapiro, 2006). MipZ is another homologue of ParA/MinD and is conserved among all α-proteobacteria that lack MinCD orthologues. MipZ is located to the *oriC* of the chromosome in *C. crescentus* by ParB, upon which MipZ forms a dimer and diffuses away from ParB by non-specific ATP dependent interaction with the chromosome (Kiekebusch et al., 2012). Eventually the intrinsic ATPase activity of MipZ causes it to hydrolyse the ATP molecule, abolishing DNA interaction in the process. MipZ then relocates to the origin region of the chromosome through interaction with ParB. This MipZ cycle creates a concentration gradient which stretches from the pole where the chromosome is tethered to the membrane by the ParB-PopZ interaction described earlier. Unlike with the Min system, in which inhibition of FtsZ polymerisation is achieved by MinC rather than the ATPase MinD, in *C. crescentus* inhibition of FtsZ polymerisation is carried out directly by MipZ (Thanbichler and Shapiro, 2006). In freshly divided cells,

the MipZ gradient is established from a single pole, while FtsZ is situated at the other pole, the site of recent division (Figure 14). When the replicated chromosome is pulled to the new pole, FtsZ is displaced by MipZ which then creates a second gradient at the new pole (Thanbichler and Shapiro, 2006). This generates a bi-polar MipZ gradient that resembles the MinD gradients seen in *E. coli* and *B. subtilis* in which there are high concentrations of MinD or MipZ at the poles but low concentrations mid cell (Figure 14). This promotes FtsZ polymerisation mid cell leading to accurate and efficient division (Thanbichler and Shapiro, 2006).

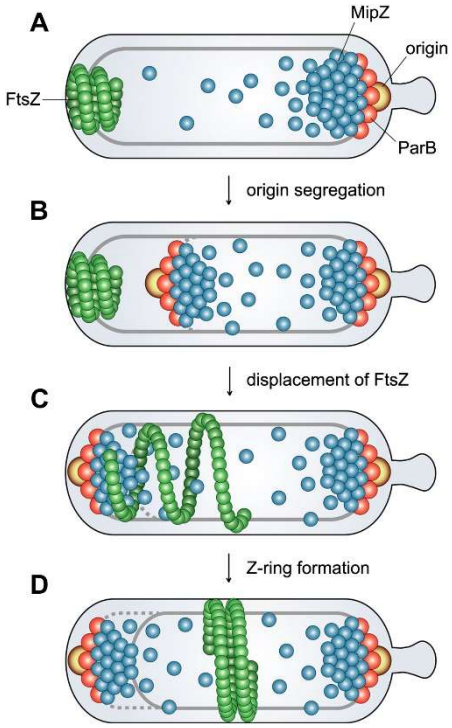

Figure 14: MipZ controls septum site placement in *C. crescentus*.

Septum site positioning is controlled by MipZ in *C. crescentus*. MipZ is located to the chromosome by the *parS* bound ParB. MipZ directly inhibits FtsZ polymerisation from occurring over the chromosome, which is tethered to the old pole. Upon chromosome replication a second ParB-*parS* segrosome is formed on the newly replicated chromosome. This causes distinct localisation of MipZ to the replicated chromosome. When the chromosome is segregated to the new pole, MipZ displaces the polar located FtsZ polymer. When the replicated chromosome is tethered to the new pole MipZ is also localised there, inhibiting FtsZ polymerisation from occurring at the new pole. Taken from Thanbichler and Shapiro (2006).

The Nucleoid Occlusion system

The negative regulators of FtsZ that we have discussed so far are involved in promoting mid cell location of the FtsZ ring. While this is important, within itself it does not protect the chromosome from being guillotined during the formation of the septum. In fact, even chromosome segregation would not be enough to prevent this as usually the terminus region of the DNA is found within the closing septa and DNA translocases are required to transport these ends into the correct compartment before the septa fully closes (Touzain et al., 2011). To ensure that chromosomes are not guillotined during division, bacteria have developed the nucleoid occlusion mechanism (Figure 15). This mechanism inhibits FtsZ ring formation from occurring over the DNA, and so far two proteins, SlmA in *E. coli* and Noc in *B. subtilis*, have been implicated in this system (Wu and Errington, 2004). While there is no sequence homology between the two proteins, with SlmA having no homologues of known function and Noc belonging to the ParB family of proteins with 40% identity to Spo0J, both proteins share similar characteristics (Sievers et al., 2002). They both bind to specific areas of the chromosome, SlmA binding sites (SBS) and Noc binding sites (NBS), which are distributed around the chromosome everywhere except for the region surrounding the terminus (Cho et al., 2011; Wu et al., 2009). The binding pattern of these two proteins would support the idea that as the chromosomes are segregated during division, a process driven from the origin, the areas covered by these nucleoid occlusion proteins would vacate the mid cell first, leaving the uncoated terminal regions at the site of division. FtsZ can then form over this region of the chromosome and begin the process of septum formation. Then, as mentioned, the terminus region of the chromosome can be removed from the closing septum by DNA translocases (Wu and Errington, 2004). There are two proposed models for the action of SlmA in *E. coli*. The first suggestion is that when SlmA binds to SBS sites around the chromosome, SlmA is able to bind to the C-terminal tail of FtsZ where it competes for binding with the other regulatory proteins of FtsZ, such as ZapD, MinC, FtsA and even other FtsZ molecules. This would not only promote further interactions of SlmA with FtsZ but eventually lead to the breakdown of FtsZ protofilaments (Du

and Lutkenhaus, 2014). The second suggestion is that SlmA spreads along DNA as a dimer of dimers forming higher order nucleoprotein complexes which sequester FtsZ preventing its formation into Z-Rings (Tonthat et al., 2013). Both of these models would indicate a regulation of FtsZ polymerisation that is independent of the GTPase activity of FtsZ (Cabre et al., 2015). In contrast to SlmA, Noc is not thought to have any direct interaction with FtsZ. Instead Noc acts by binding the chromosome to the membrane along the lateral wall, physically occupying the space that FtsZ requires in order to polymerise into the Z ring (Adams et al., 2015). So far, no nucleoid occlusion system has been shown in *C. crescentus*, but the fact that MipZ directly inhibits FtsZ polymerisation and is thought to diffuse along the chromosome from the origin, could suggest that it acts analogously to this system.

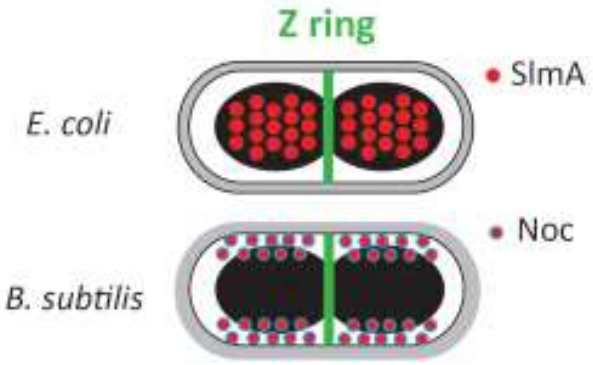

Figure 15: Nucleoid occlusion.

The nucleoid occlusion proteins SlmA (*E. coli*) and Noc (*B. subtilis*) inhibit FtsZ ring formation from occurring over the chromosome. Taken from Hajduk et al (2016).

1.3 *Streptomyces coelicolor*

After discussing the proteins which provide the mechanism for the bacterial life cycle we will now turn our attention to *Streptomyces coelicolor*, a model organism for filamentous growth from the A*ctinobacteria* phylum and the subject organism of this study.

S. coelicolor is a GC rich, Gram-positive, soil dwelling bacterium, which belongs to, and is the model organism for, a genus that produces many biologically active secondary metabolites. Unlike most other bacteria *Streptomyces* have linear

chromosomes (Lin et al., 1993), with *S. coelicolor* containing 7,825 genes and 20 possible gene clusters coding for secondary metabolites within its 8 Mbp chromosome (Bentley et al., 2002). The chromosome consists of a central core region containing many of the primary metabolic genes and the replication origin (*oriC*) which is flanked by two unstable terminal arm regions containing non-essential genes, often implicated in secondary metabolism (Bentley et al., 2002). Predictions suggest that approximately 12.5% of genes encode regulatory proteins including putative sigma factors, two component systems and DNA binding proteins reflecting its complexity of development (Bentley et al., 2002).

1.3.1 The *S. coelicolor* life cycle

As previously touched upon, unlike most other bacteria that divide by binary fission, *S. coelicolor* exhibits a far more complex life cycle (Figure 16). This begins from a single uni-genomic spore which, upon favourable conditions, produces either one or two germ tubes which extend from the spore during germination (Jyothikumar et al., 2008). These develop into a network of vegetative mycelium allowing for the uptake of nutrients and grow in a polar manner through tip extension and branching events that occur along the lateral wall of the hyphae in a similar fashion to filamentous fungi (Errington et al., 2003). These branching events allow for the increase in growth rate which is also proportionate to the rate of DNA replication (Chater, 1993; Flardh, 2003b). During vegetative growth, cell division is suspended with the placement of cross walls not undergoing full cell-cell separation. Thus exponential growth can only be achieved through the increase in number of growing tips. This stage of growth is characterised by colonies that are shiny in appearance displaying the classic bald phenotype seen in colonies blocked at this stage of development on nutrient agar. Upon nutrient depletion, a signalling cascade is initiated, which results in the erection of aerial hyphae that break the surface tension of the media and rise into the air (Kelemen and Buttner, 1998). The aerial hyphae grow as single multi-genomic individual hyphae with less branching and appear as fuzzy white colonies as seen in colonies blocked at this stage of development. After

the aerial hyphae have stopped growing, septa are placed at equal spacing along the length of the unbranched hyphae, such that each individual chromosome is packed into a single compartment, the pre-spore compartment. The spore chain then matures into uni-genomic spores with the production of a grey polyketide pigment, and thus the life-cycle is complete (Chater, 1993; Flardh and Buttner, 2009; Kelemen et al., 1998).

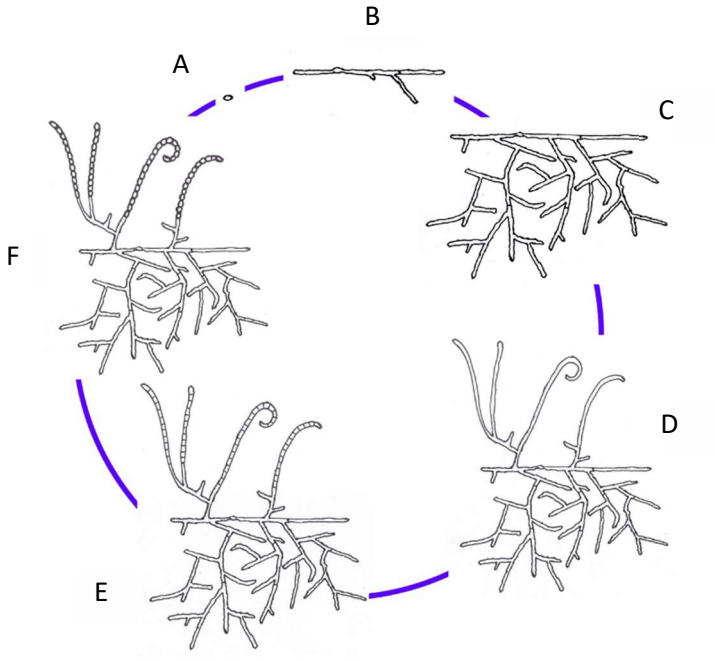

Figure 16: The *S. coelicolor* life cycle.

The life cycle of *S. coelicolor* begins with a single uni-genomic spore (A), which upon favourable conditions germinates with the protrusion of either one or two germ tubes (B). *S. coelicolor* then grows and branches forming a network of vegetative hyphae which stretch into the media in order to uptake nutrients (C). Upon nutrient depletion, aerial hyphae are erected above the surface of the media (D). After the cessation of aerial growth, septa are formed along the length of the aerial hyphae creating pre-spore compartments (E). These compartments then mature into spores from which the life cycle can begin again (F). Image curtesy of Dr Kelemen.

1.3.2 Growth in *S. coelicolor* - The TIPOC

Polar growth in *S. coelicolor* is driven by the multiprotein assembly that constitutes the Tip Organising Centre (TIPOC), otherwise known as the polarisome,

which is present at the tip of all actively growing hyphae (Flardh et al., 2012; Holmes et al., 2013) (Figure 17). This polar complex, primarily consists of three proteins; DivIVA, Scy and FilP, all of which have been implicated in growth and branching. These cytoskeletal proteins all share a similar basic coiled-coil structure and bioinformatics analysis reveals some interesting structural domains.

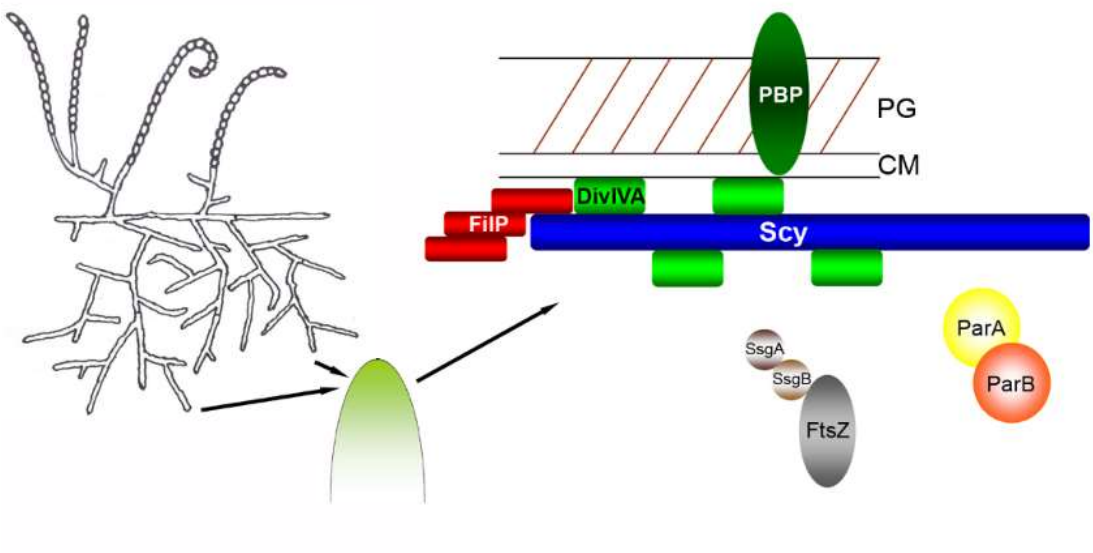

Figure 17: The TIPOC of *S. coelicolor*.

Growth and branching in *S. coelicolor* is driven by the multi-protein TIPOC. There are three key cytoskeletal proteins (DivIVA, Scy and FilP) which form the TIPOC which localises to the tips of actively growing hyphae. The TIPOC has an effect on chromosome segregation through the interaction between Scy and ParA (Holmes et al., 2013).

While DivIVA consists of two classical heptad coil-coiled domains flanking a long linker region, both Scy and FilP share an unusual domain structure consisting of N-terminal heptad coiled-coils, a linker, and a C-terminal 51mer coiled-coils (Walshaw et al., 2010). The classic heptad coiled-coil consists of a seven amino acid repeat in which the first and fourth positions are non-polar core residues while the fifth and seventh residues are exposed polar amino acids which confer specificity between the two helices formed in a homodimer through electrostatic interactions (Mason and Arndt, 2004). The C-terminal coiled-coil however has hendecad repeats (11mer) in which the first, fourth and eighth residues of the repeat are hydrophobic. The overall repeat in this domain is a 7, 11, 11, 11, 11 51mer repeat (Walshaw et al., 2010).

DivIVA was the first of these proteins to be characterised in *S. coelicolor*, named as a homologue of the division associated protein DivIVA in *B. subtilis* (Flardh, 2003a). While the DivIVA homologue in *S. coelicolor* is found to localise to the poles, in a similar manner to its *B. subtilis* counterpart and probably through a preference for negatively curved membranes, its function, as determined by the manipulation of its expression levels, is in tip growth and branching (Flardh, 2003a). Low expression levels of DivIVA, result in irregular shaped short hyphae with branching close to existing tips. Higher DivIVA levels induce hyperbranching and leads to swollen tips that lyse (Flardh, 2003a). Moreover, in *S. coelicolor divIVA* is an essential gene, which combined with the fact that cell division is a dispensable process in this organism underlines its importance to growth rather than division, although DivIVA has been localised to vegetative cross walls. Time lapse imaging techniques also demonstrate that DivIVA localises to sites of branching long before the emergence of new tips, which when DivIVA is overexpressed localises as discrete foci along the length of the hyphae where hyperbranching occurs (Hempel et al., 2008). This links DivIVA not only as a marker for growth but also as a molecular marker of future branch sites. One mechanism that has been suggested to explain the formation of new tip sites is the Tip-focussed splitting of existing DivIVA foci into smaller foci near the tip which later become the site of future branching (Flardh et al., 2012; Richards et al., 2012). This was established after monitoring tip localised DivIVA-EGFP patches which appear to break of and localise at sites of future branching. However this mechanism does not account for the majority of branching which occurs far behind existing growing tips and de novo branching is still a possibility. Another proposed method of regulation of DivIVA is through phosphorylation, which is consistent with the regulatory mechanisms of DivIVA in other bacteria. DivIVA in *S. coelicolor* has been shown to be phosphorylated by AfsK which when knocked out creates a strain that undergoes less branching (Flardh et al., 2012; Hempel et al., 2012; Saalbach et al., 2013). Phosphorylation of DivIVA is proposed to promote disassembly of DivIVA from the tip.

The second protein to make up the TIPOC is Scy (*Streptomyces* cytoskeletal protein), a large alanine/glutamate (1326 amino acids) protein with homologues found exclusively amongst filamentous *Actinomycetes*. Scy is also found to localise to

tips during active growth in *S. coelicolor,* suggesting it has a role in growth (Holmes et al., 2013). This is evident in the *scy* mutant strain which produces smaller colonies compared to the wild-type, is developmentally delayed and exhibits an over-branching phenotype. Moreover, overexpression of Scy also results in hyperbranching suggesting that, like DivIVA, Scy is important for the proper placement of branch sites and normal growth. In fact manipulation of Scy expression levels in *S. coelicolor* shows that in the presence of elevated Scy levels, DivIVA localisation is perturbed with localisation comparable to that seen when DivIVA is overexpressed and in fact co-localises with Scy at these ectopic locations. Moreover, with Scy and DivIVA interaction shown through both pelleting assays, bacterial two hybrid and co-elution experiments, it is clear that the two proteins act together, possibly forming a complex assembly, to ensure that correct growth and branching occurs. Interestingly, the *scy* mutant also shows perturbed spore formation with irregular spore size, aberrant DNA segregation and branched aerial hyphae suggesting that aberrant growth has either an indirect effect on division or there is a mechanistic regulation between growth and division via Scy (Ditkowski et al., 2013; Holmes et al., 2013).

The final protein to make up the TIPOC is the intermediate filament-like protein FilP. Originally, FilP was identified in *S. coelicolor* when the genome was mined for proteins containing a similar domain architecture to crescentin in *C. crescentus*, a protein that is responsible for the signature curvature of the organism. It was not however, the first *Streptomyces* homologue for that gene to be described. Originally that gene locus was characterised in *Streptomyces reticuli* and was identified due to its affinity to avicel, a crystalline form of cellulose and the property that led to its name avicel binding protein (AbpS) (Walter et al., 1998). The homologue in *S. coelicolor* was characterised through its relationship to growth and its cytoskeletal properties, including its similarity to crescentin, and thus its name was changed to filamentous intermediate-like protein (FilP) (Bagchi et al., 2008). FilP was originally found to localise to the tip and to inner hyphal curvatures forming long cables when expressed with a fluorescent tag, although more recent immuno-localisation suggests that it forms a network which extends along the hyphae from just behind the tip (Bagchi et al., 2008; Fuchino et al., 2013). While its role in growth

and branching still remains a mystery, with the mutant strain showing no obvious effect on this process, it has been suggested that FilP could play a role in both the strength of the wall behind the growing tip and establishing new polarity centres in response to osmotic pressures (Bagchi et al., 2008; Fuchino et al., 2017). The idea that FilP strengths walls in the filamentous *S. coelicolor* opens up the intriguing possibility that FilP could be part of a structure that allows for a stable hyphae which grows much longer than most other bacteria that reproduce via binary fission. Given that *S. coelicolor* is not motile, the formation of new polarity centres in response to osmotic shock would allow the bacteria to grow away from areas of high osmolality using its branching mechanism. One of the most interesting properties of FilP is its ability to assemble *in vitro*. Through structural studies, such as TEM and SEM, FilP has been shown to form a variety of spontaneous filamentous structures such as striation, and interlinked lace networks although the *in vivo* significance of any of these shapes is still to be determined (Bagchi et al., 2008; Fuchino et al., 2013).

1.3.3 Division in *S. coelicolor* - FtsZ

Like all bacteria, division in *S. coelicolor* is driven by FtsZ which drives the development of the bacterial septum that allows division to occur (Figure 18). Unlike in the vast majority of bacteria, ftsZ is not an essential gene in *Streptomyces* and in fact *S. coelicolor* is still viable in the absence of division (McCormick et al., 1994). While viable, in the sense that the strain can be passaged, given that division does not occur it means that the mutant strain cannot produce spores or any compartmentalisation of chromosomes in the aerial hyphae, essentially being blocked before sporulation. As well as an inability to produce sporulation septa, the FtsZ mutant is equally unable to produce crosswalls during vegetative growth, resulting in a lack of compartmentalisation. This results not only in the observed classic white phenotype of non-sporulating *S. coelicolor* but also in a strain that is unable to grow properly (McCormick et al., 1994). This suggests that the formation of crosswalls in vegetative hyphae is essential for maintaining a healthily growing colony. The fact that cell division is a dispensable process in *S. coelicolor* makes it an important organism in which to study this process. Cell division proteins that are

essential in other bacteria, and thus harder to characterised, are not essential in *Streptomyces,* creating the opportunity for gaining insights into their mechanisms.

During late development in *S. coelicolor* FtsZ has been shown to form a series of classical FtsZ rings, a precursor to septum formation, that are evenly spaced along the length of aerial hyphae in what is often termed a ladder-like formation (Schwedock et al., 1997). In order to generate such even spacing of approximately 1.3 µm, FtsZ has been shown to develop rings through a series of intermediary localisation patterns which begin in late development with an upregulation of *ftsZ* gene expression. The *ftsZ* gene is transcribed from three distinct promoters, which regulate its expression levels throughout the life cycle of *S. coelicolor* (Flardh et al., 2000). The first promoter, P1, is activated during vegetative growth while the third promoter, P3 is constitutively active throughout the life cycle. The second promoter, P2, is developmentally regulated, with a strong upregulation in aerial hyphae prior to the onset of the division process (Flardh et al., 2000). At the onset of the division process, an FtsZ ring localises to the base of the aerial hyphae, which gives rise to a basal septum which compartmentalises the hyphae into a sporogenic hyphae and the

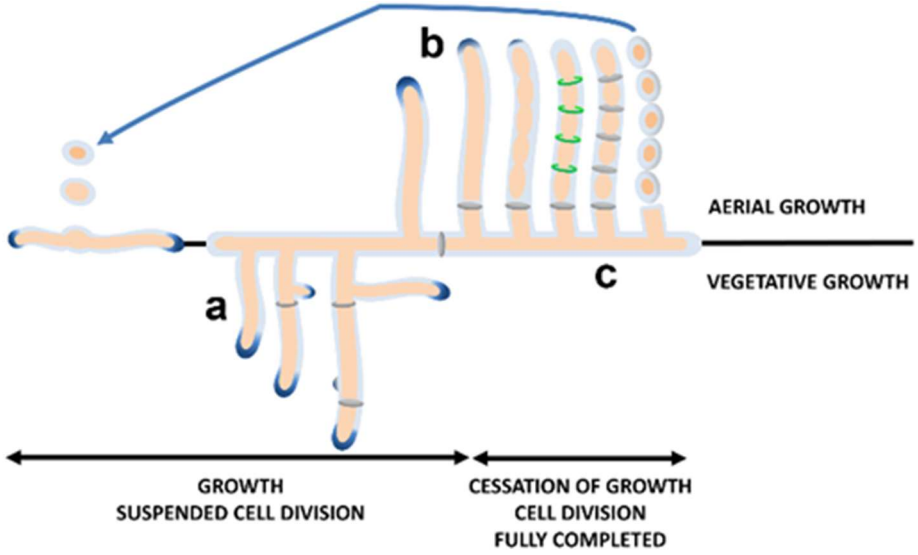

Figure 18: Septum formation during the life cycle of *S. coelicolor*.

During vegetative growth *S. coelicolor* produces irregular septa that compartmentalise hyphae (a). These septa do not undergo cell-cell separation typical of cell division. Aerial hyphae form a single basal septum in order to compartmentalise aerial hyphae (b). During sporulation many septa are placed along the length of aerial hyphae that do undergo the cell-cell separation seen in division (c). Taken from Kelemen (2017).

sub-apical stem compartment (Dalton et al., 2007; Kwak et al., 2001). After upregulation, FtsZ initially forms spiral-like intermediates from a dispersed pattern. The spirals then condense into helical filaments, before further condensation results in the many, 20-50 Z rings which form along the length of the hyphae marking the future sites of septation (Grantcharova et al., 2005). The compartmentalisation of the aerial hyphae into sporogenic hyphae and the sub apical stem is important for containment of the elevated FtsZ levels and promote its condensation into Z rings. The Z rings only occur transiently before giving way to the rise of septa (Grantcharova et al., 2005). Time lapse imaging revealed that FtsZ rings are also present, as expected, in the vegetative hyphae, which give rise to the crosswalls that compartmentalise the vegetative hyphae. Here, while the spiral intermediates are seen, the helical filaments are not, possibly due to the more dispersed formation in vegetative hyphae (Jyothikumar et al., 2008).

1.3.4 Regulating FtsZ localisation in *S. coelicolor*

Streptomyces are not known to possess the negative regulatory systems of FtsZ localisation conserved among many other bacteria, such the Min system and nucleoid occlusion. *S. coelicolor* has however, been shown to regulate FtsZ localisation through a positive regulatory system, involving SsgA and SsgB. These proteins belong to the *Streptomyces* specific SALPS, SsgA-like protein family. Previous studies showed that null mutants of both of these proteins were blocked at a stage preceding the onset of sporulation specific cell division, indicating a role in control of this process (Keijser et al., 2003; van Wezel et al., 2000). More recent localisation studies of these proteins using fluorescent microscopy have shed light on the process of this control (Willemse et al., 2011).

The progression towards fully formed FtsZ rings (Figure 19) begins with the localisation of SsgA starting at the hyphal tips followed by evenly spaced distinct foci which occur the length of the hyphae (young aerial stage I). SsgA then recruits SsgB to the side wall in an evenly spaced manner alternating between the two sides of the hyphae (early division stage IIA). FtsZ then forms long spiral-like filaments along the

length of the hyphae interacting with the alternately placed SsgB (early division stage IIB). At this point small SsgB foci are seen on the opposite side wall of the hyphae from the SsgA recruited SsgB. FtsZ then co-localises with SsgB as distinct foci along the hyphal length forming foci on opposite sides of the hyphae (pre-division foci stage IIC). FtsZ and SsgB then co-localise as rings both forming the classical laddering seen in FtsZ localisation (z-rings stage III). SsgA localises before the appearance of the other two proteins suggesting that its localisation is not dependent on FtsZ or SsgB. Indeed SsgA was shown to correctly localise in an *ftsZ* mutant background. FtsZ on the other hand failed to localise correctly in either the *ssgA* or *ssgB* null mutants suggesting that its localisation is dependent on both of these proteins. Interestingly, in these mutant strains, FtsZ forms sparsely spaced ring structures similar to the distribution of septa in vegetative hyphae and shows the same lack of constriction associated with these non-dividing septa, suggesting that at least part of the difference in septa formation between vegetative and aerial hyphae is the presence

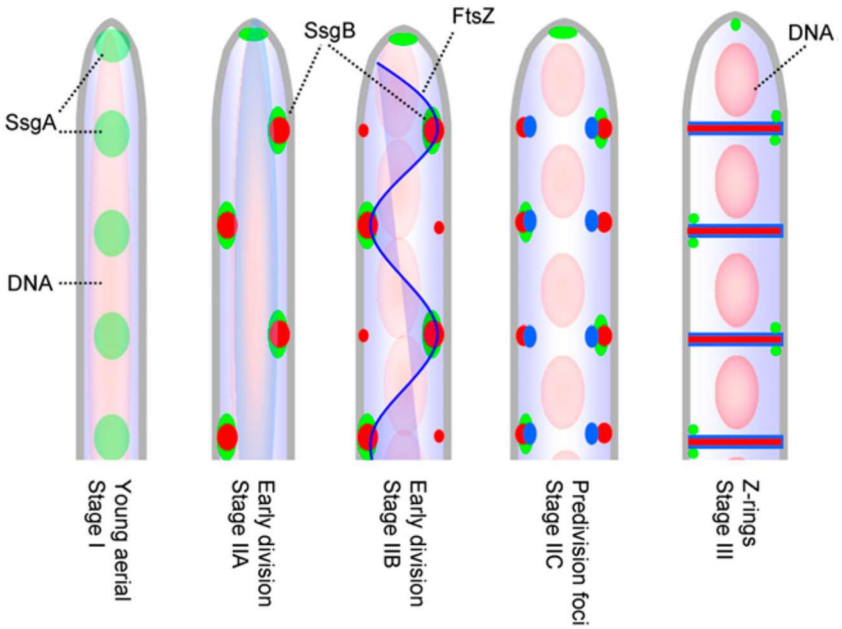

Figure 19: Positive regulation of FtsZ ring localisation by SsgA and SsgB in *S. coelicolor*.

SsgA (red) localises first as distinct regularly spaced foci along the aerial hyphae (stage I). SsgA then recruits SsgB (green) to the side wall in an evenly spaced alternating fashion (stage IIA). FtsZ (blue) forms spiral like filaments attaching at alternating sides to the now assembled SsgB foci (stage IIB). Further co-localisation of FtsZ and SsgB occurs whereby SsgB interacts with the membrane tethering FtsZ (stage IIC). FtsZ rings then form followed by chromosome condensation and segregation and formation of the sporulation septa (stage III). Taken from Willemse et al (2011).

of SsgA and SsgB. SsgB, while not able to localise correctly in an *ssgA* mutant background, does form regular foci on the lateral wall. What SsgB is not able to do it is correctly form the rings associated with the formation of Z rings. Interaction between FtsZ and SsgB was confirmed *in vivo* in *S. coelicolor* using Forster resonance energy transfer and in a heterologous host *E. coli* using a bacterial-two-hybrid assay. In addition, electron microscopy of FtsZ protein samples showed that filament length substantially increased in the presence of SsgB *in vitro* (Willemse et al., 2011).

1.3.5 Chromosome segregation in *S. coelicolor* - ParAB

Unlike most other bacteria, *Streptomyces* possess linear chromosomes in which the ends are held together by protein-protein interactions (Bentley et al., 2002). In addition, *Streptomyces* have a complex life cycle in which aerial hyphae replicate and segregate many chromosomes in order to produce hundreds of spores, each requiring exactly one complete chromosome to ensure viability. Therefore, the variations in the proteins and mechanisms of this process compared to simpler bacteria such as *E. coli* or *B. subtilis* are not only important but very exciting.

So far studies of chromosome segregation in *S. coelicolor* have mainly focussed upon the classical *parAB* operon, found at the locI SCO3886 and SCO3887 respectively, and is similar to the ParAB systems found in other bacteria. These proteins demonstrate homology with their counterparts in *B. subtilis*, with a 55% identity between ParA of *S. coelicolor* and Soj of *B. subtilis* and a 41% similarity between ParB and its homologue Spo0J (Kim et al., 2000). In addition to these genes, *S. coelicolor* also contains the other component of the system, *parS* sites, with the chromosome containing a total of 20 sites that ParB binds to in order to form the ParB-*parS* nucleoprotein complex required for the replication-partitioning cycle (Jakimowicz et al., 2002).

ParB visualisation was achieved through a ParB-EGFP translational fusion which demonstrated localisation in both vegetative and aerial hyphae. In the vegetative hyphae ParB-EGFP was confined mainly close to the growing tip although week foci could be seen at irregular intervals. In aerial hyphae however, ParB-EGFP

formed bright foci that were regularly placed throughout the hyphae, which presumably localise along with the *parS* sites found near the *oriC* of each chromosome (Jakimowicz et al., 2005).

ParA localisation, as demonstrated using immunolocalisation, begins as a single, tip associated focus in vegetative and young aerial hyphae. Prior to the appearance of FtsZ, ParA begins to form helices along the length of growing hyphae, with the majority of helices formed by the time FtsZ localises along the hyphae (Jakimowicz et al., 2007). Once the Z rings are formed in their ladder-like pattern, ParA localisation is no longer observable (Jakimowicz et al., 2007). Intriguingly, with respect to ParB localisation, ParA was not found to co-localise with ParB. Moreover, ParA disappears prior to the disassembly of ParB. However, ParB localisation was dependent upon ParA.

Knockout mutants of these genes presented spore chains with a significant amount of anucleate spores, 13% in the *parB* and *parAB* mutant strains (Kim et al., 2000) and 26% in the *parA* mutant strain (Jakimowicz et al., 2007). Although this defect is to be expected given the role that the ParAB system has in chromosome segregation the differing amounts between the *parA* and the *parAB* mutant strains could be due to the difficulty in measuring this type of phenotype.

Although *in vitro* data of the interaction between ParB and *parS* sites only demonstrated a week interaction, the presence of ParA was found to increase the affinity of ParB to *parS* sites. In fact while polymerisation of ParA is unaffected by its ATPase activity, the affinity of ParB for *parS* sites was found to be positively influenced by ATP bound ParA. Moreover, bacterial two-hybrid experiments demonstrated the ability of a ParA ATPase mutant to self-interact while at the same time abolishing interaction with ParB (Jakimowicz et al., 2007).

ParB has also been shown to recruit Topoisomerase I (TopA) to the chromosome during sporulation (Szafran et al., 2013). Topoisomerases, of which TopA is the only topoisomerase homologue in *S. coelicolor*, are important isomerase enzymes that act on the topology of DNA through over and under winding (Champoux, 2001). The *topA* null mutation is lethal and depletion strains are unable to properly sporulate with uneven pre-spore compartments formed. In addition the TopA depletion strain shows an uneven distribution of ParB foci, which usually occur

at regular intervals during sporulation in the wild-type strain (Szafran et al., 2013). This suggests that correct supercoiling of chromosomes is important for chromosome segregation.

Recent time lapse imaging of FtsZ-YPET in a *parAB* mutant background in *Streptomyces venezuelae* has revealed the temporal and spatial effects of ParAB on FtsZ ring formation (Donczew et al., 2016). In the *parAB* mutant strain FtsZ ring formation occurs significantly earlier and remains for longer compared to the wild-type. This effect however, does not seem to significantly delay the formation of mature spores which occurs at a similar time compared with the wild-type during development (Donczew et al., 2016).

1.3.6 ParA interacts with ParJ in *S. coelicolor*

Through the screening of a bacterial two-hybrid library of *S. coelicolor*, ParJ (SCO1662) was identified as a new partner for ParA (Ditkowski et al., 2010). ParJ is found exclusively in *Actinomycetes*. Its interaction with ParA was confirmed *in vitro* through surface plasmon resonance and the detection of ParA bound to immobilised ParJ on a microtiter plate, using an anti-ParA antibody.

The *parJ* mutant strain of *S. coelicolor* exhibits an interesting phenotype, sporulating earlier than the wild-type, with defects in chromosome segregation and the size of pre-spore compartments. Analyses of pre-spore compartments revealed that the mutant has around 18% mini-compartments (<0.8µm) compared to 2.5% in the wild-type. Furthermore, it has 8% anucleate spores compares to 1% in the wild-type (Ditkowski et al., 2010.

ParJ localises as distinct foci along the length of aerial hyphae, as seen using fluorescence microscopy of a ParJ-EGFP fusion and although this is only seen in 25% of unseptated hyphae, the figure increases to 65% after septation occurs (Ditkowski et al., 2010. Co-localisation of ParJ and ParA is only seen after the extension of ParA helical filaments from its tip focus and lasts after septation when ParA is absent. Correct localisation of ParJ is observed in a *parA* mutant background, indicating that ParA is not essential for ParJ localisation; the reciprocal is also true for ParA. While

no effect on localisation is observed, *in vitro* pelleting assays and dynamic light scattering indicate that ParJ both inhibits ParA filamentation and causes the depolymerisation of existing ParA polymers (Ditkowski et al., 2010).

1.3.7 From growth to chromosome segregation – ParA-Scy interaction

Providing a link between cell growth and division, ParA was found to interact with the non-canonical coiled coil domain of Scy (Ditkowski et al., 2013). This was demonstrated *in vivo* in the heterologous host *E. coli* using bacterial two-hybrid assays. In addition, the co-elution of ParA with His-Scy protein from *S. coelicolor* cells extracts confirmed the interaction in *vitro*. Co-localisation of Scy and ParA has been demonstrated both with immunofluorescence of ParA coupled with Scy-EGFP and ParA-EGFP coupled with Scy-mCherry (Ditkowski et al., 2013). This resulted in localisation at the tips of 17% of aerial hyphae, although it must be noted that in both these conditions cells contained wild-type copies of Scy, meaning that the full extent of Scy localisation may not have been observed. Interestingly, Scy localisation was observed mainly in shorter hyphae, with ParA mainly being found in longer hyphae, suggesting that co-localisation occurs only briefly at the cross over between the cessation of growth and the onset of division.

The current understanding of the relationship between Scy and ParA is of a dynamic interplay between the two proteins whereby they both inhibit polymerisation of each other (Figure 20). This was first seen in localisation studies of ParA in a *scy* mutant background whereby ParA localises along the hyphal tips even in the very short hyphae where ParA tip localisation is usually observed in the wild-type. This is confirmed in a *scy* over expression background where ParA is found mainly to localise to the tips and it fails to form extended filaments, suggesting that Scy overproduction prevents ParA polymerisation. The generation of a ParA varient that failed to interact with Scy but did interact with itself, resulted in a low level of tip localisation of ParA, demonstrating this further. Pelleting assays and dynamic light scattering show that in the presence of ATP, increased levels of ParA inhibited Scy assembly, while increased levels of Scy inhibited ParA polymerisation *in vitro*. This

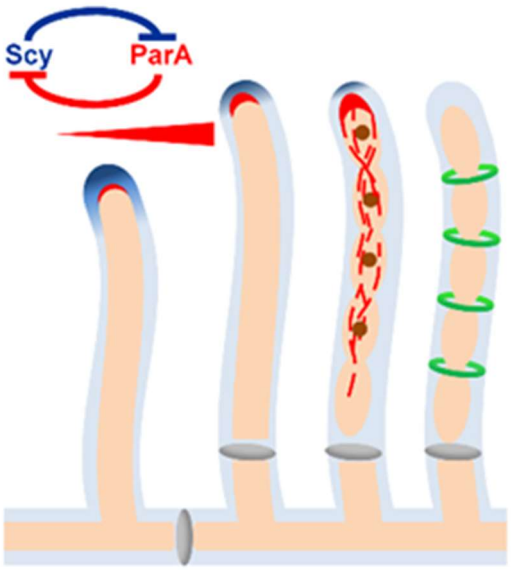

Figure 20: The interplay between ParA and Scy.

During growth ParA is sequestered to the tip where the polymerisation of ParA is inhibited by Scy. This prevents chromosome segregation from proceeding during growth. After the growth of aerial hyphal, increased levels of ParA overcomes inhibition of polymerisation by Scy and chromosome segregation begins. Increased ParA levels in turn cause depolymerisation of growth and thus curtailing growth. Taken from Kelemen (2017)

data suggests that in growing tips when ParA is at low levels, Scy inhibits its polymerisation at the tip. When cell division is due to occur ParA is up regulated which causes the depolymerisation of Scy and thus the disassembly of the TIPOC. ParA is then able to polymerise, extend along the aerial hyphae and fulfil its role in chromosome segregation (Figure 20).

Recent time lapse imaging of vegetative *S. coelicolor* hyphae has revealed a link between the TIPOC and tip localised chromosomes (Kois-Ostrowska et al., 2016). During vegetative growth ParB has been shown to form a complex on every chromosome thoughout the hyphae while ParA is found exlucively at the TIPOC. The tip localised ParA is able to ancor a single chromosome to the tip through the ParA-ParB interaction. This is maintained through chromosome replication where ParA is able to re-engage one chromosome after replication. It has been suggested that by targetting and maintaining a single chromosome at the tip during both germination and branching, efficient hyphal extension is maintained throughout the growth phase of *S. coeliocolor* development (Kois-Ostrowska et al., 2016).

1.4 Aims

ParA and MinD proteins play a key role in the processes of division in bacteria. They mediate several of the key steps of division such as initiation of chromosome replication, chromosome segregation and septum site placement. These proteins function in order to form a smooth transition thoughout the process of generating new cells. *Streptomyces* has a complex life cycle which culminates in the compartmentalisation of multigenomic aerial hyphae into uni-genomic spores. This requires the segregation of many chromosomes along the length of the sporogenic hyphea and their enclosure by septa such that each pre-spore compartment contains a single chromosome. So far the only ParA or MinD homologue that has been characterised in *S. coelicolor* is the ParA protein encoded by the *parAB* operon. ParA has been shown to facilitate chromosome segregation during sporulation. Intriguingly, recent evidence has shed light on the role that ParA plays in growth through the interplay between ParA and Scy – a key componant of the TIPOC. Given the complexity of the life cycle of *S. coelicolor* it is likely that there are other ParA and MinD homologues that function to help the division process. Through the identification of a novel ParA-like protein this study aims to fill some of the holes in our understanding of how cell division is coordinated in *S. coelicolor*. We will characterise the phenotype of the knockout strain to identify effects of this protein on the division process. We will search for partner proteins to identify possible regulatory mechanisms, both those that act upon the protein and those that the ParA-like protein acts upon. We will explore the biochemical properties of the protein to try to understand how this ParA-like protein carries out its function. We hope to propose a new model that bridges the gap between chromosome segregation and septum placement.

2 Materials and Methods

Bacterial strains, plasmids and oligonucleotides

Table 1: *E. coli* strains used in this study.

Strain	Genotype	Reference or source
DH5α	F^- λ^- *endA1 glnV44 thi-1 recA1 relA1 gyrA96 deoR nupG Φ80'lacZΔM15* Δ(*lacZYA-argF*)*U169, hsdR17*(r_K^- m_K^+)	Hanahan, 1983
BW25113	λ^- Δ(*araD-araB*)*567* Δ*lacZ4787*(*::rrnB-4*) *lacIp-4000*(*lacI*^{Q}) *rpoS369*(*Am*) *rph-1* Δ(*rhaD-rhaB*)*568 hsdR514*	Datsenko and Wanner, 2000
BL21 (DE3) pLysS	F^- *dcm ompT lon hsdS*$_B$(r_B^- m_B^-), *gal,* λ(DE3) pLysS(cm^R)	Studier and Moffatt, 1986
ET12567	*dam dcm hsdS*	MacNeil et al., 1992
BTH101	F^- *cya-99 araD139 galE15 galK16 rpsL1* (*Str* ^{R}) *hsdR2 mcrA1 mcrB1*	Karimova et al., 2000

Table 2: *Streptomyces* strains used in this study.

Strain	Genotype	Reference or source
M145	SCP1$^-$ SCP2$^-$ Pgl+	Hopwood et al., 1985
parH::aac(3)IV	M145 *parH::aac(3)IV*	This work
hyp::aac(3)IV	M145 *hyp::aac(3)IV*	This work
parH-hyp::aac(3)IV	M145 *parH-hyp::aac(3)IV*	This work

Table 3: Plasmid/Cosmid DNA used in this study.

Plasmid	Genotype	Reference or source
pIJ773	*aac(3)IV oriT bla*	Gust et al., 2003
pIJ790	*araC-P_{araB} γ β exo cat repA101ts oriR101*	Gust et al., 2003
pUZ8002	RK2 derivative with a mutation in *oriT*	Kieser et al., 2000
2StI34	Supercos-1 Cosmid with a 33.9 Kbp chromosomal fragment with *parH* and *hyp*.	Redenbach et al., 1996
2StI34/*parH::aac(3)IV*	Cosmid 2StI34 with *parH::aac(3)IV* allele	This Work
2StI34/*hyp::aac(3)IV*	Cosmid 2StI34 with *hyp::aac(3)IV* allele	This Work
2StI34/*parH-hyp::aac(3)IV*	Cosmid 2StI34 with *scy-parH-hyp::aac(3)IV* allele	This Work
pMS82	*ori* pUC18 *hyg oriT* RK2 *int ΦBT1 attP*	Gregory et al., 2003
pMS82-*P_{parH}-parH*	Plasmid pMS82 with *P_{parH}-parH*	This Work
pET28a	*ori* pBR322, T7 Promoter, His•Tag coding sequence, *lacI*, *kan*, *ori* f1	Novagen
pGS2	pET28a with *scy*	Holmes et al., 2013
pET28a-ParH	pET28a with *ParH*	This Work
pET28a-Hyp	pET28a with *Hyp*	This Work
pET28a-ParB	pET28a with *ParB*	This Work

pUT18C	pUC19 derivative with T18 domain upstream of MCS.	Karimova et al., 2000
pKT25	pSU40 derivative with T25 domain upstream of MCS.	Karimova et al., 2000
pUT18C-zip	pUT18C with leucine zipper	Karimova et al., 2000
pKT25-zip	pKT25 with leucine zipper	Karimova et al., 2000
pUT18c-ParH	pUT18C with *parH*	This Work
pKT25-ParH	pKT25 with *parH*	This Work
pUT18c-Hyp	pUT18c with Hyp	This Work
pKT25-Hyp	pKT25 with Hyp	This Work
pUT18C-Scy	pUT18C with *scy*	Walshaw et al., 2010
pKT25-scy	pKT25 with *scy*	Walshaw et al., 2010
pUT18c-ParB	pUT18c with ParB	This Work
pKT25-ParB	pKT25 with ParB	This Work
pET28a-HypN	pET28a with *HypN*	This Work
pET28a-HypC	pET28a with *HypC*	This Work

Table 4: Oligonucleotide sequences

Primer	5'-3' Sequence
I51.12knock1	AGTGGCGCGCCCCGCAACCACTTCGCCGACTACGACGAAA TTCCGGGGATCCGTCGACC
I51.12knock2	GAGCACCTCCCTGGCGAGCTGGCGGTAGGCGGCGGCACC TGTAGGCTGGAGCTGCTTC
I51.11knock1	GACGAACTCTTCCGTACGACAGGGGGAACGGCGCTCCAG ATTCCGGGGATCCGTCGACC

I51.11knock2	GTTCGAGGTCATGGCCCCCGCAGGCTACCGCTACCGCCCT GTAGGCTGGAGCTGCTTC
ParH GFP BglII Forward	GGATCAAGATCTTATGGTCACTTTGCGATTCTCG
1772 XbaI NdeI FRW	GGATCATCTAGAGCATATGAGTATGGATGGCCAACACG
1772 Eco UTC	GGATCAGAATTCTCTCACTCGGCGTGACACCGGGC
1771 XbaI NdeI FRW	GGATCATCTAGAGCATATGAGTCTGCCGGGGGCCGACG
1771 Eco UTC	GGATCAGAATTCTCCTACCGCCCGCGCAGCCGTCG
ParB XbaI NdeI FRW	GATCATCTAGAGCATATGCCGCTGCTACCGAACGAGC
ParB Eco UTC	GATCAGAATTCTCAGGACTCGGCGTCCCCGTCC
HypN Eco UTC	GATCACGAATTCCTAGTCGTGGCGCTCACGGCCGCTGG
HypC XbaI NdeI FRW	GATCACTCTAGAGCATATGCGCCACGACGAGAAGATCACC

Table 5: Antibiotic concentrations used in this study.

Antibiotic	Stock (mg/ml)	*Streptomyces* final concentration (µg/ml)	*E. coli* final concentration (µg/ml)
		SFM	LB
Ampicillin	100	-	100
Apramycin	100	50	50
Chloramphenicol	25	-	25
Hygromycin	50	50	50
Kanamycin	100	50	50
Nalidixic Acid	25	25	-

Generation of *S. coelicolor* knock out mutant strains

Mutant alleles of *parH*, *hyp* and *parh-hyp* were generated in cosmid StI34 using the redirect PCR targeting method. An apramycin resistance cassette (apramycin resistance gene and an oriT) was amplified using appropriate primers: I51.12knock1 and I51.12knock2 (*parH*), I51.11knock1 and I51.11knock2 (*hyp*), I51.12knock1 and I51.11knock2 (*parh-hyp*). The cassettes were subsequently introduced into BW25113 carrying pIJ790 to generate StI34/ΔparH::apr, StI34/Δhyp::apr and StI34/ΔparH-hyp::apr mutants in Escherichia coli. The cosmids were then introduced into the dcm-dam- ET12567 strain containing pUZ8002and conjugated into Streptomyces coelicolor M145. Double cross-over exconjugants were determined by testing colonies for resistance to apramycin and sensitivity to kanamycin. Spore counts were measured after collecting spores from confluent lawns of the WT and the mutant strains after 5 d of growth following the inoculation of ∼500 spores on Lysogeny broth agar (LBA).

Macroscopic analysis of *S. coelicolor* knock out mutant strains

Approximately 10^6 of *S. coelicolor* spores were plated onto soya flour medium (SFM) in a triangular shape before incubation at 30°C for up to 7 days. Images were taken daily using an Epsom scanner.

Microscopic analysis of *S. coelicolor* knock out mutant strains

Coverslip microscopy: Approximately 10^5 spores of *S. coelicolor* spore stock was inoculated in a 1 cm^2 confluent patch (0.5 cm by 2 cm) on SFM. A glass coverslip, 22x22 mm with a thickness of 0.13-0.17 mm, was inserted into the patch at an approximate angle of 70˚ to the horizontal plain of the medium. Plates were incubated at 30°C before the coverslips were removed and stained.

Cellophane microscopy: Approximately 1000 colonies per cm^2 of *S. coelicolor* spores were inoculated onto the surface of cellophane membranes positioned on solid SFM medium to restrict hyphal growth in two dimensions. The plates were incubated at 30°C for approximately 16-18 hours after which a 1 cm^2 cellophane patch was extracted and used for staining.

Staining: Cells on both cellophane membrane and coverslips were fixed with ice-cold methanol for 1 min before further staining with WGA-Alexa488 (50 µg/mL; Molecular Probes) and/or propidium iodide (25 µg/mL; Sigma) for 20 min. After several washes with PBS, samples were mounted using 20% (vol/vol) glycerol and viewed using an Axioplan 2 Imaging E (Carl Zeiss) Universal microscope with an AxioCamMR camera. A Plan Apochromatic 100x/1.40 Oil (440780) objective was used in combination with FS 38 GFP and FS 45 TxR filters.

Optimising production of *S. coelicolor* proteins in *E. coli*

Cultures of *E. coli* BL21 (DE3) pLysS cells containing the relevant plasmid (pGS2 (Scy), pET28a-ParH (ParH), pET28a-Hyp (Hyp), pET28a-ParB (ParB), pET28a-HypN (HypN) and pET28a-HypC (HypC) were grown at 37°C for 4 h and, after induction with 1 mM isopropylβ-D-thiogalactopyranoside (IPTG), cultures were grown overnight at 15°C, 25°C and 37°C. Samples were taken pre induction and 4 h and 20 h after induction. The cells were lysed by sonication and both supernatant and pellet protein fractions were analysed on 10% (wt/vol) SDS-PAGE.

Purification of His-Scy using *E. coli*

A culture of *E. coli* BL21 (DE3) pLysS cells containing the plasmid pGS2 was grown for 4 h at 37°C before induction with 1 mM isopropylβ-D-thiogalactopyranoside (IPTG). Cells were collected 20 h after induction and His-Scy was purified from the supernatant of cell lysates in Tris buffer A (Scy): 50 mM Tris-HCl, 300 mM NaCl, 20

mM $MgCl_2$, 0.05% Tween, 10 mM imidazole pH 8 under native conditions using a HisTrap HP 5 ml nickel affinity column (GE Healthcare). After washing with Tris buffer A (Scy) containing 27 mM imidazole, His-Scy was eluted with a step increase in imidazole concentration to 250 mM in Tris buffer A (Scy). His-Scy fractions were dialyzed against 20 mM Tris·HCl (pH 8) and further purified using a MonoQ 5/50 anion exchange column (GE Healthcare). The protein was eluted using a linear gradient increase in NaCl from 10 mM to 500 mM in 20 mM Tris·HCl (pH 8.0). Fractions containing His-Scy were dialyzed against 50 mM Tris-HCl, 150 mM NaCl, 10 mM $MgCl_2$, pH 8.

Purification of His-ParH using *E. coli*

A culture of *E. coli* BL21 (DE3) pLysS cells containing the plasmid pET28a-ParH was grown for 4 h at 37°C before induction with 1 mM isopropylβ-D-thiogalactopyranoside (IPTG). Cells were then grown at 37°C and collected 20 h after induction. His-ParH was purified from the supernatant of cell lysates in Tris buffer A: 50 mM Tris-HCl, 300 mM NaCl, 20 mM $MgCl_2$, 10 mM imidazole pH 8 under native conditions using a HisTrap HP 5 ml nickel affinity column (GE Healthcare). After washing with Tris buffer A containing 27 mM imidazole, His-ParH was eluted with a linear gradient increase in imidazole concentration from 27 mM to 300 mM in Tris buffer A. Fractions containing His-ParH were dialyzed against 50 mM Tris-HCl, 150 mM NaCl, 10 mM $MgCl_2$, pH 8.

Purification of His-Hyp using *E. coli*

A culture of *E. coli* BL21 (DE3) pLysS cells containing the plasmid pET28a-Hyp was grown for 4 h at 37°C before induction with 1 mM isopropylβ-D-thiogalactopyranoside (IPTG). Cells were then grown at 25°C and collected 20 h after induction. His-Hyp was purified from the supernatant of cell lysates in Tris buffer A:

50 mM Tris-HCl, 300 mM NaCl, 20 mM $MgCl_2$, 10 mM imidazole pH 8 under native conditions using a HisTrap HP 5 ml nickel affinity column (GE Healthcare). After washing with Tris buffer A containing 27 mM imidazole, His-Hyp was eluted with a linear gradient increase in imidazole concentration from 27 mM to 300 mM in Tris buffer A. Fractions containing His-Hyp were dialyzed against 50 mM Tris-HCl, 150 mM NaCl, 10 mM $MgCl_2$, 200 mM arginine, pH 8.

Purification of His-ParB using *E. coli*

A culture of *E. coli* BL21 (DE3) pLysS cells containing the plasmid pET28a-ParB was grown for 4 h at 37°C before induction with 1 mM isopropylβ-D-thiogalactopyranoside (IPTG). Cells were then grown at 37°C and collected 20 h after induction. His-ParB was purified from cell lysates generated under denaturing conditions in denaturing loading buffer: 8 M urea-HCl, 0.1 M NaH_2PO_4, 0.01 M Tris pH 8 using a gravity flow column from Novogen which contained approximately 2 ml Nickel Sepharose. After washing with denaturing washing buffer: 8 M urea-HCl, 0.1 M NaH_2PO_4, 0.01 M Tris pH 6.3, His-ParB was eluted with denaturing eluting buffer: 8 M urea-HCl, 0.1 M NaH_2PO_4, 0.01 M Tris pH 4.5. Fractions containing His-ParB were dialyzed against 50 mM Tris-HCl, 150 mM NaCl, 10 mM $MgCl_2$, pH 8.

Purification of His-HypN using *E. coli*

A culture of *E. coli* BL21 (DE3) pLysS cells containing the plasmid pET28a-HypN was grown for 4 h at 37°C before induction with 1 mM isopropylβ-D-thiogalactopyranoside (IPTG). Cells were then grown at 37°C and collected 20 h after induction. His-Hyp was purified from the supernatant of cell lysates in Tris buffer A: 50 mM Tris-HCl, 300 mM NaCl, 20 mM $MgCl_2$, 10 mM imidazole pH 8 under native conditions using a HisTrap HP 5 ml nickel affinity column (GE Healthcare). After washing with Tris buffer A containing 27 mM imidazole, His-HypN was eluted with a

linear gradient increase in imidazole concentration from 27 mM to 300 mM in Tris buffer A. Fractions containing His-HypN were dialyzed against 20 mM Tris, 150 mM NaCl, 10 mM $MgCl_2$, 200 mM arginine, pH 8.

Purification of His-HypC using *E. coli*

A culture of *E. coli* BL21 (DE3) pLysS cells containing the plasmid pET28a-HypC was grown for 4 h at 37°C before induction with 1 mM isopropylβ-D-thiogalactopyranoside (IPTG). Cells were then grown at 37°C and collected 4 h after induction. His-HypC was purified from cell lysates generated under denaturing conditions in denaturing loading buffer: 8 M urea-HCl, 0.1 M NaH_2PO_4, 0.01 M Tris pH 8 using a gravity flow column from Novogen which contained approximately 2 ml Nickel Sepharose. After washing with denaturing washing buffer: 8 M urea-HCl, 0.1 M NaH_2PO_4, 0.01 M Tris pH 6.3, His-HypC was eluted with denaturing eluting buffer: 8 M urea-HCl, 0.1 M NaH_2PO_4, 0.01 M Tris pH 4.5. Fractions containing His-HypC were dialyzed against 20 mM Tris, 150 mM NaCl, 10 mM $MgCl_2$, 200 mM arginine, pH 8.

Analytical gel filtration

Analytical gel filtration was performed using a Superdex 200 10/300 GL column from GE Healthcare. Proteins were analysed on the column in either a Tris buffer 20 mM Tris-HCl, 150 mM NaCl, 10 mM $MgCl_2$ pH 7.5 (ParH and protein standards) or a Tris-arginine buffer 20 mM Tris-HCl, 150 mM NaCl, 10 mM $MgCl_2$, 200 mM arginine pH 7.5 (Hyp, HypN and HypC). The column was calibrated using six protein standards: Blue Dextran (2000 kDa), Ferritin (446 kDa), Alcohol Dehydrogenase (150 kDa), Bovine Serum Albumen (66 kDa), Egg Albumin (45 kDa) and Cytochrome C (12.4 kDa). Elution profiles of the proteins were determined either by monitoring UV absorbance at 280 nm (ParH, Hyp and the protein standards) or through analysis on 15% (wt/vol) SDS-PAGE (HypN and HypC). The molecular weights of the target proteins was

calculated from the partition coefficient (K_{av}) of each protein and comparing it to the partition coefficient of the protein standards.

$$K_{av} = \frac{(V_e - V_o)}{(V_t - V_o)}$$

Ferguson Plot

His-ParH (200 pmol) was analysed across four different concentrations of native-PAGE (6%, 8%, 10% and 12%). Band migration was measured on each gel and the relative migration (mobility (R_f)) calculated by division with the migration of the leading edge of the gel represented by the dye. The retardation coefficient (K_r) of each protein oligomer was determined by plotting the log (R_f x 100) against the acrylamide percentage (T%) and determining the -slope of the curve (K_r). A standard curve of K_r values was generated using the bottom two bands (monomer and dimer) seen in His-ParH samples.

Crosslinking of ParH

His-ParH (12 µM) was incubated for one hour at 37°C in the presence of increasing concentrations of Dimethyl pimelimidate (DMP) (0 mM, 0.1 mM, 0.5 mM, 1 mM and 10 mM) in a Hepes buffer 50 mM Hepes-KOH, 100 mM KCl, 5 mM MgCl2 pH 8.5. Resulting oligomers were analysed on 10% (wt/vol) SDS-PAGE.

Pelleting assays

Proteins were incubated for 30 min in a Tris based buffer (50 mM Tris-HCl, 150 mM NaCl, 10 mM MgCl2 pH 8) before centrifugation at 450,420 g for 30 minutes at 4°C in a Beckman Optima TLX Ultracentrifuge with a Beckman Coulter TLA 100 Fixed Angle Rotor. Pellet and supernatant fractions were analysed on 10% (wt/vol) SDS-PAGE. In appropriate samples 1 mM nucleotides were added to the reaction.

ATPase assay

Nucleotides (AMP, ADP and ATP) were resolved by HPLC on a Phenomenex (Macclesfield, UK) Synergi Hydro-RP column eluted isocratically at 1 mL min-1 with a buffer derived from solvent reservoirs containing (A) 50mM NaH2PO4 and (B) acetonitrile/methanol/water (40/50/10, v/v/v) mixed in ratio (A/B, 70/30). Both reservoirs contained 4 mM tetrabutyl ammonium hydroxide as ion-pair reagent (Caddick et al., 2008). Peaks of nucleotide were integrated with the chromatography software (Jasco ChromNav) and percentage conversion of ATP to ADP determined.

3 ParH - a novel ParA-like protein?

The ParA/MinD superfamily of proteins plays an important role in coordinating the cell division process from the correct segregation of chromosomes to the efficient placement of septa (Lutkenhaus, 2012). Many bacteria contain multiple homologues of these proteins with diverse methods of action. *C. crescentus* for example has ParA, which actively segregates chromosomes through positioning of ParB (Ptacin et al., 2014). It also has another homologue from this superfamily, MipZ, which inhibits FtsZ ring formation from occurring near the cell poles and thus limits septum formation to the mid-cell (Thanbichler and Shapiro, 2006). *B. subtilis* also has two homologues that have been characterised, Soj (ParA) which is involved in regulating the initiation of chromosome replication and sporulation, and MinD which, like MipZ, is involved in septum positioning (Marston and Errington, 1999; Murray and Errington, 2008). *E. coli* on the other hand only has one characterised protein from this superfamily, MinD which is also involved in septum positioning (de Boer et al., 1992). Given there are many uncharacterised genes within the genomes of these bacteria it is entirely possible that there are other ParA/MinD homologues that are yet to be characterised.

So far in *S. coelicolor* the only homologue from the ParA/MinD superfamily that has been characterised is ParA encoded by the *parAB* operon (Jakimowicz et al., 2007). This ParA homologue has been implicated in chromosome segregation during sporulation, when it forms helical filaments along the length of aerial hyphae from which it positions ParB in an ATP dependent manner (Jakimowicz et al., 2007). This in turn positions the multiple chromosomes allowing their segregation and eventual compartmentalisation into pre-spore compartments (Jakimowicz et al., 2007). In the absence of ParA, the chromosomes are exhibit missegregation resulting in uneven pre-spore compartments with a prevalence of bigger compartments containing multiple chromosomes and micro-compartments that are anucleate (Jakimowicz et al., 2007). This indicates how important this system is in managing the process by which multi-genomic aerial hyphae differentiate into uni-genomic spores. In addition to this this system also has an important role during vegetative growth. At this time

ParA is localised to the tip through interaction with Scy, a key component of the multi-protein assembly – the TIPOC which drives growth (Ditkowski et al., 2013). As well as suppression by Scy of the polymerisation of ParA, which inhibits chromosome segregation during growth, localisation of ParA to the tip also anchors a chromosome to the tip to ensure that there is efficient growth and branching (Kois-Ostrowska et al., 2016). Finally, increased ParA production after the formation of aerial hyphae causes Scy to depolymerise, which in turn disassembles the TIPOC and curtails growth before allowing cell division to occur (Ditkowski et al., 2013). All of this underlines the importance of the *parAB* operon throughout the *S. coelicolor* life cycle. Thus far no other ParA or MinD proteins have been characterised in *S. coelicolor* and there is no mechanism found which negatively regulates FtsZ ring formation such as the Min systems described in *B. subtilis* and *E. coli* or the MipZ system in *C. crescentus*. A Blast search of the *S. coelicolor* genome using both Soj and MinD from *B. subtilis* reveals multiple potential homologues of ParA and MinD (Figure 21).

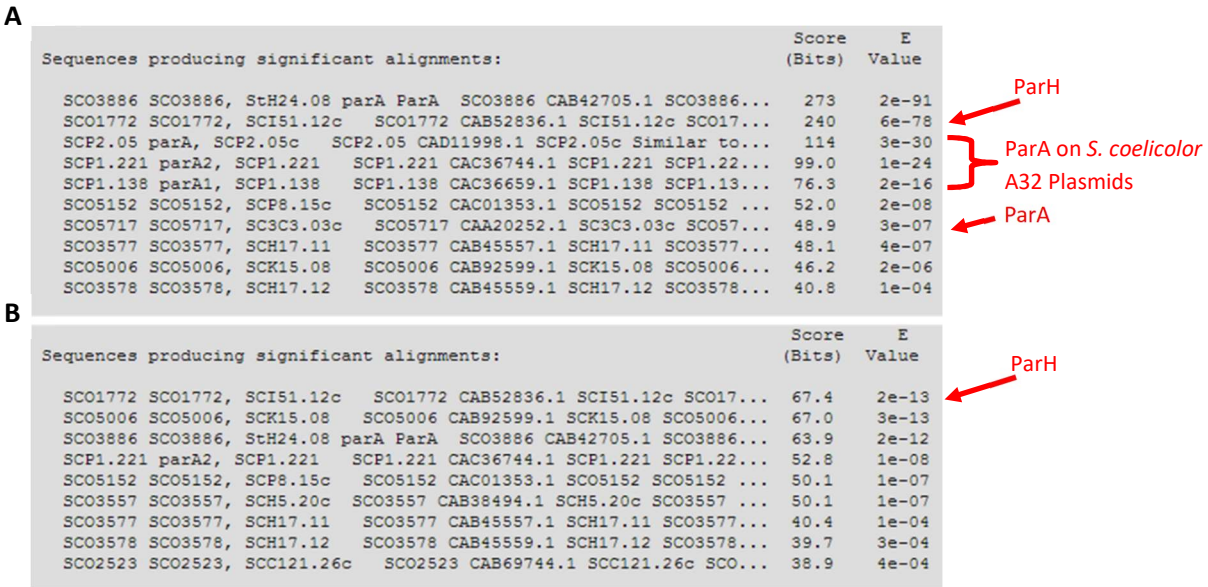

Figure 21: Homologues of ParA and MinD in the *S. coelicolor* genome.

The amino acid sequence of (A) Soj (Uniprot P37522) and (B) MinD (Uniprot Q01464) from *B. subtilis* was Blast against the *S. coelicolor* genome. The top hit from Soj is the already characterised *S. coelicolor* ParA (SCO3886) protein which is encoded in the *parAB* operon. There were several hits (SCP2.05, SCP1.221, SCP1.138) that represent potential ParA proteins encoded on the two plasmids (SCP1 and SCP2) associated with the *S. coelicolor* A3(2) wild type strain. The second hit from the Blast search with Soj and the top hit from MinD is the uncharacterised ParA-like protein we have designated ParH.

The protein with the highest homology to *B. subtilis* Soj is the already characterised *S. coelicolor* ParA (SCO3886) protein which is encoded by the *parAB* operon. Several of the hits (SCP2.05, SCP1.221, SCP1.138) corresponded to ParA proteins encoded on the two plasmids (SCP1 and SCP2) associated with the *S. coelicolor* A3(2) wild-type strain. These proteins may be involved in the segregation of these two plasmids. The strain of *S. coelicolor* utilised by the group (M145) is deficient for these plasmids. The second hit from the Blast search with Soj and the top hit from MinD is the uncharacterised ParA-like protein we have designated ParH (SCO1772). We chose to characterise this protein because it is the uncharacterised protein most similar to other ParA and MinD homologues with 49% identity to *B. subtilis* Soj and 30% identity to *B. subtilis* MinD.

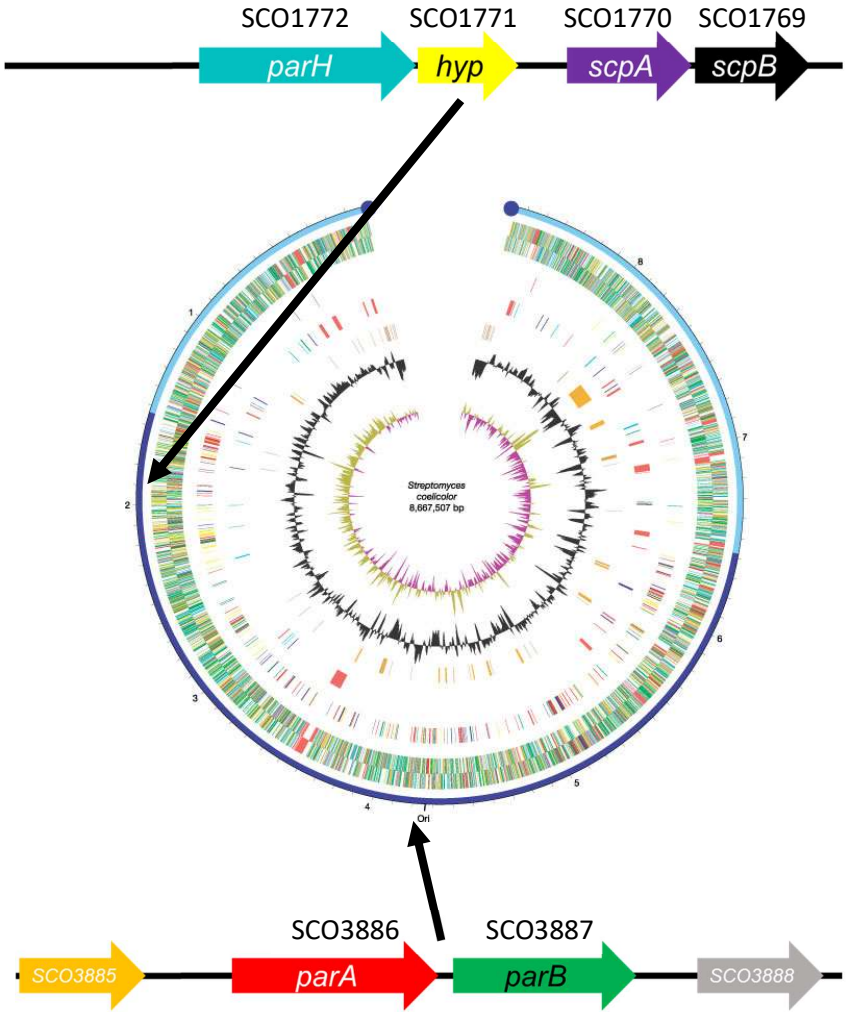

Figure 22: Chromosomal location of *parA* and *parH*.

ParH is encoded by a gene found halfway between the origin and the terminator region to the left of the origin while ParA is encoded by the *parAB* operon located near the origin.

The *parAB* operon is located near the origin of the chromosome, around which the ParB binding sites, *parS*, are clustered. This is therefore the region of the chromosome upon which the ParAB system acts. The *parH* gene however is located half way between the origin and the terminus region to the left of the origin (Figure 22). The *parH* gene is translationally coupled to a downstream gene (SCO1771) that encodes a small hypothetical protein, which we have designated Hyp (Figure 23). The fact that the genes are translationally coupled would suggest that their products have a shared function. Other ParA and MinD proteins are encoded in operons with partner proteins whether this is the *parAB* operon or the *minCDE* operon. Also located downstream of *parH* and *hyp* are the genes *scpA* (SCO1770) and *scpB* (SCO1769). These encode the ScpAB proteins that are functionally involved with SMC which together act as the bacterial equivalent of eukaryotic condensin helping to package and orientate chromosomes.

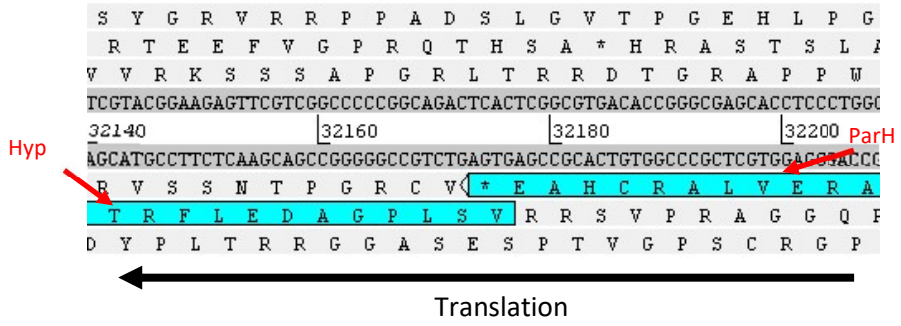

Figure 23: *parH* and *hyp* are translationally coupled.

The *parH* gene and the downstream gene, *hyp*, are translationally coupled, suggesting that they have a shared function in *S. coelicolor*.

Although ParH is a ParA-like protein and therefore is homologous to many other ParA-like and MinD-like proteins, we wished to determine if we could identify other ParA-like proteins that are located alongside similar genes. We therefore searched other genomes for gene arrangements that are similar to this one in *S. coelicolor*. We found similar gene arrangements throughout *Actinobacteria*, but not outside this phylum (Figure 24). This suggests that this ParA-like protein is specific to *Actinobacteria*. Interestingly, while the gene encoding Hyp is found throughout *Streptomyces* species, it is not found in all *Actinobacteria*, notably being absent from

the genomes of mycobacteria and corynebacteria. Also of note is the presence of a gene encoding the protein XerD, which is found upstream if the gene encoding ParH in many organisms, although not in *Streptomyces* species. XerD is a site-specific tyrosine recombinase involved in the resolution of chromosome dimers after replication. The linear chromosomes of *Streptomyces* species mean that they are not required to resolve replicated chromosomes and so the absence of this protein is expected.

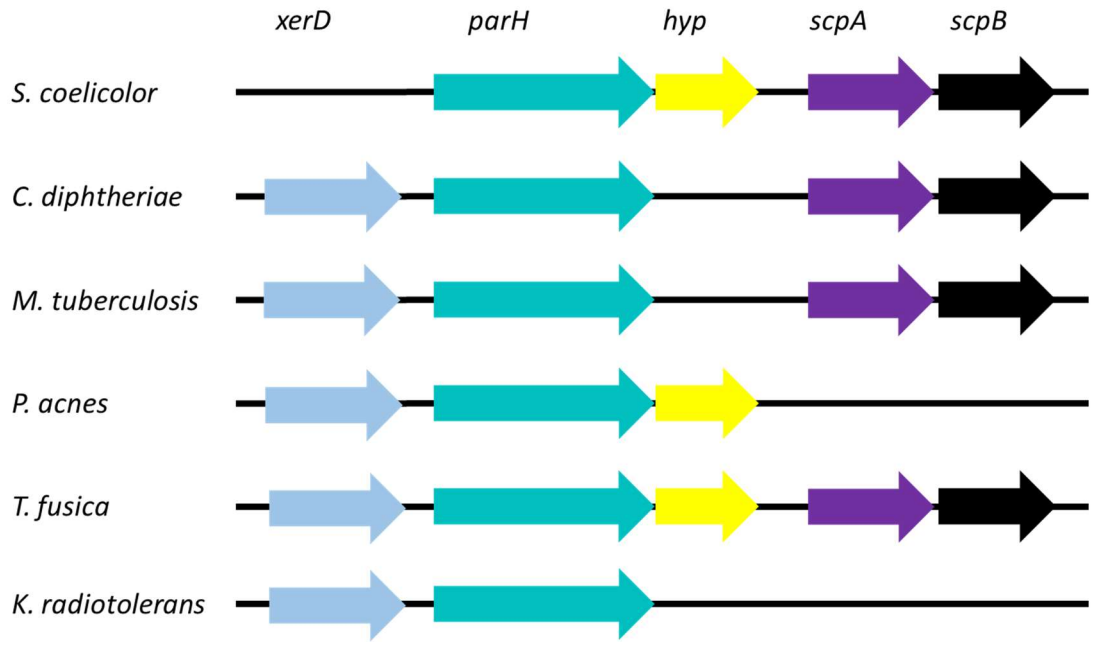

Figure 24: Comparison of the genomic context of *parH* across *Actinobacteria*.

A sequence alignment of ParH and ParA homologues shows that ParH contains residues and motifs that are important to the function ParA (Figure 25). This include both Walker A and Walker B motifs which are important for nucleotide binding and ATPase hydrolysis respectively (Koonin, 1993; Motallebi-Veshareh et al., 1990). ParH homologues also contain important conserved residues that have been characterised in ParA homologues. This includes the arginine residues R189 and R218 that are important for DNA binding in *B. subtilis* Soj (Hester and Lutkenhaus, 2007); the lysine residue K20 that is essential for ATP binding (Fung et al., 2001); the glycine residue (G16) that allows dimerisation of ParA to occur (Leonard et al., 2005); and the aspartate residue (D44) that is important for ATP hydrolysis (Lutkenhaus and Sundaramoorthy, 2003).

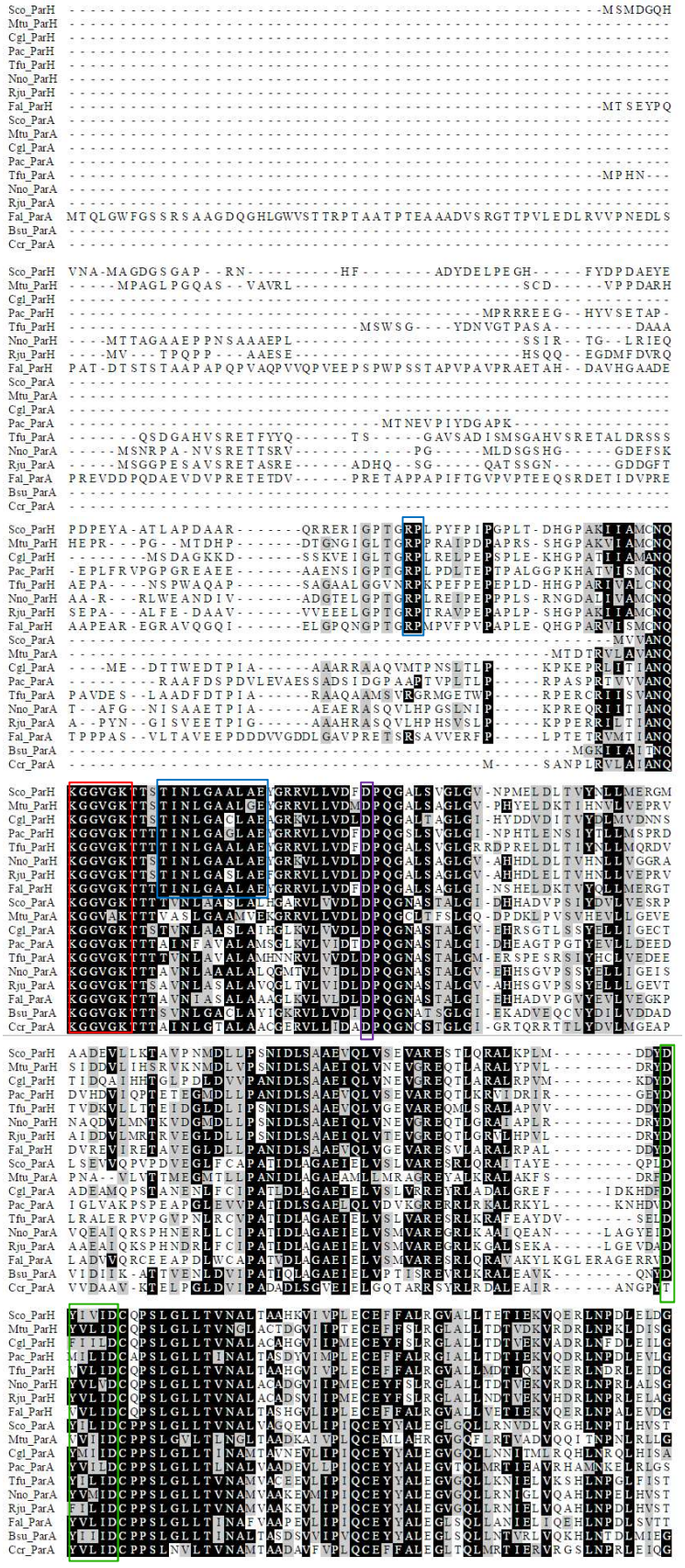
Sco_ParH
Mtu_ParH
Cgl_ParH
Pac_ParH
Tfu_ParH
Nno_ParH
Rju_ParH
Fal_ParH
Sco_ParA
Mtu_ParA
Cgl_ParA
Pac_ParA
Tfu_ParA
Nno_ParA
Rju_ParA
Fal_ParA
Bsu_ParA
Ccr_ParA

Figure 25: Sequence alignment of ParA and ParH homologues.

Homologues of ParA and ParH were aligned using Clustal omega with the default alignment settings. The output was processed with box shade to highlight common residues. Features highlighted: Walker A motif (red box); Walker B motif (green box); arginine residues R189 and R218 that are important for DNA binding (yellow box); the lysine residue K20 that is essential for ATP binding and the glycine residue (G16) that allows dimerisation of ParA to occur are found in the Walker A motif; the aspartate residue (D44) that is important for ATP hydrolysis (purple box); and residues conserved in ParH that are absent from ParA (blue box).

The fact that so many residues important for the function of ParA proteins are also conserved across ParH proteins suggests that ParH should share similar biochemical properties with ParA proteins. However, it is also clear there are conserved ParH residue that are not shared with ParA proteins, which indicates that ParH should also have some properties absent from ParA proteins. These include -RP- residues upstream of the Walker A motif and a conserved -TINLGAALAE- motif immediately downstream of the Walker A box (Figure 25).

After finding ParH homologues we wished to find homologues of Hyp, the protein encoded by the gene downstream of *parH*. A search across bacteria revealed that homologues of Hyp were exclusively found among the *Actinobacteria*. As stated before though not all *actinobacteria* contain a homologue of Hyp, However, in those that do, the gene encoding Hyp is always found downstream of the gene encoding the homologue of ParH. No homologues of Hyp have thus far been characterised, meaning that it is not possible to determine a possible function from analysis of the

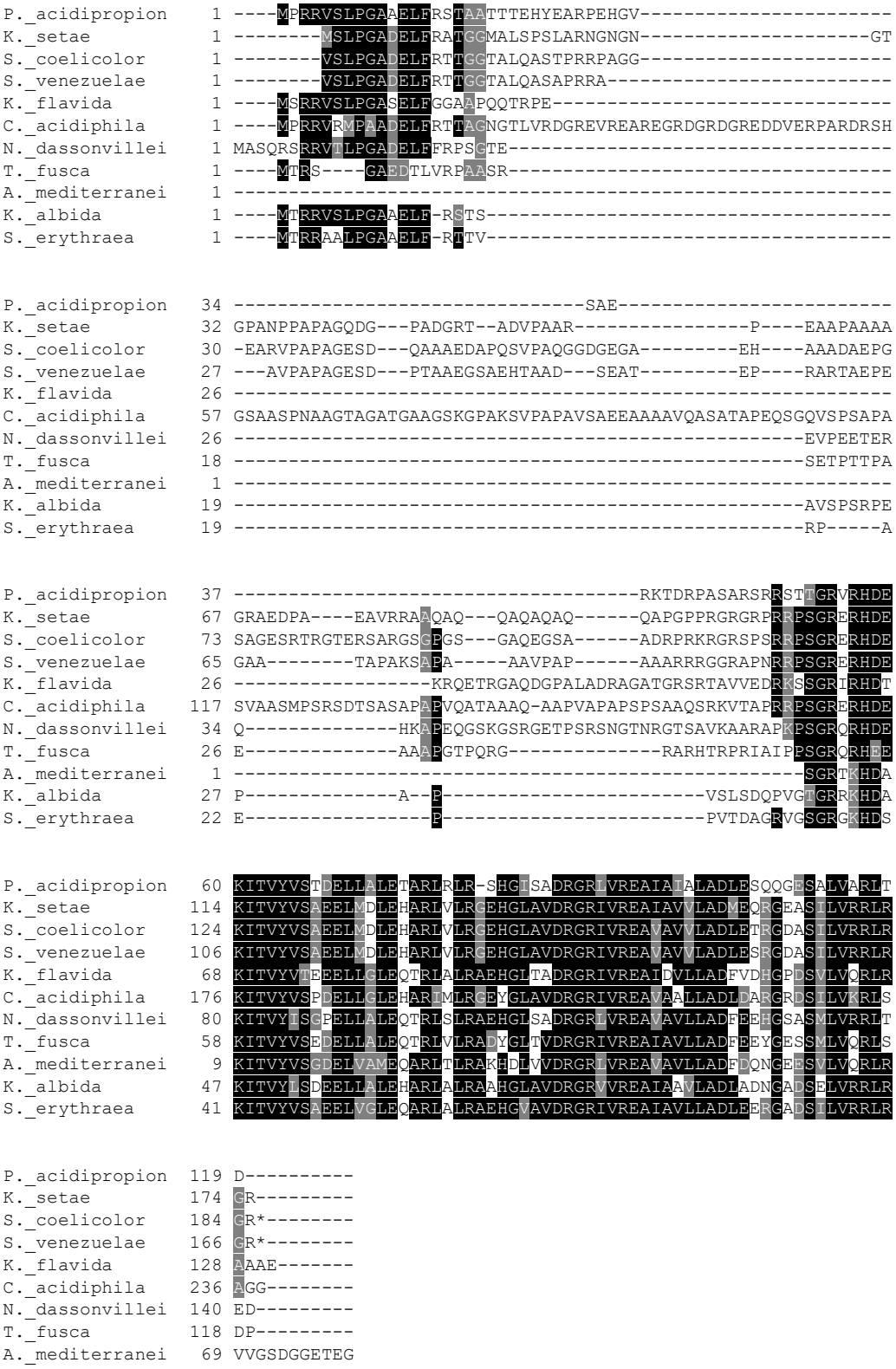

Figure 26: Sequence alignment of Hyp homologues

The N-terminus of the protein has low conservation among the homologues of Hyp while the C-terminus shows high similarity.

homologues. Sequence alignment of the homologous of Hyp shows that there is a small conserved region at the N-terminus of the protein followed by a largely non-conserved region (Figure 26). This non-conserved region differs in length across the Hyp homologues. Finally, the C-terminus is highly conserved across the Hyp homologues, probably indicating a domain that is responsible for a function that is shared across the homologues.

As we could not gain any functional or structural information about Hyp by analysing the homologues of Hyp we attempted to derive this information using protein prediction software (Figure 27). This suggested that the N-terminal region of Hyp, approximately the first 120 amino acids, is disordered. This corresponds to the region of low conservation in the sequence alignment. According to the prediction software, the highly conserved C-terminal region of Hyp contains possible α-helices and β-strands as well as possible DNA binding residues.

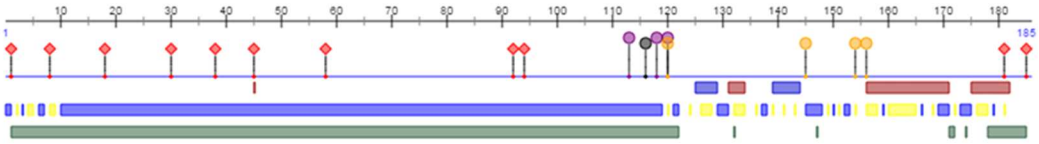

Figure 27: Secondary structure prediction of Hyp.

The amino acid sequence was analysed by online protein secondary structure prediction software (Protein Predict). This indicated that the N-terminal region of the protein is highly disordered (green bar bottom) while the C-terminal region contains possible α-helices (red bar top) and β-strands (blue bar top). The C-terminal region also contains potential DNA binding residues (yellow dots).

3.1 Generating mutant strains in *S. coelicolor*

After identifying the novel ParA-like protein ParH and the hypothetical protein Hyp, encoded by the gene located downstream of the gene encoding ParH, we wished to generate *S. coelicolor* mutants of the genes encoding these proteins. To create gene knockouts in *S. coelicolor* for *parH*, *hyp* and *parH-hyp*, the REDIRECT© PCR-targeting system was used (Gust et al., 2003). Previously generated cosmids containing *S. coelicolor* chromosomal DNA inserted into supercos-1, can be targeted

with a PCR generated apramycin resistance cassette containing 39 bp flanking regions that are homologous to the flanking regions of the targeted gene. The cosmid containing the target gene can be modified by the cassette in an *E. coli* strain (BW) which expresses the phage lambda Red recombinase (λ RED) (Datsenko and Wanner, 2000). The recombinase allows for homologous recombination between the flanking regions of the cassette and the flanking regions of the target gene in order to replace the target gene with the resistance cassette. Once the insertion of the cassette has been confirmed by restriction digest, the cosmid can be conjugated into *S. coelicolor* M145 via the non-methylating *E. coli* strain ET12567 (MacNeil et al., 1992). Ex-conjugants that have undergone a double crossover event either side of the resistance cassette can then be selected for through first the selection of apramycin resistant colonies and then through screening for the loss of the kanamycin resistance gene found on the backbone of the cosmid.

To generate the knock out cassettes, the apramycin cassette from pIJ773 was liberated from pIJ773 using *Eco*R1 and *Hin*dIII before purification through gel extraction. The template (≈1.3 Kb) was then used for PCR using the primers to generate cassettes for the knockout of *parH* (I51.12knock1 and I51.12knock2), *hyp* (I51.11knock1 and I51.11knock2), and *parH-hyp* (I51.12knock1 and I51.11knock2). The PCR was performed with two distinct cycles the first had a lower annealing temperature of 50°C to allow for the primers to anneal to the initial template which will allow the annealing of either 19 bp or 20 bp of the primers. After the initial round of cycles the PCR template is able to anneal to the full length of the primers (39 bp or 40 bp) so the second round of cycle has an increased annealing temperature of 55°C. The PCR products were desalted using a self-made mini gel filtration column.

The cosmid I34, which contains a 38.5 Kbp fragment of the *S. coelicolor* chromosome containing the *parH* locus, was transformed in the *E. coli* strain BW25113 carrying pIJ790 which encodes the λRED recombinase genes *gam*, *bet* and *exo* which are transcribed by the L-arabinose inducible promoter $Para_{BAD}$. The plasmid also encodes a temperature-sensitive replication initiation protein (repA101ts) to allow for its loss when the strain is grown at temperatures higher than 30°C. The disruption cassettes were transformed into *E. coli* BW25113 cells carrying I34 which were induced with L-arabinose to promote expression of the recombinase

enzymes which cause a homologous recombination event to occur between the flanking regions of the cassette and the flanking regions of the target genes. Cells containing cosmids that had undergone successful recombination were selected for using plates supplemented with apramycin and grown at 37°C to induce loss of pIJ790. Recombination events in *E. coli* BW25113 only target a small proportion of the multicopy cosmid, so the cosmid DNA from a single transformant from each disruption was extracted and transformed into *E. coli* DH5α, after which a single colony was picked and a large scale cosmid extraction was performed. To determine whether the target gene was successfully disrupted the purified cosmid DNA was digested with *Xba*I and the resulting products observed on 0.7% agarose (Figure 28)

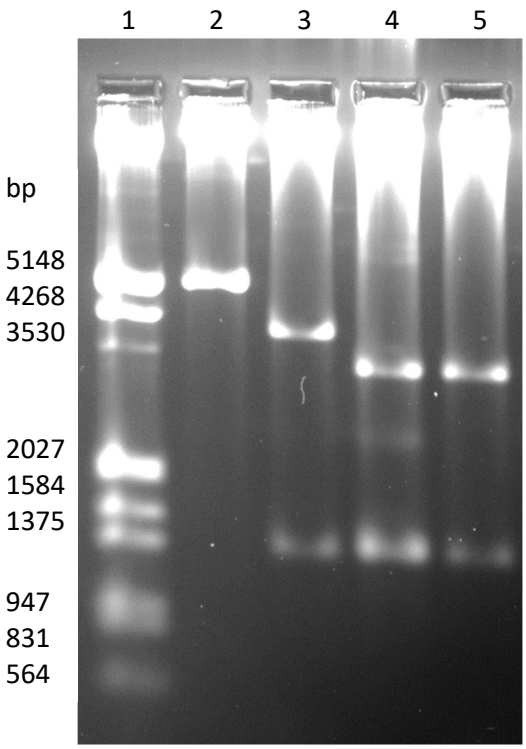

Figure 28: Confirmation of mutant cosmids using *Xba*I and *Eco*RI digestion.

The cosmids I34 (Lane2); I34/parH::aac(3)IV (Lane 3); I34/hyp::aac(3)IV (Lane 3); and I34/parH/hyp::aac(3)IV (Lane 5) were digested with *Xba*I. The digests were analysed on 0.7% agarose. Lane 1 contains λ DNA digested with HindIII and EcoRI. Fragment sizes of marker shown in bp.

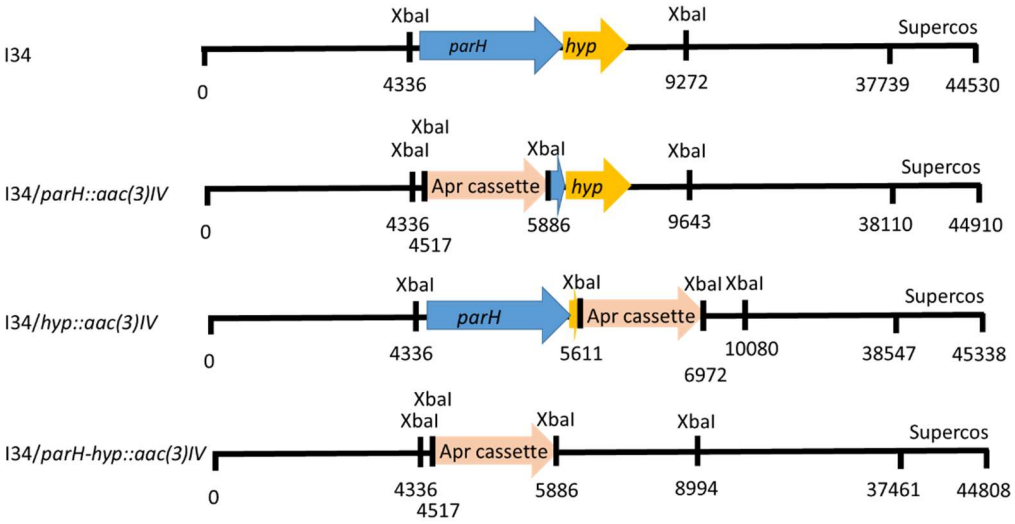

Figure 29: Pictorial representation of cosmid restriction pattern.

Restriction maps of I34 cosmids containing the disruption cassettes.

Table 5: Table showing expected fragment sizes generated from *Xba*I digestion of I34 cosmids containing the disruption cassettes

	I34	I34/*parH::aac(3)IV*	I34/*hyp::aac(3)IV*	I34/*parH/hyp::aac(3)IV*
1	39594	39594	39594	39594
2	4936	3757	3108	3108
3		1369	1369	1369
4		181	1275	181

The expected sizes of the fragments generated by *Xba*I digest of I34 and mutant cosmids is set out in figure 29 and table 5. The I34 *Xba*I digest resulted in the two bands of around 39.5 Kbp and 5 Kbp which correspond to the two expected bands. The mutant cosmid XbaI digests all contained the larger fragment of 39.5 Kbp as expected. They also all contain a fragment of around 1400 bp which corresponds to the fragment containing the apramycin cassette. In addition they all contain the other theoretical fragments that each construct was expected to contains confirming that all of the disruption cassettes were successfully integrated into the I34 cosmid. After confirming that the mutant cosmids had been successfully generated they were

transformed into the non-methylating *E. coli* strain ET12567/pUZ8002. This strain serves two folds, overcoming the methyl-specific restriction endonuclease system by removing the methylation of the cosmid DNA and allowing conjugation of plasmids/cosmids containing *oriT* into *S. coelicolor* through the action of pUZ8002. After conjugation, we sort to select for colonies that had successfully up taken the cosmid, which given that the cosmid was unable to replicate in *S. coelicolor*, could only have happened through integration into the chromosome by homologous recombination. Selection was achieved by overlaying plates with both apramycin, which the cosmid conferred resistance to, and nalidixic acid to kill the *E. coli* cells. Selection using apramycin did not distinguish between the desired double crossover event, which results in a single copy of the gene cluster with the mutation, or the single crossover event which would result in two copies of the gene locus, wild type and mutant. To differentiate between the two scenarios we used replica plating to identify colonies that were sensitive to kanamycin and had thus lost the back bone of the cosmid, a unique identifier of a double crossover event. Colonies identified as double crossover were then processed to generate spore preps, for which the spore concentration was calculated, before being stored at -20°C for further analysis.

3.2 The *parH* mutant strain is developmentally delayed

To determine the macroscopic phenotype of the mutant strains, approximately 10^6 spores of each mutant strain were plated on SFM along with the wild type control, M145. The spores were plated in a triangle shape with all the triangles of equal size to ensure that development was unaffected by the concentration of spores plated. Development is linked to nutrient depletion so importance was paid to ensuring that each spore confluent triangle had access to the same nutrients per spore. The plates were incubated at 30°C and development monitored daily (Figure 30).

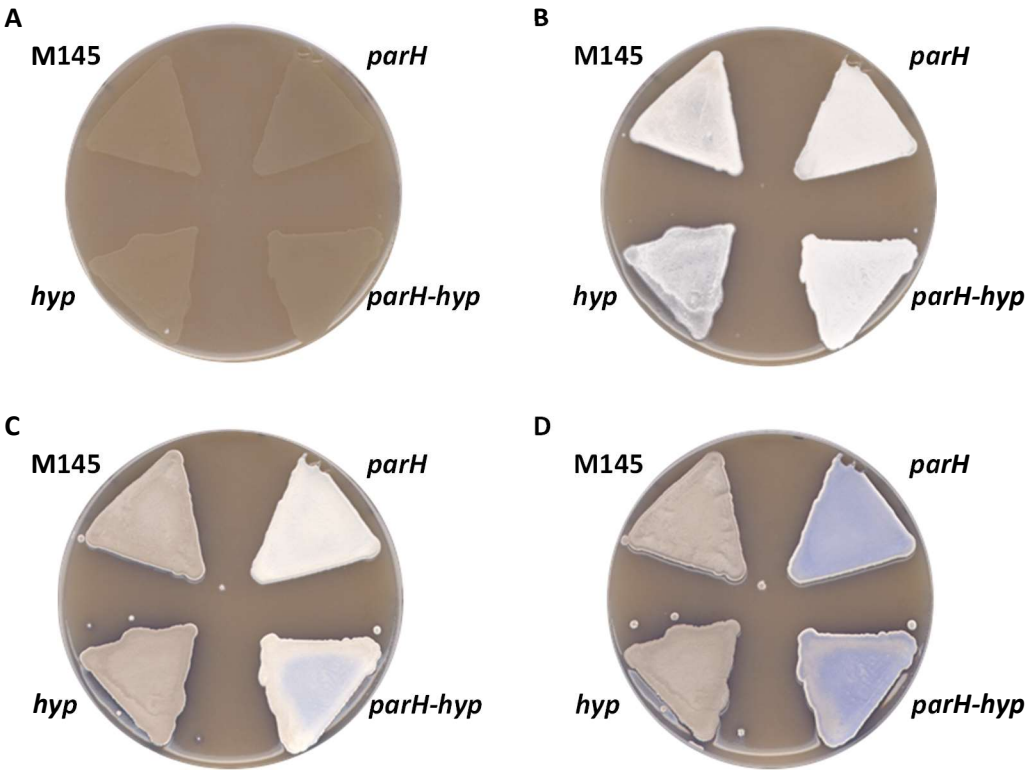

Figure 30: Macroscopic analysis of *parH* and *hyp* mutant strains

Approximately 10^6 spores of M145 (wild type) and the mutant strains were plated in a triangle patch on SFM. The plates were incubated and monitored at regular time intervals (A) 1 day, (B) 2 days, (C) 3 days and (D) 4 days. The *parH* and *parH-Hyp* mutants are developmentally delayed compared to the wild type and *hyp* mutant. While all strains develop vegetative (A) and aerial hyphae (B) at the same rate the *parH* and *parH-hyp* mutants are delayed in sporulating (C). These mutants are also impaired in producing the grey pigment associated with spore maturation (D).

The macroscopic phenotype of the *parH* and *parH-hyp* mutants have a delayed development phenotype when compared to the wild type strain, M145. After two days of growth the *parH* and *parH-hyp* mutant strains have both developed vegetative and aerial hyphae in a comparable time to the wild type strain. We can observe this through the shiny appearance of the bacterial lawns one day after plating which is consistent with the development of vegetative hyphae. After two days the colonies have developed the fuzzy white morphology associated with the growth of aerial hyphae. After this stage we start to see a divergence in development

of the strains. At 3 days, the wild type shows the classic grey pigment associated with spore maturation and the end of the life cycle. In the same time the parH and *parH-hyp* mutant strains still show the white morphology of aerial hyphae development, suggesting they have yet to sporulate. In fact even after 4 days of growth these strains are yet to express the grey spore pigment instead gaining the strong blue colour of the antibiotic actinorhodin (Figure 31). This colouration could be due to the lack of the grey pigment although observations of the back of the plate could suggest that more actinorhodin is being produced. Rather than an upregulation of gene transcription this apparent increase in production could be because the time between aerial hyphae development and sporulation is elongated because of delayed sporulation. Antibiotic production in *Streptomyces* is often developmentally linked and a delay in development could lead to the strain being in the window of antibiotic production for longer thus leading to higher amounts of antibiotics being produced. The *hyp* mutant did not appear to have a macroscopic phenotype with the strain looking very similar to the wild type at all stages of development.

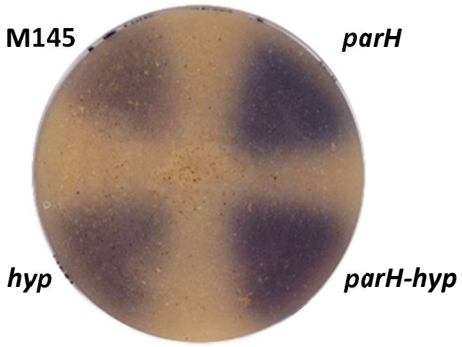

Figure 31: Antibiotic production of *parH* and *hyp* mutant strains

Approximately 10^6 spores of M145 (wild type) and the mutant strains were plated in a triangle patch on SFM. The plates were incubated for 5 days and monitored for antibiotic production. The *parH* and *parH-Hyp* mutants produce more actinorhodin than the wild type or the *hyp* mutant.

3.3 The *parH* mutant strain has irregular septum site placement

After observing the macroscopic phenotype of the mutants we wished to investigate the microscopic phenotypes of the mutants. To do this we visualised both vegetative and aerial hyphae using an epi-fluorescence microscope. In order to properly observe the effects on the chromosome and cell division of the mutants we decided to use two dyes; propidium iodide (PI) and wheat germ agglutinin (WGA) Alexa Flour® 488 conjugate. Propidium iodide is a compound that intercalates between bases of DNA where it undergoes a conformational change increasing its fluorescence (Arndt-Jovin and Jovin, 1989; Waring, 1965). WGA conjugates bind to sialic acid and N-acetylglucosaminyl residues and have been well documented to bind to the cell wall and septum of Gram-positive bacteria (Pogliano et al., 1997; Wright, 1984).

For viewing vegetative hyphae approximately 1000 spores/cm^2 were inoculated onto SFM with a cellophane on the surface. In order to view the aerial hyphae, around 10^5 spores were grown on SFM after inoculation in a streak pattern into which glass coverslips were embedded at a 70° angle from the horizontal plain of the media. Plates were grown at 30°C and hyphae were observed after overnight growth for observations of vegetative hyphae on cellophane and after 2 to 4 days growth on coverslips for observations of aerial hyphae and spore development. Prior to staining samples were treated with methanol in order to permeabilise the cell wall and allow for uptake of PI into the cell and for the better incorporation of WGA conjugate into the cell wall (Allen et al., 1973).

M145 was monitored microscopically to act as a comparison upon which to judge the microscopic phenotype of the mutant strains (Figure 32). Growth began from a single spore from which most often either one or two germ tubes grew before branching to create a network of hyphae in order to access the available nutrients in the media. The branching pattern was irregular and the hyphae grew in a generally straight fashion, although where it does curve those curves are smooth (Jyothikumar et al., 2008). After the depletion of nutrients the erection of aerial hyphae above the surface begins. This exhibits as the very smooth and curly hyphae which unlike

vegetative hyphae do not undergo any branching events. So far the DNA in the hyphae is dispersed and so we can visualise the propidium iodide filling the inside of the hyphae although there are occasional gaps seen, especially in the aerial hyphae, which could indicate that the DNA is beginning to align in preparation for sporulation. After the cessation of growth division septa are laid down in the aerial hyphae which is the ladder-like structures that are seen with WGA. The chromosomes have undergone segregation with clear gaps having emerged between each individual chromosome. These septa have been placed with great regularity and each

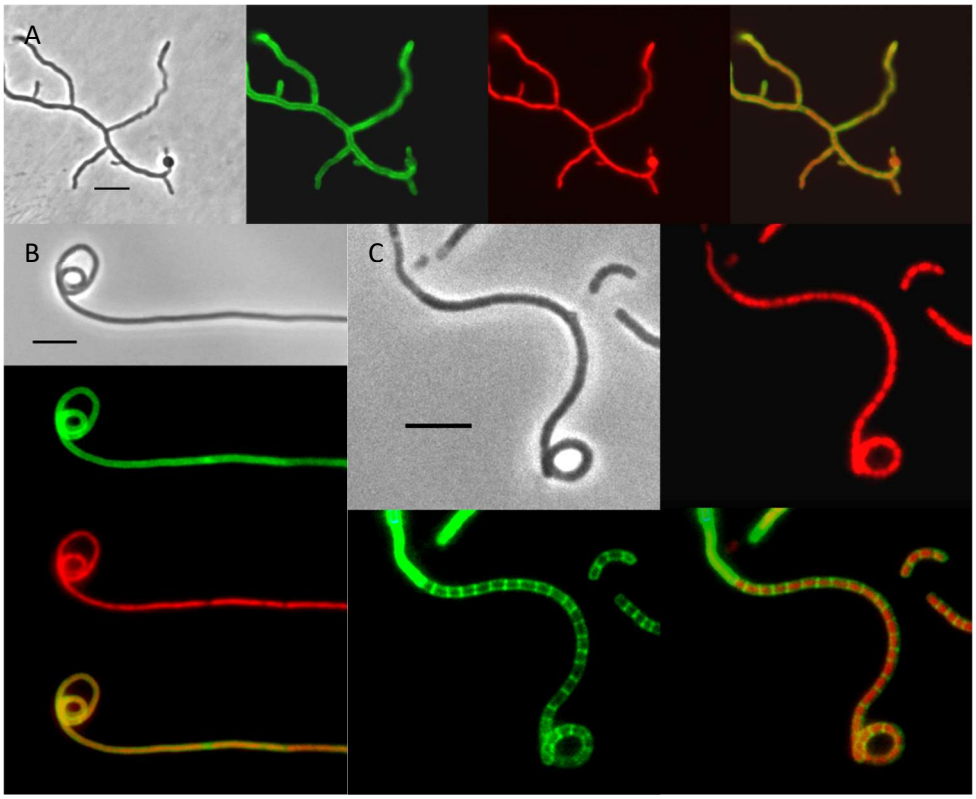

Figure 32: Fluorescence microscopy showing the developmental stages of the wild type M145

M145 was plated onto SFM either with cellophane (A) or beside a coverslip (B-C) before being stained with PI (red – DNA) and WGA (green – cell wall). (A) M145 vegetative hyphae germinate before branching and forming a hyphal network of straight and gently curved hyphae. (B) Aerial hyphae are erected above the media forming curly hyphae containing dispersed DNA with irregular segregation events. (C) After the cessation of growth, septa are positioned along the length of the hyphae in a ladder like fashion creating multiple pre-spore compartments containing a single chromosome. These will go on to mature into spores. Scale bar corresponds to 5µm

chromosome enclosed with a septum on each flank. These pre-spore compartments are then ready to undergo maturation, with the thickening of the cell wall into full spores, which will lay dormant until the optimal conditions once again present themselves and germination is triggered once again.

Monitoring the *parH* mutant strain by microscopy reveals some interesting characteristics which are divergent from the wild type. Firstly, there are observable differences in vegetative hyphae where there appears a greater propensity for more germ tubes to protrude from the spore during germination (Figure 33). We can also observe instances of the germination of two connected spores both undergoing germination individually with the protrusion of germ tubes. These appear to have a connecting cell wall that has not undergone thickening during spore maturation, although the other walls of the spores have. Despite these abnormalities there are also numerous instances of normal vegetative hyphae development and growth. It is difficult to judge whether the distribution of DNA is affected in vegetative hyphae as segregation at this stage is very irregular so the distribution observed could be comparable to the wild type. So, even if there is a difference it is clearly not obvious at this stage. As we move onto observing the aerial hyphae in the *parH* mutant we find the same smooth curls seen in the wild type (Figure 34). This suggests that the mechanism that controls the direction of hyphal growth is unaffected by the absence of ParH. Again at this stage there does not appear to be a disruption to the distribution of DNA. While aerial hyphae appear to develop normally, it is possible that the hyphae grow to a longer length compared to the wild type. This is difficult to measure as often aerial hyphae break during the staining and mounting process meaning that finding complete aerial hyphae is somewhat rare. There is also a possibility from observations of the aerial hyphae that they may undergo branching events although at this stage it is difficult to determine the beginning of any given aerial hyphae.

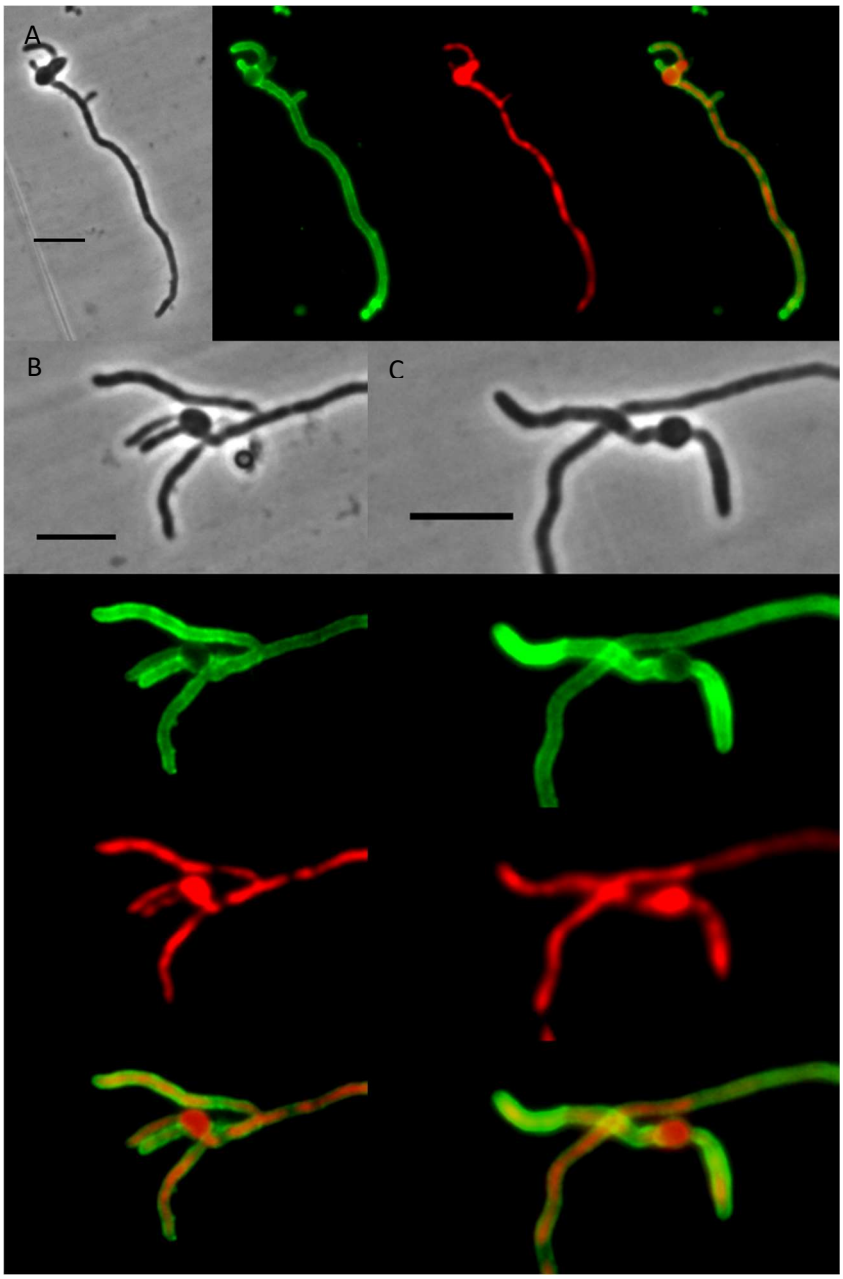

Figure 33: Fluorescence microscopy showing vegetative hyphae in the *parH* mutant strain.

The *parH* mutant strain was plated onto SFM with cellophane before being stained with PI (red – DNA) and WGA (green – cell wall). (A) The strain sometimes has two spores that remain connected by a non-thickened spore wall. (B) There are higher instances of more than two germ tubes emanating from a single spore. (C) Lots of spores develop vegetative hyphae normally. Scale bar corresponds to 5 µm.

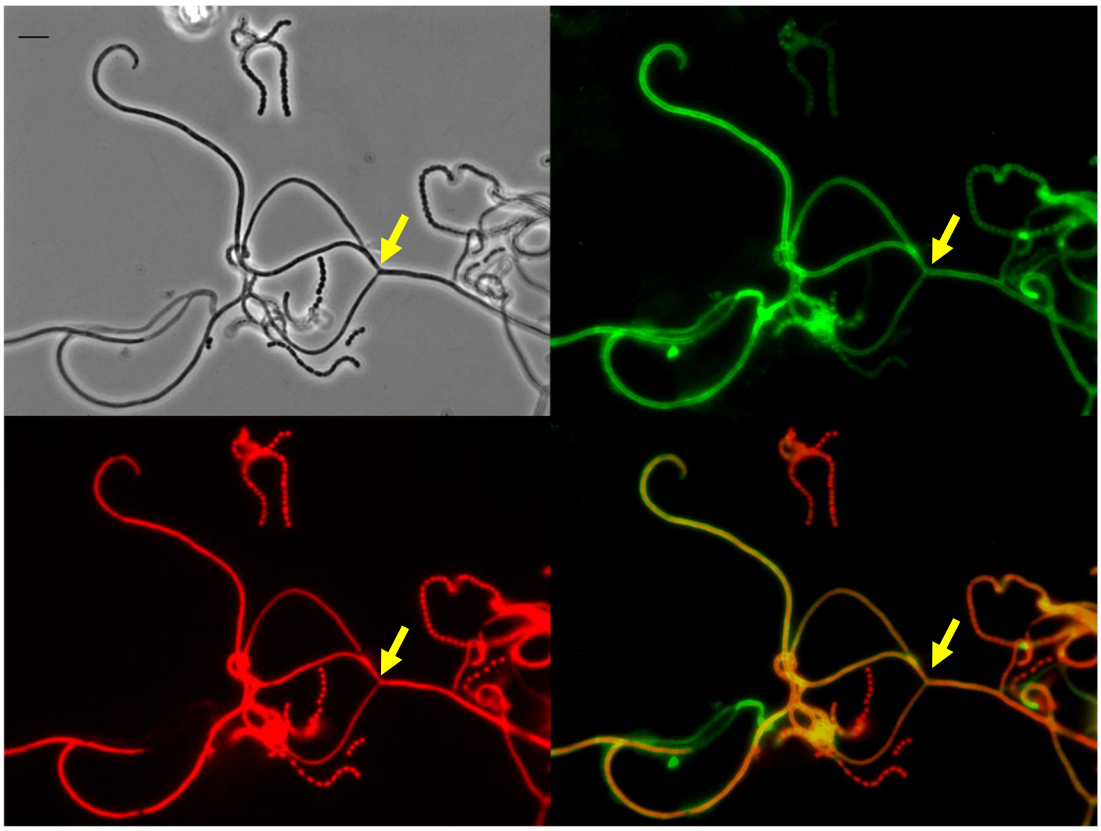

Figure 34: Fluorescence microscopy showing aerial hyphae in the *parH* mutant strain.

The *parH* mutant strain was plated onto SFM beside a coverslip before being stained with PI (red – DNA) and WGA (green – cell wall). The *parH* mutant seems to develop aerial hyphae that are longer than in the wild type. There is also the indication that the aerial hyphae branch in this mutant (arrow). Scale bar corresponds to 5 µm.

As we turn towards looking at spore development in the *parH* mutant we see the greatest divergence from the wild type phenotype. Unlike the wild type, where we saw evenly placed septa that flanked well segregated individual chromosomes, in the *parH* mutant we observe irregular septum placement along the length of the hyphae (Figure 35). We see both pre-spore compartments that are far larger than the compartments seen in the wild type as well as many that are smaller. There are, however, hyphae that are better able to distribute the septa in an even manner but many of the hyphae show this uneven laddering. When we inspect the compartments we see that the incidence of anucleate spores is very low. In fact it is very hard to find any compartments that contain no DNA. This is in stark contrast to the reported number of anucleate spores in the *parA* mutant strain where it stands at around 24% (Jakimowicz et al., 2007). When we observe the DNA distribution in these spore chains we clearly observe both larger and smaller foci of DNA. This DNA is clearly

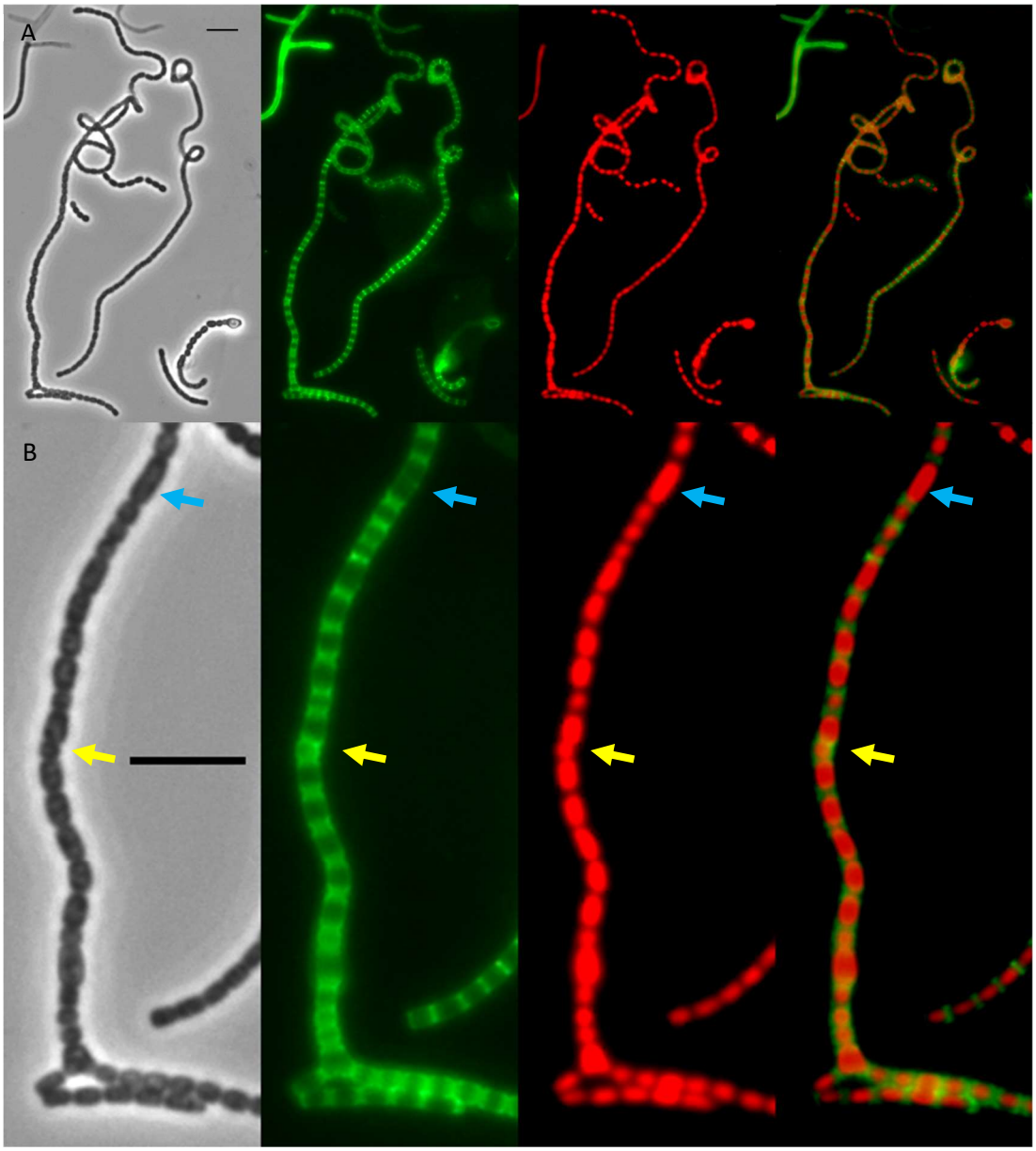

Figure 35: Fluorescence microscopy showing septum placement in aerial hyphae in the *parH* mutant strain.

The *parH* mutant strain was plated onto SFM beside a coverslip before being stained with PI (red – DNA) and WGA (green – cell wall). The *parH* mutant has irregular placement of septa in aerial hyphae with pre-spore compartments both larger (blue arrow) and smaller (yellow arrow) compared to the standard size of pre-spore compartments typically seen in the wild type strain. Image B is an enlarged section of image A. Scale bar corresponds to 5 µm,

completely segregated and flanked by septa just as in the wild type. The unevenness of thenucleoid size indicates that the number of chromosomes in each package is different. This would therefore include DNA in pre-spore compartments that are too small to contain a complete chromosome and, of course, the reciprocal should be

true and that is compartments with DNA foci that contain multiple chromosomes. This opens up the possibility that we are observing the possible guillotining of chromosomes during division. The abundance of anucleate pre-spore compartments in the *parA* mutant strain combined with the miss-segregation of the chromosomes indicates that in this strain, while the chromosomes are not segregating properly the septa are still being placed in the gaps between chromosomes and therefore there is no guillotining of the DNA. However, it is possible that in the *parH* mutant strain we are seeing the opposite happening. The chromosomes are perhaps aligning properly prior to septa formation but the septa are being unevenly distributed along the hyphae and over the DNA, guillotining the chromosomes when the septa close and thus creating the uneven size of DNA distribution in the pre-spore compartments.

With the appearance of septa we can also more easily distinguish the boundaries of aerial hyphae and thus observe aerial branching (Figure 36). As previously stated, in the wild type branching is a process exclusive to vegetative mycelium and is completely absent from aerial hyphae. Branching in the aerial hyphae of the *parH* mutant is a relatively common occurrence, observable in around 10% of all aerial hyphae. This would indicate that ParH has some kind of interaction with the TIPOC which possibly affects the action of the TIPOC. While this observation of aberrant branching in the aerial hyphae is so clear due to the fact that branching in the aerial hyphae is not seen in the wild type, the fact that there is no clear effect on branching in vegetative hyphae in the *parH* mutant, could simply be because subtle aberrant branching in vegetative hyphae is difficult to measure. As the pre-spore compartments begin to develop into mature spores we can also observe the fate of small pre-spores which in all likelihood contain less than a complete chromosome. While many small pre-spore compartments develop into mature spores, with the associated thicker cell walls, it is noticeable that some small pre-spores do not undergo this thickening, although they do show the more rounded spore-like shape. There are also small compartments that do not even become more rounded in appearance, maintaining the straight edges present associated with pre-spore apartments. It is difficult to say whether these ever develop into mature spores or simple stall at a particular stage of development. However, if the DNA is being guillotined which is a distinct probability then it stands to reason that some

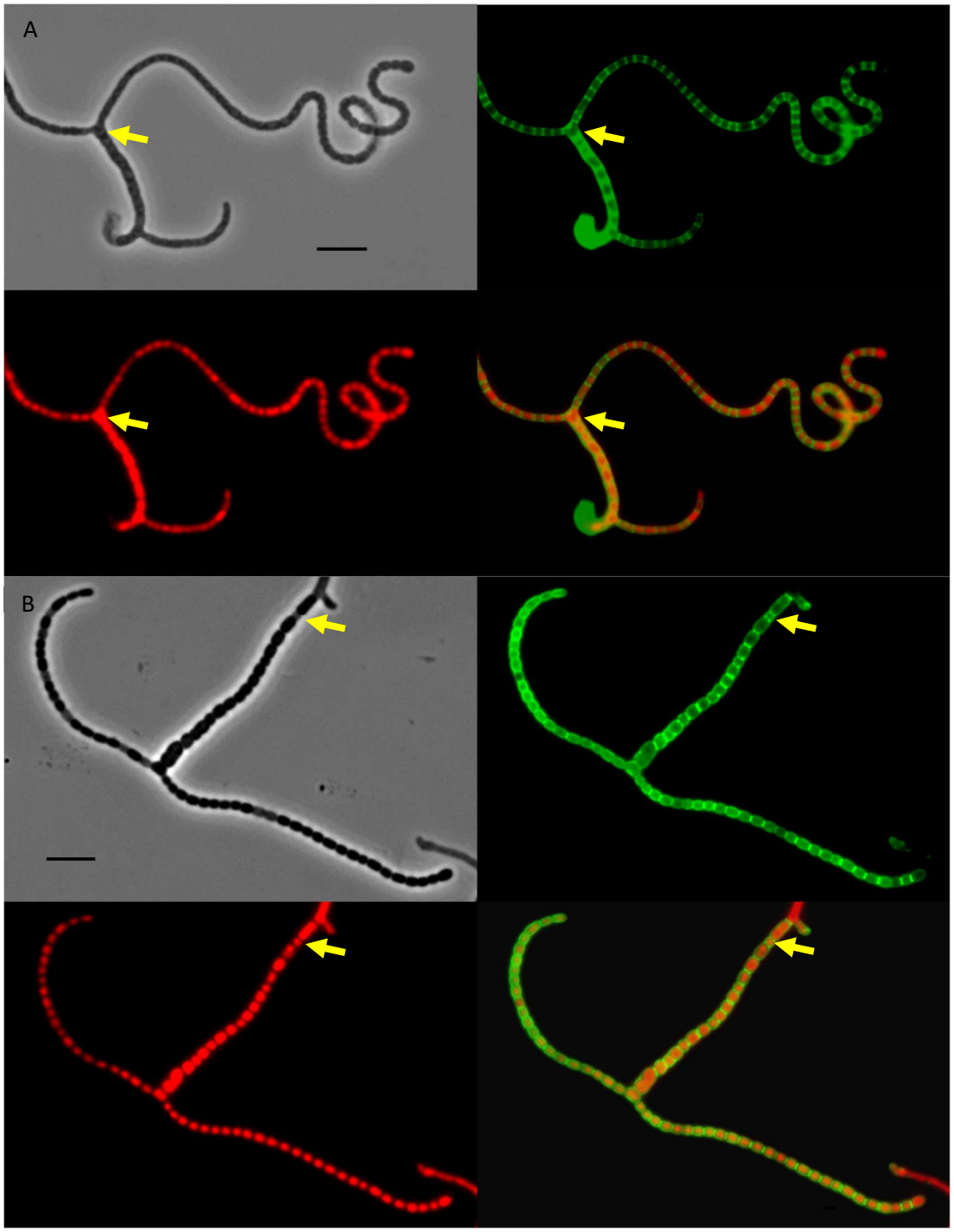

Figure 36: Fluorescent microscopy showing branching and stalled spore formation in aerial hyphae in the *parH* mutant strain.

The *parH* mutant strain was plated onto SFM beside a coverslip before being stained with PI (red – DNA) and WGA (green – cell wall). (A) The *parH* mutant has aberrant branching (arrow) of aerial hyphae in stark contrast to the wild type in which aerial hyphae do not branch. (B) Some very small pre-spore compartments fail to develop into mature spores (arrow), indicating that they are missing key genes required for spore maturation, an indication that chromosomes have been guillotined during septa formation. Scale bar corresponds to 5 µm.

maturation. The fact that some very small compartments do appear to complete spore maturation would indicate that the maturation of spores is not dependent on a complete chromosome but merely requires the specific genes responsible for spore development. It is of course unclear whether all of these spores would undergo germination and continue the life cycle. One noticeable aspect of sporulation in the *parH* mutant strain is the synchronicity with which sporulation progresses. In the wild type strain the onset of septa formation, i.e. the moment that ladders become visible, to the formation of mature spores occurs within a few hours, with the synchronous progression of all aerial hyphae into spores. The *parH* mutant however, appears to exhibit an extended period in which aerial hyphae contain septa but have not progressed to full spore chains. We find that a full 24 hours after the onset of the first sporulation septa becoming visible in a sample we can still find aerial hyphae in this stage of development. In the absence of live imaging it is not yet clear whether this is solely a result of different aerial hyphae undergoing sporulation at different times or whether this is because there is a long delay between the onset of septation and the progression into spores.

The microscopy of the *hyp* mutant strain reinforces the findings from the macroscopic analysis, that the strain is phenotypically similar to the wild type strain (Figure 37). The spores germinate with the growth of mostly one or two germ tubes per spore. These then create a network of branching mycelium in which the DNA is dispersed throughout the hyphae. Aerial hyphae are then erected above surface and display the wild type smooth curves with irregularly segregated DNA. We can then see the formation of septa along the length of the hyphae which are placed at regular positions and encompass correctly segregated chromosomes into pre-spore compartments. These pre-spore compartments then develop into full spores after undergoing maturation. We are unable to detect any of the abnormalities that are present in the *parH* mutant strain. This is important in understanding the *parH* mutant phenotype as it is likely that transcription of the *hyp* gene in the *parH* mutant is disrupted by the polar effect from the apramycin resistance cassette used to knock out the *parH* gene. The lack of a phenotype different from the wild type in the *hyp* mutant means that the observation made in the *parH* mutant are because of the disruption of *parH* and are not a cumulative effect of a *parH-hyp* knock out.

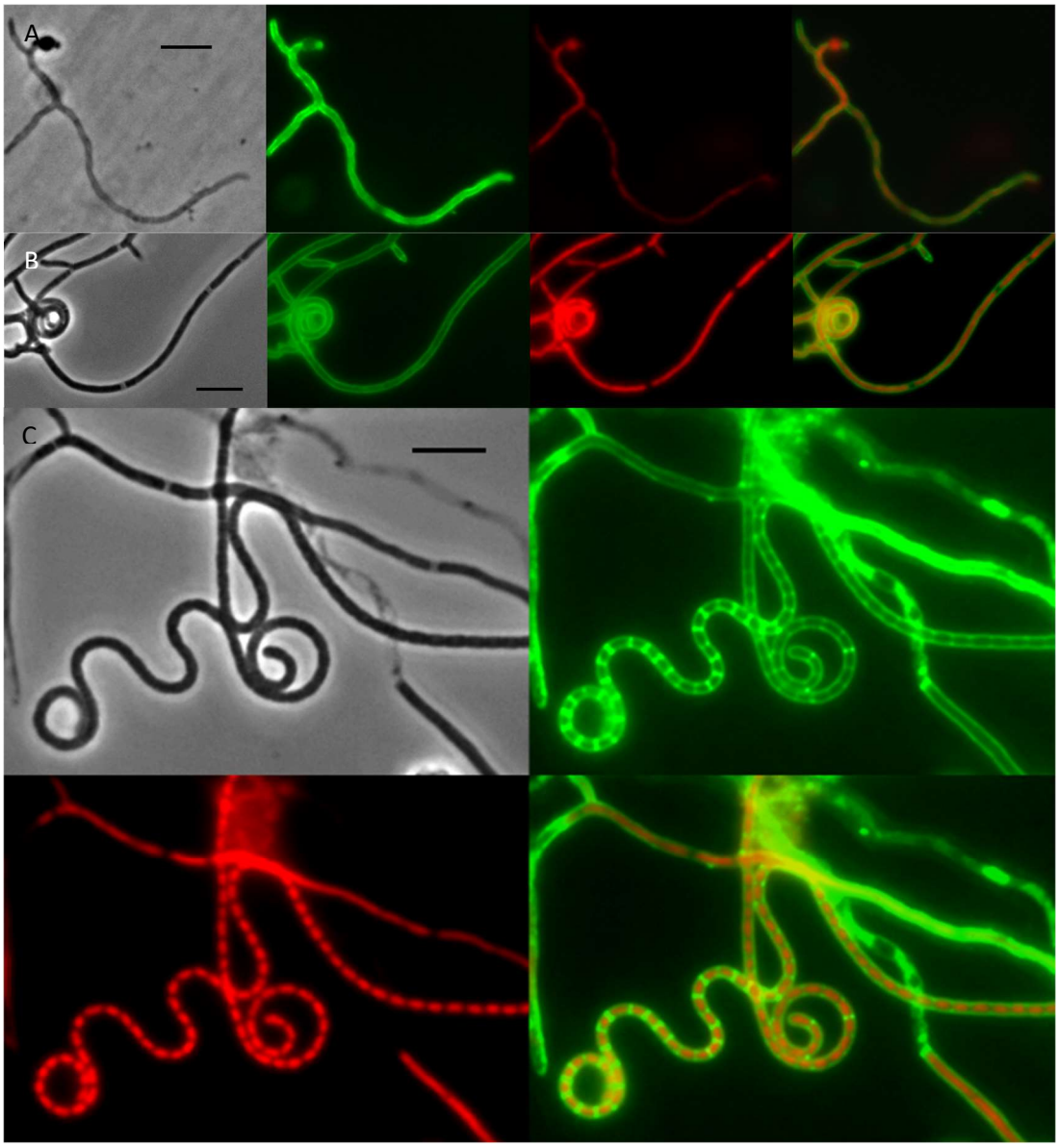

Figure 37: Fluorescent microscopy showing the developmental stages of the *hyp* mutant strain

The *hyp* mutant strain was plated onto SFM either with cellophane (A) or beside a coverslip (B-C) before being stained with PI (red – DNA) and WGA (green – cell wall). The *hyp* mutant has a microscopic phenotype comparable to the wild type. (A) Vegetative hyphae germinate before branching and forming a hyphal network of straight and gently curved hyphae. (B) Aerial hyphae are erected above the media forming curly hyphae containing dispersed DNA with irregular segregation events. (C) After the cessation of growth, septa are positioned along the length of the hyphae in a ladder like fashion creating multiple pre-spore compartments containing a single chromosome. These will go on to mature into spores. Scale bar corresponds to 5 µm.

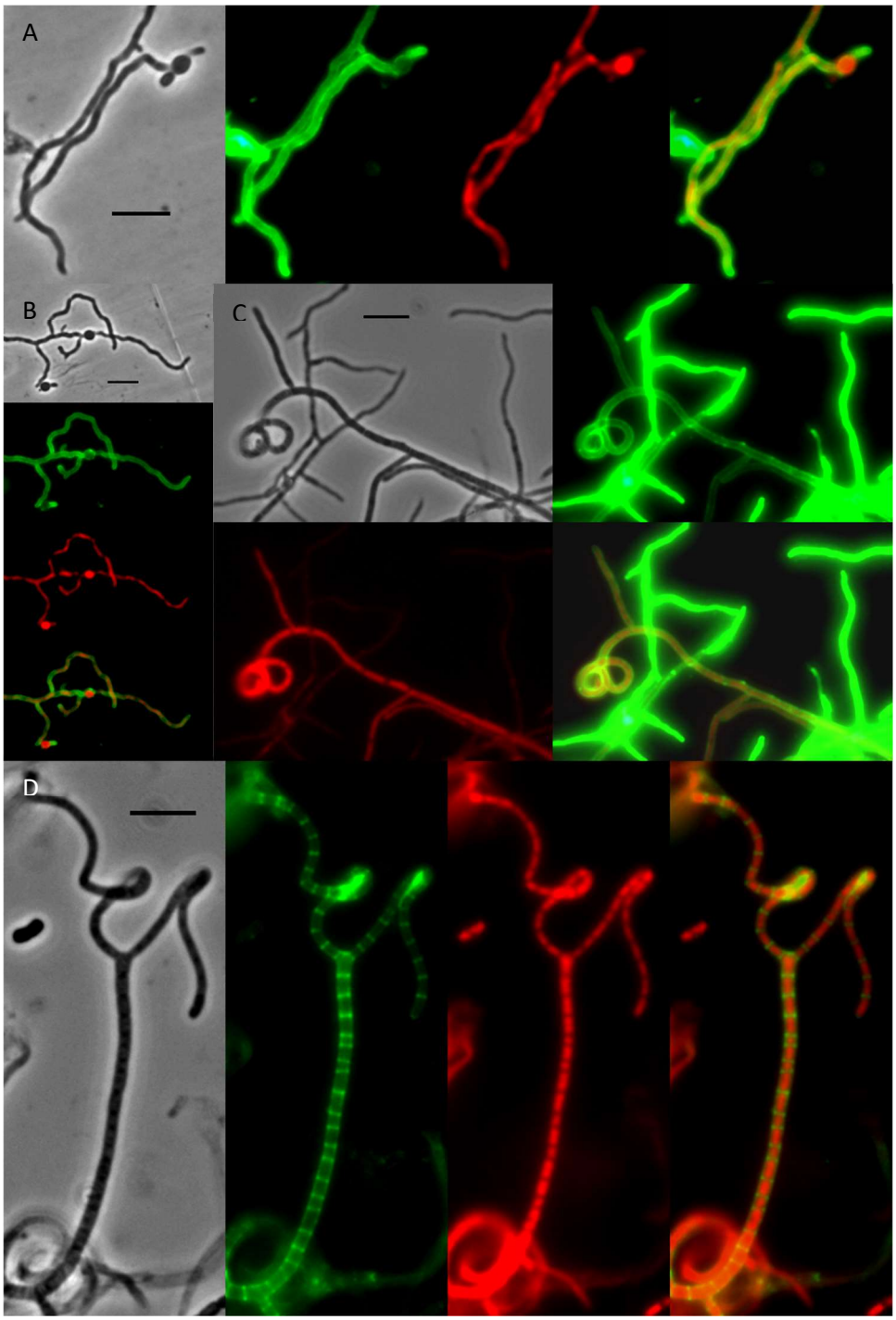

Figure 38: Fluorescent microscopy showing the developmental stages of the *parH-hyp* mutant strain

The *parH-hyp* mutant strain was plated onto SFM either with cellophane (A-B) or beside a coverslip (C-D) before being stained with PI (red – DNA) and WGA (green – cell wall). The *parH-hyp* mutant has a microscopic phenotype comparable to the *parH* mutant strain. (A-B) The strain sometimes has two spores that remain connected by a non-thickened spore wall and there are higher instances of more than two germ tubes emanating from a single spore. (C-D) Aerial hyphae have aberrant branching and place septa at irregular intervals along the hyphae. Scale bar corresponds to 5 µm.

Based upon the microscopic phenotypes seen for the *parH* mutant and the *hyp* mutant strains it was expected that the *parH-hyp* mutant strain would have the same microscopic phenotype as the *parH* mutant strain. This appears to be the case (Figure 38). In vegetative hyphae, we are able to observe the same deficiencies as in the parH mutant with spores being connected and the higher occurrence of multiple germ tubes growing from a single spore. In aerial hyphae we see the same extended length and branching phenotype that is not seen in the wild type strain. Septa are laid down at irregular intervals throughout the aerial hyphae which create pre-spore compartments containing varying amounts of DNA. These observations from the *parH-hyp* mutant strain help to validate the results of the microscopy of the *parH* mutant strain

To understand the irregularity of septum placement in the *parH* mutant, we undertook to measure the distance between septa in the *parH* mutant strain and compare the resulting distribution to the wild-type. Images were analysed using the Zeiss Axiovision software, which has a measuring tool, with the data collated in Excel and histograms generated. The histogram for the *parH* strain was plotted against that of the wild-type strain to determine how the placement of septa in the *parH* mutant strain, varied from the wild type (Figure 39). The *parH* mutant strain had a larger distribution of sizes with many larger and smaller than the mode of 1.1 µm. Interestingly the mode of 1.1 µm was the same for all both the *parH* mutant strain and the wild-type strain suggesting that septum formation still occurs with a gap of 1.1 µm more often than any other size of gap. This is similar to data found in *B. subtilis* in the absence of the Min and NO systems. In this strain the septum is still located at the mid cell more often than at any other position in the cell. This is despite the greater variety of cell size which occurs due to the miss-placement of the septum.

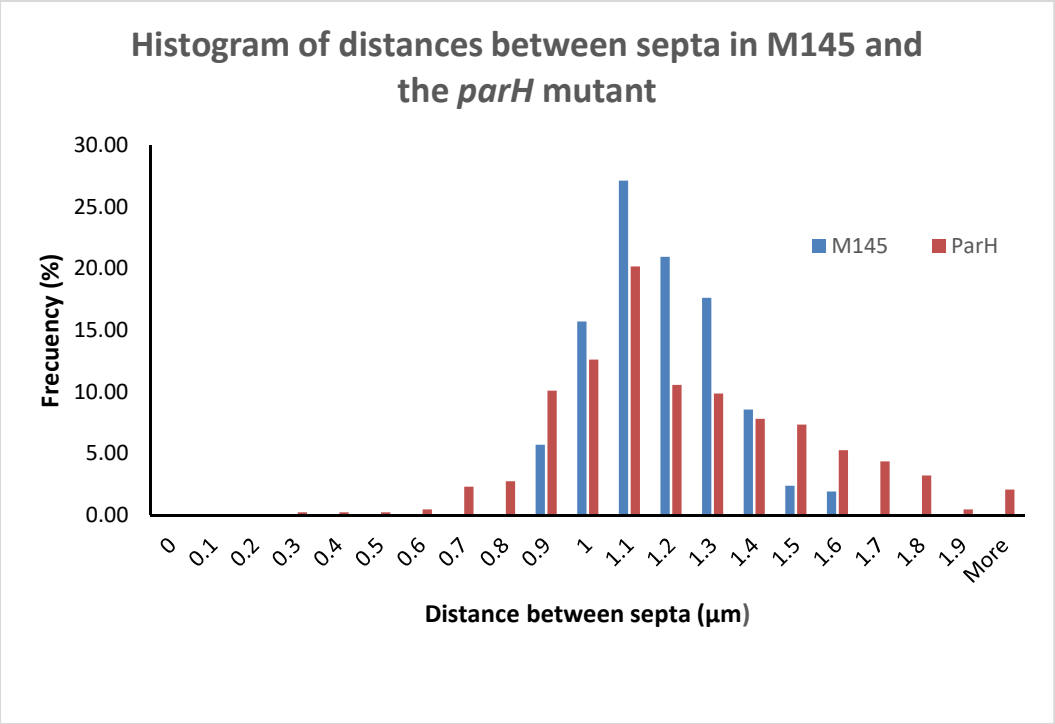

Figure 39 Distribution of septa distances in the wild-type, M145, and the *parH* mutant strain.

The distance between 400 septa was measured for both the wild-type strain M145 and the *parH* mutant strain of *S. coelicolor*. The *parH* mutant strain has a much broader distribution compared to the wild-type, suggesting that the septa are not placed at regular intervals in the aerial hyphae.

3.4 The *parH* mutant strain has smaller colonies and fewer viable spores

So far we have established that in the *parH* mutant, septa are placed in an irregular distribution compared to the wild-type where there is a regular ladder pattern of septa placement. This leads to a greater variation in pre-spore compartments. It is likely that when these mature into spores, the spores contain varying amounts of DNA, with some spores containing an incomplete copy of the chromosome and other spores containing multiple copies. It is therefore also likely

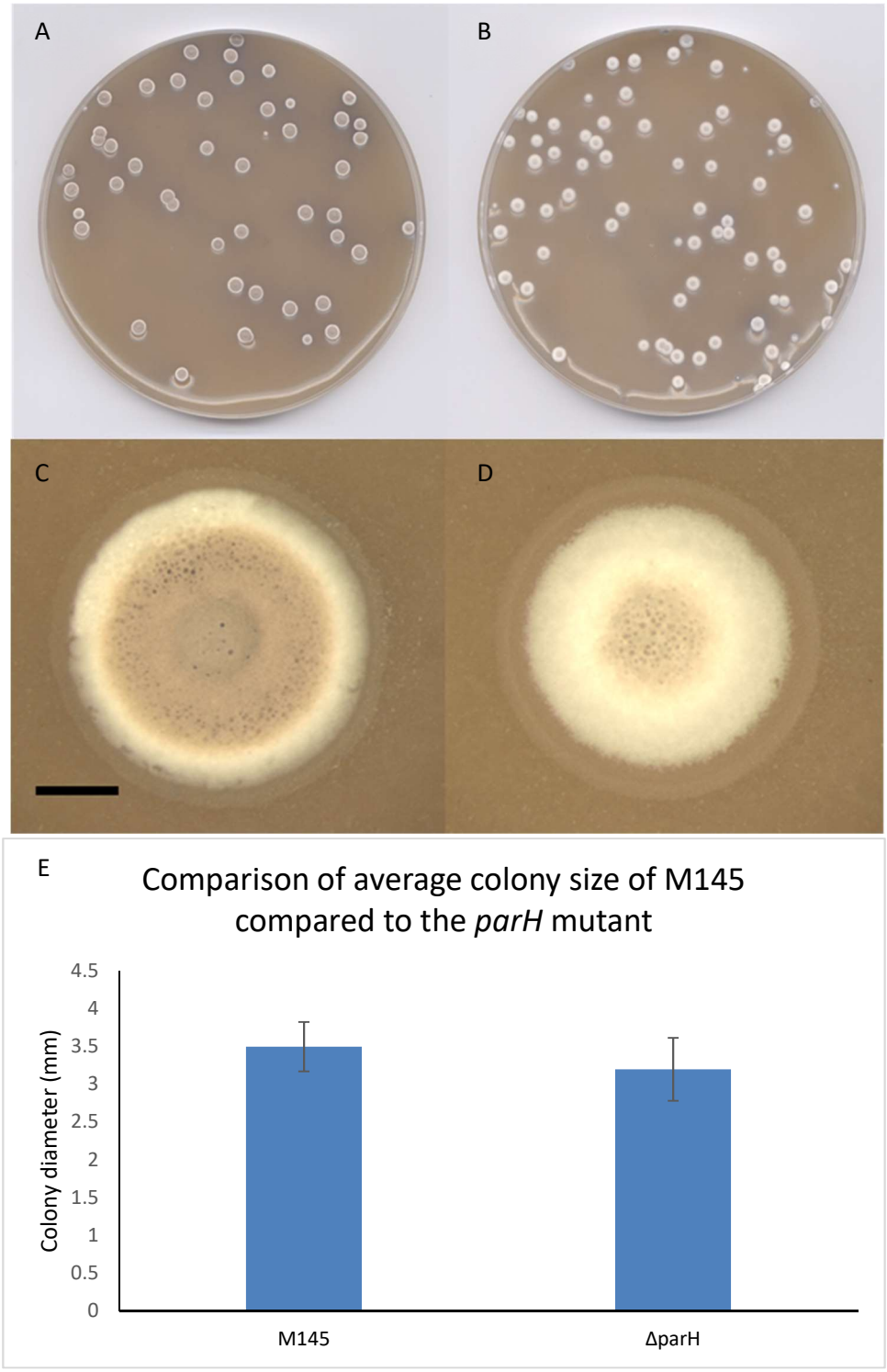

Figure 40: Comparisons of M145 and *parH* mutant strain colonies.

Approximately 50 colonies of M145 (A) and the *parH* mutant strain (B) were grown on SFM for 5 days. An individual colony of M145 (C) and the *parH* mutant strain (D) were imaged using a dissection microscope. Scale bar 10 mm. (E) Colony sizes were measured for both strains and are shown in the bar chart.

that the DNA is, in cases, being guillotined during septum formation. We wished to determine whether potentially having incomplete chromosomes would lead to a

heterogeneous colony population due to the loss of genetic material. We have also observed aberrant branching in aerial hyphae. This suggests that the mutant has a growth defect as well as a defect in cell division. To observe this we monitored the development of single colonies. To do this we inoculated both the wild type and *parH* mutant strains onto SFM such that approximately 50 colonies would grow on the plate. The plates were incubated at 30°C and colony growth monitored (Figure 40). We find that, as for the wild type, we get a homogeneous colony morphology across the plate. This suggests that all spores that are able to grow and progress through the life cycle contain at least one complete chromosome. Spores containing an incomplete chromosome probably fail to germinate and develop into a full colony. Visualising single colonies with a dissection microscope shows that the *parH* mutant strain develops smaller colonies that take longer to sporulate than the wild-type. This indicates that as well as a defect in cell division the *parH* mutant strain also has impaired growth. Measurements of colony sizes show that the mutant strain is approximately 10 % smaller than the wild-type. This could suggest that ParH has an effect on the TIPOC.

So having established that the *parH* mutant produces smaller colonies, the next question to answer is how the *parH* mutant compares to the wild type in its ability to produce viable spores. To measure this we inoculated both the wild type and *parH* mutant strains onto SFM such that approximately 1000 colonies would grow on the plate. The plates were incubated at 30°C and colony growth monitored for development of spores in the *parH* mutant strain as that has delayed development. Once the *parH* mutant strain appeared to sporulate the spores were collected from each plate (2 for each strain) and spore stocks were generated from each plate in a final volume of 1 ml of 20% glycerol. Spore counts were performed on these to determine the number of viable spores collected and a comparison was made between the *parH* mutant and the wild type control (Table 7). The *parH* mutant produces only around 13% of the number of viable spores that the wild type is able to produce. This difference could be a result of several factors. The colonies are smaller than that of the wild type, although not by enough that would account for the scale of difference in viable spores. This could be down to two fundamental reasons, either less spores are produced by the *parH* mutant, or the spores that are

produced are not viable and therefore do not lead to the formation of a visible colony on the plate.

Table 7: Spore viability test of the *parH* mutant

Strain	Spore Concentration Plate 1 (spores/ml)	Spore Concentration Plate 2 (spores/ml)	Average Spore Concentration (spores/ml)	Percentage of M145
M145	$6.13x10^{08}$	$4.63x10^{08}$	$5.38x10^{08}$	100
parH	$5.18x10^{07}$	$8.68x10^{07}$	$6.93x10^{07}$	12.9

3.5 The *parH* mutant strain is complemented by the *parH* gene

To ensure that the observed phenotype of a mutant is as a result of the gene knockout rather than some other genetic abnormality we decided to complement the mutant by placing a copy of *parH* under its native promoter *in cis* in the *parH* mutant strain. If we were able to restore the wild-type phenotype in this strain then we could conclude that the mutant phenotype was a true reflection of the effects of *parH* deletion in *S. coelicolor*. To achieve this we decided to utilise the plasmid pMS82, a vector that integrates at the ϕBT1 attachment site in *S. coelicolor,* leading to each chromosome containing a single copy of the plasmid (Gregory et al., 2003). The vector also contains a hygromycin resistance gene which allows for selection in the apramycin resistant *S. coelicolor* mutant strain. To complement the *parH* mutant strain the primers ParH GFP BglII Forward and 1772 Eco UTC were used to amplify a portion of the *S. coelicolor* genome containing the *parH* gene and a 400 bp upstream region of DNA, which should ensure that the full promoter was present. The PCR product was blunt cloned into the EcoRV site of pMS82. Sequencing was used to confirm the successful generation of the complementation construct pMS82-P_{parH}-*parH* (Figure 41). After confirming a successful construct, it was then conjugated into both M145 and the *parH* mutant strains using the non-methylating *E. coli* strain ET12567/pUZ8002. In addition the empty pMS82 vector was also conjugated into the same strains in order to provide a control to ensure that complementation is a result of the complementation fragment and not an effect of the vector. The strains were

then processed to generate spore preps, for which the spore concentration was calculated, before being stored at -20°C for further analysis.

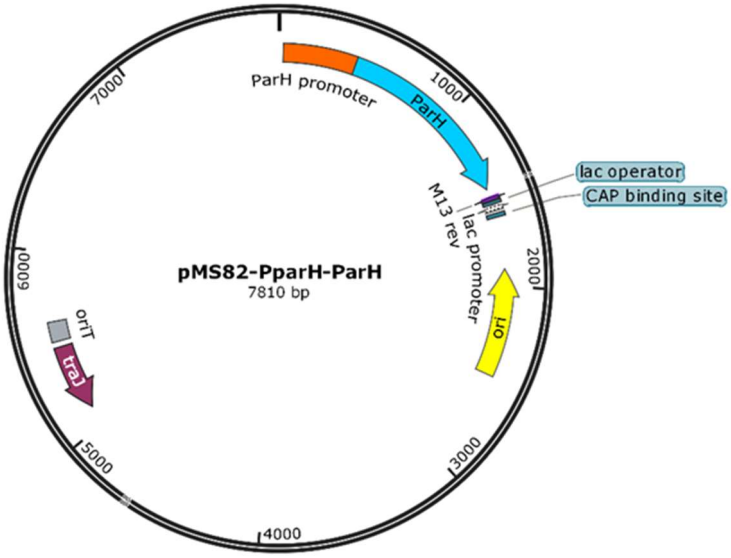

Figure 41: Plasmid map of pMS82-PparH-ParH.

The plasmid pMS82-PparH-ParH.is a derivative of pMS82 with the *parH* gene and its promoter blunt end cloned using the restriction site *Eco*RV.

To assess whether the construct pMS82-P_{parH}-*parH* complements the *parH* mutant strain the macroscopic phenotype was analysed in the same manner as the mutant strains before. Approximately 10^6 spores of each mutant strain were plated on SFM in a triangle shape with all the triangles of equal size to again ensure that development was unaffected by the concentration of spores plated. The plates were incubated at 30°C and development monitored daily (Figure 42).

The complementation vector restored *parH* mutant strain to the wild-type phenotype. In the first two days of growth all strains developed at the same rate developing first vegetative hyphae after 1 day and the beginnings of aerial hyphae development after two days. At 3 days after inoculation the wild type strains and the *parH* mutant strain containing pMS82-P_{parH}-*parH* all had begun to sporulate with the *parH* strain containing pMS82 as a control still exhibited a white phonotype. After 4 days of growth the *parH* mutant strain containing pMS82 still showed a blue colour and lacked the strong grey pigment associated with mature spores, consistent with

previous results. This suggests that the *parH* mutant strain was successfully complemented by the introduction, *in cis*, of the *parH* gene driven by the native *parH* promoter. This means that, macroscopically at least, the phenotype observed in the *parH* mutant strain is the result of the deletion of the parH gene and not as a result of an unforeseen secondary mutation event.

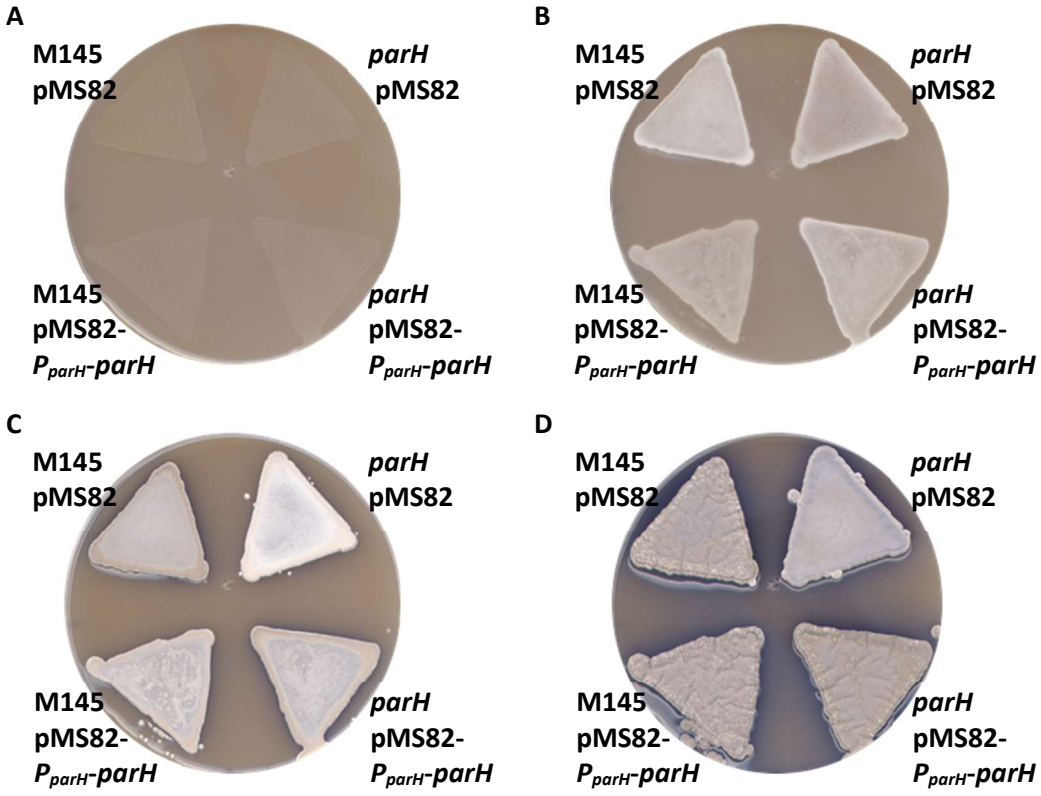

Figure 42: Macroscopic analysis of the complementation of the *parH* mutant strain

Approximately 10^6 spores of the complementation and control strains were plated in a triangle patch on SFM. The plates were incubated and monitored at regular time intervals (A) 1 day, (B) 2 days, (C) 3 days and (D) 4 days. The complemented strain shows development consistent with the control strains suggesting that the *parH* mutant is in fact complemented by pMS82-P_{parH}-*parH*. The *parH* strain containing paMS82 has a macroscopic phenotype comparable to that of the *parH* mutant, suggesting that complementation is as a result of the complementation fragment cloned into pMS82.

3.6 Summary

In this chapter we set out to identify novel ParA-like proteins in *S. coelicolor*. We searched the genome for homologues of both Soj and MinD from *B. subtilis*. We identified the gene locus SCO1772, which encodes a ParA-like protein, with 49% identity to *B. subtilis* Soj and 30% identity to *B. subtilis* MinD. We designated this protein ParH. Its gene overlaps with the downstream gene, which encodes a small hypothetical protein. Also downstream of this locus are genes encoding ScpA and ScpB, proteins that function with SMC as part of the chromosome organising machinery. By searching for ParA-like proteins that are surrounded by the same genes we were able to identify homologues for ParH, which were found exclusively in *Actinobacteria*. We also searched for potential homologues of the small hypothetical protein that is encoded by the gene immediately downstream of *parH*. Homologues of this protein are found only in Actinobacteria, but as of yet none have been characterised. We therefore gave the protein the working title of Hyp.

After identifying these proteins, we proceeded to create mutant strains in *S. coelicolor*. We generated a *parH* mutant strain, a *hyp* mutant strain and a *parH-hyp* double mutant strain. Macroscopic analysis of the *parH* mutant strain showed that it had a delayed sporulation phenotype compared to the wild-type strain. Closer inspection using fluorescence microscopy revealed that the *parH* mutant strain had irregular septation compared to the wild-type strain as well as aberrant branching in the aerial hyphae. This suggests that ParH has an effect on both growth and division. Further analysis of the *parH* mutant strain showed that it developed smaller colonies than the wild-type strain as well as produced fewer viable spores. We were able to complement the *parH* mutant phenotype *in cis* by inserting the *parH* gene under the control of its native promoter into the chromosome of a *parH* mutant strain. Analysis of the *hyp* mutant strain did not reveal a significant phenotype under the conditions tested, while the *parH-hyp* double mutant resembled the phenotype of the *parH* mutant strain in its phenotype

4 The Oligomerisation of ParH and Hyp

In the previous chapter, we identified a novel ParA-like protein that is specific to *Actinobacteria*. The protein, which we designated ParH, is found in a gene operon with a small hypothetical protein (*hyp*), although this gene is not conserved across all *Actinobacteria*. We generated *S. coelicolor* mutant strains for these genes, for which we analysed the phenotypes both macroscopically and microscopically. While we were unable to detect a phenotype for the *hyp* mutant strain under the conditions tested, the *parH* mutant strain showed a defect in septum placement during sporulation. We wished to progress investigation of these proteins by looking at their biochemical properties. This chapter will explore purification of these proteins as well as the purification of Scy and ParB. We decided to explore a possible link between ParH and Scy for two reasons. Previous research has already shown a link between ParA and Scy, which demonstrated that the interplay between the two proteins controls the switch between growth and cell division (Ditkowski et al., 2013). The premise of this interplay is that during growth, Scy sequesters ParA to the tip and inhibits polymerisation of ParA. This in turn prevents chromosome segregation from occurring during growth. After aerial hyphae formation, upregulation of a developmentally regulated *parA* promoter leads to increased ParA accumulation at the tip, which overcomes the inhibition of ParA polymerisation by Scy, and begins chromosome segregation. Polymerisation of ParA causes depolymerisation of Scy in an ATP dependent manner, which curtails growth. Given the homology that exists between ParA and ParH we wished to explore whether ParH shares a similar interplay with Scy. In addition the *parH* mutant strain had branching aerial hyphae, suggesting that it could have an effect on the TIPOC, and Scy is a good candidate for this given the already established ParA-Scy link. We also decided to explore a link between ParH and ParB as we wished to find a protein that could link ParH to the chromosome as septum positioning could be regulated by chromosome positioning. As ParB is localised to

the origin of the chromosome during cell division we thought it would be a good candidate to help facilitate this. Moreover, interaction between the homologue of ParH in *C. glutamicum* (PdlP) and ParB has already been demonstrated (Donovan et al., 2010).

In the second part of this chapter, we will investigate the oligomerisation of ParH and how this may be affected by ATP interaction. A key feature of ParA and MinD proteins is the oligomers that they form. This oligomeric state is often regulated by binding to nucleotides, such as ATP. This regulated state has been linked to both the function of these proteins and also their localisation. For example, in *B. subtilis,* Soj (ParA) has an ATP dependent dimeric state which leads to the over initiation of DNA replication through interaction with DnaA. When not bound to ATP, Soj is monomeric and blocks the activity of DnaA, which inhibits chromosome replication. Monomeric Soj also activates sporulation in *B. subtilis* (Gruber and Errington, 2009; Scholefield et al., 2011). In *E. coli* dimerisation of MinD is also ATP dependent. Unlike Soj in *B. subtilis*, monomeric MinD is bound to ADP *in vivo* (Hu et al., 2002; Hu et al., 2003; Lackner et al., 2003). As well as just monomers and dimers, ParA proteins are also able to assemble into filaments. This is also an ATP dependent polymerisation as shown by the ParA protein encoded on the *E. coli* plasmid pB171 (Gerdes et al., 2010). When not bound to ATP the protein forms monomers which then filament in the presence of ATP. The regulation of this oligomerisation creates a pulling effect on the ParB bound to the plasmid. As the filament retracts, due to the loss of ATP, it pulls the plasmid in order to achieve plasmid segregation during cell division (Ebersbach and Gerdes, 2004; Ebersbach et al., 2006). We hope that by investigating the oligomerisation of ParH and the effect of ATP on this, we will be able to understand the beginnings of a regulatory mechanism.

4.1 Protein Purification

Purification of *Streptomyces* proteins was achieved through the use of the heterologous host *E. coli*. The well-established pET vector system was utilised with the vector pET28a used to amplify the desired protein (Figure 43). The pET28a

vector is a medium copy number plasmid with around 20-60 copies per *E. coli* cell. The plasmid can be used to add an N-terminal His-Tag followed by a thrombin cleavage site to the gene of interest, while also carrying the kanamycin resistance gene for selection. All genes where cloned into the vector using the *Nde*I and *Eco*RI restriction sites. Overlapping the ATG start site of the gene with the ATG from the *Nde*I restriction site ensures that the beginning of the gene is in frame with the N-terminal His-tag and placed under the control of the T7 promoter (Dubendorff and Studier, 1991; Studier et al., 1990).

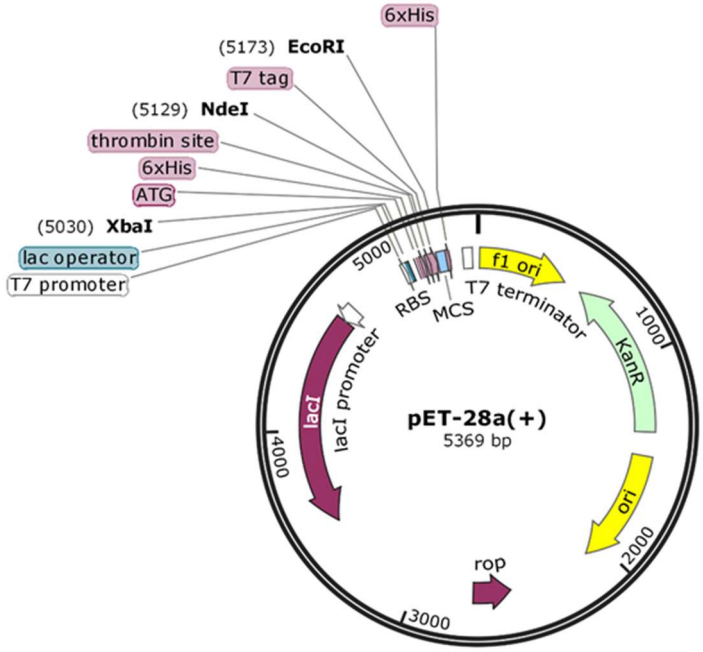

Figure 43: Plasmid map of pET28a.

The plasmid pET28a is a medium copy number plasmid designed to overexpress and purifiy proteins through metal affinity chromatography. A His-tag can be added to a gene if it is cloned inframe with the residues encoding the histadine tag. The T7 polymerase is under the control of the *lacI* promoter which can be induced by IPTG. The vector contains a kanamycin resistance gene for selection. Genes were inserted using the *Nde*I and *Eco*RI restriction sites.

Expression of proteins was carried out in the *E. coli* strain BL21(DE3)pLysS. BL21 being deficient in the proteases Lon and OmpT, DE3 encoding the T7 RNA polymerase gene required for expression of the target gene, and pLysS encoding T7 lysozyme which inhibits basal levels of expression of the target gene (Moffatt and Studier, 1987; Studier, 1991). Protein synthesis is achieved using IPTG, which

inhibits the action of the *lac* repressor allowing synthesis of T7 polymerase and in turn the gene of interest.

Purification was achieved using metal affinity chromatography in which the His-tagged protein is passed through a column containing immobilised nickel ions. The His-tag, which has affinity for the nickel ions, binds to the column while other non-tagged proteins flow through the column. The bound protein can be eluted with higher concentrations of imidazole which, due to structural similarities to histidine, will displace the His-tagged bound protein from the column.

4.1.1 Purification of His-Scy

In order to purify His-Scy, we utilised the previously generated construct pGS2 which is a pET28a derivative with the full Scy gene cloned into the *Nde*I and *EcoR*I sites of pET28a (Figure 44). This generates an N-terminally His-tagged Scy protein with an approximate molecular weight of 148 kDa and a theoretical pI of 4.98. The cloning method does change the start codon of the native Scy protein from a GTG to an ATG. This was done to allow the start site of the *scy* gene to be incorporated into the *Nde*I restriction site in order to allow in frame translation of the *scy* gene from the translational start site of the His-tag. The extinction coefficient of His-Scy is approximately 12950 $M^{-1}cm^{-1}$. The absorbance coefficient is a measure of the proteins ability to absorb UV light at 280 nm (Pace et al., 1995). This property is conferred through the presence of aromatic amino acids, tryptophan and tyrosine as well as the number of cystine residues (Pace et al., 1995). These residues all contribute to the extinction coefficient of any given protein with tryptophan having the highest absorbance value followed by tyrosine and then cystine (Pace et al., 1995).

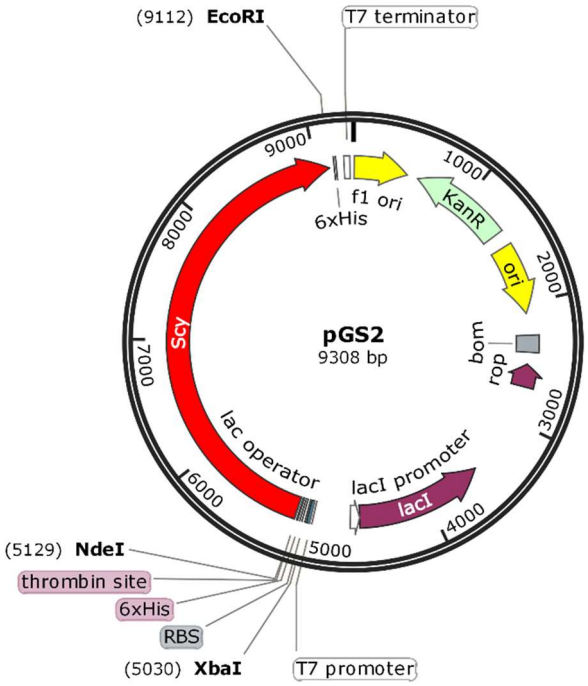

Properties of His-Scy:

Molecular Weight 148 kDa
pI 4.98
Extinction Coefficient 12950 $M^{-1}cm^{-1}$

MGSSHHHHHHSSGLVPRGSHMRGYESQEREPAADVDHLSRFEAEMKRLKTEREKAIQHAEDLGYQVEVLR
AKLHEARRTIMSRPAFDGGDIGYQAEQLLRNAQTQADQLRADAERELSQARAQTQRILQEHAEQAARLQAE
LHQEAVTRRQQLDQELAERRQTVESHVNENVAWAEQLRARTEQQARRLLDESRAEAEQAMAAARAEAER
LTAEARQRLRSDAESARAEADQILRRARTDAERLLNAASTQAQEATDHAEQLRSSTASESESTRREVQELSRA
AEQRMSEAEEALRKAQAEAEKVVAQAEEAAAKALSSAEATNEQRTRTAKEQVARLVGEATKDAESTRSEAE
QVVADARAEAERIVAEAAEKARTITAEESATQLSKAAKTAEDVLNKASEDAKRTTKAATEEAERIRTEAEAEAD
RLRAEAHDIAAELKGAAKDDTKEYRAKTVELQEEARRLRGEAEQLRADAVAEGEKIRAEARKEAVAQIEEAAK
TAEELLAKAKADADELRQTATADGEKVRAEAIERATTLRRQAEETLERTRAEAERHRAEAAERVEELQAEAER
AARELREETERAVEARQAEAAEELTRLHTEAEERRSAAEEALSGAREEGERIRREAAEESERLRTEAAERVRTL
QQQAETEAERLRTEAAADASASRAEGEAVAVRLRSEASNEAERLKTEAQESADRVRAEAQTAAERIAAEASE
ALAAAQEEAARRRREAEELLGSARQEADQERERVREQSEELLASARNRVEEAQAEAVRLVEEADRRATEMV
SAAEQHAAQVRESVAGLHEQAQEEITGLRSAAEHAAERTRTEAQEEADRVRADAYAERERASEDAGRLRRE
AQEETEAAKALAERTVSEAITEADRIRSDVSEHAQRVRTEASDAIAEAEQSASRTRADAREDANRIRSDAATQ
ADTLITEARSEAERLTTETAAETDRIRTQTLAEAERVTAEAASESERVRTEAATEAERLRTETIAEADRVRAEAG
ARAEQLVSDATGEAERLRAEAADTVGSAQQHAERLRTEADRVRREAAAEAERVTTAAREEAERTLDEARKD
ANKRRSEAAEQVDTLITETAAEADKLLTEAQQQAQKTTADAESQADTMVGAARSEADRIVQEATVEGNTRV
EKARTDADELLVGARRDATAIRERAEELRERLTSEIEELHERARREAAETMKSAGDRCDALIKAAEEQLAKAEA
KAKELVSEANSEAGKVRIAAVKKAEGLLKEAEQKKATLVREAEELKAEAVREARATVDEGKRELEVLVRRREDI
NAEISRVQDVLEALESFEAPGGAKDNGVKAGATVGAPRSGGKSSDG

Figure 44: Plasmid map of pGS2.

The plasmid pGS2 (pET28a-Scy) is a derivative of pET28a with the *scy* gene cloned using the restriction sites *Nde*I and *Eco*RI. When induced with IPTG it it leads to the production of His-Scy, which has an approximate molecular weight of 148 kDa and a theoretical pI of 4.98. The protein has an extinction coefficient of approximately 12950 $M^{-1}cm^{-1}$.
The amino acid sequence of His-Scy encoded by pGS2 is shown. The His-tag is labelled in red while the individual His residues are underlined.

4.1.1.1 Not all His-Scy binds to the column

Purification of His-Scy was attempted using an Amersham FRC FPLC machine and a HisTrap FF 1 ml column from GE Healthcare. It had previously been established that optimal production of Scy protein in *E. coli* is achieved when induced with 1 mM IPTG and incubated for 4 hours after induction at 37°C. Production of Scy was started from a single, freshly transformed BL21(DE3)pLysS colony carrying pGS2 which was inoculated into a 10 ml LB starter culture containing kanamycin and grown overnight at 37°C. The overnight growth was sub-cultured into 500 ml of LB and grown for 4 hours before induction with 1 mM IPTG. Cells were collected four hours after induction by centrifugation and washed twice with phosphate buffer (50 mM NaH_2PO_4-HCl, 50 mM NaCl; pH 8) before being re-suspended in phosphate loading buffer (50 mM NaH_2PO_4-HCl, 300 mM NaCl; 10 mM imidazole pH 8). The cells were lysed using a high pressure homogeniser French press at pressure of 1000 psi and centrifuged, after which the lysate was aliquoted and stored at -20°C.

A 3 ml sample of cell extract was loaded onto the column with a low flow rate (0.2 ml/min) to allow effective binding of His-Scy to the nickel ions in phosphate loading buffer. Once loaded, the column was washed with a higher concentration of imidazole (27 mM) and a higher flow rate (0.5 ml/min) to remove non-target proteins from the column. After washing, the remaining bound protein was eluted at 0.2 ml/min using a step increase to 300 mM Imidazole concentration (Figure 45). Fractions were collected in 1 ml aliquots in a serpentine manner with the first row consisting of fractions labelled A1-A15, the second row B15-B1, the third row C1-C15 and so forth.

From the chromatogram, appropriate samples from the load, wash and elution steps were analysed by 10% SDS-PAGE (Figure 46). It is clear that His-Scy was expressed by *E.coli*, with a large band at the approximate molecular weight of His-Scy (142 kDa) seen in the pre-load fraction of the gel. However, it is evident from the gel that only a small fraction of the His-Scy protein successfully bound to the column

as there is only comparably weak His-Scy bands in the elution fractions compared to the pre-load. Moreover, there is still a lot of His-Scy in the flow-through.

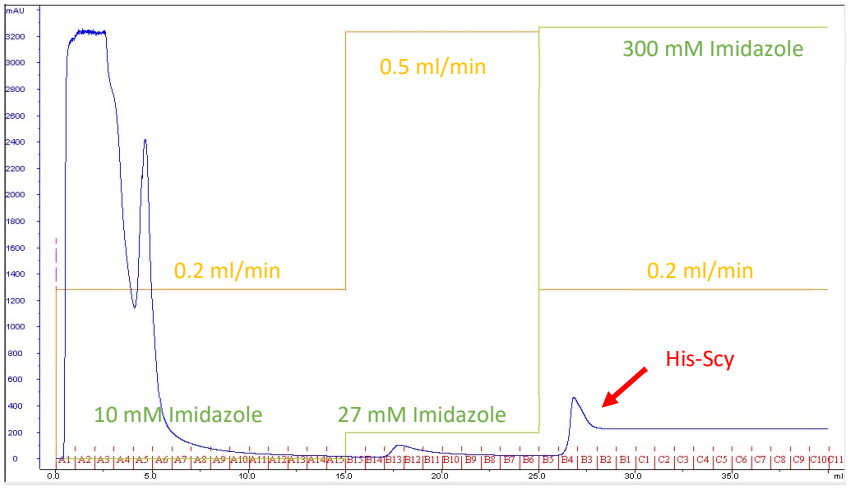

Figure 45: FPLC Chromatogram readout for the purification of His-Scy using phosphate buffer.

Cell extract was loaded onto the column in the presence of 10 mM imidazole at a low speed (0.2 ml/min, orange line), before being washed with 27 mM imidazole (green line) at a higher speed (0.5 ml/min, orange line). Elution was carried out at a low speed (0.2 ml/min, orange line) with a step increase in imidazole concentration up to 300 mM (green line). Absorbance at 280 nm was measured and is indicated by the blue line, with the scale shown on the Y axis. Samples were collected in 1 ml fractions.

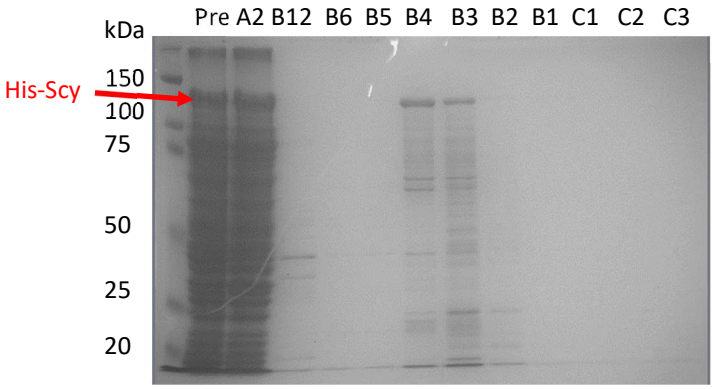

Figure 46: Purification of His-Scy in a phosphate buffer.

Fractions from Nickel-NTA affinity purification of His-Scy were analysed on 10% SDS-PAGE. Samples loaded include the pre-load (Pre), flow through (A2), wash (B12), last wash (B6) and elution fractions (B5 to C3). 5 µl of Precision Plus Protein™ All Blue Standards from Bio-Rad was loaded in the first lane (Molecular weight of marker proteins shown in kDa). Visualised by Coomassie staining.

The fact that not all the His-Scy protein bound to the column could be due to the protein being degraded after production, such that the His-tag is not present on all of the protein or that there is translation of Scy without the His-tag. Alternatively, His-Scy could be forming higher order assemblies such that the His-tag is not exposed, or that His-Scy protein that is already strongly bound to the column via the His-tag is then binding, perhaps weakly, to other nickel ions along with the rest of the column.

To test whether the His-Scy that passed through the column still possessed the His-tag another purification was performed using the collected flow through from the first purification. Should His-Scy protein from the flow through fractions still bind to the column, it would indicate that His-Scy is being inhibited from binding to the column in an efficient manner. Accordingly, the flow through was loaded onto the column, followed by washing and elution. This was done using the same conditions used in the previous purification (Figure 47).

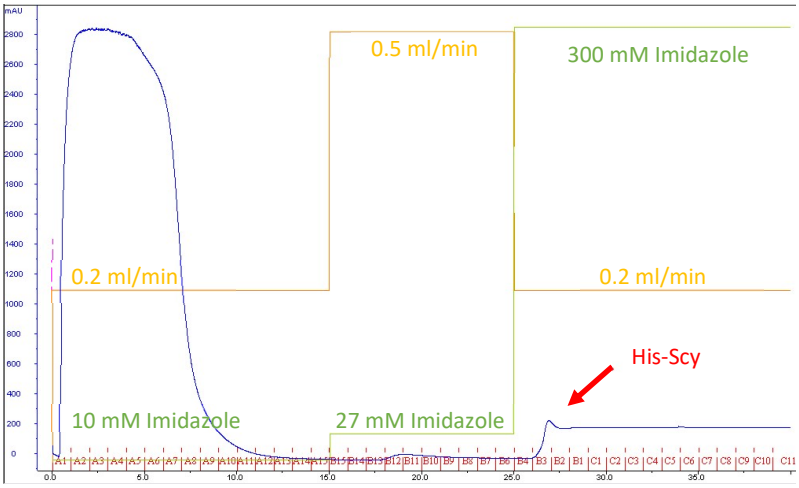

Figure 47: FPLC Chromatogram readout for the purification of His-Scy using the flow through from the previous purification.

The flow through from the previous purification was loaded onto the column in the presence of 10 mM imidazole at a low speed (0.2 ml/min, orange line), before being washed with 27 mM imidazole (green line) at a higher speed (0.5 ml/min, orange line). Elution was carried out at a low speed (0.2 ml/min, orange line) with a step increase in imidazole concentration up to 300 mM imidazole (green line). Absorbance at 280 nm was measured and is indicated by the blue line, with the scale shown on the Y axis. Samples were collected in 1 ml fractions.

From the chromatogram (Figure 47), appropriate samples from the load, wash and elution steps were analysed on 10% SDS-PAGE (Figure 49). As before His-Scy was observable in the flow through, while some His-Scy bound to the column and was successfully eluted. This suggests that the His-Scy from the flow through in the previous purification did have an intact His-tag and that its inability to bind the column was due to unavailable nickel ions in the column.

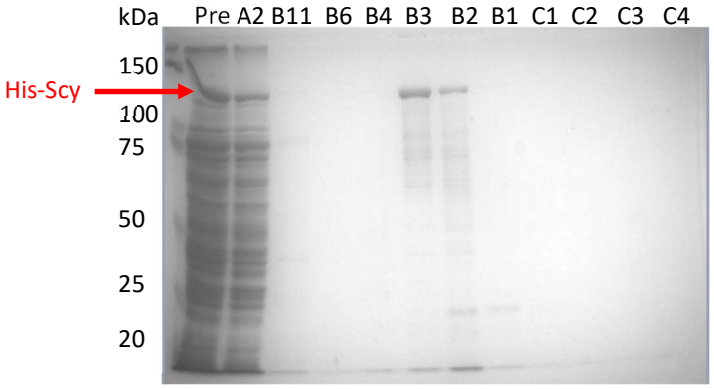

Figure 48: Purification of His-Scy using flow through from previous purification.

Fractions from Nickel-NTA affinity purification of His-Scy using flow through from previous purification were analysed on 10% SDS-PAGE. Samples loaded include the pre-load (Pre), flow through (A2), wash (B11), last wash (B6) and elution fractions (B4 to C4). 5 µl of Precision Plus Protein™ All Blue Standards from Bio-Rad was loaded in the first lane (Molecular weight of marker proteins shown in kDa). Visualised by Coomassie staining.

4.1.1.2 Magnesium allows full His-Scy binding

Previous studies in the group have shown that non-tagged Scy has some degree of affinity to Ni-Sepharose. To test whether preventing non-specific Scy interaction with the matrix would increase the binding efficiency of His-Scy we decided to try to purify His-Scy in the presence of 20 mM $MgCl_2$. This would prevent week ionic interactions between the His-Scy elemental homodimer (Walshaw et al., 2010) that could cause the His-tag to be buried within aggregated His-Scy protein as well as help prevent week ionic interactions with the binding matrix. In addition, 0.05% Tween 20 was also added as a solubilising agent to help prevent

protein aggregation. However, in a phosphate buffer, precipitation would occur due to the production of insoluble magnesium phosphate and so a Tris based buffer was used for the purification.

To test this new buffer system, production of His-Scy was carried out in a smaller scale from a cell culture of 50 ml LB. After collection by centrifugation, the cells were lysed in the Tris loading buffer (50 mM Tris-HCl, 300 mM NaCl, 20 mM $MgCl_2$, 0.05% Tween, 10 mM imidazole pH 8) using a high pressure homogeniser French press. Half of the cell extract was loaded onto the column before being washed and eluted using the same conditions used in previous purifications.

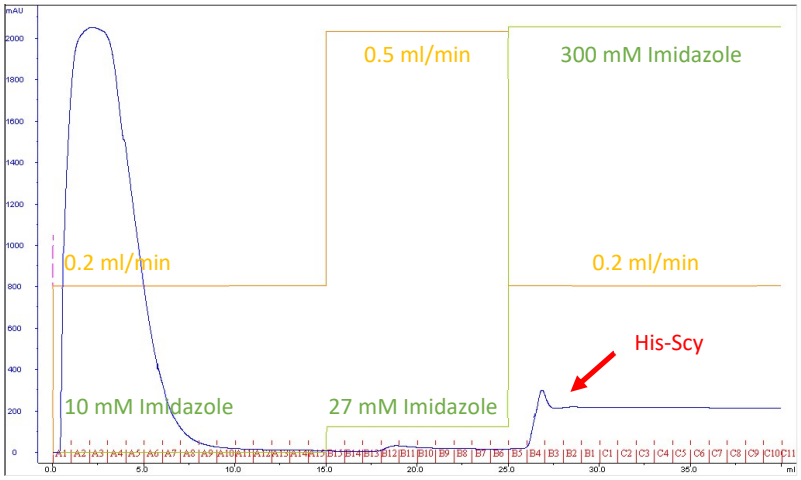

Figure 49: FPLC Chromatogram readout for the purification of His-Scy using a Tris buffer system with magnesium and Tween 20.

His-Scy was loaded onto the column in a Tris based buffer containing 20 mM $MgCl_2$ and 0.05% Tween 20 in the presence of 10 mM imidazole at a low speed (0.2 ml/min, orange line), before being washed with 27 mM imidazole (green line) at a higher speed (0.5 ml/min, orange line). Elution was carried out at a low speed (0.2 ml/min, orange line) with a step increase in imidazole concentration up to 300 mM (green line). Absorbance at 280 nm was measured and is indicated by the blue line, with the scale shown on the Y axis. Samples were collected in 1 ml fractions.

From the chromatogram (Figure 49), appropriate samples from the load, wash and elution steps were analysed using 10% SDS-PAGE (Figure 50). Unlike before very little His-Scy was present in the flow through, with the majority of the protein binding to the column. This was then successfully eluted by the step increase to 300 mM imidazole.

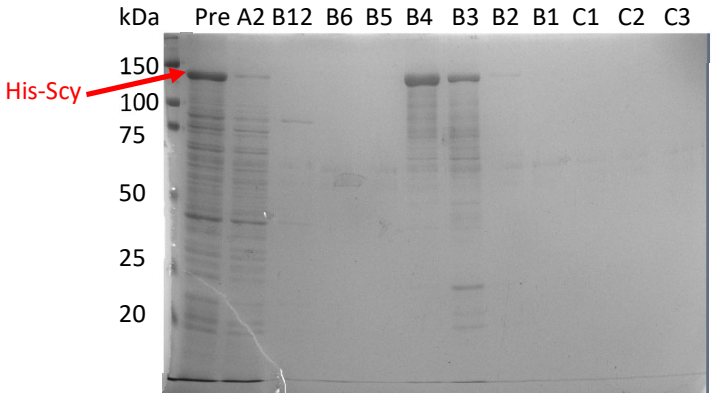

Figure 50: Purification of His-Scy in a Tris buffer system.

Fractions from Nickel-NTA affinity purification of His-Scy in a Tris buffer were analysed on 10% SDS-PAGE. Samples loaded include the pre-load (Pre), flow through (A2), wash (B12), last wash (B6) and elution fractions (B5 to C3). 5 µl of Precision Plus Protein™ All Blue Standards from Bio-Rad was loaded in the first lane (Molecular weight of marker proteins shown in kDa). Visualised by Coomassie staining.

4.1.1.3 Large Scale Purification of Scy

After successfully determining the optimal conditions for purifying His-Scy from *E. coli*, a larger purification was carried out to produce a good quantity of purified His-Scy protein. Production of His-Scy was carried out in 500 ml of LB using the established protocol previously laid out. The cells were lysed in the Tris loading buffer (50 mM Tris-HCl, 300 mM NaCl, 20 mM $MgCl_2$, 0.05% Tween, 10 mM imidazole pH 8) and purified as before but using a 5ml HisTrap HP column from GE Healthcare (Figure 51). Fractions were collected in 1 ml aliquots in a serpentine manner with the first row consisting of fractions labelled A1-A15, the second row B15-B1, the third row C1-C15 and so forth.

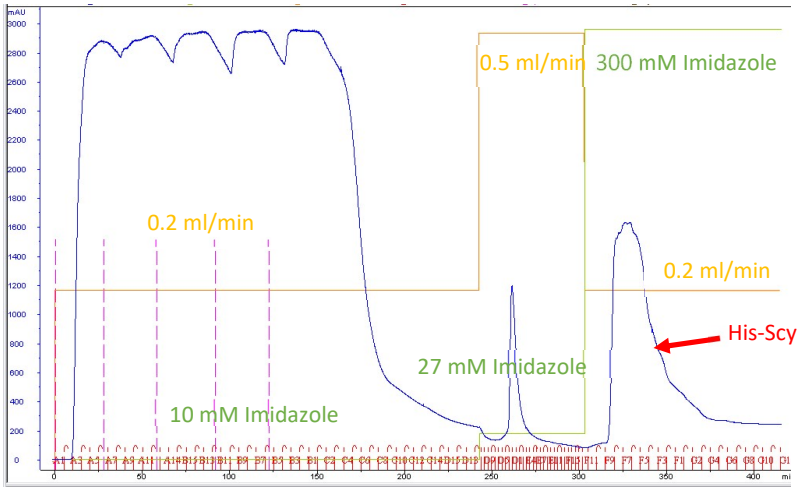

Figure 51: FPLC Chromatogram readout for the large scale purification of His-Scy using a Tris buffer system with magnesium and Tween 20.

His-Scy was loaded on to the column in a Tris based buffer containing 20 mM $MgCl_2$ and 0.05% Tween 20 in the presence of 10 mM imidazole at a low speed (0.2 ml/min, orange line), before being washed with 27 mM imidazole (green line) at a higher speed (0.5 ml/min, orange line). Elution was carried out at a low speed (0.2 ml/min, orange line) with a step increase in imidazole concentration up to 300 mM (green line). Absorbance at 280 nm was measured and is indicated by the blue line, with the scale shown on the Y axis. Samples were collected in 1 ml fractions.

From the chromatogram, appropriate samples from the load, wash and elution steps were analysed with 8% SDS-PAGE (Figure 52). His-Scy was successfully bound to the column with only a small amount of His-Scy seen in the last flow-through fraction. The wash step removed a lot of weakly bound proteins from the column, while His-Scy was eluted with a step increase in imidazole concentration. There were lots of other proteins seen in the elution, although this is relatively low compared to the amount of His-Scy. It could be that some of the contamination is degradation products of His-Scy or His-Scy which was not fully translated due to it being a large protein. Alternatively it may be *E. coli* proteins that interact with His-Scy.

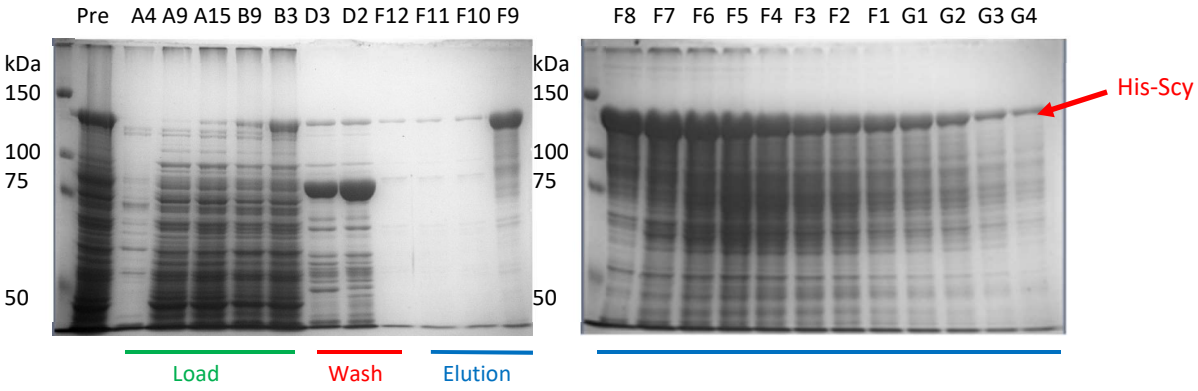

Figure 52: Large scale purification of His-Scy protein in a Tris buffer.

Fractions from the large scale FPLC nickel purification of His-Scy in a Tris buffer were analysed on 8% SDS-PAGE. Samples loaded include the pre-load (Pre), load (A4 to B3), wash (D3 and D2), last wash (F12) and elution fractions (F9 to G4). Load fractions are indicated by the solid green line under the gel while wash and elution fractions are indicated by red and blue lines respectively. 5 µl of Precision Plus Protein™ All Blue Standards from Bio-Rad was loaded in the first lane (Molecular weight of marker proteins shown in kDa). Visualised by Coomassie staining.

In order to further purify the His-Scy protein obtained through nickel purification, the protein was subjected to anion exchange chromatography using a MonoQ 5/50 (GE Healthcare) column. Routinely, proteins bind to the gel matrix in the MonoQ column under low or no salt concentrations whilst proteins are eluted with buffer containing increasing amounts of salt. Samples containing high concentrations of His-Scy were from figure 52 were combined and dialysed against a Tris based buffer (20 mM Tris-HCl pH 8). The concentrated sample was applied onto the MonoQ column using the Amersham AKTA FRC FPLC machine in the same buffer in which the His-Scy protein was dialysed against (Figure 53). Purification was monitored using Once loaded with protein the column was washed in with 10mM NaCl, before the protein was eluted using a gradient increase in concentration of NaCl up to 500 mM. Samples were collected in 1 ml fractions.

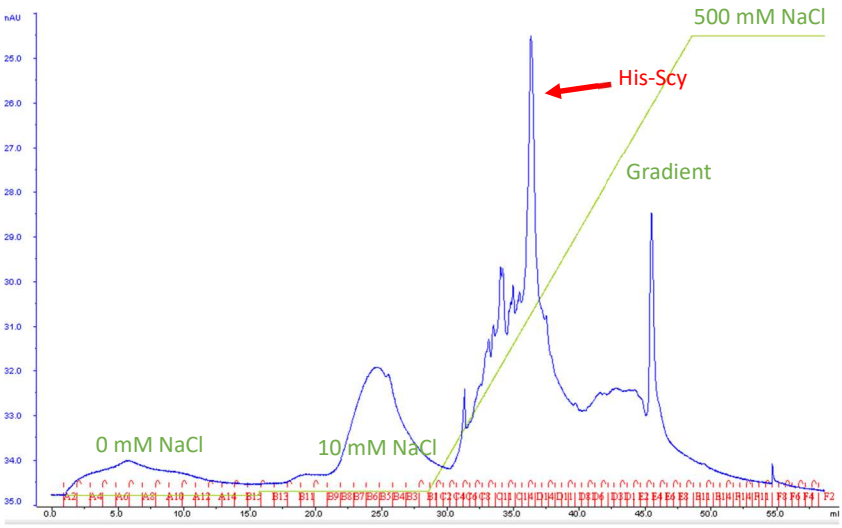

Figure 53: FPLC Chromatogram readout for ion exchange chromatography of His-Scy

Purified His-Scy obtained from nickel purification was loaded on to the column in a Tris based buffer (20 mM Tris pH 8) before being washed with 10 mM NaCl (green line). Elution was achieved with a gradient increase in NaCl concentration up to 500 mM (green line). Absorbance at 280 nm was measured and is indicated by the blue line, with the scale shown on the Y axis. Samples were collected in 1 ml fractions.

From the chromatogram, appropriate samples from the load, wash and elution steps were analysed with 8% SDS-PAGE (Figure 54A). His-Scy was eluted from the column in and is further purified compared to the nickel purification step. As not much His-Scy yield was achieved from the purification ion exchange purification was performed several times in order to produce sufficient quantities of purified His-Scy. The fractions containind eluted His-Scy were combined and dialysed against a Tris based buffer (50 mM Tris-HCl, 150 mM NaCl, 10 mM $MgCl_2$, pH 8). After dialysis we achieved a final concentration of 1.55 mg/ml purifying a total of 23.25 mg from a 500 ml culture (Figure 54B).

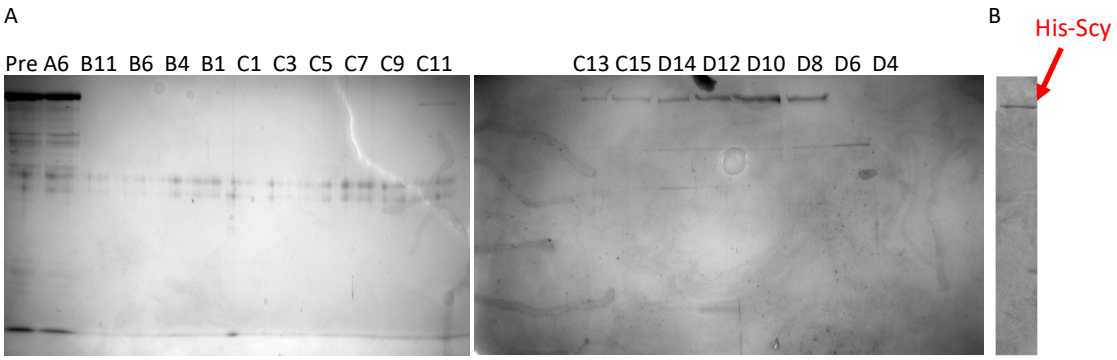

Figure 54: Purification of His-Scy protein using ion exchange chromatography.

(A) Fractions from the FPLC ion exchange chromatography purification of His-Scy in a Tris buffer were analysed on 8% SDS-PAGE. Samples loaded include the pre-load (Pre), load (A6), wash (B11), and elution fractions (B6 to D4).
(B) Final purified His-Scy protein (30 pmol)
Both gels visualised by Coomassie staining.

4.1.2 Purification of His-ParH

In order to purify ParH using nickel affinity chromatography the *parH* gene was cloned into pET28a in order to create pET28a-ParH (Figure 55). The *parH* gene was amplified from *S. coelicolor* using the primers '1772 *Xba*I *Nde*I FRW' and '1772 Eco UTC REV' before being digested with *Nde*I and *Eco*RI and cloned into pET28a. The forward primer adds an *Nde*I site which incorporates the ATG start codon from *parH* into the restriction site and allows for the in frame fusion of ParH with the His-tag. The generated His-ParH protein has an approximate molecular weight of 39 kDa with a theoretical pI of 5.09. His-ParH has an extinction coefficient higher than Scy at an estimated 19620 $M^{-1}cm^{-1}$.

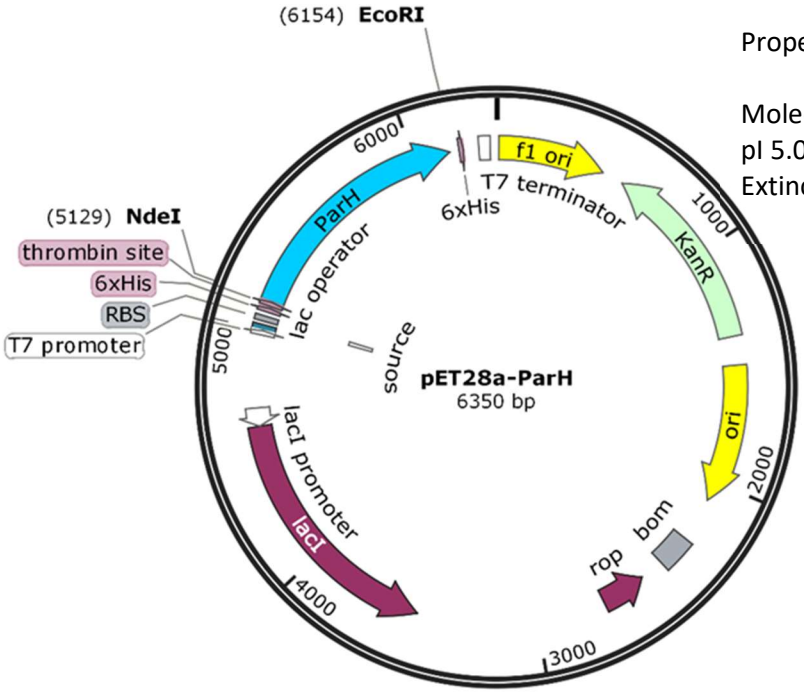

Properties of His-ParH:

Molecular Weight 39 kDa
pI 5.09
Extinction Coefficient 19620 $M^{-1}cm^{-1}$

MGSSHHHHHHSSGLVPRGSHMSMDGQHVNAMAGDGSGAPRNHFADYDELPEGHFYDPDAEYEPDPEYAA
TLAPDAARQRRERIGPTGRPLPYFPIPGPLTDHGPAKIIAMCNQKGGVGKTTSTINLGAALAEYGRRVLLVDFDP
QGALSVGLGVNPMELDLTVYNLLMERGMAADEVLLKTAVPNMDLLPSNIDLSAAEVQLVSEVARESTLQRALK
PLMDDYDYIVIDCQPSLGLLTVNALTAAHKVIVPLECEFFALRGVALLTETIEKVQERLNPDLELDGILATMYDSRT
VHSREVLARVVEAFDDHVYHTVIGRTVRFPETTVAGEPITTYASNSVGAAAYRQLAREVLARCHAE

Figure 55: Plasmid map of pET28a-ParH.

The plasmid pET28a-ParH is a derivative of pET28a with the *parH* gene cloned using the restriction sites *Nde*I and *Eco*RI. When induced with IPTG it it leads to the production of His-ParH, which has an approximate molecular weight of 39 kDa and a theoretical pI of 5.09. The protein has an extinction coefficient of approximately 19620 $M^{-1}cm^{-1}$.
The amino acid sequence of His-ParH produced by pET28a-ParH is shown. The His-tag is labelled in red while the individual His residues are underlined.

In order to determine the optimal conditions for production of His-ParH from *E. coli*, an expression test was carried out. *E. coli* BL21(DE3)pLysS cells carrying pET28a-ParH were sub cultured from an overnight culture and grown at 37°C for 4 hours in 10 ml LB containing kanamycin before induction with 1 mM IPTG. Expression was tested at 37°C, 25°C and 15°C, with 1 ml samples collected by centrifugation including pre induction, and then four hours and twenty hours after induction. The cells were re-suspended in Tris-magnesium buffer (20 mM Tris-HCl, 10 mM $MgCl_2$, pH 8) and were lysed on ice using five 15 second bursts of sonication

with 30 second intervals. The lysate was centrifuged resulting in pellet and supernatant fractions which were analysed with 10% SDS-PAGE (Figure 56). His-ParH was found to be best expressed when incubated for 20 hours after induction at 37°C. Under these conditions we see large band at the expected size of 39 kDa in the pellet fraction indicating that most of the protein is in soluble. However a small amount of His-ParH can be seen in the supernatant fractions, with the highest amount of soluble His-ParH found in the fraction corresponding to a four hour induction at 37°C. We decided to use these conditions for the production of His-ParH in order to purify the protein.

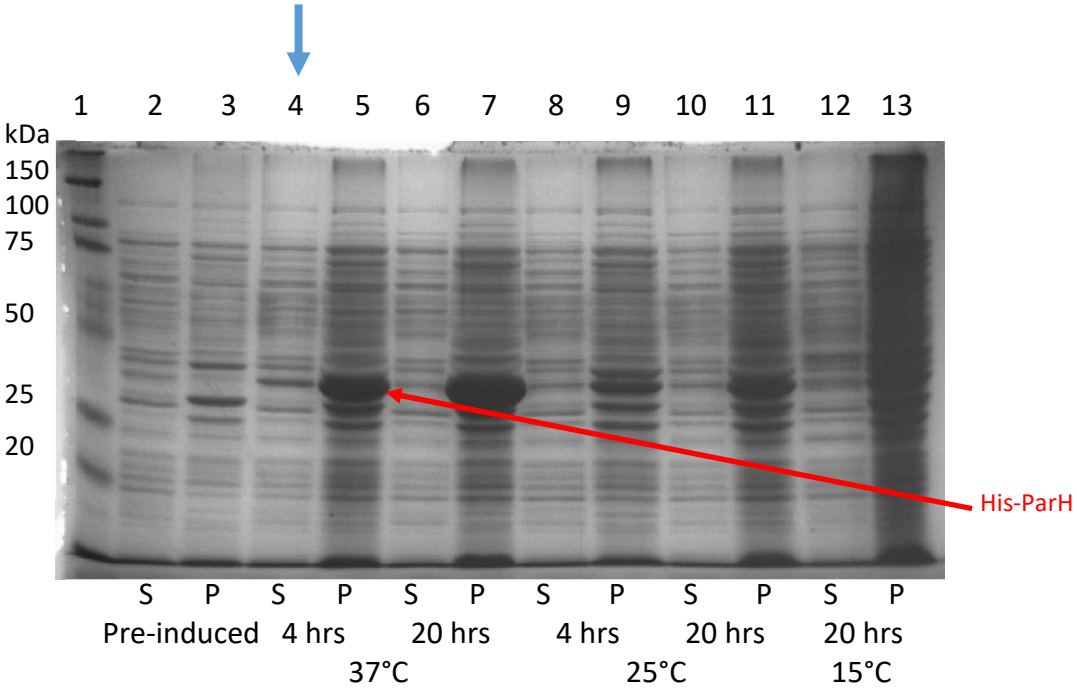

Figure 56: His-ParH expression trial.

Supernatant and pellet fractions from the His-ParH (39 kDa) expression trial in *E.coli* were run on 10% SDS-PAGE. Supernatant fractions were loaded into even lane numbers, while odd lane numbers contain pellet fractions. The samples were loaded as follows; pre-induced (2 and 3), four hours induction 37°C (4 and 5), twenty hours induction 37°C (6 and 7), four hours induction 25°C (8 and 9), twenty hours induction 25°C (10 and 11), and twenty hours induction 15°C (12 and 13). The blue arrow indicates the lane containing the fraction corresponding to the conditions used to purify His-ParH. 5 µl of Precision Plus Protein™ All Blue Standards from Bio-Rad was loaded into lane one (Molecular weight of marker proteins shown in kDa). Visualised by Coomassie staining.

For purification of ParH, a single, freshly transformed *E. coli* BL21(DE3)pLysS colony carrying pET28a-ParH was picked and grown. Induction was carried out in a 500 ml culture using the optimal conditions determined for the production of His-ParH protein. The cells were lysed in the loading buffer (50 mM Tris-HCl, 300 mM NaCl, 20 mM $MgCl_2$, 10 mM imidazole pH 8) using a Mitsubishi Electric E1061 cell disruptor set to a pressure of 30 Kpsi. Purification was carried out using a 5ml HisTrap HP nickel column (GE Healthcare) using the same protocol used for His-Scy purification with one modification. Elution was carried out using a gradient increase in imidazole concentration to 300 mM over 50 minutes instead of the step increase used for His-Scy purification. As before absorbance of proteins exiting the column was monitored at 280 nm and fractions collected in 1 ml aliquots during loading and washing but in 500 µl fractions during the elution. Fractions were collected in a serpentine manner with the first row consisting of fractions labelled A1-A15, the second row B15-B1, the third row C1-C15 and so forth.

From the chromatogram of the purification (Figure 57) appropriate samples were analysed using 10% SDS-PAGE (Figure 58A) in order to determine whether His-ParH protein was successfully purified. As can be seen from the chromatogram readout and the associated protein gels, His-ParH was successfully bound and eluted from the column. Weakly bound impurities were removed from the column during the wash step and at the lower concentration range of the gradient elution. The majority of His-ParH eluted at an imidazole concentration between 155 mM and 200 mM, although small quantities of His-ParH continued to be eluted up to as imidazole concentration of 300 mM. After purification, His-ParH was dialysed against a Tris-magnesium buffer (50 mM Tris-HCl, 150 mM NaCl, 10 mM $MgCl_2$, pH 8). After dialysis approximately 7 ml solution of His-ParH was recovered at a concentration of 1 mg/ml (Figure 58B). We successfully purified and dialysed approximately 7 mg of His-ParH from a 500 ml cell culture.

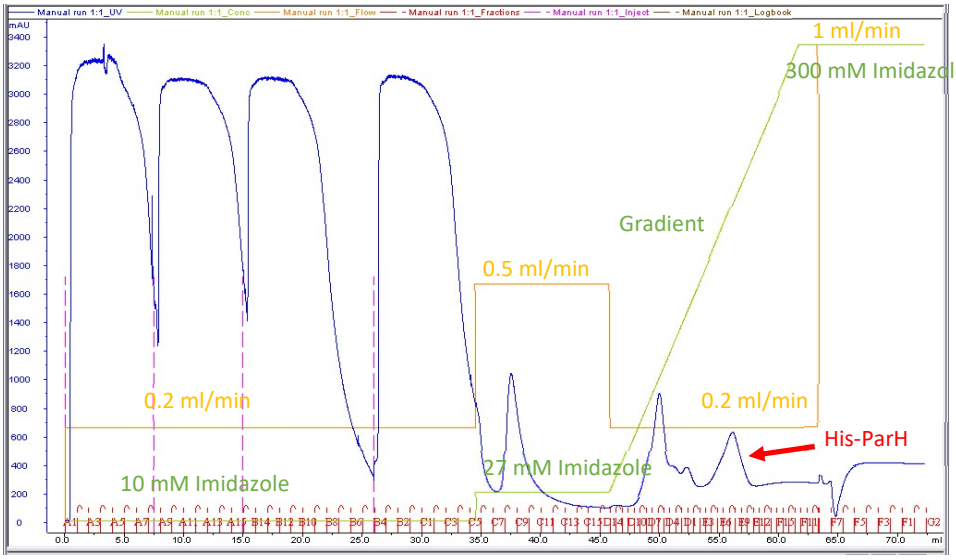

Figure 57: FPLC Chromatogram readout for the purification of His-ParH using Tris buffer.

Cell extract was loaded onto the column in the presence of 10 mM imidazole at a low speed (0.2 ml/min, orange line), before being washed with 27 mM imidazole (green line) at a higher speed (0.5 ml/min, orange line). Elution was carried out at a low speed (0.2 ml/min, orange line) with a gradient increase in imidazole concentration up to 300 mM imidazole (green line). Absorbance at 280 nm was measured and is indicated by the blue line, with the scale shown on the Y axis. Samples were collected initially in 1ml fractions throughout the load and wash steps before being collected in 500 µl fractions for the elution (red lines).

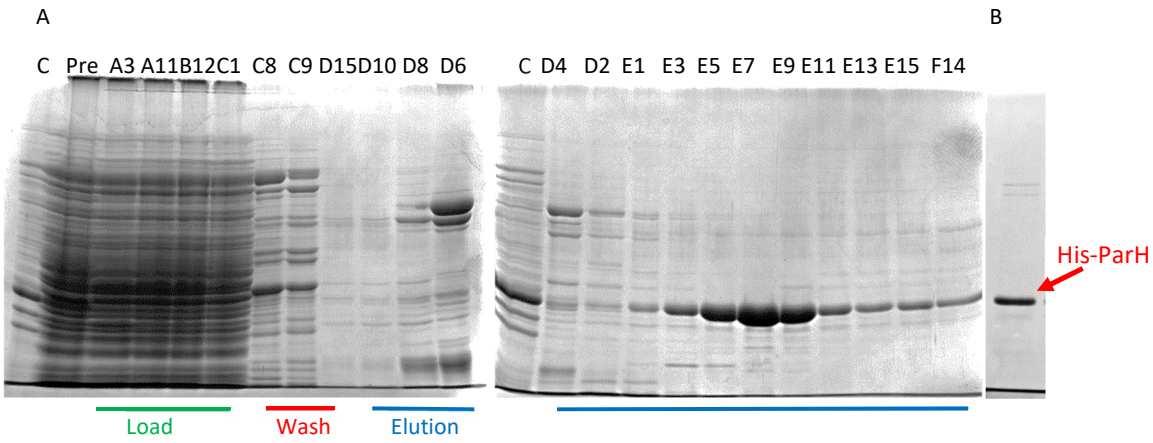

Figure 58: Purification of His-ParH

(A) Fractions from the large scale Nickel-NTA purification of His-ParH in a Tris buffer were analysed on 10% SDS-PAGE. Samples loaded include a control (C, Lane 5 from figure 56) the pre-load (Pre), load (A3 to C1), wash (C8 and C9), last wash (D15) and elution fractions (D10 to F14). Load fractions are indicated by the solid green line under the gel while wash and elution fractions are indicated by red and blue lines respectively.
(B) Final purified His-ParH protein (60 pmol)
Both gels visualised by Coomassie staining.

4.1.3.1 Purification of His-Hyp

After successfully purifying His-ParH we then moved onto purify Hyp protein using nickel affinity chromatography. To do this the *hyp* gene was cloned into pET28a in order to create pET28a-Hyp (Figure 59). The *hyp* gene was amplified from *S. coelicolor* using the primers 1771-XbaI-NdeI-FRW and 1771-Eco-UTC-REV before being digested with *Nde*I and *Eco*RI and cloned into pET28a. As before the forward primer adds an *Nde*I site which incorporates the ATG start codon from *hyp* into the restriction site and allows for the in frame fusion of Hyp to the His-tag. The generated His-Hyp protein has an approximate molecular weight of 21.5 kDa with a theoretical PI of 6.81. His-Hyp has a very low extinction coefficient at an estimated 1490 $M^{-1}cm^{-1}$.

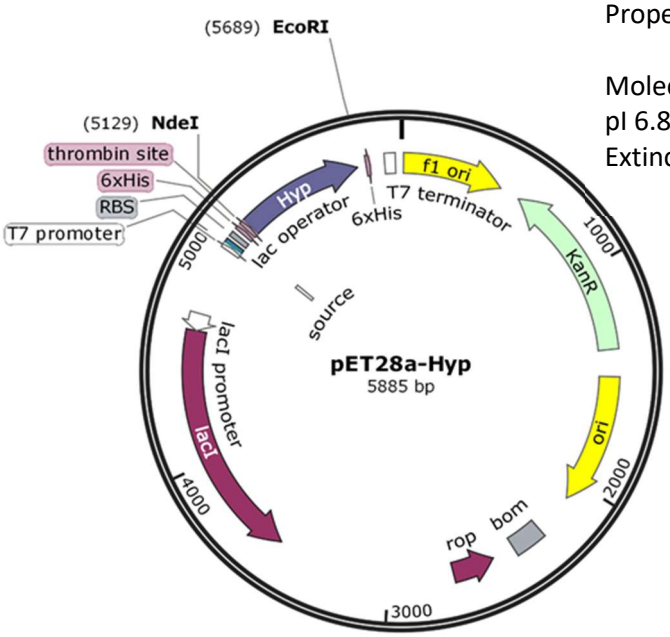

Properties of His-Hyp:

Molecular Weight 21.5 kDa
pI 6.81
Extinction Coefficient 1490 $M^{-1}cm^{-1}$

MGSSHHHHHHSSGLVPRGSHMSLPGADELFRTTGGTALQASTPRRPAGGEARVPAPAGESDQAAAEDAP
QSVPAQGGDGEGAEHAAADAEPGSAGESRTRGTERSARGSGPGSGAQEGSAADRPRKRGRSPSRRPSGRE
RHDEKITVYVSAEELMDLEHARLVLRGEHGLAVDRGRIVREAVAVVLADLETRGDASILVRRLRGR

Figure 59: Plasmid map of pET28a-Hyp.

The plasmid pET28a-Hyp is a derivative of pET28a with the *hyp* gene cloned using the restriction sites *Nde*I and *Eco*RI. When induced with IPTG it it leads to the production of His-Hyp, which has an approximate molecular weight of 21.5 kDa and a theoretical pI of 6.81. The protein has an extinction coefficient of approximately 1490 $M^{-1}cm^{-1}$.
The amino acid sequence of His-Hyp produced by pET28a-Hyp is shown. The His-tag is labelled in red while the individual His residues are underlined.

As with the purification of His-ParH, we set out to determine the optimal conditions for production of His-Hyp in *E. coli*. We used the same expression test that we utilised to determine the optimal conditions for His-ParH production. Pellet and supernatant fractions from the expression test were analysed using 12% SDS-PAGE (Figure 60). Best expression of His-Hyp was seen after induction for 20 hours at 25°C with a large band of approximately 21.5 kDa appearing in the pellet fraction under these conditions. A small amount of His-Hyp was also visible in the supernatant fraction collected under the same conditions. We decided to use these conditions for the production of His-Hyp in order to purify the protein.

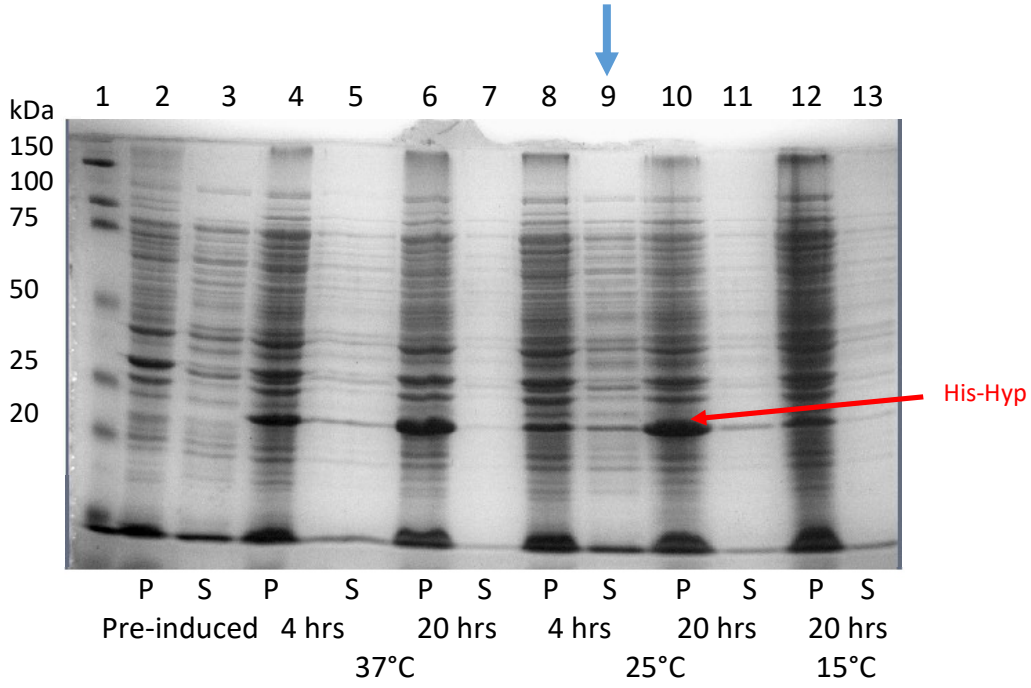

Figure 60: His-Hyp expression trial.

Supernatant and pellet fractions from the His-Hyp (21.5 kDa) expression trial in *E.coli* were analysed using 12% SDS-PAGE. Supernatant fractions were loaded into odd lane numbers, while even lane numbers contain pellet fractions. The samples were loaded as follows; pre-induced (2 and 3), four hours induction 37°C (4 and 5), twenty hours induction 37°C (6 and 7), four hours induction 25°C (8 and 9), twenty hours induction 25°C (10 and 11), and twenty hours induction 15°C (12 and 13). The blue arrow indicates the lane containing the fraction corresponding to the conditions used to purify His-Hyp. 5 µl of Precision Plus Protein™ All Blue Standards from Bio-Rad was loaded into lane one (Molecular weight of marker proteins shown in kDa). Visualised by Coomassie staining.

Purification of His-Hyp was carried out in the same way as the purification of His-ParH after production using the conditions determined in the expression trials. A 5ml HisTrap HP nickel column (GE Healthcare) was used for purification and protein leaving the column was monitored by UV absorbance at 280 nm (Figure 61). During loading of the column and the column wash, fractions were collected every 1 ml while the elution was collected in 0.5 ml fractions. Fractions were collected in a serpentine manner with the first row consisting of fractions labelled A1-A15, the second row B15-B1, the third row C1-C15 and so forth. Appropriate fractions were analysed using 12% SDS-PAGE in order to fractions containing the eluted His-Hyp protein (Figure 62A). His-Hyp was successfully purified through nickel affinity chromatography. The protein completely bound to the column with no His-Hyp seen in the flow through. Some of the non-specifically bound protein was removed during the wash step while His-Hyp remained bound to the nickel. During elution His-Hyp was successfully eluted, although during the first part of its elution profile impurities were also eluted from the column. Samples containing the purest His-Hyp elution fractions were chosen and dialysed for utilisation in further experiments.

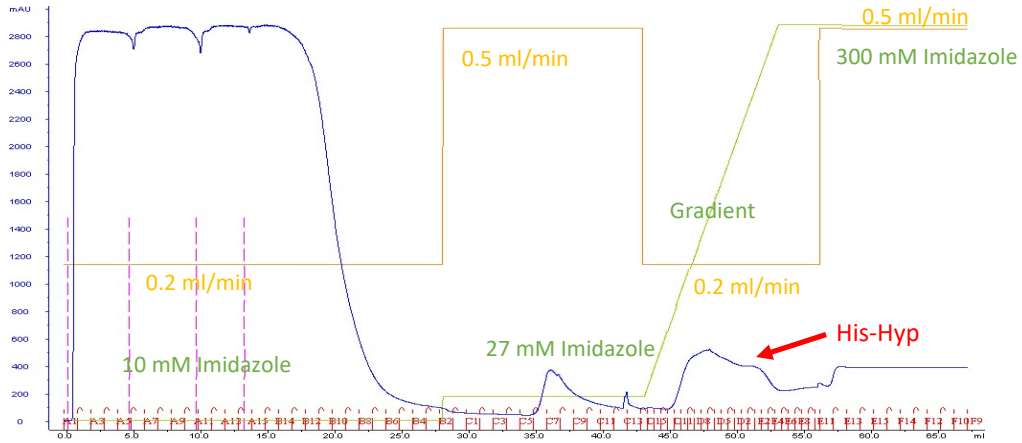

Figure 61: FPLC Chromatogram readout for the purification of His-Hyp using Tris buffer.

Cell extract was loaded onto the column in the presence of 10 mM imidazole at a low speed (0.2 ml/min, orange line), before being washed with 27 mM imidazole (green line) at a higher speed (0.5ml/min, orange line). Elution was carried out at a low speed (0.2 ml/min, orange line) with a gradient increase in imidazole concentration up to 300 mM (green line). Absorbance at 280 nm was measured and is indicated by the blue line, with the scale shown on the Y axis. Samples were collected initially in 1 ml fractions throughout the load and wash steps before being collected in 500 µl fractions for the elution (red lines).

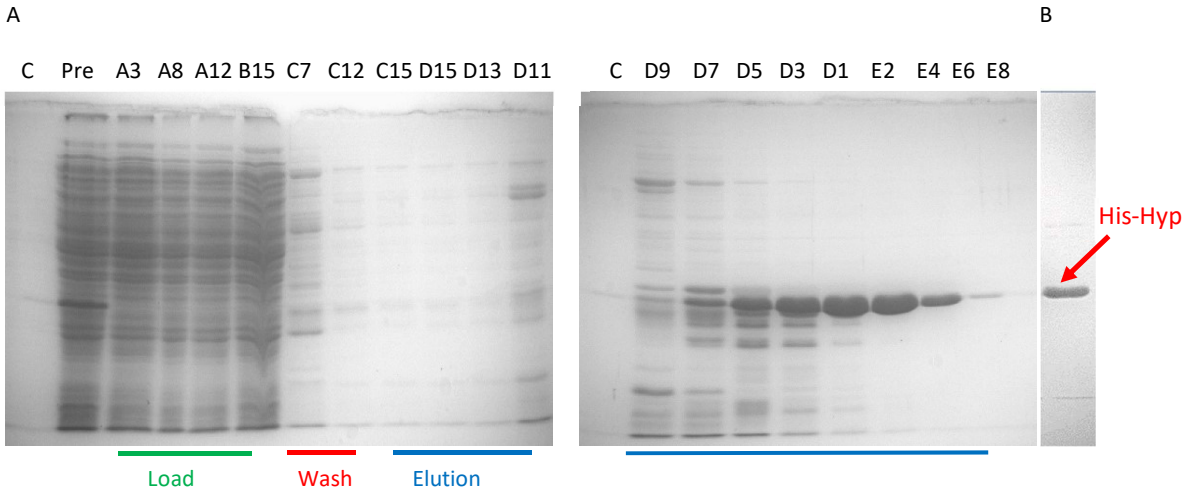

Figure 62: Purification of His-Hyp.

Fractions from the large scale Nickel-NTA purification of His-Hyp in a Tris buffer were analysed on 12% SDS-PAGE. Samples loaded include a control (C, Lane 9 from figure 60) the pre-load (Pre), load (A3 to B15), wash (C7), last wash (C12) and elution fractions (C15 to E8). Load fractions are indicated by the solid green line under the gel while wash and elution fractions are indicated by red and blue lines respectively.
(B) Final purified His-Hyp protein (60 pmol)
Both gels visualised by Coomassie staining.

4.1.3.2 Dialysis of Hyp

Initial attempts to dialyse Hyp into a Tris based buffer and remove the imidazole present in the elution buffer led to the precipitation of His-Hyp protein. This is not necessarily surprising given that previous estimates show that around 25-57% of soluble non-membrane proteins aggregate or precipitate during concentration. In fact, between 33-50% of all non-membrane proteins are insoluble to begin with (Golovanov et al., 2004; Shukla and Trout, 2011). One demonstrated method for maintaining protein solubility during dialysis and concentration is through the addition of charged L-amino acids, such as arginine and glutamate. As well as maintaining solubility during concentration, these additives have also been shown to increase the lifetime and stability of protein samples by preventing the degradation and precipitation seen in protein samples when left for periods of time. To test for a buffer that allowed His-Hyp to be maintained in a soluble form a series

of dialysis were carried out against Tris buffer (30 mM Tris-HCl, 150 mM NaCl, 10 mM $MgCl_2$, pH 7.5) containing different additives (Table 8). Concentration of His-Hyp was measured both before and after dialysis into each of the buffer conditions. From this experiment it is clear that His-Hyp had a lower solubility limit without the addition of arginine, with less than 50% of the protein recovered after dialysis. The addition of 100mM and 200 mM arginine to the buffer resulted in increased recovery rates after dialysis of 79% and 89% respectively. Therefore we decided to dialyse His-Hyp against a Tris buffer containing 200 mM arginine (50 mM Tris-NaOH, 150 mM NaCl, 10 mM $MgCl_2$, 200 mM Arginine pH 8). After dialysis approximately 5 ml solution of His-Hyp was recovered at a concentration of 2.97 mg/ml (Figure 62B). We successfully purified and dialysed approximately 14.85 mg of His-Hyp protein from a 500 ml cell culture.

Table 8: Table showing the percentage recovery of His-Hyp after dialysis with different additives.

Buffer Additive	Concentration of His-Hyp before dialysis (mg/ml)	Volume before dialysis (µl)	Concentration of His-Hyp after dialysis (mg/ml)	Volume after dialysis (µl)	Amount of His-Hyp before dialysis (µg)	Amount of His-Hyp after dialysis (µg)	Recovery (%)
None	0.13	440	0.09	550	58.29	47.41	81.34
None	1.50	200	0.40	250	300	100	33.33
10% Glycerol	1.50	200	0.51	270	300	138.04	45.97
100mM Arginine	1.45	200	0.67	320	289.01	226.99	78.54
200mM Arginine	1.45	200	0.81	320	289.01	257.80	89.20

4.1.4 Purification of His-ParB

We next wished to purify ParB, so the *parB* gene was cloned into pET28a in order to create pET28a-ParB (Figure 63). The *parB* gene was amplified from *S. coelicolor* using the primers 'ParB XbaI NdeI FRW' and 'ParB Eco UTC REV' before being digested with *Nde*I and *Eco*RI and cloned into pET28a. Like with other genes, the forward primer adds an *Nde*I site which incorporates the ATG start codon from *parB* into the restriction site and allows for the in frame fusion of ParB to the His-tag. The generated His-ParB protein has an approximate molecular weight of 38 kDa with a theoretical pI of 5.67. His-ParB has a very low extinction coefficient at an estimated 3105 $M^{-1}cm^{-1}$.

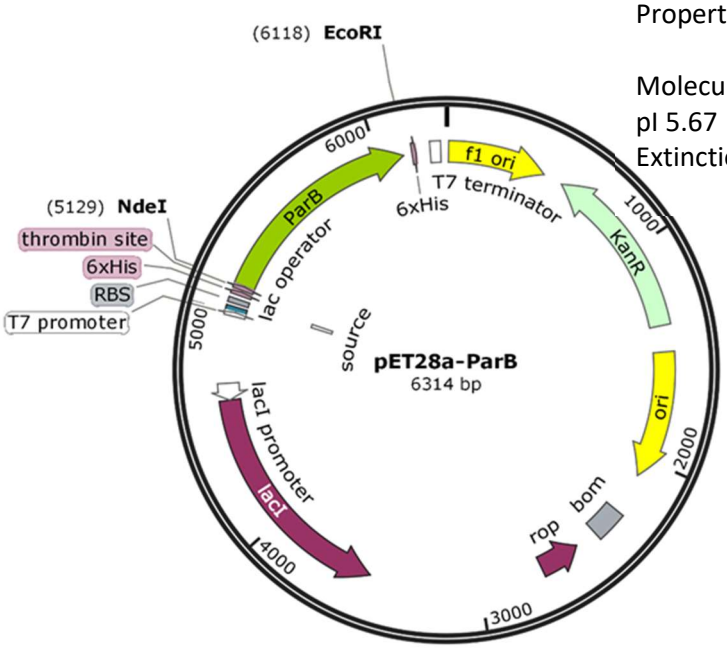

Properties of His-ParB:

Molecular Weight 38 kDa
pI 5.67
Extinction Coefficient 3105 $M^{-1}cm^{-1}$

MGSSHHHHHHSSGLVPRGSHMPLLPNERGVAAAKVATLQHVSRETEELTAPQGVEGLRPPMGAHFAEVPL
DAITPNPKQPRKDFDDDALAELVTSIREVGLLQPVVVRPTEPGRYELIMGERRFRACRELELDAIPAIVRATED
EKLLLDALLENLHRAQLNPLEEAFAYDQLLKDFNCTHDQLADRIGRSRPQVSNTLRLLKLSPKVQNRVAAGVL
SAGHARALLSVDDPEEQDRLAHRIVAEGLSVRSVEEIVTLMGSRPQKPQRAKGPRAGSLVSPALSDLATRLSD
RFETRVKVDLGQKKGKITVEFASMDDLERILGSLAPGEGPVLQKGLLEGEDEDGDAES

Figure 63: Plasmid map of pET28a-ParB.

The plasmid pET28a-ParB is a derivative of pET28a with the *parB* gene cloned using the restriction sites *Nde*I and *Eco*RI. When induced with IPTG it it leads to the production of His-ParB, which has an approximate molecular weight of 38 kDa and a theoretical PI of 5.67. The protein has an extinction coefficient of approximately 3105 $M^{-1}cm^{-1}$.
The amino acid sequence of His-ParB produced by pET28a-ParB is shown. The His-tag is labelled in red while the individual His residues are underlined.

The optimal conditions for the production of His-ParB were investigated using the same protocol employed to determine optimal production of His-ParH and His-Hyp. In order to determine the optimal conditions for production of His-ParB *E. coli*, an expression test was carried out. Pellet and supernatant fractions from the expression test were analysed using 10% SDS-PAGE (Figure 64). A band of approximately 38 kDa was observable in pellet fractions under the conditions tested. This is not surprising as previous studies had indicated this to be the case (Jakimowicz et al., 2002). In those studies ParB was purified using a GST tag designed to solubilise proteins using Glutathione S-transferase, which can then be cleaved. As we did not have the materials to purify GST-tagged ParB we decided to attempt to purify ParB under denaturing conditions using urea.

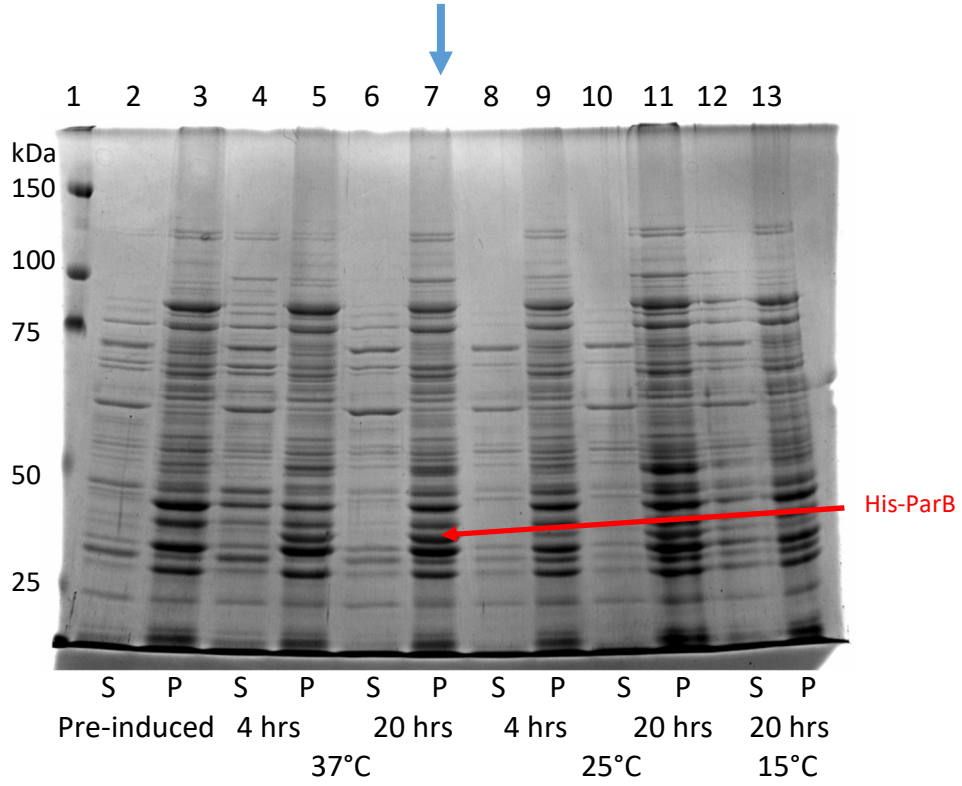

Figure 64: His-ParB expression trial.

Supernatant and pellet fractions from the His-ParB (38 kDa) expression trial in *E.coli* were analysed using 10% SDS-PAGE. Supernatant fractions were loaded into even lane numbers, while odd lane numbers contain pellet fractions. The samples were loaded as follows; pre-induced (2 and 3), four hours induction 37°C (4 and 5), twenty hours induction 37°C (6 and 7), four hours induction 25°C (8 and 9), twenty hours induction 25°C (10 and 11), and twenty hours induction 15°C (12 and 13). The blue arrow indicates the lane containing the fraction corresponding to the conditions used to purify His-ParH. 5 µl of Precision Plus Protein™ All Blue Standards from Bio-Rad was loaded into lane one (Molecular weight of marker proteins shown in kDa). Visualised by Coomassie staining.

This breaks down all proteins and membranes to their basic state without any structure, allowing the purification of previously insoluble proteins. After purification, the protein can be re-folded through dialyses to an aqueous buffer. His-ParB was produced in its highest quantities when induced over night at 37°C, and thus these conditions were used for purification.

Production of His-ParB, in order to achieve large scale purification, was carried out in a 500 ml LB culture using the optimal conditions derived from the expression test. Cell lyses was initially carried out under native conditions using the same method utilised in purification of His-ParH and His-Hyp. After lyses the supernatant was discarded and the pellet re-suspended in denaturing loading buffer (8 M urea-HCl, 0.1 M NaH_2PO_4, 0.01 M Tris pH 8). Purification was carried out using the denaturing purification protocol using a gravity flow column from Novogen which contained approximately 2 ml Nickel Sepharose. Purification of proteins under denaturing conditions requires elution based on a change in pH. Histidine residues bind to Ni^{2+} ions due to it being deprotonated above pH 7. Below this the amino acid becomes deprotonated and loses affinity to Ni^{2+} ions. Thus the wash set was done in urea buffer at pH 6.3 and elution at pH 4.5, also in a urea buffer. The load and wash were collected in single fractions while the elution was collected in 1 ml aliquots. Fractions were analysed by 10% SDS-PAGE (Figure 65A).

From the gel, it is clear that His-ParB was produced in much higher quantities than we achieved in the expression trial. There is a very strong band with a molecular weight consistent with the molecular weight of His-ParB (38 kDa). It could be that the cells were not in an optimal growth phase when induced during the expression trial. While not all the His-ParB protein bound to the column, there was probably a greater amount than the binding capacity of the column, we were able to elute concentrated His-ParB. Our initial attempt to re-fold the protein by dialysing against a Tris buffer (50 mM Tris-HCl, 150 mM NaCl, 10 mM $MgCl_2$, pH 8) resulted in the protein precipitating. We theorised that this could either be because the protein was in buffer conditions with changing pH from pH 4.5 to pH 8, which passes through the pI of the protein (5.67) which would remove all charge, or because the protein is not soluble at the concentration in which it eluted. We decided to solubilise the protein by centrifuging the precipitate and re-suspending in the denaturing loading buffer (8

M urea, HCl 0.1 M NaH_2PO_4, 0.01 M Tris pH 8). We also diluted the protein to one tenth its initial concentration. We hoped that this would help to prevent precipitation during dialyses. We again dialysed the protein against the same buffer as before. The protein again precipitated during dialyses, although this time some of the protein remained in solution. We tried to measure the protein concentration but it was very dilute so a reading was difficult to achieve. We decided therefore to test whether we could concentrate the protein to a usable concentration. After concentration, we recovered around 1 ml of purified His-ParB protein with a concentration of 0.5 mg/ml (Figure 65B). We therefore managed to successfully purify and dialyse approximately 0.5 mg of His-ParB protein from a 500 ml cell culture.

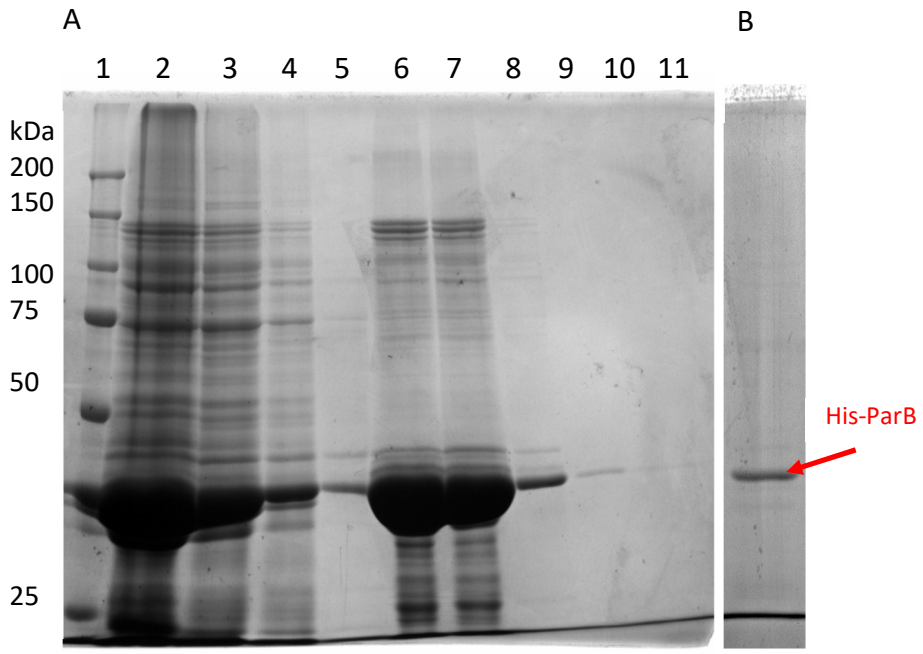

Figure 65: Purification of His-ParB under denaturing conditions.

Fractions from the purification of His-ParB (38 kDa) were analysed on 10% SDS-PAGE. Pre-load (2), Flow through (3), Wash (4) and Elution fractions (5-11) were analysed alongside a protein marker (1). 5 µl of Precision Plus Protein™ All Blue Standards from Bio-Rad was loaded into lane one (Molecular weight of marker proteins shown in kDa).
(B) Final purified His-Hyp protein (60 pmol)
Both gels visualised by Coomassie staining.

4.1 Protein Purification

4.2.1 Analytical Gel Filtration

A key feature of ParA like proteins is their ability to form higher order assemblies or dimers, usually in the presence of ATP. The oligomeric state often affects the role of the protein in a cell with the switch between different states acting as a regulator in the cell for cell division and chromosome segregation (Gerdes et al., 2010; Gruber and Errington, 2009; Ptacin et al., 2010). One method for determining the oligomeric state of a protein is though size exclusion chromatography, or gel filtration when using an aqueous solution. This technique allows for the separation and elution of proteins based upon their molecular weight.

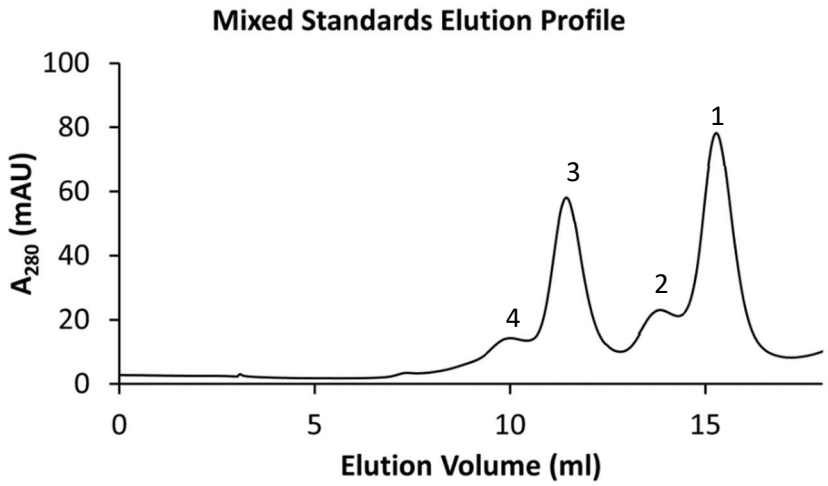

Figure 66: Elution profile of protein standards.

Standard proteins standards were analysed using a Superdex 200 10/300 GL column from GE Healthcare. The elution profile of (1) Egg Albumin (45 kDa), (2) Bovine Serum Albumen (66 kDa), (3) Alcohol Dehydrogenase (150 kDa) and (4) Ferritin (446 kDa) were monitored via UV absorbance at 280nm. The proteins were analysed using a Superdex 200 10/300 GL column from GE Healthcare. Blue Dextran (2000 kDa) and Cytochrome C (12.4 kDa) were analysed separately and are not shown.

For analytical gel filtration, a Superdex 200 10/300 GL column from GE Healthcare was used, which has a resolution between 10 kDA and 600 kDa. In order to calibrate the column such that the molecular weight of a protein of unknown molecular weight could be determined by its elution profile, several proteins of known molecular weight were passed through the column. Blue Dextran, which has a molecular weight of 2000 kDa, was used to determine the void volume of the column, while Cytochrome C (12.4 kDa), Egg Albumin (45 kDa), Bovine Serum Albumen (66 kDa), Alcohol Dehydrogenase (150 kDa) and Ferritin (446 kDa) were used to generate a calibration curve. Proteins were loaded onto the column in a 500 µl volume containing approximately 0.5 mg of each protein at a speed of 0.5 ml/min and run in a buffer containing 20 mM Tris-HCl, 150 mM NaCl, 10 mM $MgCl_2$ pH 7.5. The elution was measured by UV absorbance at a wavelength of 280 nm to determine the elution volume for each protein (Figure 66).

The calibration curve was calculated by working out the partition coefficient (K_{av}) of each protein (Table 9) in which V_e represents the elution of the protein, V_o the void volume and V_t the total volume of the column (24ml).

$$K_{av} = \frac{(V_e - V_o)}{(V_t - V_o)}$$

This determines the partition coefficient by dividing the elution of a protein from the void volume of the column (V_e-V_o) with the fraction of the stationary phase that is available for diffusion (V_t-V_o). The K_{av} was then plotted against the logarithmic weight of each protein to generate the calibration curve (Figure 67).

Table 9: Table showing protein standard measurements for calibration of Superdex 200 10/300 GL column

Protein	MW (kDa)	Log (MW)	Elution Volume (ml)(V_e)	V_e-V_o	V_t-V_o	K_{av}
Blue Dextran	2000	N/A	7.43 (V_o)	N/A	N/A	N/A
Ferritin	446	2.65	9.99	1.34	16.57	0.15
Alcohol Dehydrogenase	150	2.18	11.49	1.55	16.57	0.25
Bovine Serum Albumen	66	1.82	13.89	1.87	16.57	0.39
Egg Albumin	45	1.65	15.29	2.06	16.57	0.47
Cytochrome C	12.4	1.09	17.93	2.41	16.57	0.63

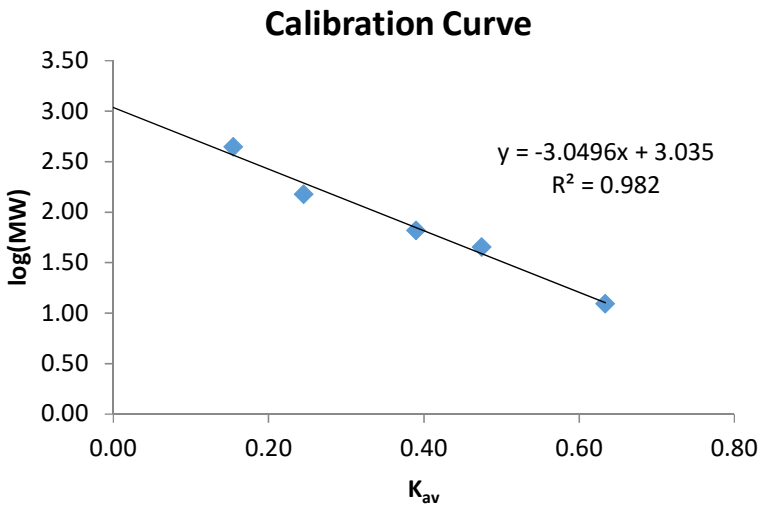

Figure 67: Calibration curve of the Superdex 200 10/300 GL column from GE Healthcare.

The partition coefficient (Kav) was plotted against the logarithmical molecular weight of each protein.

4.2.2 Analytical Gel Filtration of ParH reveals that it has multiple oligomeric states

After calibration of the gel filtration column, His-ParH was applied onto the column so that its oligomeric state could be determined. Around 350 µg of His-ParH was loaded in 500 µl of 20 mM Tris-HCl, 150 mM NaCl 10 mM $MgCl_2$ pH 7.5 buffer on to the gel filtration column at a speed of 0.5 ml/min. The running buffer was the same as the loading buffer with the addition of 5 mM DTT and the elution profile of His-ParH was monitored by measuring UV absorbance at 280 nm of the eluate (Figure 68). The elution volume of the peaks obtained were measured against the calibration curve and the molecular weight determined for each of the peaks observed (Table 10).

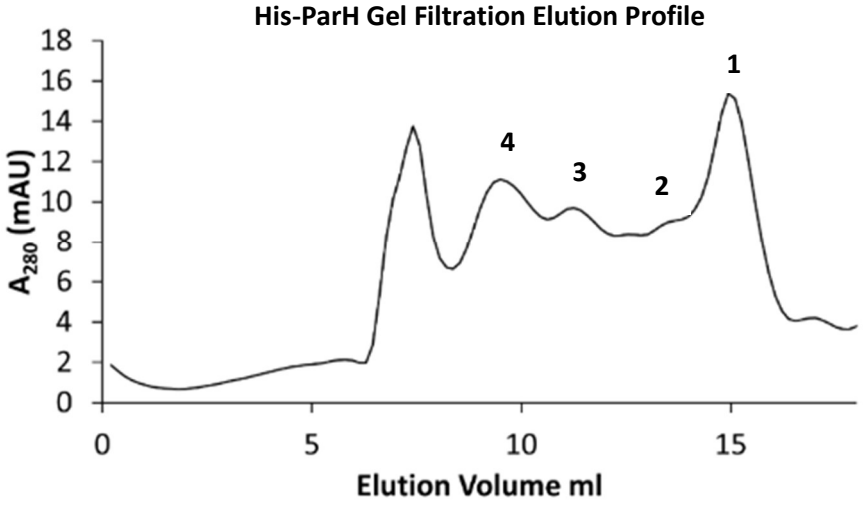

Figure 68: His-ParH elution profile determined by analytical gel filtration.

Approximately 350 µg of His-ParH was loaded onto a Superdex 200 10/300 GL column from GE Healthcare. The eluate was monitored by UV absorbance measured at 280 nm. ParH exhibited multiple peaks, suggesting that it exists as multiple forms of oligomers.

Table 10: Table showing calculations of oligomeric state of His-ParH peak measurements from Superdex 200 10/300 GL column

Peak	V_e (ml)	K_{av}	$Log_{(MW)}$	Molecular Weight (kDa)	Theoretical Oligomer
1	14.94	0.45	1.65	44.92	Monomer
2	13.5	0.37	1.92	82.73	Dimer
3	11.26	0.23	2.33	214.03	Pentamer
4	9.5	0.12	2.65	451.42	11mer

His-ParH eluted as multiple peaks from the analytical gel filtration column suggesting that it exists as different oligomers. The smallest oligomer of His-ParH eluted 14.94 ml after loading which is consistent with a protein of 44.92 kDa. This is close to the molecular weight of monomeric His-ParH which would be 39 kDa suggesting that ParH has monomeric units from which to build higher order assemblies. The next smallest oligomer eluted 13.5 ml (82.73 kDa) after loading which would most likely correspond to a dimer of His-ParH (78 kDa). Oligomers higher than monomers and dimers become hard to differentiate as the difference in molecular weight becomes smaller relative to the size of the oligomer. Thus while peaks can be detected that correspond to a pentamer and an 11mer, there is little confidence in the accuracy of these measurements. What is probable is that His-ParH forms many different oligomers within the resolution range of the column. In addition, His-ParH also eluted in the void volume suggesting that ParH is able to form higher order assemblies with over 15 monomeric subunits. What is noticeable is that the monomeric His-ParH peak had the highest UV absorption of all of the observable peaks. This suggests that the His-ParH sample contains more monomers than any other oligomeric state. Assuming a linear increase in extinction coefficient relative to the oligomeric state then the amount of monomeric His-ParH in the solution is relatively high.

4.2.3 Hyp is a tetrameric protein

After the oligomeric state of His-ParH was determined, His-Hyp was also analysed by analytical gel filtration to determine its oligomeric state. Around 1.5 mg of His-Hyp was loaded in 500 µl of 20 mM Tris-NaOH, 150 mM NaCl 10 mM $MgCl_2$, 200 mM arginine pH 7.5 buffer on to the gel filtration column at a speed of 0.5 ml/min. The running buffer was the same as the loading buffer with the addition of 5 mM DTT and the elution profile of His-Hyp was monitored by measuring UV absorbance at 280 nm of the eluate (Figure 69). The elution volume of the peak obtained was measured against the calibration curve and the molecular weight determined.

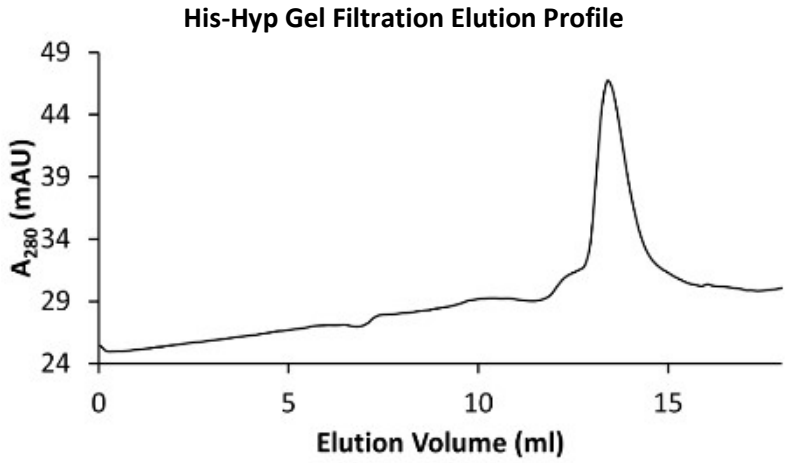

Figure 69: His-Hyp elution profile determined by Analytical Gel Filtration.

Approximately 1.5 mg of His-Hyp was loaded onto a Superdex 200 10/300 GL column from GE Healthcare. The eluate was monitored by UV absorbance measured at 280 nm. His-Hyp exhibited a single peak with an elution volume consistent with a tetrameric His-Hyp oligomer.

His-Hyp eluted as a single peak from the analytical gel filtration column, suggesting that it exists as a single oligomer. The peak eluted 13.6 ml after loading which is consistent with a molecular weight of 80 kDa. This is very close to the

molecular weight of a tetrameric His-Hyp, which would have a molecular weight around 84 kDa.

4.2.4 ParH has a pattern to its oligomeric assembly

While analytical gel filtration indicated that ParH formed multiple oligomers, it was not possible to distinguish the stoichiometry of the assemblies higher than a dimer. Thus in order to determine whether there was an ordered pattern of the different ParH oligomers, native-PAGE was carried out using purified His-ParH protein. In SDS-PAGE, proteins are denatured to monomers in order that proteins will run according to their monomeric molecular weight when compared to protein standards. This is achieved by subjecting the protein to SDS, which applies a negative charge to the protein in proportion to its mass, DTT or β-mercaptoethanol, which reduces any disulphide bonds, and boiling, which disrupts quaternary, tertiary and secondary structures. Native-PAGE on the other hand involves running proteins in an acrylamide gel while maintaining higher order assemblies and the native shape of the protein. The fact that protein shape and charge is maintained means that it is not possible to compare the migration patterns of different proteins to understand molecular weight. It does however, allow different oligomers of the same protein to be observed, and thus determine if any pattern exists.

To test the oligomers of His-ParH using native PAGE, His-ParH protein (200 pmol/10 μM) was incubated both independently and in the presence of His-Hyp either in a 1:2 ratio (400 pmol/20 μM), or 1:4 ratio (800 pmol/40 μM) for 30 minutes at room temperature in a phosphate salt buffer (50 mM NaH_2PO_4-HCl, 150 mM NaCl pH 8.5). After incubation the samples were analysed using 6% native-PAGE and run for 2 hours at a low voltage (100 V) to avoid overheating the gel so that the native protein remained intact. The gel was then silver stained to observe the ParH oligomers (Figure 70).

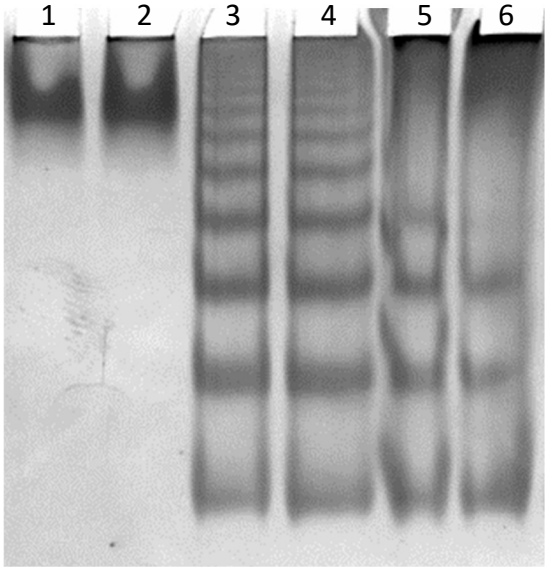

Figure 70: Native-PAGE of His-ParH and His-Hyp

His-ParH (200 pmol/10 µM) and His-Hyp were incubated both separately and together before analysis using 6% native-PAGE. His-Hyp (Lane 1 400 pmol/20 µM, Lane 2 800 pmol/40 µM) ran as a single band consistent with analytical gel filtration. His-ParH (lanes 3 and 4) produced multiple bands in a ladder-like formation. When the proteins were mixed either in a 1:2 ratio (Lane 5) or a 1:4 ratio (Lane 6) some of the higher weight His-ParH bands disappeared, suggesting interaction between His-Hyp and His-ParH. Visualised by silver staining.

In its native form, His-ParH appears as multiple bands in a ladder-like formation with at least 10 bands being discernible (Figure 70). This complements the analytical gel filtration data for His-ParH which indicated the presence of different oligomers. A key feature of the His-ParH bands is the regular spacing of the bands on the gel which get closer together the higher the oligomer. This spacing pattern is probably the result of a regular increase in size being offset by the resolution of the gel. This suggests that each oligomer is built from the previous oligomer through the addition of a common subunit, for example a monomer or a dimer. Analytical gel filtration, through which we were able to discern both monomeric and dimeric His-ParH, suggests this subunit to be a monomer. His-Hyp on the other hand, forms a single band which is consistent with the analytical gel filtration data that suggested Hyp is tetrameric. When the proteins were mixed, there is a disappearance, not only

of His-ParH bands but the His-Hyp band as well. In their place is a band at the very top of the gel and a short smear underneath. This suggests that both proteins interact with each other, forming a higher order assembly. Interestingly the three lowest His-ParH bands remain unchanged, which could indicate that this interaction is between Hyp and higher oligomers of ParH.

4.2.5 ParH oligomers are built from monomer subunit

As previously stated it is not possible to determine the molecular weight of individual ParH oligomers from their migration using native PAGE in a similar fashion to SDS-PAGE. One technique that overcomes the individual properties of proteins make them incomparable in native PAGE is the so called Ferguson plot. This technique involves measuring the migration pattern of proteins across a range of

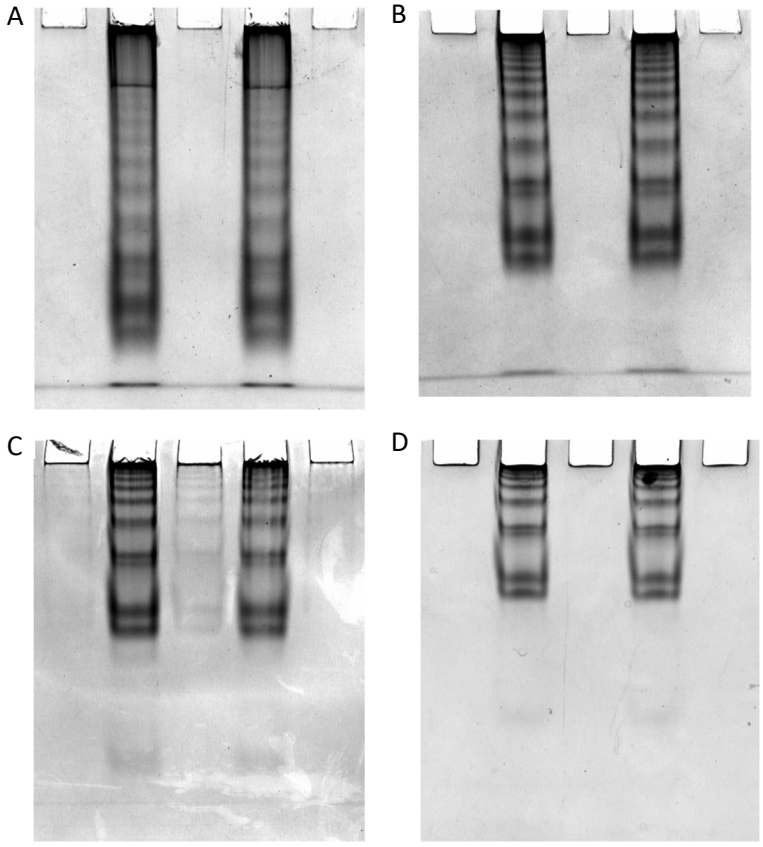

Figure 71: Native-PAGE of His-ParH used for Ferguson plot.

His-ParH was run on four gels with differing acrylamide percentage; (A) 6%, (B) 8%, (C) 10% and (D) 12%. The migration distance (mm) of the first six bands were measured to calculate a Ferguson Plot. Visualised by silver staining.

different percentage acrylamide gels. Each band will migrate a different distance on each gel, which when measured, the log of relative migration (mobility) can be plotted against the percentage of the gel. From this the retardation coefficient (Kr), which is the gradient of the line that intercepts the points, for each band can be found. By having two bands of known molecular weight, the Kr values of these bands can then be plotted against their molecular weight, generating a calibration curve for the native gels.

In order to calculate the Ferguson plot, four different concentrations of native-PAGE (6%, 8%, 10% and 12%) were made and His-ParH loaded in a Tris Buffer (50 mM Tris-HCl, 150 mM NaCl, 10 mM $MgCl_2$ pH 7.5). The gels were run simultaneously at a low voltage (100 V) for 3 hours and then silver stained (Figure 71). Surprisingly the bands appeared as a doublet when His-ParH was maintained in a Tris buffer system compared to the single bands that were visible in the phosphate system. The reason for moving to a Tris based buffer was in order to be able to perform experiments with ATP. Protein-ATP binding is promoted by the presence of Mg^{2+} ions, and as discussed before $MgCl_2$ is not compatible with a phosphate based buffer system. The doublets could be due to two different conformations that the protein can form depending on how it interacts with its environment.

After silver staining the migration of each of the first six bands was measured along with the migration of the leading edge of the gel. For each band, its mobility (R_f) was calculated by dividing the migration of the band by the leading edge of the individual gel. This value was then multiplied by 100, so that the log (R_f) was a positive number. The log (R_f x 100) was plotted against the acrylamide percentage (T%) to generate a curve for each band (Figure 72).

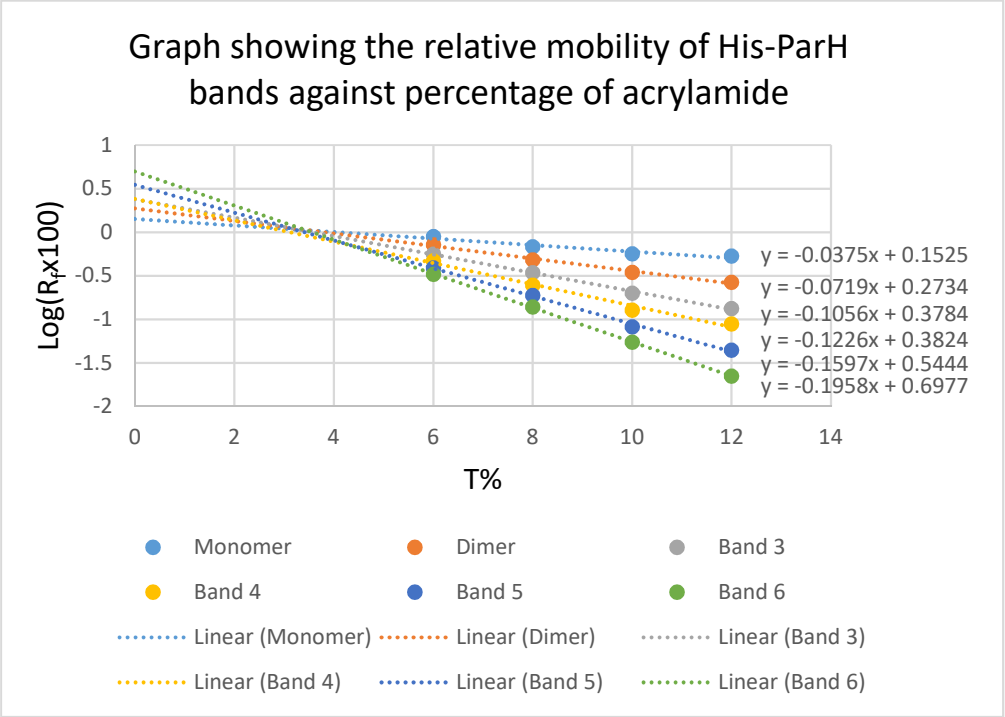

Figure 72: Mobility of bands (log(R_fx100)) plotted against acrylamide percentage T%.

The mobility of each band was plotted against the percentage of acrylamide in which the band was run. This gave a curve for each of the first six bands across each of the gels. The gradient of the curves corresponds to the retardation coefficient (K_r).

The gradient of each curve (-slope) corresponds to the retardation coefficient of that protein (K_r). Based upon the data from the analytical gel filtration of His-ParH it is assumed that the first two bands in each gel correspond to the monomer and dimer forms of the protein. Thus they were assigned K_r values of 0.0375 and 0.0719 respectively and plotted against the theoretical molecular weights of the monomer (39 kDa) and the dimer (78 kDa). These two points acted as a calibration curve upon which to extrapolate the molecular weight of the other bands (Figure 73).

The calibration curve generated by the Ferguson plot indicates that oligomers of ParH conform to an n+1 monomer progression (Table 11). The third band is estimated to be a protein with a molecular weight of approximately 116 kDa, which compares well with the molecular weight of a His-ParH trimer (118 kDa). The next three bands have calculated molecular weights of 136 kDa, 177 kDa and 219 kDa which could be said to correspond to a tetramer (157 kDa), a pentamer (196 kDa) and a hexamer (219 kDa) although they are not perfect in matching the theoretical molecular weights. This could be because the charge may change between the different oligomers, or that the shape changes significantly which would change the relative gradients of the oligomers. However overall the data suggests that each oligomer of ParH contains a monomer increase of the previous oligomer.

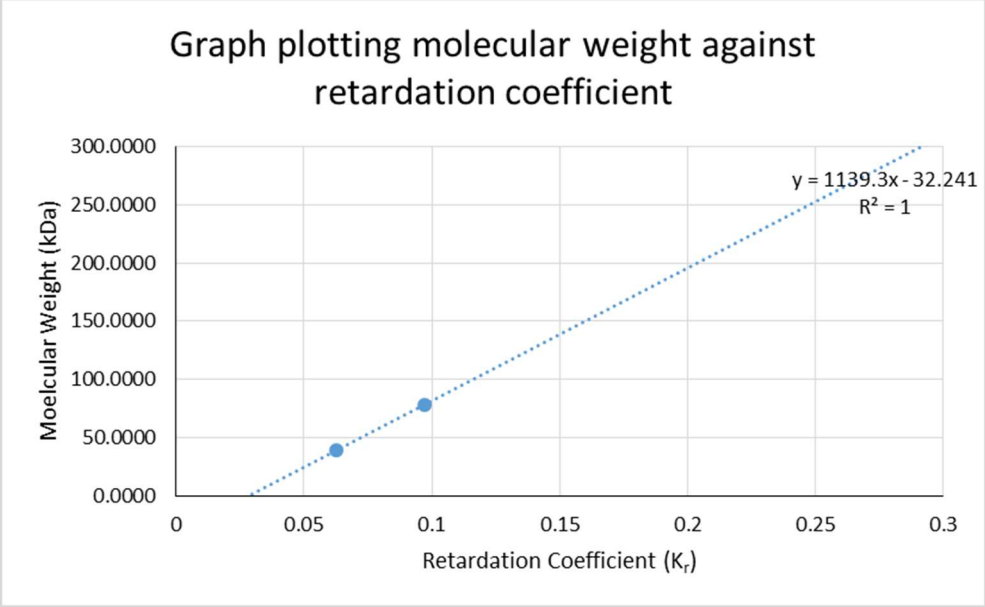

Figure 73: Ferguson plot of molecular weight against retardation coefficient.

The known molecular weight of the monomer and dimer of His-ParH was plotted against their retardation coefficient as determined by native PAGE. The calibration curve generated was used to estimate the molecular weight of bands of unknown oligomers of His-ParH.

Table 11: Table showing the molecular weight calculations of His-ParH oligomers using the Ferguson plot.

Band	K_r	Estimated Molecular Weight (kDa)	Theoretical Molecular Weight (kDa)	Possible Oligomer
1	0.0375	39	39	Monomer
2	0.0719	78	78	Dimer
3	0.1056	118	116	Trimer
4	0.1226	157	136	Tetramer
5	0.1597	196	177	Pentamer
6	0.1958	235	219	Hexamer

4.2.6 Crosslinking of ParH reveals the trimer

Another way of testing protein oligomers using electrophoresis, is to crosslink the proteins using a chemical cross linker. These small molecules have a reactive group at each end which form bonds with certain amino groups. Dimethyl pimelimidate (DMP) is one such cross linker that has imidoester reactive groups at both ends of the molecule. Imidoester groups form bonds with primary amines, such as those found at the N-terminus of each peptide chain as well as the side chains of lysine residues. The cross linker will form reversible bonds between two primary amines at alkaline pH values (pH 8-10) to form an amide bond. If two primary amines are within 8 Å of each other, then they will be cross linked together (Hand and Jencks, 1962). These bonds are not broken by SDS-PAGE and thus the protein will run according to its oligomeric state rather than in its monomeric form.

His-ParH (240 pmol/12 µM) was incubated in a Hepes buffer (50 mM Hepes-KOH, 100 mM KCl, 5 mM $MgCl_2$ pH 8.5) along with increasing concentration of DMP

cross linker. The reactions were incubated at 30°C for 1 hour before being analysed on 10% SDS-PAGE and stained with Coomassie (Figure 74). His-ParH without cross linker ran as a single band at a position consummate with the size of a ParH monomer. Increasing concentrations of DMP cross linker resulted in the appearance of bands at positions consistent with dimeric, trimeric and tetrameric ParH. The presence of multiple bands at each of the positions could indicate that the cross linking formed bonds that change the shape of the complexes which led to different migrations of oligomers. The fact that not all of the protein crosslinked, as evidenced by the large amount of monomeric His-ParH, would indicate that the cross linking is inefficient and explain why the cross linking led to multiple bands. The data does however, support the previous results that indicate that oligomerisation of ParH is built upon a monomeric subunit.

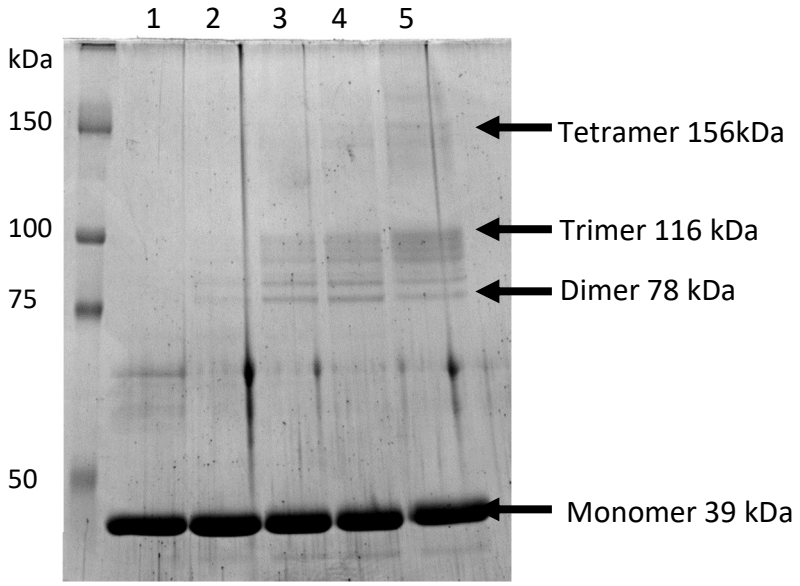

Figure 74: 10% SDS-PAGE of DMP cross linked His-ParH

His-ParH (240 pmol/12 µM) was incubated in Hepes buffer (50 mM Hepes-KOH, 100 mM KCl, 5 mM $MgCl_2$ pH 8.5) for 60 minutes at 30°C in the presence of increasing concentrations of DMP and loaded as follows (1) 0 mM, (2) 0.1 mM, (3) 0.5 mM, (4) 1 mM and (5) 10 mM. His-ParH appeared to form dimers, trimers and tetramers. Molecular weights of Bio-Rad Precision Plus Protein™ Standard are shown in kDa. Visualised by Coomassie staining.

4.2.7 ATP has no effect on the oligomerisation of His-ParH

A feature of ParA proteins is that ATP can influence their oligomeric state. In *B. subtilis* for example, in the absence of ATP Soj (ParA) is a monomeric protein, however once bound with ATP Soj dimerises (Gruber and Errington, 2009). As has been shown, His-ParH already forms many oligomers even in the absence of ATP. This does not however, preclude the possibility that ATP may affect this oligomerisation by either causing polymerisation, or by causing a bias to one oligomeric state.

To investigate this, His-ParH (240 pmol/12 µM) was incubated in the absence and presence of ATP (1 mM) for 1 hour at 30°C in a Tris buffer (50 mM Tris-HCl, 150 mM NaCl, 5 mM $MgCl_2$ pH 7.5). After incubation the reactions were loaded in to an 8% PAGE gel and run for 2 hours at 100 V (Figure 75). No discernible difference was found in the oligomers of His-ParH when incubated in the presence or absence of ATP compared to when incubated separately. This suggests that either ATP is binding to His-ParH but not affecting its oligomerisation, or that there is no ATP binding. it is

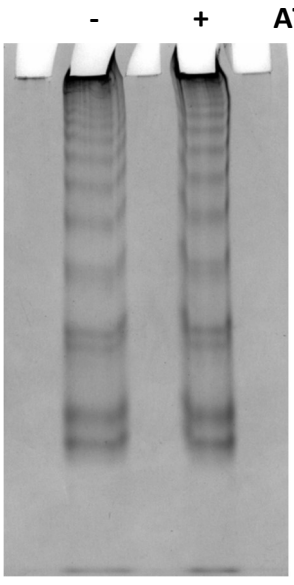

Figure 75: The effect of ATP on ParH polymerisation.

His-ParH (240 pmol/12 µM) was incubated in the absence and presence of ATP (1 mM) for 1 hour at 30°C in Tris buffer (50 mM Tris-HCl, 150 mM NaCl, 5 mM $MgCl_2$ pH 7.5). There is no discernible difference in the oligomerisation state of His-ParH whether in the presence or absence of ATP. Visualised by silver staining.

possible however, that either the ability of ParH to bind ATP depends upon a partner protein, or that changes in oligomerisation of ATP bound ParH requires activation by a partner protein.

4.3.8 ParH oligomers have a dynamic equilibrium

After confirming that ParH oligomers follow an N+1 monomer assembly pattern we wished to test whether their formation was dynamic. That is, could higher

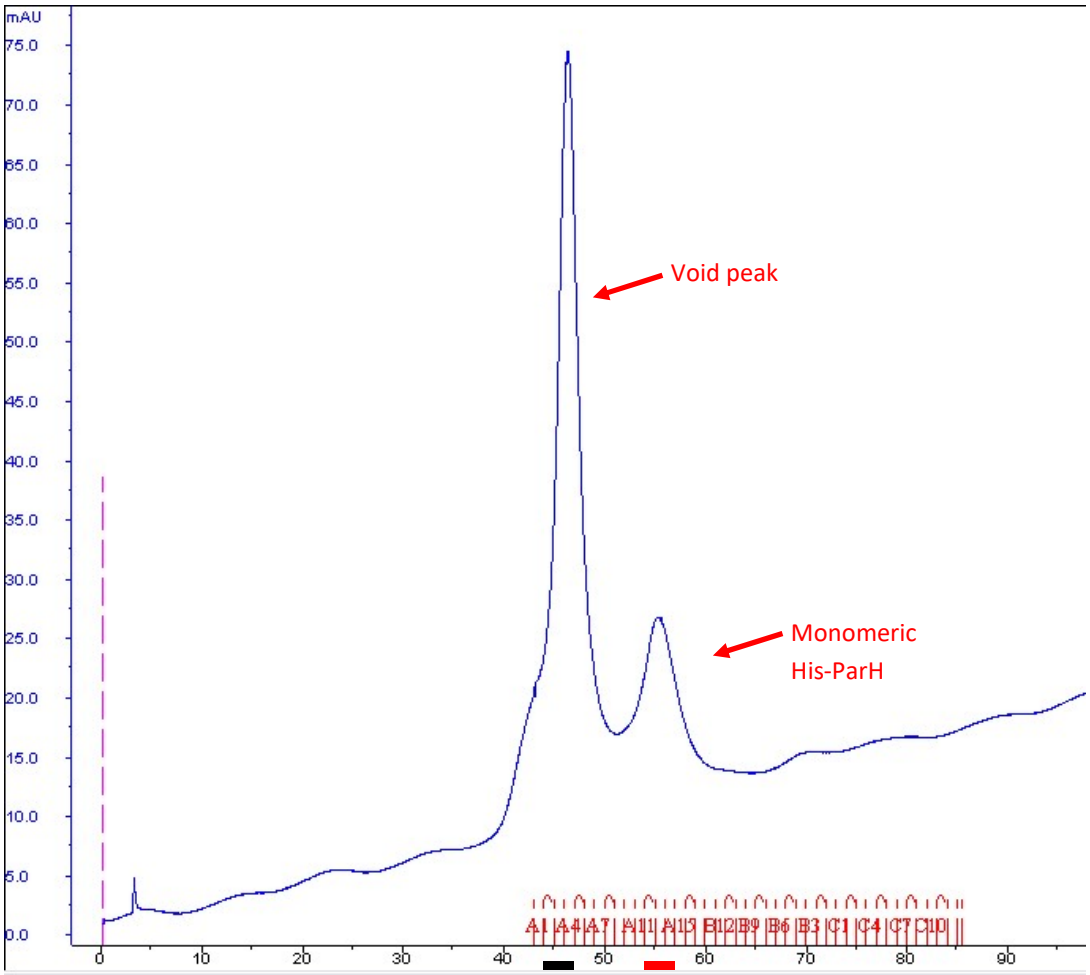

Figure 76: Chromatogram of the purification of monomeric His-ParH using gel filtration.

His-ParH (3 mg) was loaded onto a HiLoad 16/600 Superdex 75 pg column from GE Healthcare in Tris buffer (20 mM Tris-HCl, 150 mM NaCl, 5 mM $MgCl_2$, 5 mM DTT pH 7.5). The UV absorbance of the elution was monitored for the void volume and the peak representing monomeric His-ParH. Fractions representing these two peaks were collected and analysed. Fractions A2 to A4 (Black line) were collected for higher His-ParH oligomers, while fractions A12-A14 (Red line) were collected for monomeric His-ParH.

order oligomers be reconstituted from the monomeric form and *vice versa*? To separate out the monomer from higher oligomers, gel filtration was carried out on His-ParH using a HiLoad 16/600 Superdex 75 pg column from GE Healthcare.

This gel filtration column has a resolution between 3 kDa and 70 kDa, thus monomeric His-ParH (39 kDa) will elute within the resolution range of the column, while all the oligomers higher than the monomer will elute at the void volume. To this end, 2 ml of purified His-ParH protein (3 mg) was loaded onto the column in a Tris buffer (20 mM Tris, 150 mM NaCl, 10 mM $MgCl_2$, 5 mM DTT pH7.5) at a speed of 1 ml/min. Fractions were collected in 1ml aliquots, beginning a short time before the estimated void volume of the column (Figure 76).

As expected the elution profile of His-ParH using HiLoad 16/600 Superdex 75 pg column showed a single peak within the resolution range of the column, which represented monomeric His-ParH. The remainder of His-ParH eluted in the void, suggesting a molecular weight over 70 kDa, consistent with the other oligomers being dimers and higher. Fractions representing these two peaks (Figure 76) were collected and combined before being concentrated using a vivaspin6 concentrator with a molecular weight cut off of 3 kDa. The fractions were then run on the Superdex 200 10/300 GL column to check their elution profiles (Figure 77).

As expected the fraction containing monomeric His-ParH from the preparative gel filtration column showed one peak when run on the analytical gel filtration column. There was a shoulder visible after peak, which is probably due to the drifting of the UV detector. This suggests that monomeric His-ParH was successfully isolated from the mixed population. However the void fraction, while containing the expected higher order assemblies, unexpectedly contained a peak at the monomeric His-ParH elution volume. The monomeric peak was also smaller relative to the other peaks, indicating that monomeric units make up a smaller proportion of the population compared to the original population. Surprisingly, there was also no detectable peak which would correspond to dimeric His-ParH. One explanation for the appearance of monomeric His-ParH in the void fraction is that the monomeric oligomer was generated in the sample after separation of the oligomers. In addition the monomeric fraction was applied to the column directly after gel filtration while the void fraction was incubated on ice. Even with this delay

in the analysis of the void fraction, the monomeric fraction was still incubated during the concentration process. It could be that the disassembly of the oligomers into monomers is faster than the creation of higher oligomers of ParH from the monomer. It may also be why the dimer was not detected in the void fraction as it had disassembled into monomeric form. One reason for the speed of monomer

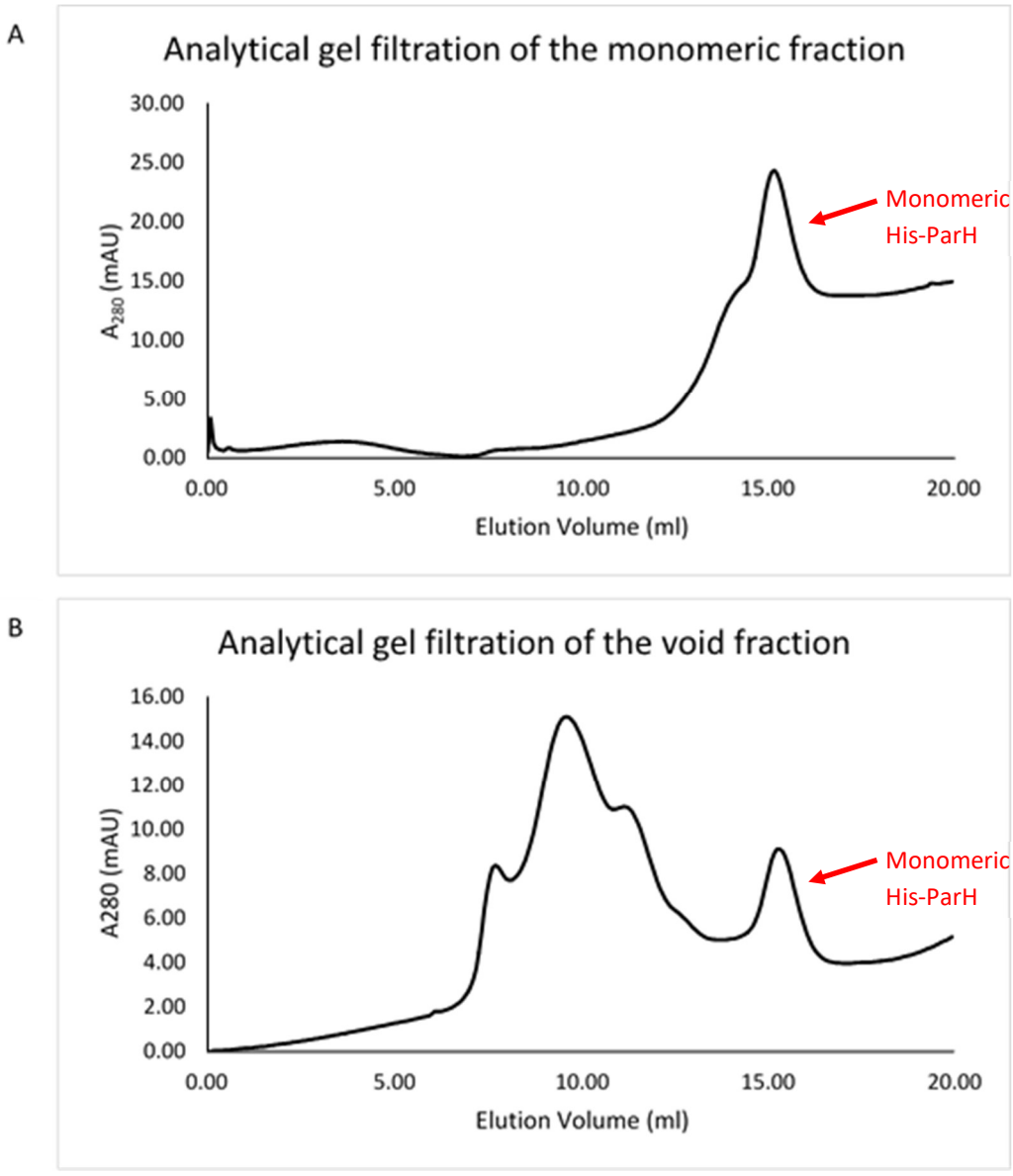

Figure 77: His-ParH monomer and void fraction analytical gel filtration elution profile.

Concentrated monomer and void fractions from figure 74 were analysed by analytical gel filtration using the Superdex 200 10/300 GL column. (A) The monomer fraction consisted of a single peak with an elution volume consistent with monomeric His-ParH. (B) The void fractions had peaks associated with higher order His-ParH oligomers. It also had an unexpected peak at the monomer elution volume.

formation is that all oligomers have the ability to form a monomer through the loss of a subunit, while any given higher oligomer can only be formed from a limited number of oligomers in the sample at any given time. This would also explain why the monomeric form is the dominate oligomer in the original His-ParH population. Moreover, this data starts to suggest that the oligomeric population of ParH is dynamic with oligomers gaining and losing subunits.

To test whether the monomer fraction would revert to a population mixture closer to the original His-ParH population, the concentrated monomeric fraction (240 pmol/12µM) was incubated for 48 hours in the presence and absence of ATP (1 mM) before being analysed on 6% native-PAGE (Figure 78). It is evident that the higher order oligomers were reconstituted from the monomeric form which occurred independently of ATP. This provides further evidence that the oligomers are undergoing dynamic assembly generating an equilibrium of oligomers within the population.

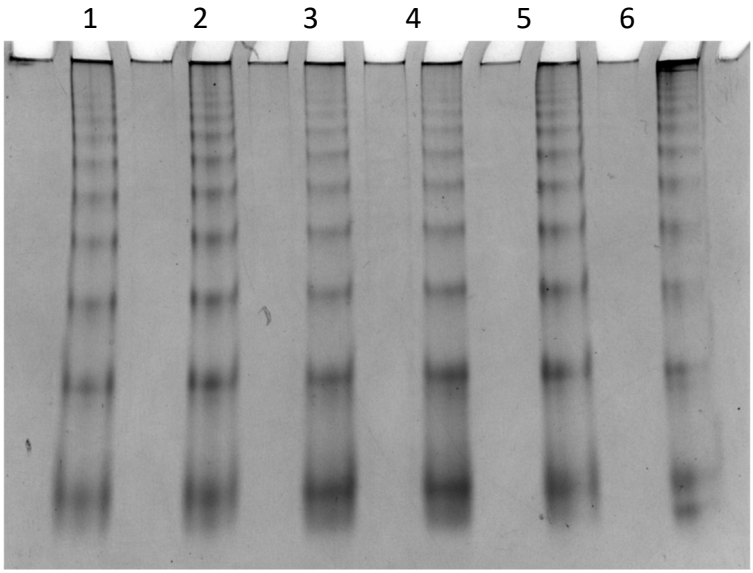

Figure 78: Native-PAGE of monomeric His-ParH fraction incubated with and without ATP for 48 hours.

The monomeric His-ParH fraction (240 pmol/12 µM) was incubated in the absence (Lanes 1, 2 and 5) and presence (Lanes 3 and 4) of ATP (1 mM). The original His-ParH (240 pmol12 µM) was also analysed (Lane 6). The higher order oligomers of ParH were constituted from the monomeric form independently of ATP. Visualised by silver staining.

4.3 Summary

In this chapter we set out to purify four S. coelicolor proteins ParH, Hyp, ParB and Scy using the heterologous host *E. coli*. After generating pET28a constructs for the purification of each protein we optimised both the production of each protein and large scale purification using metal affinity chromatography. Three of the proteins, Scy, ParH and Hyp, were purified from solution, while the fourth protein, ParB, was purified under denaturing conditions. After purification we successfully dialysed the proteins into buffers for *in vitro* assays. However we determined that Hyp required the presence of arginine in order to remain soluble.

In the second part of this chapter we investigated the oligomerisation of ParH using analytical gel filtration, native-PAGE, chemical cross linking and a Ferguson plot. Through these techniques we were able to demonstrate that ParH assemblies into multiple oligomers. Remarkably ATP had no effect on this oligomerisation, at least under the conditions we tested. This finding is different to the observations made for other ParA-like proteins where dimerisation and oligomerisation are dependent upon ATP binding. Our observations show that these oligomers are built upon a monomeric subunit with an n+1 monomer progression. We also demonstrated that these oligomers can be reformed from the monomeric form of ParH. This also occurred independently of ATP, further demonstrating that ATP is not required for oligomerisation. Interestingly we were able to show interaction between ParH and Hyp, which occurred only between the higher order oligomers of ParH and Hyp. This demonstrates that the oligomeric state of ParH is important for interaction with Hyp and possibly suggests that a regulatory mechanism could exist which would regulate oligomerisation of ParH and in turn regulate ParH-Hyp interaction. Through the same techniques we were also able to demonstrate that Hyp is tetrameric protein.

5 Investigating Interactions of ParH and Hyp

So far, we have established that ParH is a ParA homologue that is important for correct and efficient positioning of septa during *S. coelicolor* sporulation. In the last chapter we investigated the oligomerisation of ParH, showing that it has multiples forms of oligomers which exist in equilibrium likely built upon a common monomeric subunit. The monomeric form also appears to be the most prevalent oligomer present. We also demonstrated that ATP on its own has no effect on the oligomerisation of ParH. This does not however preclude the possibility that a partner protein is required to influence the interaction between ParH and ATP. As well as the oligomerisation of ParH, we investigated the oligomerisation of Hyp, which was found to form a tetramer. Interaction between ParH and Hyp was also seen through native-PAGE. This interaction seemed to depend on higher oligomer assemblies of ParH and Hyp suggesting that oligomerisation is important for this interaction. After investigating the oligomerisation of ParH and Hyp in the last chapter, we wished to next investigate potential interactions of these proteins.

Partner proteins of ParA/MinD proteins are important for regulating the function and localisation of these proteins (Lutkenhaus, 2012). Often this is due to regulating the oligomerisation state of the ParA/MinD protein. These proteins are often found downstream of the gene locus of the ParA/MinD protein. MinD in *E. coli*, for example interacts with the protein MinE, with both genes located in the *minCDE* operon. This interaction affects the oligomeric state of MinD by regulating its ATPase activity (Hu and Lutkenhaus, 2001). In its ATP bound state, when its ATPase activity is low, MinD forms a dimer, which is able to interact with MinE. Upon interaction, the ATPase activity of MinD is upregulated and it hydrolyses its bound ATP which generates a MinD monomer bound to ADP (Hu and Lutkenhaus, 2001). This form of the protein does not interact with MinE. This interaction, regulating the nucleotide binding properties of MinD drives the pole-to-pole oscillations of MinD localisation (Raskin and de Boer, 1999). The homologue of MinD from *B. subtilis* has a stable interaction with DivIVA, which is not encoded in

a gene in an operon with *minD*. This allows for static localisation of the gene at the poles and closing septum during the division process (Cha and Stewart, 1997). The MinD proteins from both of these bacteria interact and localise MinC which is the inhibitor of FtsZ ring formation (Dajkovic et al., 2008). These two homologues are an example for how bacteria can use different protein partners of these proteins with different mechanisms of interaction to ultimately achieve the same outcome. These types of interactions are found across the whole family of ParA/MinD proteins with the ParA-ParB interaction of the *parAB* operon found in *C. crescentus* and *S. coelicolor* and the MipZ interaction with ParB in *C. crescentus*, all demonstrating how interaction with partner proteins plays an important role in the function of these proteins (Jakimowicz et al., 2007; Kiekebusch et al., 2012).

In the last chapter we already set out why we chose to test interaction of ParH with Hyp, Scy and ParB and this will be discussed again later in the chapter. To understand these interactions we utilised four methods. For protein-protein interaction we will test interaction both *in vivo* using bacterial two-hybrid assays in the heterologous host *E. coli*, and *in vitro* using pelleting assays. For protein-DNA interaction we will test *in vitro* also using pelleting assays as well as electrophoretic mobility shift assays. Finally we will see if the ATPase activity of ParH is regulated by partner proteins in vitro through reverse phase HPLC where we will monitor the turnover rate of ATP to ADP by ParH.

The bacterial two-hybrid assay measures protein-protein interaction in the heterologous host *E. coli*, for which we used the BACTH system (Karimova et al., 2000). This system utilises the fact that the adenylate cyclase of *Bordetella pertussis* can be split into two non-functioning domains, T25 and T18 (Figure 79). They can then be fused to two proteins of interest which when co-expressed have the potential to form an interaction which allows for the two domains to coalesce to form active adenylate cyclase. Adenylate cyclase is an important enzyme which catalyses the conversion of ATP to cyclic AMP (cAMP) which in turn binds to the catabolite activator protein (CAP). The cAMP-CAP complex activates reporter genes, which in this case is *lacZ*. The reporter gene *lacZ* is important for lactose metabolism, and is activated when lactose is the carbon source for the bacteria. The bacteria are therefore grown on LB agar deficient in glucose but supplemented

with the lactose analogue X-gal. When cleaved by β-galactosidase, the protein encoded by *lacZ*, X-gal is broken down into a product that is insoluble and blue. Thus interacting proteins can be observed through the appearance of blue *E. coli* colonies. To generate the tagged proteins, two vectors, pUT18c and pKT25, were used (Figure 80). These vectors have a multiple cloning site (MCS) downstream of the either the T18 (pUT18c) or T25 (pKT25) tag encoding genes allowing genes of interest to be fused to their C-terminus. This generates fusions where the tag is located at the N-terminus of the protein of interest. The two plasmids have different resistance markers and have separate replicons allowing co-transformation into the adenylate cyclase deficient *E. coli* strain BTH101 after which β-galactosidase activity can be monitored. All genes were cloned into the vectors using *Xba*I and *Eco*RI such that the gene is in frame with the sequence encoding the corresponding domain of adenylate cyclase.

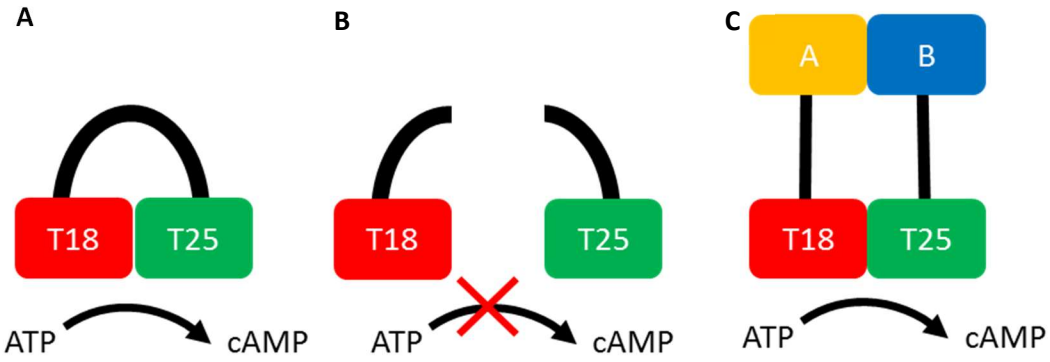

Figure 79: The bacterial two-hybrid system.

Adenylate cyclase from *B pertussis* consists of two domains, T25 and T18, which convert ATP to cAMP (A). When separated, this process is lost and cells can no longer produce cAMP (B). Fusing the domains to proteins that interact leads to the reconstitution of this process and cAMP is produced (C). Production of cAMP is monitored using *lacZ*, a as a reporter gene which in the presence of X-gal will allow blue/white screening.

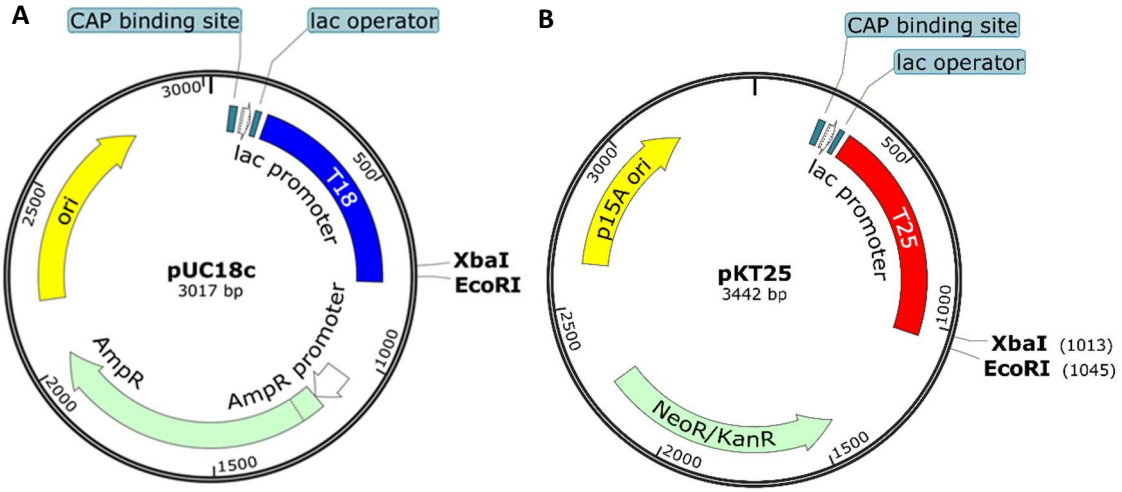

Figure 80: The bacterial two-hybrid plasmids pUT18c and pKT25

The vectors used to generate plasmids used in bacterial two-hybrid assays pUT18c and pKT25 each contain a domain of adenylate cyclase from *Bordetella pertussis*. (A) The vector pUT18c contains the T18 domain which is driven by the *lac* promoter and proceeds a MCS containing restriction sites *Xba*I and *Eco*RI which were used for cloning. It also contains an origin of replication from pUC18 and an ampicillin resistance gene. (B) The vector pKT25 contains the T25 domain which is driven by the lac promoter and proceeds a MCS containing restriction sites *Xba*I and *Eco*RI which were used for cloning. It also contains the *E. coli* p15A origin of replication which is distinct and compatible with the pUC origin of replication in pUT18c, allowing co-transformation. Vector maps were generated using SnapGene.

Monitoring protein interaction *in vitro* using pelleting assay relies on the change in sedimentation properties of protein complexes based on their relative density in relation to the density of the medium. Proteins that form lower oligomers will remain in the supernatant when subjected to ultracentrifugation due to being less dense than the media. Upon oligomerisation or through the formation of protein-protein interactions in which complexes are formed, the protein can have higher density than the media and will thus pellet when subjected to ultracentrifugation. We tested this property by incubating proteins for 30 min in a Tris based buffer (50 mM Tris-HCl, 150 mM NaCl, 10 mM $MgCl_2$ pH 8) before centrifuging them at 450,420 g for 30 minutes at 4°C in a Beckman Optima TLX Ultracentrifuge with a Beckman Coulter TLA 100 Fixed Angle Rotor. This generates

two fractions, pellet and supernatant, that can be analysed by SDS-PAGE from which it can determined in which fraction the protein entered. Once this is determined then nucleotides, DNA and other proteins can be added to the reaction and the fractions analysed. Should the protein move from one fraction to the other we can estimate that the protein interacted with the additive, or underwent either polymerisation or depolymerisation depending upon to and from which fraction it moved. This method has been previously used using *S. coelicolor* proteins to show Scy-DivIVA and Scy-ParA interaction (Ditkowski et al., 2013; Holmes et al., 2013).

5.1 ParH and Hyp show interaction in pelleting assay

ParA/MinD proteins often interact with their downstream partner, whether this is ParA interacting with ParB, or MinD interacting with MinE. Given that the *hyp* gene is located downstream of *parH* and is translationally coupled we believed that it was likely that the two proteins interact. In the last chapter, we had already observed interaction *in vitro* using native-PAGE, and we wished to confirm this interaction again *in vitro* using pelleting assay and *in vivo* bacterial two-hybrid assay in the heterologous host *E. coli*. To demonstrate interaction between ParH and Hyp using the pelleting assay we needed to show that both proteins are found in a single fraction, although not necessarily the same one, and does this pattern change when the proteins are mixed. To achieve this reactions were set up in which His-ParH (40 pmol/2 µM) and His-Hyp (240 pmol/12 µM) were incubated separately and then together in 1:2 (80 pmol/4 µM His-Hyp), 1:4 (160 pmol/8 µM His-Hyp) and 1:6 (240 pmol/12 µM His-Hyp) molar ratios in which the amount of His-ParH (40 pmol/2 µM) remained constant. Incubations were carried out for 30 min at room temperature in a Tris buffer (50 mM Tris-HCl, 150 mM NaCl, 10 mM $MgCl_2$ pH 8). After incubation the samples were centrifuged using ultracentrifugation for 30 minutes at 450,420 g at 4°C. After centrifugation the supernatant was collected and the pellet fraction re-suspended in the reaction buffer. To test whether ATP had an effect on the polymerisation state of these

proteins we also incubated the samples in the presence of ATP (1 mM). In the presence of ATP, His-ParH was incubated separately and with His-Hyp in 1:2 (80 pmol/4 µM His-Hyp) and 1:4 (160 pmol/8 µM His-Hyp) molar ratios. All fractions were then analysed using SDS-PAGE (Figure 81).

The pelleting assay reveals that His-ParH is mainly in the supernatant with a very small proportion found in the pellet fraction. This was expected given the observations from the oligomerisation experiments in the previous chapter (Figure 70). It is likely that lower oligomers of His-ParH are being separated into the supernatant, while some of the higher oligomers are pelleting. His-Hyp is found exclusively in the supernatant fractions when subjected to ultracentrifugation. The

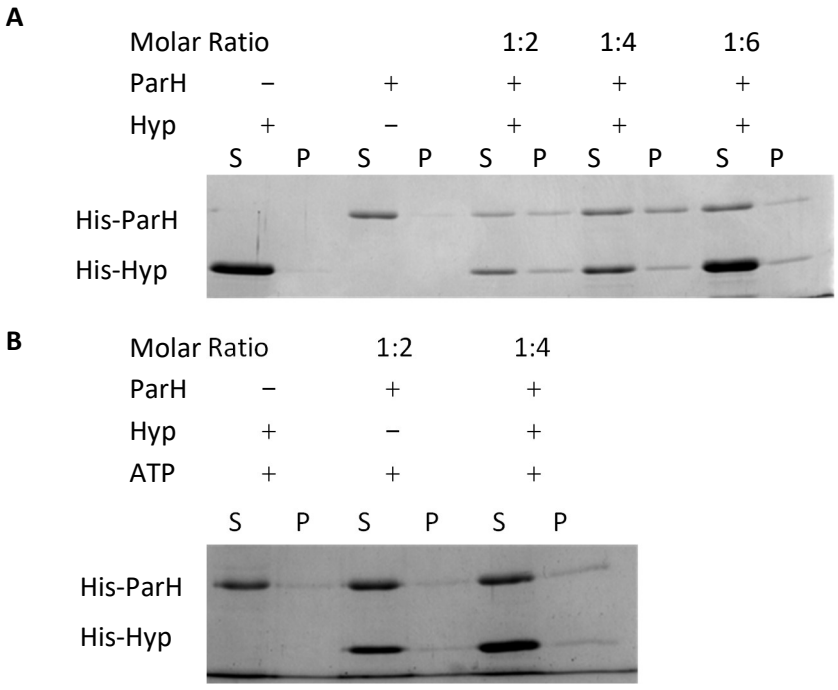

Figure 81: Pelleting assay of His-ParH and His-Hyp.

(A) His-ParH (40 pmol/2 µM) and His-Hyp (240 pmol/2 µM) were incubated separately and then together in 1:2 (80 pmol/4 µM His-Hyp), 1:4 (160 pmol/8 µM His-Hyp) and 1:6 (240 pmol/12 µM His-Hyp) molar ratios in which the amount of His-ParH (40 pmol/2 µM) remained constant.
(B) In the presence of ATP (1 mM), His-ParH was incubated separately and with His-Hyp in 1:2 (80 pmol/4 µM His-Hyp) and 1:4 (160 pmol/8 µM His-Hyp) molar ratios.
After a 30 min incubation at room temperature in a Tris buffer (50 mM Tri-HCl, 150 mM NaCl, 10 mM $MgCl_2$ pH 8) the samples were centrifuged for 30 minutes at 450,420 g at 4°C generating both supernatant and pellet fractions. Samples were analysed on 10% SDS PAGE and visualised using Coomassie staining.

addition of ATP had no effect on the amount of His-ParH pelleting, which is again concordant with the data from the previous chapter which indicated that ATP has no effect on the oligomerisation of His-ParH. When the two proteins are incubated together, a proportion of each protein is then pulled to the pellet fraction which suggests that the two proteins interact. One thing to note is that increasing the molar ratio of Hyp compared to ParH does not appear to increase the amount of either protein seen in the pellet fraction. This suggests that the interaction is perhaps limited to a subsection of the population or that not all interaction between the two proteins leads to complexes that result in pelleting. Interestingly this compares favourably with the observations seen when the proteins were run on native PAGE. In that experiment we showed that only higher oligomers of ParH interacted with Hyp, suggesting only a subset of the ParH population interacted with Hyp. It also suggests that His-ParH is the limiting factor in interaction and therefore increasing the amount of His-ParH relative to His-Hyp could pull more of the His-Hyp protein to the pellet. The addition of ATP had no effect on the observable interaction between His-ParH and His-Hyp, suggesting it is not important for interaction and is suggestive of the fact that ATP does not change the nature of the interaction between His-ParH and His-Hyp.

5.2 ParH and Hyp do not show interaction using bacterial two-hybrid assay

In order to analyse protein interactions of ParH and Hyp using bacterial two-hybrid assay, the two genes were cloned into the bacterial two-hybrid vectors pUT18c and pKT25. These vectors will create fusions of the genes to the C-terminus of the adenylate cyclase domains T18 (pUT18c) and T25 (pKT25). Four constructs were generated to analyse the proteins: pUT18c-ParH, pKT25-ParH, pUT18c-Hyp and pKT25-Hyp (Figures 82 and 83). To generate the constructs the *parH* gene was amplified from *S. coelicolor* chromosomal DNA using the primers '1772 *Nde*I *Xba*I FRW' and '1772 Eco UTC REV', while the *hyp* gene was amplified from the same template using the primers '1771 *Nde*I *Xba*I FRW' and '1771 Eco UTC REV'.

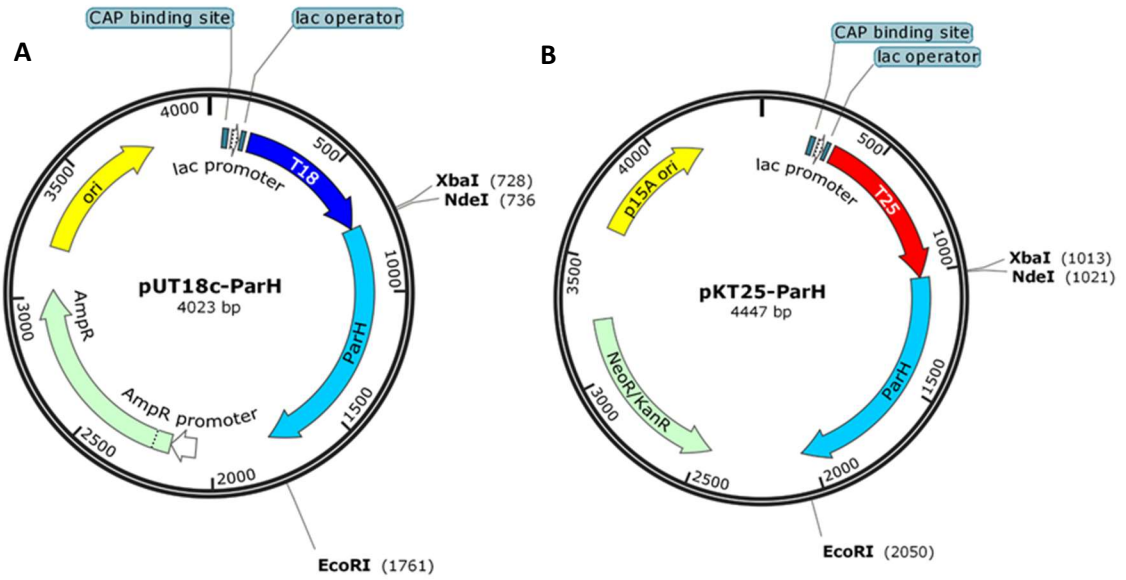

Figure 82: The ParH bacterial two-hybrid plasmids pUT18c-ParH and pKT25-ParH

(A) The plasmid pUT18c-ParH is a derivative of pUT18c with the *parH* gene cloned using the restriction sites *Xba*I and *Eco*RI.
(B) The plasmid pKT25-ParH is a derivative of pKT25 with the *parH* gene cloned using the restriction sites *Xba*I and *Eco*RI.
The *parH* gene was amplified from *S. coelicolor* chromosomal DNA using the primers '1772 *Nde*I *Xba*I FRW' and '1772 Eco UTC REV'.

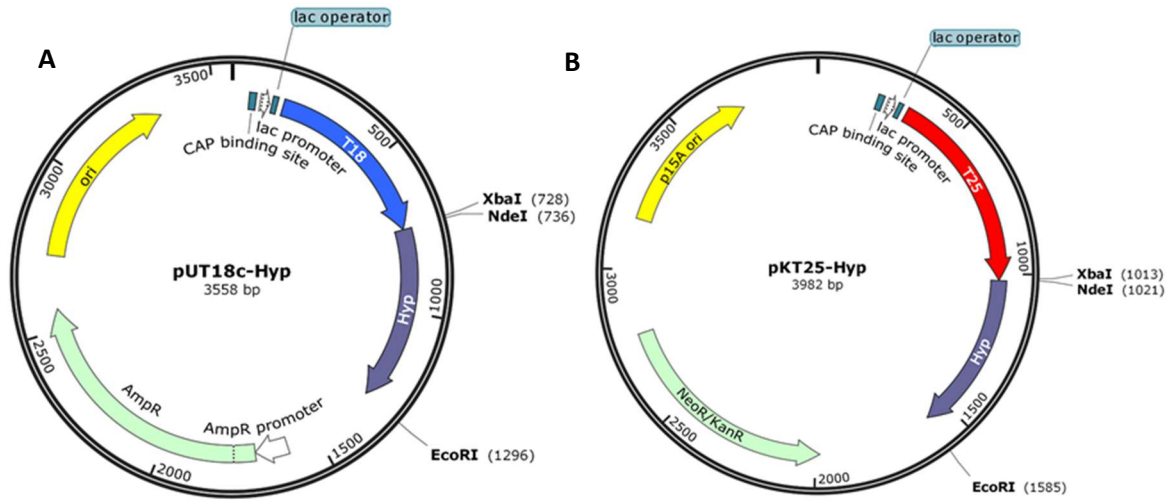

Figure 83: The Hyp bacterial two-hybrid plasmids pUT18c-Hyp and pKT25-Hyp

(A) The plasmid pUT18c-Hyp is a derivative of pUT18c with the *hyp* gene cloned using the restriction sites *Xba*I and *Eco*RI.
(B) The plasmid pKT25-Hyp is a derivative of pKT25 with the *hyp* gene cloned using the restriction sites *Xba*I and *Eco*RI.
The *hyp* gene was amplified from *S. coelicolor* chromosomal DNA using the primers '1771 *Nde*I *Xba*I FRW' and '1771 Eco UTC REV'.

The primers allow cloning of the genes in frame downstream of the adenylate cyclase domains using *Xba*I and *Eco*RI. Clones containing recombinant DNA were sequenced to confirm mutation free constructs.

To test interaction, the *E. coli* strain BTH101, which is adenylate cyclase deficient, was co-transformed with pUT18c-ParH and pKT25-Hyp, and with pUT18c-Hyp and pKT25-ParH. Both combinations of constructs were transformed so that we could observe whether expression levels affect interaction. The two plasmids have different copy numbers, with pUT18c being a high copy vector and pKT25 a low copy vector. Thus fusions expressed from pUT18c will be produced in a higher quantity than those expressed from pKT25. We also tested self-interaction of ParH and Hyp, and so co-transformed BTH101 with pUT18c-ParH and pKT25-ParH, and with pUT18c-Hyp and pKT25-Hyp. After transformation, three colonies were picked along with colonies containing both positive and negative controls and plated onto LB agar deficient in glucose, before being incubated at 30°C to allow best visualisation of the blue/white colony screen. Colonies were monitored over two days to observe the colour (Figure 84). Colonies carrying pUT18c-ParH with pKT25-ParH, and pUT18c-Hyp with pKT25-Hyp bacterial two-hybrid constructs, turned blue when compared to the negative control and were comparable in colour to the positive control. This was not surprising given the established oligomerisation of these proteins. Both proteins are able to form higher order assemblies and this is reflected in the bacterial two-hybrid assay. Therefore we have been able to show self-interaction both in vitro and in vivo using the heterologous host E. coli. However, we were unable to confirm interaction between ParH and Hyp using bacterial two-hybrid. Colonies carrying ParH and Hyp bacterial two-hybrid constructs in both combinations were negative for this assay. Interaction is probably not observable due to the interaction between the two proteins forming in a conformation that does not bring the two domains from adenylate cyclase (T18 and T25) close enough in order to restore the enzymatic activity of the protein.

5.3 Hyp is a DNA binding protein

As has previously been discussed, one feature of ParA proteins is their association with the downstream DNA binding protein ParB. Classically, ParB binds to *parS* sites which predominantly cluster around the chromosomes origin of replication. The interaction between ParB and ParA then helps to pull the chromosome to the poles in the case of *C. crescentus*, or to align chromosomes along the length of the hyphae during division in *S. coelicolor*. Although Hyp is not a homologue of ParB and in fact has no homologues of known function, we wanted to test whether Hyp could in fact also be a DNA binding protein. To test this an Electrophoretic mobility shift assay (EMSA) was performed using purified Hyp protein and the plasmid pIJ8660 which is a shuttle vector that can be manipulated in *E. coli* and then used to introduce recombinant genes into the *S. coelicolor* chromosome where it integrates at the ϕC31 attachment site. Increasing concentrations of Hyp protein were incubated with a fixed concentration of pIJ8660 plasmid, purified from *E. coli*, for 30 minutes at room temperature. After incubation the samples were run on 0.7% agarose gel made with TAE buffer without the addition of ethidium bromide. After running the gel at 10 V for 16 hours, it was incubated for 1 hour in TA buffer containing 2 µg/ml ethidium bromide in order to stain the DNA (Figure 85).

It is evident from this experiment that Hyp is a DNA binding protein. There is a clear shift in the position of pIJ8660 DNA in the gel after incubation with His-Hyp protein when compared to the control lane. What is also clear is that as the concentration of His-Hyp protein increases with relation to the amount of DNA, that shift gets higher. This suggests that the binding is non-specific, otherwise the shift would have occurred to a specific position and then not shifted any further. Interestingly this was observed in the absence of $MgCl_2$, suggesting that Mg^{2+} ions are not necessary for this interaction.

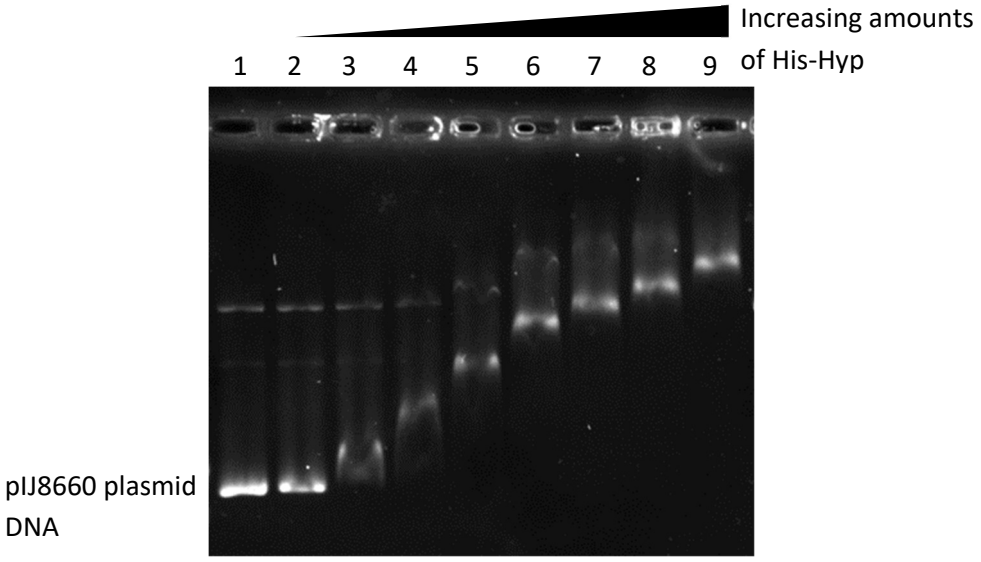

Figure 85: Electrophoretic mobility shift assay of His-Hyp and pIJ8660

An electrophoretic mobility shift assay was performed in which pIJ8660 was incubated for 30 minutes at room temperature both in the absence (Lane 1) and with increasing amounts (Lanes 2-9) of purified His-Hyp protein in a phosphate buffer (50 mM NaH_2PO_4-HCl, 150 mM NaCl, pH 8). The amount of His-Hyp increased as follows: 13 pmol/0.65 µM (Lane 2), 26 pmol/1.3 µM (Lane 3), 39 pmol/1.95 µM (Lane 4), 52 pmol/2.6 µM (Lane 5), 65 pmol/3.25 µM (Lane 6), 78 pmol/3.9 µM (Lane 7), 91 pmol/4.55 µM (Lane 8), and 104 pmol/5.2 µM (Lane 9). Samples were analysed on a 0.7% agarose gel made with TAE buffer without the addition of ethidium bromide. The gel was subsequently incubated for 1 hour in TAE buffer containing 2 µg/ml ethidium bromide to stain the DNA.

One possible reason for the shift could involve His-Hyp changing the supercoiling of the DNA which would explain the step increase as the supercoiling would change proportionately to the amount of His-Hyp protein that is present. To test this we decided to test the ability of His-Hyp to shift linear DNA. As such, pIJ8660 was linearized through digestion with *Eco*RI for which it contains a single cut site. After digestion the plasmid was gel purified using a gel extraction kit from QIAgen. As well as this we also tested linear DNA generated by PCR. To generate the PCR DNA, the gene *sepF1* from *S. coelicolor* chromosomal DNA was amplified using the primers 'SepF1 *Xba*I *Nde*I FRW' and 'SepF1 Eco UTC FRW' and the resulting product desalted. The linearized plasmid and PCR product was then incubated as before in the absence and presence of Hyp protein before being analysed on 0.7% agarose gel (Figure 86).

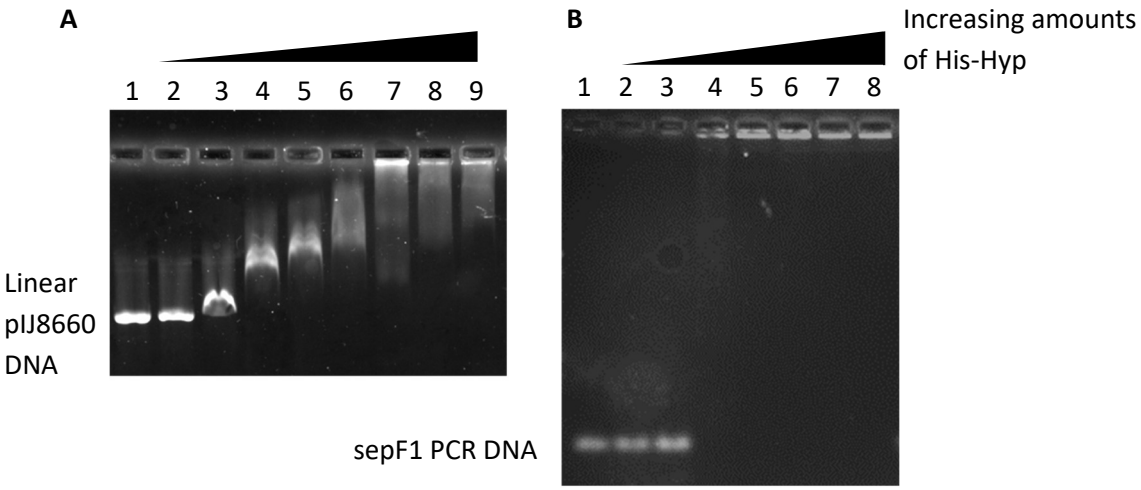

Figure 86: Electrophoretic mobility shift assay of His-Hyp and linear DNA

An electrophoretic mobility shift assay was performed on linear DNA using purified Hyp protein. (A) Linearized pIJ8660 (digested with *Eco*RI) was incubated for 30 minutes at room temperature both in the absence (Lane 1) and with increasing amounts (Lanes 2-9) of purified His-Hyp protein in a phosphate buffer (50 mM NaH_2PO_4-HCl, 150 mM NaCl, pH8). The amount of His-Hyp increased as follows: 13 pmol/0.65 µM (Lane 2), 26 pmol/1.3 µM (Lane 3), 39 pmol/1.95 µM (Lane 4), 52 pmol/2.6 µM (Lane 5), 65 pmol/3.25 µM (Lane 6), 78 pmol/3.9 µM (Lane 7), 91 pmol/4.55 µM (Lane 8), and 104 pmol/5.2 µM (Lane 9).
(B) A PCR fragment containing the *sepF1* gene from *S. coelicolor* was incubated for 30 minutes at room temperature both in the absence (Lane 1) and with increasing concentrations (Lanes 2-8) of purified Hyp protein in a phosphate buffer (50 mM NaH_2PO_4-HCl, 150 mM NaCl, pH8). The amount of His-Hyp increased as follows: 13 pmol/0.65 µM (Lane 2), 26 pmol/1.3 µM (Lane 3), 39 pmol/1.95 µM (Lane 4), 52 pmol/2.6 µM (Lane 5), 65 pmol/3.25 µM (Lane 6), 78 pmol/3.9 µM (Lane 7), 91 pmol/4.55 µM (Lane 8). Samples were analysed on a 0.7% agarose gel made with TAE buffer without the addition of ethidium bromide. The gel was subsequently incubated for 1 hour in TAE

Both forms of DNA shifted in the presence of His-Hyp protein. In the case of linearized pIJ8660 the pattern observed was similar to that seen on the circular form of the plasmid. This suggests that the pattern is not due to changes in the supercoiling of the plasmid caused by an interaction with His-Hyp. When it comes to the test with linear PCR DNA, the DNA entirely shifted to the well after a certain increase in the concentration of Hyp in the reaction. There does not appear to be a step increase, although if there were it may not be possible to resolve in this experiment. As the PCR product is an *S. coelicolor* gene, it will have higher GC content than pIJ8660 which may have an effect on His-Hyp-DNA binding.

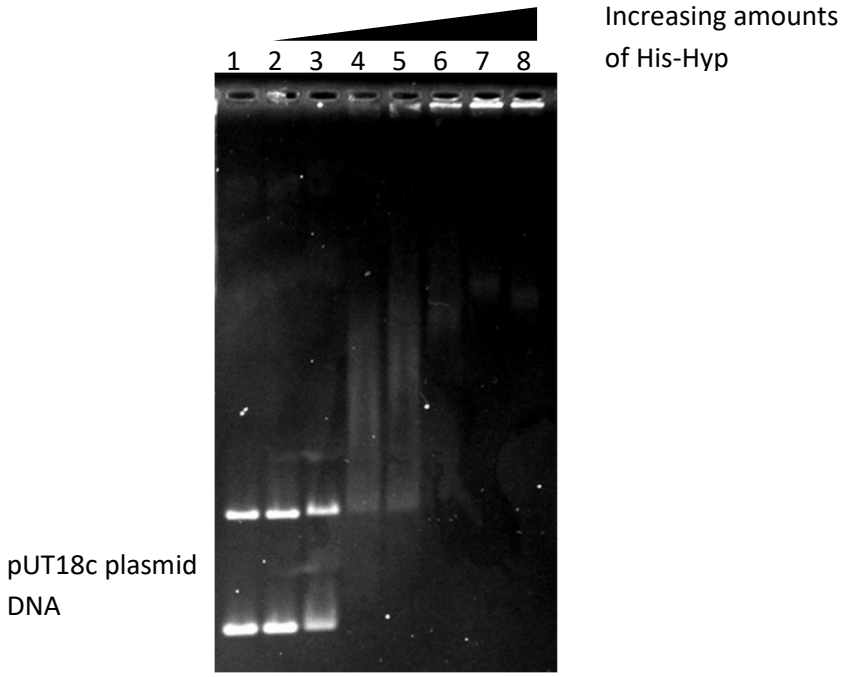

Figure 87: Electrophoretic mobility shift assay of His-Hyp and AT rich plasmid pUT18c.

An electrophoretic mobility shift assay was performed in which pUT18c was incubated for 30 minutes at room temperature both in the absence (Lane 1) and with increasing amounts (Lanes 2-8) of purified His-Hyp protein in a phosphate buffer (50 mM NaH2PO4-HCl, 150 mM NaCl, pH8). The amount of His-Hyp increased as follows: 13 pmol/0.65 µM (Lane 2), 26 pmol/1.3 µM pmol (Lane 3), 39 pmol/1.95 µM (Lane 4), 52 pmol/2.6 µM (Lane 5), 65 pmol/3.25 µM (Lane 6), 78 pmol/3.9 µM (Lane 7), 91 pmol/4.55 µM (Lane 8). Samples were analysed on a 0.7% agarose gel made with TAE buffer without the addition of ethidium bromide. The gel was subsequently incubated for 1 hour in TAE buffer containing 2 µg/ml ethidium bromide to stain the DNA.

To see whether a low GC content would affect Hyp-DNA interaction we carried out an EMSA using pUT18c. This vector is a derivative of pUC19 and thus an E. coli vector with high AT content. The reaction was set up as before and analysed 0.7% agarose gel (Figure 87). The AT rich plasmid pUT18c had a different shift pattern with the addition of His-Hyp compared to that observed with pIJ8660. Rather than observing the clear incremental step increase of DNA, pUT18c appears to shift almost entirely to the well of the gel when incubated with higher amounts of His-Hyp. In addition in samples were the DNA is shifted, but not to the well, it forms a smear on the gel rather than the discreet bands seen in the shift of pIJ8660

by His-Hyp. This is probably due to the smaller size (around 3 Kbp) of the plasmid pUT18c compared to the much larger (around 8 Kbp) size of the plasmid pIJ8660.

5.4 ParH does not shift DNA

After demonstrating His-Hyp-DNA interaction, we wished to test whether His-ParH had the same DNA binding activity. It has previously been demonstrated that Soj (ParA) from *B. subtilis* is able to non-specifically bind DNA in an ATP dependent manner, in which Soj dimerises when bound to ATP forming a nucleoprotein complex with DNA in its regulation of DnaA (Hester and Lutkenhaus, 2007; Murray and Errington, 2008). To test whether ParH is able to shift DNA, reactions were set up as before using pIJ8660 as the substrate DNA, in the absence and presence of increasing amounts of purified His-ParH protein in a Tris based buffer (50 mM Tris-HCl, 150 mM NaCl, 10 mM $MgCl_2$ pH 8). The change to a Tris buffer was to allow for the addition of ATP to reactions. EDTA was left out of the gel and running buffer to prevent chelating of Mg^{2+} ions from the buffer, which are important for protein-nucleotide binding. This was performed both in the presence and absence of ATP (1 mM). Reactions were incubated either at room temperature for 30 minutes before being analysed on a 0.7% agarose gel (Figure 88).

There was no detectable shift of pIJ8660 DNA under any of the conditions tested, even with the addition of ATP. Although this does not exclude the possibility that ParH does bind DNA in a manner that would not induce a shift in agarose gel. For protein-DNA complexes to show a shift in an electrophoretic mobility shift assay, the interaction between the DNA and protein needs to be strong, otherwise the interaction could be abolished when subjected to electrophoresis. It is possible that ParH requires a partner protein in order to stabilise perhaps otherwise week binding to DNA.

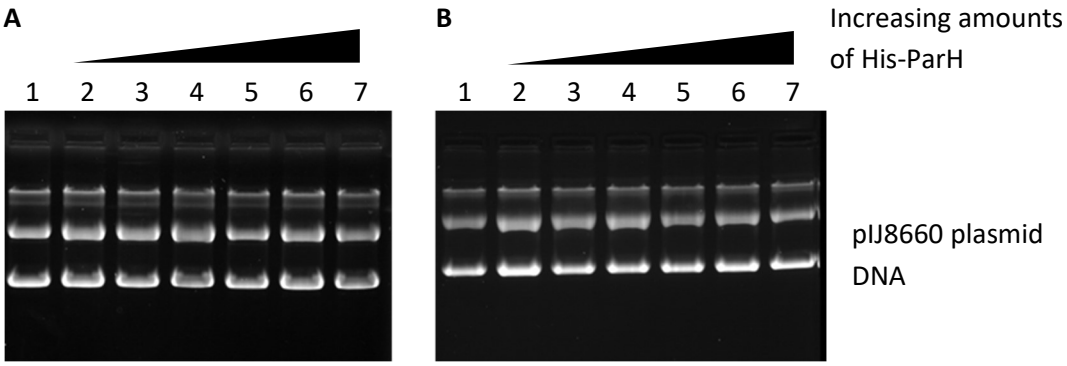

Figure 88: Electrophoretic mobility shift assay of His-ParH and pIJ8660

(A) An electrophoretic mobility shift assay was performed in which pIJ8660 was incubated for 30 minutes at room temperature both in the absence (Lane 1) and with increasing amounts (Lanes 2-7) of purified His-ParH protein in a Tris buffer (50 mM Tris-HCl, 150 mM NaCl, 10 mM $MgCl_2$ pH8). The amount of His-ParH increased as follows: 13 pmol/0.65 µM (Lane 2), 26 pmol/1.3 µM pmol (Lane 3), 39 pmol/1.95 µM (Lane 4), 52 pmol/2.6 µM (Lane 5), 65 pmol/3.25 µM (Lane 6), 78 pmol/3.9 µM (Lane 7).
(B) The same reactions were set up in the presence of 1 mM ATP.
Samples were analysed on a 0.7% agarose gel made with TA buffer without the addition of ethidium bromide. The gel was subsequently incubated for 1 hour in TA buffer containing 2 µg/ml ethidium bromide to stain the DNA.

We therefore wished to investigate whether either ParH or Hyp affected DNA binding of the other protein. To test this, reactions were set up to observe a gel shift of pIJ8660 in the presence of increasing amounts of purified His-Hyp protein, increasing amounts of purified His-ParH protein, and increasing amounts of purified His-Hyp protein in the presence of a fixed amount of His-ParH. The reactions were carried out in the presence of ATP (1mM) and were incubated for 30 minutes at room temperature in a Tris based buffer (50 mM Tris-HCl, 150 mM NaCl, 10 mM $MgCl_2$ pH 8). Samples were analysed on 0.7% agarose gel (Figure 89).

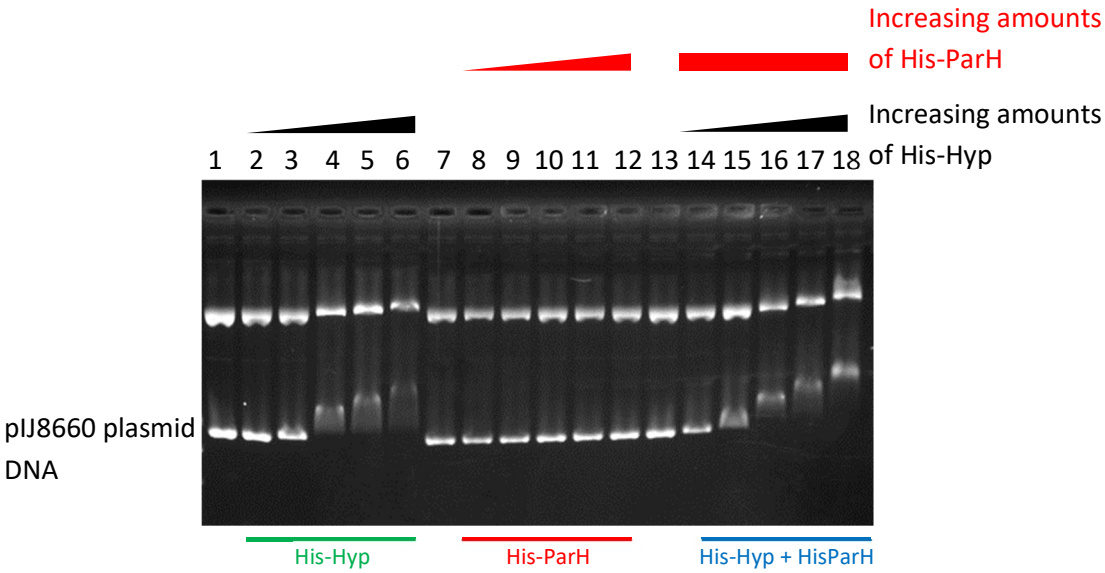

Figure 89: Electrophoretic mobility shift assay of His-Hyp, His-ParH and pIJ8660

An electrophoretic mobility shift assay was performed in which pIJ8660 was incubated for 30 minutes at room temperature both in the absence (Lanes 1, 7 and 13) and with increasing amounts of either His-Hyp (Lanes 2-6) or His-ParH (Lanes 8-12) protein in a Tris buffer (50 mM Tris-HCl, 150 mM NaCl, 10 mM $MgCl_2$ pH8). The amount of protein was increased as follows: 13 pmol/0.65 µM (Lanes 2 and 8), 26 pmol/1.3 µM (Lanes 3 and 9), 39 pmol/1.95 µM (Lanes 4 and 10), 52 pmol/2.6 µM (Lanes 5 and 11) and 65 pmol/3.25 µM (Lanes 6 and 12). The plasmid was also incubated with increasing amounts of His-Hyp with the addition of a constant amount of His-ParH (65 pmol/3.25 µM). The amount of His-Hyp was increased as follows: 13 pmol/0.65 µM (Lane 14), 26 pmol/1.3 µM (Lane 15), 39 pmol/1.95 µM (Lane 16), 52 pmol/2.6 µM (Lane 17) and 65 pmol/3.25 µM (Lane 18). Samples were analysed on a 0.7% agarose gel made with TA buffer without the addition of ethidium bromide. The gel was subsequently incubated for 1 hour in TA buffer containing 2 µg/ml ethidium bromide to stain the DNA.

As with previous experiments, the addition of His-Hyp caused pIJ8660 DNA to shift in correlation with the amount of His-Hyp protein, while His-ParH did not cause any observable shift. The addition of His-ParH to the His-Hyp-pIJ8660 reaction results in a clear increase in the observable shift. This increase could be due to ParH-Hyp interaction leading to the formation of a larger nucleoprotein complex on the DNA. This would cause a larger shift compared with a nucleoprotein complex consisting solely of just His-Hyp. Alternatively, this increase in shift could be the result of His-Hyp promoting His-ParH DNA binding leading to stable His-ParH-DNA nucleoprotein complexes which are able to be maintained

during electrophoresis. This nucleoprotein complex could then migrate along the DNA creating separate complexes from those formed between His-Hyp and DNA. This would also lead to a larger shift in DNA as the total mass of the protein-DNA molecule increases.

5.5 The pelleting assay shows ParH-DNA interaction

After visualising protein-DNA interaction using electrophoretic mobility shift assays, we wished to also test the interaction using pelleting assay. Both purified His-Hyp (160 pmol/8 μM) and His-ParH (40 pmol/2 μM) protein were incubated in the presence of circular pIJ8660 for 30 minutes at room temperature in a Tris buffer (50 mM Tris-HCl, 150 mM NaCl, 10 mM $MgCl_2$ pH 8). They were also incubated together in a 1:2 (40 pmol/2 μM His-ParH, 80 pmol/4 μM His-Hyp) and 1:4 (40 pmol/ 2 μM His-ParH, 160 pmol His-Hyp) molar ratio in the presence of DNA. After incubation the samples were centrifuged using the same conditions as before, after which the supernatant was collected and the pellet fraction re-suspended. All fractions were then analysed using 10% SDS-PAGE (Figure 90). In the previous ultracentrifugation experiment, we demonstrated that His-Hyp is found in entirely in the supernatant, while the majority His-ParH is found in the supernatant with a small proportion pelleting. However, in the presence of DNA, His-Hyp is almost entirely pulled into the pellet fraction. This is consistent with the observations from the electrophoretic mobility shift assays involving His-Hyp, and confirms the strong DNA binding properties of His-Hyp. In addition around half of the His-ParH in the reaction was pulled into the pellet by the DNA. Along with the inability to observe a shift with His-ParH in the electrophoretic mobility shift assays, indicates that on its own His-ParH has week affinity for DNA. It could also suggest that only specific oligomers of His-ParH are able to bind DNA. If this is the case then it is possible that a partner protein that affects the oligomerisation of His-ParH could regulate the DNA binding affinity of His-ParH. There were no additional effects on the pelleting of the proteins when His-ParH and His-Hyp were incubated together with pIJ8660, regardless of the molar ration between the two

proteins. While this would indicate that the proteins are not affecting the DNA binding properties of each other it does not completely rule it out. This assay does not measure the strength of protein-DNA interaction. It is entirely possible that while His-Hyp is not promoting any additional interactions between His-ParH and DNA, it is possible that the affinity of those His-ParH molecules that are able to bind DNA is enhanced by the presence of His-Hyp.

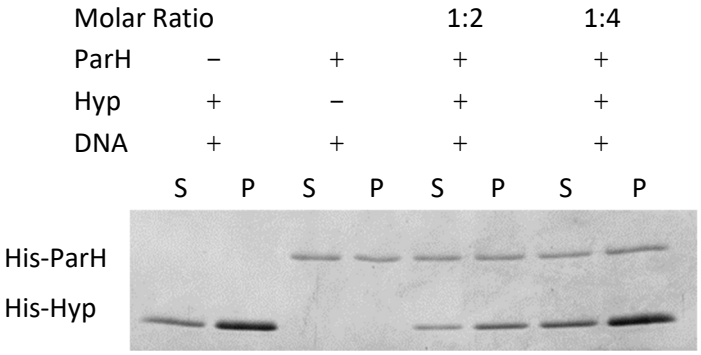

Figure 90: Pelleting assay of His-ParH, His-Hyp and pIJ8660

His-ParH (40 pmol/2 µM) and His-Hyp (160 pmol/8 µM) were incubated separately and then together in a 1:2 (80 pmol/4 µM His-Hyp) and 1:4 (160/8 µM pmol His-Hyp) molar ratio in which the amount of His-ParH (40/2 µM pmol) remained constant. Reactions were all carried out in the presence of pIJ8660.
After a 30 minute incubation at room temperature in a Tris buffer (50 mM Tris-HCl, 150 mM NaCl, 10 mM $MgCl_2$ pH 8) the samples were centrifuged for 30 minutes at 450,420 g at 4°C generating both supernatant and pellet fractions. Samples were analysed on 10% SDS PAGE and visualised using Coomassie staining.

5.6 ParH interacts with Scy – a key component of the TIPOC

As previously discussed there a link between growth and division has already been shown in *S. coelicolor* (Ditkowski et al., 2013). This was demonstrated through the interaction between Scy, a component of the TIPOC, and ParA, which is involved in chromosome segregation. The interaction between Scy and ParA indicated that at lower levels of ParA, Scy is able to sequester ParA to the tip, and

thus block chromosome segregation. At late development, ParA is upregulated which overcomes the block on polymerisation by Scy and in turn cause ParA to disassemble Scy, ending the growth phase of *S. coelicolor*. We wished to see whether such a regulatory mechanism existed between Scy and ParH, which as we have shown is a homologue of ParA.

To investigate this possible link we first used bacterial two-hybrid assay to determine whether the two proteins interact. The bacterial two-hybrid constructs for Scy, pUT18c-Scy and pKT25-Scy (Figure 91), had already been generated and used in publications by the group (Holmes et al., 2013; Walshaw et al., 2010).

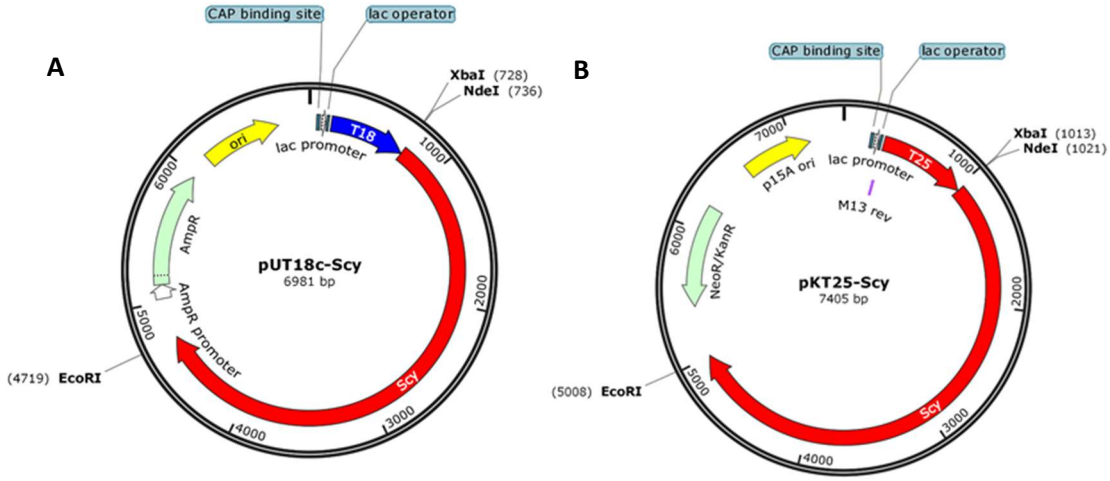

Figure 91: The Scy constructs used in bacterial two-hybrid assays, pUT18c-Scy and pKT25-Scy.

Scy was cloned into the *Xba*I and *Eco*RI sites of both pUT18c and pKT25 to generate plasmids pUT18c-Scy (A) and pKT25-Scy (B). In both constructs Scy was cloned to the C-terminus of the T18 and T25 domains of adenylate cyclase such that a fusion protein is generated.

To test interaction, the *E. coli* strain BTH101, which is adenylate cyclase deficient, was co-transformed with pUT18c-ParH and pKT25-Scy, and with pUT18c-Scy and pKT25-ParH. After transformation, three colonies were picked along with colonies containing both positive and negative controls and plated onto LB agar deficient in glucose, before being incubated at 30°C to allow best visualisation of the blue/white colony screen. Colonies were monitored over two days to observe

the colour (Figure 92). In both combinations the colonies containing ParH and Scy bacterial two-hybrid constructs, turned blue when compared to the negative control and were comparable in colour to the positive control. This suggests, that like ParA, ParH also interacts with Scy. This is not surprising given the observations from the *S. coelicolor parH* mutant strain, which had branching aerial hyphae. This had suggested some relationship between ParH and the TIPOC, the multi-protein assembly important to growth and division.

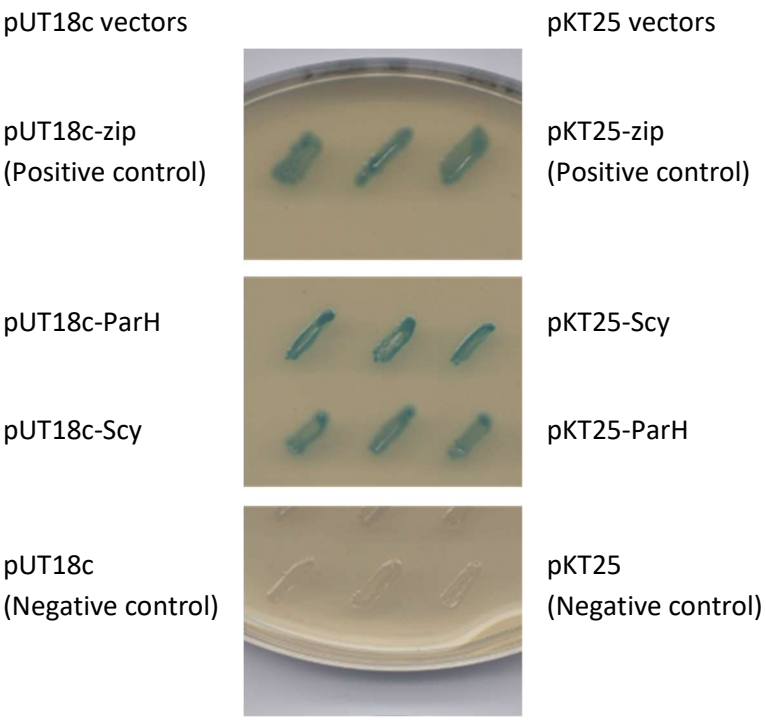

Figure 92: Bacterial two-hybrid assay of ParH and Scy

E. coli strain BTH101 was co-transformed with pUT18c-ParH and pKT25-Scy, and with pUT18c-Scy and pKT25-ParH. Also co-transformed were the positive controls pUT18c-zip and pKT25-zip as well as negative controls pUT18c and pKT25. Three colonies from each transformation were picked and streaked on an LB plate deficient with glucose but supplemented with IPTG, X-gal, ampicillin and kanamycin. The plate was incubated for 2 days at 30°C

After showing interaction using bacterial two-hybrid assay, we decided to test if the nature of the ParH-Scy interaction was similar to the ParA-Scy interaction. Previous pelleting assays has shown that in the absence of other proteins Scy is found in the pellet fraction (Holmes et al., 2013). ParA on the other hand is found in the supernatant fraction (Ditkowski et al., 2013). However, when

incubated with ATP, the oligomerisation of ParA changes and it is pulled to the pellet fraction (Ditkowski et al., 2013). Interestingly when Scy and ParA are incubated together in the presence of ATP both proteins are pulled to the supernatant suggesting a reciprocal depolymerisation effect. In order to fully pull Scy to the supernatant, ParA needs to be in at least 4 molar excess of Scy (Ditkowski et al., 2013). To test if we could observe a similar effect on His-Scy with His-ParH, reactions were set up in which His-Scy (30 pmol/ 1.5 µM) and His-ParH (240 pmol/ 12 µM) were incubated separately and then together in 1:2 (60 pmol/3 µM His-ParH), 1:4 (120 pmol/6 µM His-ParH) and 1:8 (240 pmol/12 µM His-ParH) molar ratios in which the amount of His-Scy (30 pmol/1.5 µM) remained constant. The same reactions were also set up in the presence of 1 mM ATP to observe the effects of ATP the interaction. Incubations were carried out for 30 minutes at room temperature in a Tris buffer (50 mM Tris-HCl, 150 mM NaCl, 10 mM $MgCl_2$ pH 8). Reactions were incubated for 30 minutes at room temperature in a Tris based buffer (50 mM Tris-HCl, 150 mM NaCl, 10 mM $MgCl_2$ pH 8). After incubation the samples were centrifuged using the same conditions as before, after which the supernatant was collected and the pellet fraction re-suspended. All fractions were then analysed using 10% SDS-PAGE (Figure 93).

In agreement with established observations, His-Scy was found in the pellet fraction in both the presence and absence of ATP. As before, His-ParH was found mainly in the supernatant, with a small amount visible in the pellet. This was also true in the presence of ATP, showing that ATP has no effect on His-ParH oligomerisation. When His-ParH and His-Scy are mixed a proportion of the His-ParH protein is pulled into the pellet with His-Scy suggesting interaction between the proteins, which are probably forming some kind of complex. At the same time a small amount of His-Scy is moved to the supernatant in the presence of His-ParH. The amount of His-Scy that is moved to the supernatant fraction increases in relation to increases in the amount of His-ParH in the reaction suggesting that this change in His-Scy oligomerisation is dependent on interaction with His-ParH. The addition of ATP to the reaction causes an increase in the amount of His-Scy and His-ParH that is found in the supernatant. This is true at all molar ratios tested

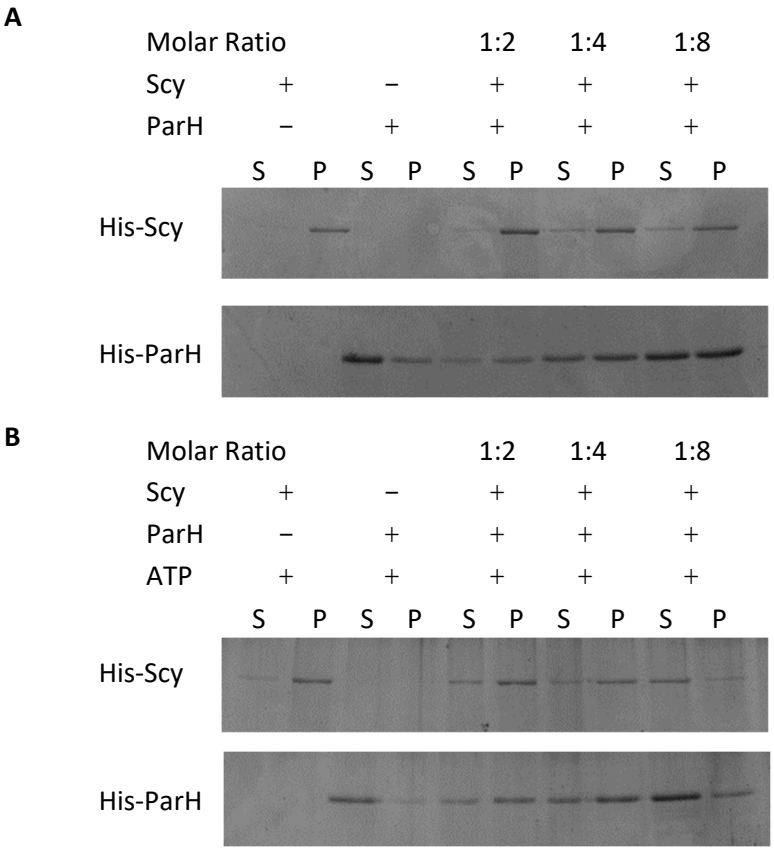

Figure 93: Pelleting assay of His-ParH and His-Scy.

(A) His-Scy (30 pmol/1.5 µM) and His-ParH (240 pmol/12 µM) were incubated separately and then together in 1:2 (60 pmol/3 µM His-ParH), 1:4 (120 pmol/6 µM His-ParH) and 1:8 (240 pmol/12 µM His-ParH) molar ratios in which the amount of His-Scy (30 pmol/1.5 µM) remained constant.
(B) Reactions were set up as described for (A) in the presence of 1 mM ATP.
After a 30 minute incubation at room temperature in a Tris buffer (50 mM Tris-HCl, 150 mM NaCl, 10 mM $MgCl_2$ pH 8) the samples were centrifuged for 30 minutes at 450,420 g at 4°C generating both supernatant and pellet fractions. Samples were analysed on 10% SDS PAGE and visualised using Coomassie staining.

between the proteins, reaching almost all of His-Scy at a 1:8 His-Scy:His-ParH molar ratio. This suggests that in the presence of ATP and with a higher molar ratio of His-ParH, His-Scy begins to disassemble. This data is similar to that found in the pelleting assays between ParA and Scy. However there are a couple off differences. Firstly, the molar excess to cause His-Scy to move to the supernatant is higher for His-ParH than it is for His-ParA. This could be because, at least under these conditions, His-ParH is less effective at binding ATP than would ParA. Thus in order to get enough of the right oligomer bound to ATP that will cause depolymerisation

of His-Scy, there needs to be a lot more His-ParH overall. The second difference is that, as we are unable to show oligomerisation of His-ParH in response to ATP, and in the pelleting assay this interaction does not result in pelleting, we cannot say that His-Scy is causing a depolymerisation of His-ParH in this condition. In fact the presence of His-ParH in the supernatant in this condition could be the result of it interacting with a lower order assembly of His-Scy and forming a complex that does not pellet. Overall this data further demonstrates interaction between Scy and ParH. It could also suggest that the nature of this interaction is similar to the relationship between ParA and Scy, which would suggest that there is a regulatory role for ParH in the functioning of the TIPOC. This fits in with the phenotype seen in the *parH* mutant strain of *S. coelicolor*, in which aerial hyphae exhibited a branching phenotype. It is probable that ParH helps to maintain the correct organisation of the TIPOC by stabilising Scy assemblies, ensuring that growth and branching is carried out in the most efficient and effective manner. Also of note, is that this is the first experiment with ParH that shows a clear effect with the addition of ATP, suggesting that there probably is a functional role to the ATP binding of ParH.

5.7 ParH interacts with ParB – a key component of chromosome segregation.

After demonstrating a link between ParH and Scy, and thus a possible link between growth and division, we wished to explore the possibility of a link between ParH and the mechanism of chromosome segregation in *S. coelicolor*. The current established model of chromosome segregation in *S. coelicolor* revolves around the ParAB chromosome segregation machinery which we discussed earlier. Given that ParH has a non-ParB like partner protein (Hyp) we decided to explore whether there was crosstalk between the ParA system and the ParH system through a ParH-ParB interaction. We wished to again utilise bacterial two-hybrid assay to determine a ParH-ParB interaction and so *parB* was cloned into the bacterial two-hybrid vectors to generate pUT18c-ParB and pKT25-ParB.

(Figure 94). To generate the constructs the *parB* gene was amplified from *S. coelicolor* chromosomal DNA using the primers 'ParB *Nde*I *Xba*I FRW' and 'ParB Eco UTC REV'. The primers allow cloning of the *parB* gene in frame downstream of the adenylate cyclase domains using *Xba*I and *Eco*RI. Clones containing recombinant DNA were sequenced to confirm mutation free constructs.

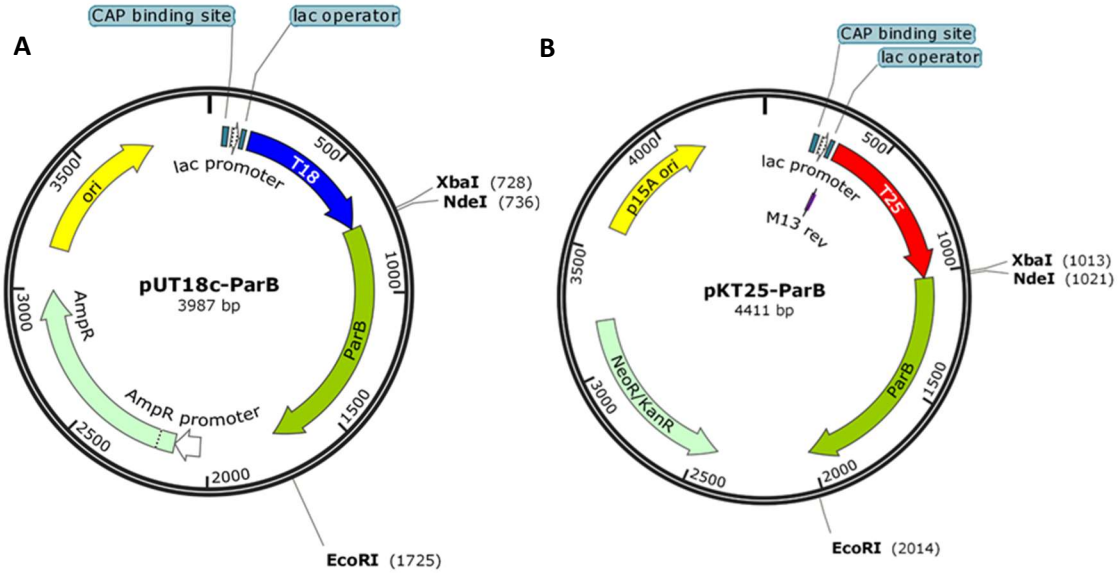

Figure 94: The ParB bacterial two-hybrid plasmids pUT18c-ParB and pKT25-ParB.

(A) The plasmid pUT18c-ParB is a derivative of pUT18c with the *parB* gene cloned using the restriction sites *Xba*I and *Eco*RI.
(B) The plasmid pKT25-ParB is a derivative of pKT25 with the *parB* gene cloned using the restriction sites *Xba*I and *Eco*RI.
The *parB* gene was amplified from *S. coelicolor* chromosomal DNA using the primers 'ParB *Nde*I *Xba*I FRW' and 'ParB Eco UTC REV'.

To test interaction, the *E. coli* strain BTH101, which is adenylate cyclase deficient, was co-transformed with pUT18c-ParH and pKT25-ParB, and with pUT18c-ParB and pKT25-ParH. After transformation, three colonies were picked along with colonies containing both positive and negative controls and plated onto LB agar deficient in glucose, before being incubated at 30°C to allow best visualisation of the blue/white colony screen. Colonies were monitored over two days to observe the colour (Figure 95). In both combinations the colonies containing ParH and ParB bacterial two-hybrid constructs, turned blue when compared to the negative control and were comparable in colour to the positive

control. This suggests that ParH interacts with ParB. This would indicate that there is cross-talk between the ParH-Hyp system and the ParAB system, which would perhaps create a link between chromosome segregation and septum placement.

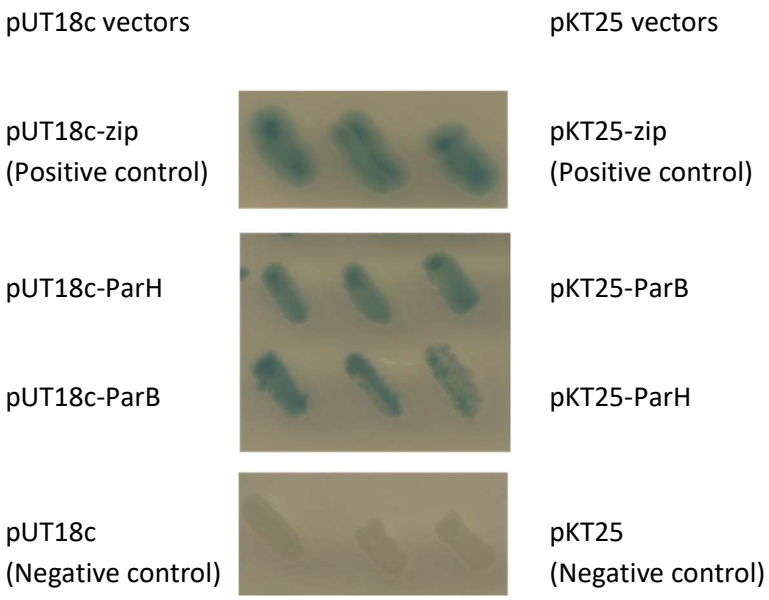

Figure 95: Bacterial two-hybrid assay of ParH and ParB

E. coli strain BTH101 was co-transformed with pUT18c-ParH and pKT25-ParB, and with pUT18c-ParB and pKT25-ParH. Also co-transformed were the positive controls pUT18c-zip and pKT25-zip as well as negative controls pUT18c and pKT25. Three colonies from each transformation were picked and streaked on an LB plate deficient with glucose but supplemented with IPTG, X-gal, ampicillin and kanamycin. The plate was incubated for 2 days at 30°C

After showing interaction through bacterial two-hybrid, we decided to further test interaction between ParB and ParH using the pelleting assay. Reactions were set up in which His-ParH (120 pmol/6 µM) and His-ParB (120 pmol/6 µM) were incubated both separately and together in a 1:1 molar ratio. The reactions were carried out in the absence and presence of ATP (1 mM) and were incubated for 30 minutes at room temperature in a Tris based buffer (50 mM Tris-HCl, 150 mM NaCl, 10 mM $MgCl_2$ pH 8). After incubation the samples were centrifuged using the same conditions as before, after which the supernatant was collected and the pellet fraction re-suspended. All fractions were then analysed using 8% SDS-PAGE (Figure 96).

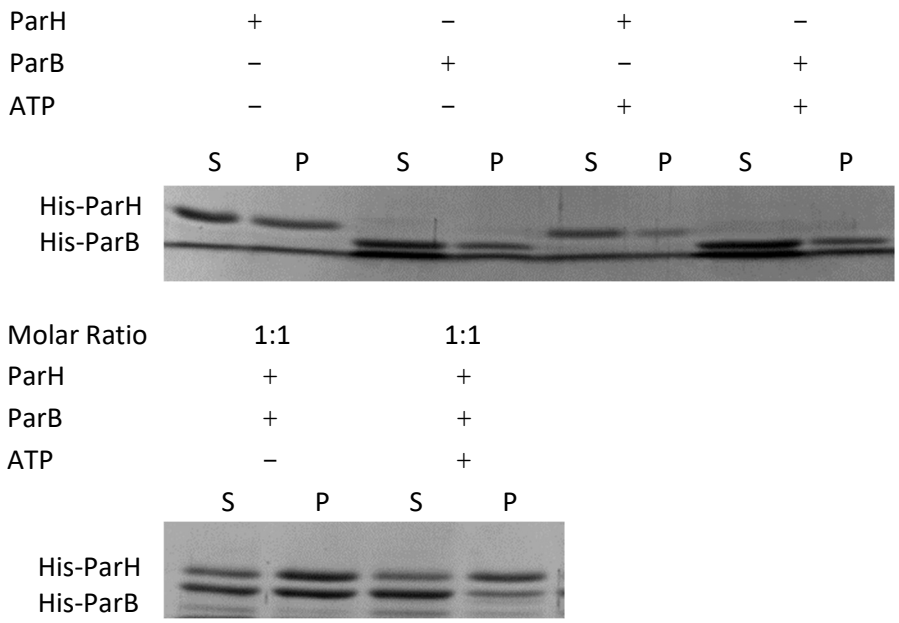

Figure 96: Pelleting assay of His-ParH and His-Hyp.

(A) His-ParH (120 pmol/6 µM) and His-ParB (120 pmol6 µM) were incubated separately in the presence and absence of 1 mM ATP.
(B) His-ParH (120 pmol6 µM) and His-ParB (120 pmol6 µM) were incubated together in a 1:1 molar ratio in the presence and absence of 1 mM ATP.
After a 30 minute incubation at room temperature in a Tris buffer (50 mM Tris-HCl, 150 mM NaCl, 10 mM $MgCl_2$ pH 8) the samples were centrifuged for 30 minutes at 450,420 g at 4°C generating both supernatant and pellet fractions. Samples were analysed on 8% SDS PAGE and visualised using Coomassie staining.

As with the previous observations, His-ParH was found mainly in the supernatant in both the absence and presence of ATP, with a small amount of His-ParH pelleting under both conditions. Likewise His-ParB was found mainly in the supernatant under these two conditions, although again a small amount of His-ParB was also found in the pellet fraction. There is no published data on how ParB from *S. coelicolor* behaves in pelleting assay so we have taken this result at face value. When mixed together in the absence of ATP, both proteins are moved to the pellet fraction, although some remains in the supernatant. This data suggests that the proteins are able to interact and form a complex which pellets when subjected to ultracentrifugation. While interaction between the proteins is unsurprising given the interaction observed *in vivo* using bacterial two-hybrid, it is surprising that the interaction does not appear to require ATP. The well-established interaction between ParB and ParA in *S. coelicolor* is ATP dependent,

with mutants that are deficient in ATP binding losing their ability to interact with ParB. We had expected to find the same requirements for ParB-ParH interaction, but this does not appear to be the case. The most surprising and interesting result was the apparent effect on this interaction from the addition of ATP. In these conditions His-ParB is moved back to mainly being in the supernatant, while the majority of His-ParH remains in the pellet fraction. This indicates two things, firstly that interaction between His-ParH and His-ParB is abolished by the presence of ATP. The fact they end up in different fractions would indicate that they are no longer bound in a complex. Secondly, and most importantly, that the oligomerisation of His-ParH has changed in response to the presence of both His-ParB and ATP. The fact that the interaction between the proteins has been abolished suggests that this change of state is likely to be due to ATP binding. Given that we are not able to observe a change in oligomerisation of His-ParH in the presence of ATP in other circumstances could mean that His-ParB is promoting the interaction between His-ParH and ATP which is subsequently leading to a change in oligomerisation. Therefore perhaps ParB is a partner protein of ParH, which activates its interaction with ATP.

5.8 Neither ParB or Hyp increase the ATPase activity of ParH

After exploring protein interactions of ParH, we wished to determine whether any of these proteins regulate the ATPase activity of ParH. As we have previously discussed the regulation of ATPase activity is an important regulatory mechanism of ParA/MinD proteins. In *S. coelicolor*, the ATPase activity of ParA is regulated by its partner protein ParB, encoded from the gene downstream of *parA* (Jakimowicz et al., 2007). Although we have been able to show interaction between ParH and Hyp, translationally coupled to ParH, and with ParB, neither of these interactions appear to be ATP dependent. However, we decided to test whether these protein could stimulate ATPase activity. To this end, His-ParH (10 µM) was incubated in the presence of 1 mM ATP. In addition His-ParH and ATP were also incubated in the presence of His-Hyp in a 1:4 (10µM His-ParH, 40 µM

His-Hyp) molar ratio and in the presence of His-ParB in a 1:1 (10 µM His-ParH, 10 µM His-ParB) molar ratio. The reactions were set up in a Tris buffer (50 mM Tris-HCl, 150 mM NaCl, 10 mM $MgCl_2$ pH 8) and incubated at 30°C over a period of 20 hours. Samples were taken before incubation, and at 2 hours, 4 hours and 20 hours of incubation. The relative ADP-ATP content was measured by reverse-phased HPLC to determine the concentration of ADP in the sample (Figure 97)

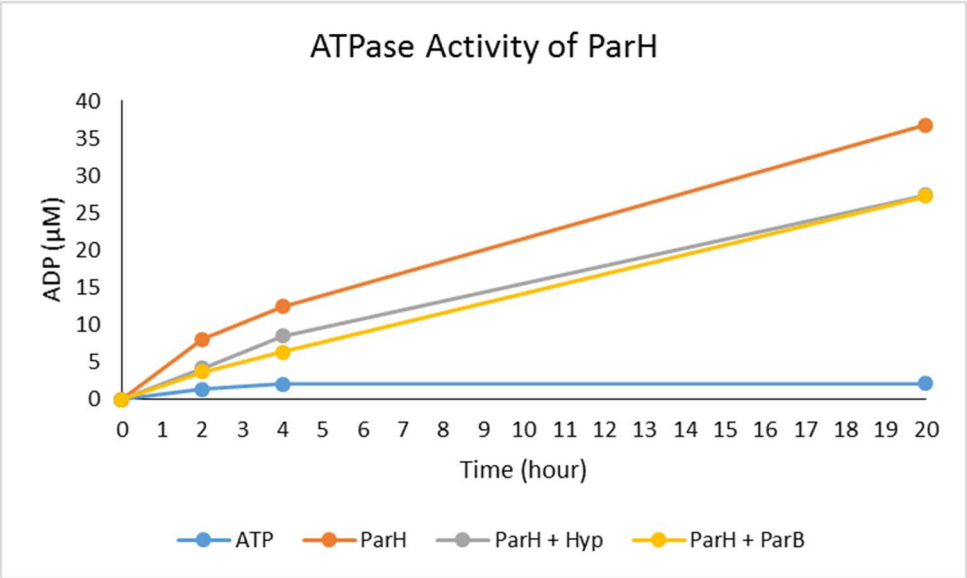

Figure 97: ATPase assay of His-ParH.

His-ParH (10 µM) was incubated in the presence of 1 mM ATP on its own and in the presence of His-Hyp in a 1:4 (10 µM His-ParH, 40 µM His-Hyp) molar ratio or His-ParB in a 1:1 (10 µM His-ParH, 10 µM His-ParB) molar ratio. ATP was also incubated separately as a control. Reactions were incubated at 30°C with samples analysed by reversed-phased HPLC to monitor ADP concentration after 2 hours, 4 hours and 20 hours incubation.

The ATPase assay of His-ParH shows that it is a very weak ATPase. After 2 hours incubation the concentration of ADP in the solution had increased to less than 10 µM which would correspond to less than 1% of the total amount of starting ATP. The reaction was set up such that the ratio of ATP to His-ParH was 1:100 meaning that the amount of ATP hydrolysed in two hours suggests that one molecule of His-ParH hydrolyses one molecule of ATP every two hours. The absolute rate of ATP hydrolysis was not that important, we wished to know

whether either His-Hyp or His-ParB would increase the rate and indicate a regulatory mechanism. Unfortunately, neither protein increased the rate when added to the reaction. If anything we observed a slight decrease in activity but we do not think this is significant as this experiment was an attempt at an indicative result rather than an accurate measurement of activity. Under these conditions tested, we have not found an indication of regulation. This does not rule out the possibility that these proteins do regulate the ATPase activity of ParH, it maybe that they require another component such as DNA.

5.9 Summary

In this chapter we have sort to understand the partner proteins of ParH and how those interactions may work. We first investigated interaction between ParH and Hyp. Although we had already observed this interaction in the last chapter using native-PAGE we wished to confirm this interaction. While we were able confirm interaction *in vitro* using a pelleting assay, we were unable to see interaction in vivo using bacterial two-hybrid in the heterologous host *E. coli*, although this is likely due to the limitations of the assay rather than non-interaction. The *in vitro* interaction we observed is not dependent upon, nor is it affected by the presence of ATP suggesting interaction occurs independently of ATP.

We were able to demonstrate that Hyp is a DNA binding protein in vitro using both an electrophoretic mobility shift assay and pelleting assay. Therefore, while Hyp is not a ParB homologue, it is a DNA binding partner of a ParA-like protein. We have not yet shown a specific DNA target sequence for Hyp, but it is a possibility that one exists. We were however able to show that ParH also has affinity for DNA although given that we had interaction in the pelleting assay but not with the electrophoretic mobility shift assay, it is probably a weak interaction. Surprisingly, DNA binding activity of ParH was once again unaffected by the addition of ATP in the conditions we tested. Interestingly we were able to see a bigger shift in the electrophoretic mobility shift assay when Hyp was incubated in

the presence of ParH. This further confirms interaction between ParH and Hyp and opens up the possibility that they have a shared function involving DNA.

We then turned to observing interaction between ParH and both Scy and ParB. We observed positive interaction for both proteins using the bacterial two-hybrid assay. Interaction between ParH and Scy indicates that the growth defect seen in the *parH* mutant strain is due to the effect that ParH has on the TIPOC through its interaction with Scy. The pelleting assay using the two proteins also suggested that the ParH-Scy interaction has a similar dynamic to the ParA-Scy interaction. ParH may play a similar role in regulating the switch from growth to cell division prior to sporulation. The ParH interaction with ParB is arguably more fascinating than the ParH-Scy interaction. The observations made in the pelleting assay between ParH and ParB suggests not only that the proteins interact in the absence of ATP, but that ParB might induce a conformational change in ParH in the presence of ATP. Interaction between ParH and ParB in the absence of ATP is different from the ParA interaction with ParB which is ATP dependant. This suggests that the ParH-ParB interaction occurs to effect a different outcome than the ParA-ParB interaction, which further suggests different roles in the cell for ParA and ParH.

Finally, we investigated the ATPase activity of ParH. While we were able to show basal levels of ATPase activity of ParH comparable with other ParA-like proteins we were not able to show upregulation with either ParB or Hyp suggesting, under these conditions at least, they are not regulating this activity. It does not however, rule out the possibility that there is another protein regulating this activity.

6 Structural Studies of Hyp

In the preceding chapters we identified established that Hyp is a DNA binding protein that, according to analytical gel filtration, forms a tetramer. As has already been discussed, based on its amino acid sequence Hyp is an *Actinomycete* specific protein with homologues of no known function. While sequence similarity is important in identifying closely related homologues of a protein it is not the only way the proteins can share homology. While it was known that FtsZ was an important gene in the formation of septa during the bacterial division process, for a while it was considered a protein that was specific to bacteria and archaea with no related proteins in eukaryotes. It was only in the discovery of its structure that the resemblance of FtsZ to the eukaryotic Tubulin was identified (Figure 98)(Nogales et al., 1998).

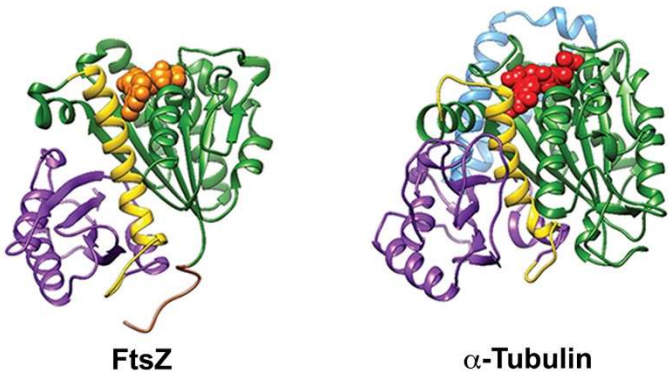

Figure 98: Comparison of the 3D structures of FtsZ and tubulin showing a conserved fold. Taken from Palumbo et al., (2015).

This structural identity between FtsZ and Tubulin played a key role in establishing the bacterial cytoskeleton. Before this, it was thought that bacterial shape was maintained through their cell wall, rather than underlying cytoskeletal proteins, such as those found in eukaryotes. As structural data has expanded, more proteins from bacteria with no sequence similarity to eukaryotic proteins have been found to share structural similarity with eukaryotic proteins. This is especially true for proteins involved in the bacterial cytoskeleton. After the discovery that FtsZ is a

structural homologue of Tubulin, the structure of MreB, which is responsible for lateral cell wall extension, was solved (van den Ent et al., 2001). This structure showed similarity to another eukaryotic cytoskeletal element, actin (Figure 99).

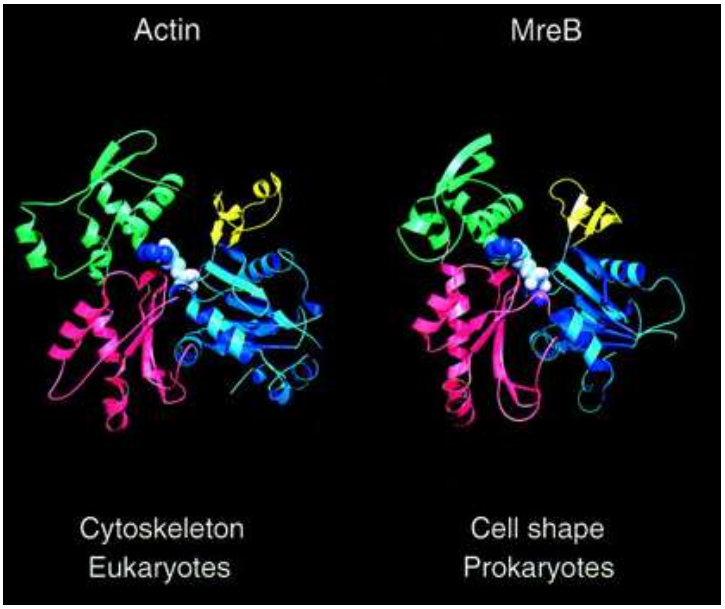

Figure 99: Comparison of the 3D structures of MreB and actin showing a conserved fold. Taken from Carballido-Lopez and Errington, (2003).

Thus, through structural data, structural homologues of two of the three cytoskeletal elements from eukaryotes, tubulin and actin, have been found in prokaryotes. The remaining class of eukaryotic cytoskeletal proteins, intermediate filaments, has thus far not been identified in bacteria using structural data. However, secondary structural predictions of Crescentin from *C. crescentus*, his identified it as a possible prokaryotic homologue of the eukaryotic intermediate filaments (Ausmees et al., 2003). This has given rise to a new class of prokaryote cytoskeleton proteins known as intermediate filament-like proteins. Suggested other members of this class include FilP and Scy in *S. coelicolor*. Structural studies of ParA and ParB have demonstrated that these are cytoskeletal proteins that are unique to prokaryotes and show no structural similarity to known eukaryotic proteins. Soj (ParA) is an ATPase with a deviant Walker A motif while ParB contains a helix-turn-helix DNA binding domain (Figure 100) (Leonard et al., 2004, 2005).

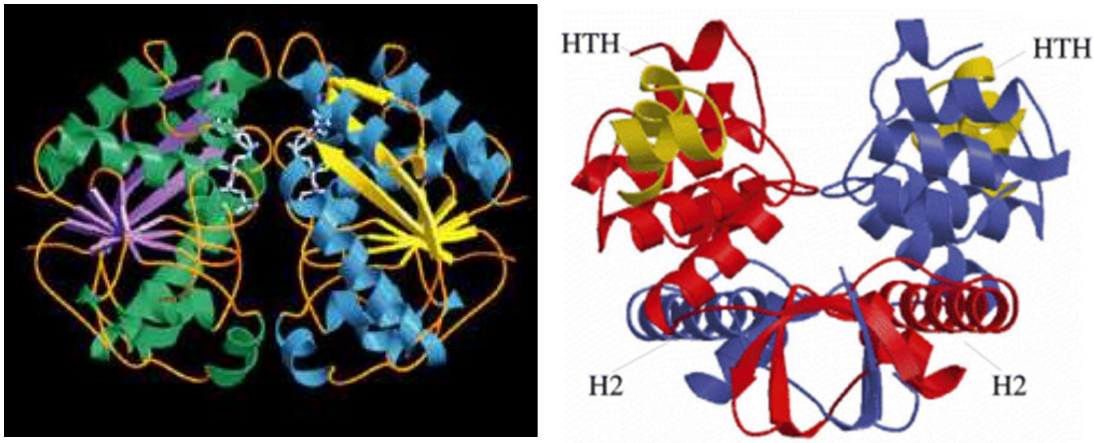

Figure 100: The structures of Soj (ParA) and ParB.
Both Soj (A) and ParB (B) are prokaryote cytoskeletal components with no known eukaryotic proteins sharing structural homology. Taken from Leonard et al., (2004, 2005).

The structure of Soj consists of a core consisting of one antiparallel and seven parallel and β-strands which hare surrounded by α-helices. At the centre of the dimer is the nucleotide binding motifs of the protein. ParB on the other hand consists of a dimer which is held together by an α-helix domain with each subunit containing the HTH DNA binding domain.

The fact that Hyp only had homologues of unknown function and that we have established it as a DNA binding protein, led us to question whether Hyp has a novel DNA binding motif or whether we could identify structural homologues for the protein. We also selected Hyp to undertake structural studies because it forms a single oligomer, a tetramer, whereas ParH multiple forms of oligomers, which is not suitable for crystallography. To achieve this we used X-ray crystallography, which requires protein crystals from which native X-ray diffraction data can be collected. Once data is collected, the crystal structure can be solved either through molecular replacement via comparison with the known structure of a similar protein or through experimental phasing such as single wavelength anomalous dispersion (SAD), which relies on soaking the crystal in heavy-metal salts and observing anomalies in the diffraction pattern to solve the phase problem. After the generation of an electron density map, a final protein structure can be generated through repeated rounds of model binding and refinement.

6.1 Crystallisation of Hyp

For X-ray crystallography it is necessary to grow a well ordered crystal that will strongly diffract X-rays. To prevent contaminant molecules which will compete for binding sites on growing crystals and introduce internal disorder into the crystal it is necessary to obtain protein over 90% pure. In addition, the protein should be purified in a single batch and not aggregate in order to achieve the greatest chance for successful crystallisation (Benvenuti and Mangani, 2007). We have previously shown purification from solution of His-Hyp using the heterologous host *E. coli*. We therefore set out to purify His-Hyp from a 500 ml LB culture in which His-Hyp was

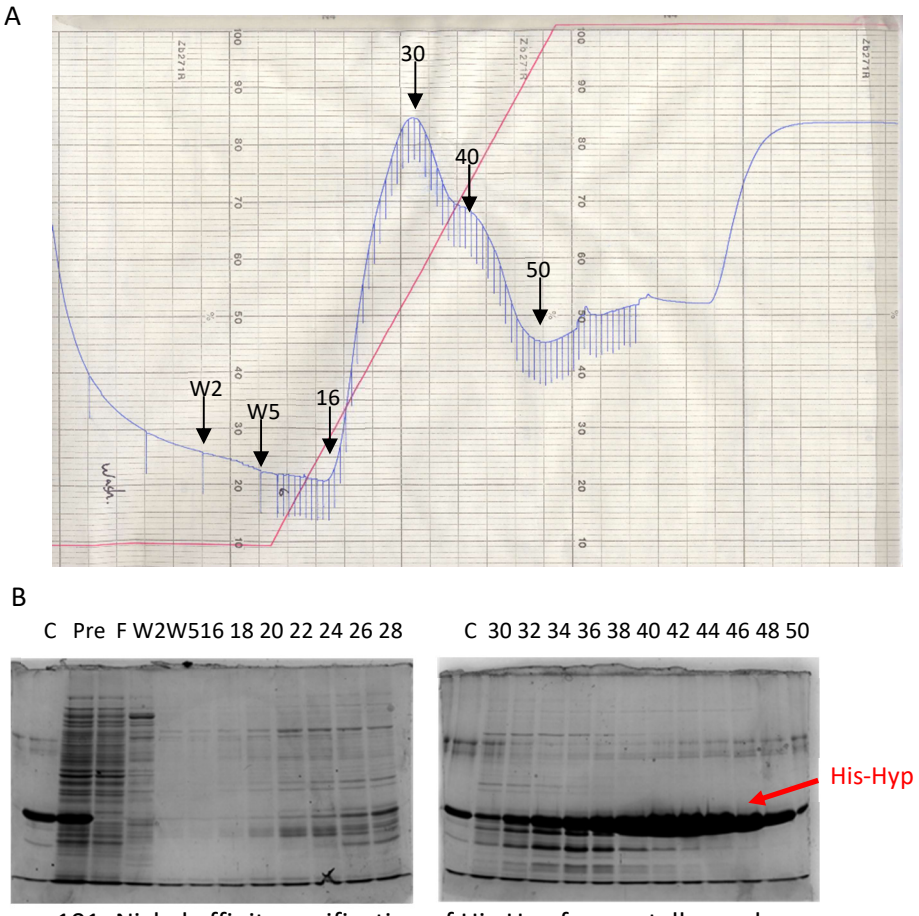

Figure 101: Nickel affinity purification of His-Hyp for crystallography.

(A) UV absorbance measured at 280 nm of nickel affinity purification of His-Hyp for crystallography.
(B) Fractions from purification were analysed by 12% SDS-PAGE to determine the elution fractions containing purified His-Hyp protein. Fractions loaded include a control (C) containing purified His-Hyp protein, a pre-load fraction (Pre), a flow through fraction (F), 2 wash fractions (W2 and W5), and elution fractions (16-50) for which every other fraction was loaded. The gel was visualised using Coomassie staining.

produced under the optimal conditions set out in chapter 4. His-Hyp was purified as before through nickel affinity chromatography, but using an AKTA machine set up to purify proteins at 4°C. Purification was performed at this temperature to minimise any chance of the protein degrading prior to undergoing crystallisation trials. A 5ml HisTrap HP nickel column (GE Healthcare) was used for purification which was undertaken in a Tris based buffer (50mM Tris, 150 mM NaCl, 20 mM $MgCl_2$, 10 mM imidazole pH8). The protein was eluted using a gradient increase in imidazole up to 300 mM imidazole concentration. UV absorbance at 280 nm was used to monitor proteins eluting from the column. Fractions were collected in 5 ml aliquots during loading and washing, but in 1 ml aliquots during elution. Appropriate fractions were analysed on 12% SDS-PAGE for the presence of His-Hyp protein (Figure 101). From the first step of purification, nickel affinity chromatography, elution fractions containing His-Hyp protein (Fractions 32 to 50, Figure 101B) were combined and

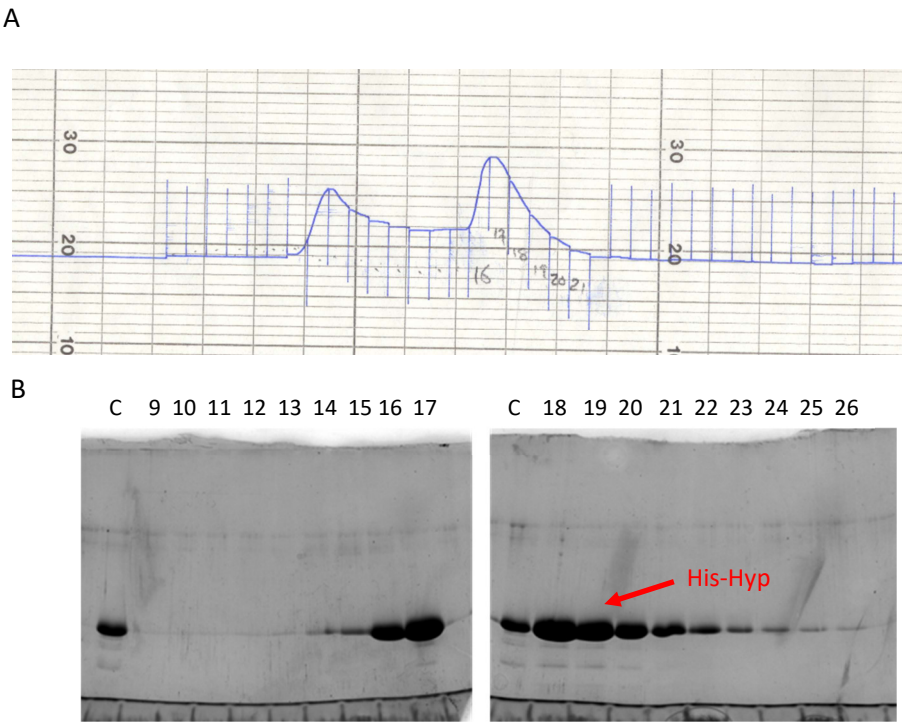

Figure 102: Gel filtration of His-Hyp for crystallography.

(A) UV absorbance measured at 280 nm of gel filtration purification of His-Hyp for crystallography.
(B) Fractions from purification were analysed by 12% SDS-PAGE to determine the elution fractions containing purified His-Hyp protein. Fractions loaded include a control (C) containing purified His-Hyp protein and elution fractions (9-26) for which every fraction was loaded. The gel was visualised using Coomassie staining.

dialysed against a Tris buffer containing arginine (50 mM Tris-HCl, 150 mM NaCl, 10 mM $MgCl_2$, 200 mM arginine pH 8) in order to maintain solubility (Chapter 4). After dialysis His-Hyp was concentrated to a 2 ml volume which contained approximately 34 mg of Hi-Hyp protein. The protein was then further purified by gel filtration using a Superdex 16/600 200 pg column (GE Healthcare). The extra purification was performed in order to obtain the very pure His-Hyp protein required for crystallisation. The protein was purified at a speed of 1 ml/min at 4°C with the elution monitored by UV absorbance measured at 280 nm with fractions collected in 2 ml aliquots. Appropriate fractions were analysed on 12% SDS-PAGE for the presence of His-Hyp protein (Figure 102).

Elution fractions 16-21 (Figure 102) were combined giving a total volume of 12 ml of His-Hyp protein. This was then concentrated to a final volume of 1 ml containing 20 mg of purified His-Hyp protein in a Tris buffer (50 mM Tris, 150 mM NaCl, 10 mM $MgCl_2$, 200 mM arginine pH8).

There are three steps to crystallisation: nucleation, growth and cessation of growth. To achieve nucleation and growth, the protein is required to reach supersaturation which is achieved by subjecting the protein to a variety of buffer conditions with variable conditions such as pH, temperature, precipitants and solvents (Saludjian et al., 1992). To help with this process the slow evaporation of the solvent can induce reaching the solubility limit of the protein and force either crystal formation or protein precipitation. To promote the formation of crystals, the protein was mixed 1:1 (v:v) from two different starting concentrations, 20 mg/ml and 10 mg/ml with buffers from three different crystallisation screens: Hampton Research (PEG/Ion Screens 1 and 2, 96 conditions); Molecular Dimensions (JCSG-plus MD1-37, 96 tests; and Structure MD1-03, 94 tests. The mixture was then incubated in a sitting drop configuration, with a reservoir located just below the drop at two different temperatures, 16°C and 4°C, and observed for the formation of crystals. After two months a single crystal grew from a precipitate in 200 mM KH_2PO_4, 20% PEG 3350, which was picked, mixed with a cryo-protectant containing 20% glycerol and stored in liquid nitrogen before being transported to Diamond Light Source, where X-ray diffraction data on the crystal was collected (Figure 103). As discussed before, molecular replacement was unavailable due to a lack of homologues with a solved

A B

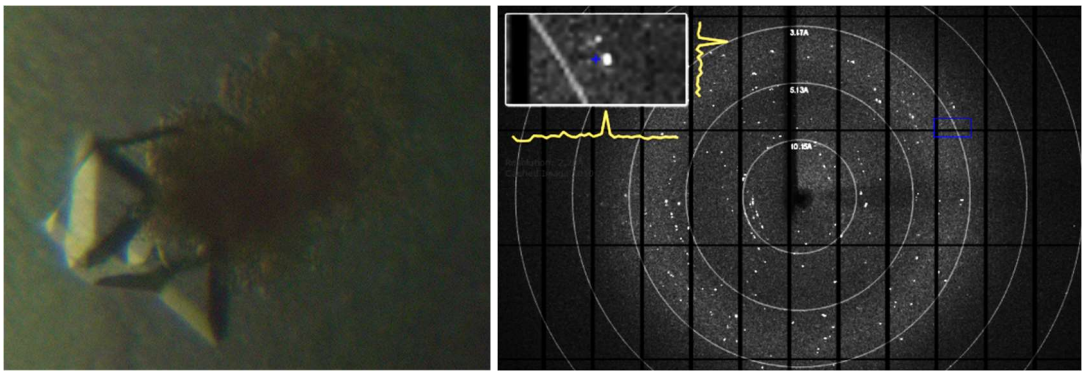

Figure 103: X-ray crystallography of His-Hyp

(A) A crystal of His-Hyp, which grew from a precipitate in 200 mM KH_2PO_4 20 % PEG 3350 Da, was picked and mixed with cryo-protectant (20% glycerol) before being sent for data collection.
(B) The diffraction pattern collected by the detector after the crystal was bombarded with X-rays during data collection.

structure. Therefore, in order to solve the phase problem, another crystal, which grew in 4 % (v/v) Tacsimate pH 6.0, 12 % w/v PEG 3350, was harvested and soaked in 1 M NaBr for SAD before being processed in the same way as the previous crystal. In collaboration with Dr Andrew Hemmings, SHELXC/D was used to solve the heavy atom substructure and to calculate approximate phases, followed by SHELXE for density modification by solvent flattening. The model was refined using PHENIX refine with the final refinement containing one Ramachandran outlier (Table 11).

Table 11: Data collection and refinement statistics for the Hyp structure

Data Processing	
Space Group	P 1 2_1 1
Unit Cell a,b,c (Å) α,β,γ (°)	 51.1, 58.4, 51.8 90, 119.7, 90
Resolution (Å)	29.175-2.128
(I)/sd(I)	1.36
Completeness (%)	97.53
Refinement	
Total Atoms Water	2030 60
R_{work} (%)	21.8
R_{free} (%)	27
Mean B-value (Å^2)	27.98
RMSD Bonds (Å)	0.008
RMSD Angles (Å)	1.157
RMSD Planes (Å)	0.004

6.2 The structure of the C-terminus of Hyp

Although the entire Hyp protein was purified and subjected to crystallisation trials, only the C-terminal region of the protein was present in the crystal that grew. The crystallised protein consisted of a domain starting at His121 and ending at Arg183 (Figure 104). This part of the protein corresponds to a structured domain and is highly conserved among the homologues of Hyp across *Actinobacteria*. The N-terminal region, which was not found in the crystal is a highly disordered domain with low conservation across the homologues. It is likely that this part of the protein underwent proteolysis during incubation, allowing for the C-terminal domain to form an ordered crystal. The structure obtained consists of two dimers which form a tetramer (Figure 105). This is consistent with the data we observed using analytical gel filtration which demonstrated that Hyp is tetrameric. Each subunit of the domain consists of a β-strand followed by two larger α-helices and a very small third α-helix. These structures are highly conserved across the homologs of Hyp, suggesting that they are important for properties that are shared across the proteins (Figure 104). Closer inspection of a single dimer (Figure 106)

shows that the β-strands from two subunits interact to form an antiparallel dimer, which possibly acts to stabilise each individual β-strand as individual strands are unable to maintain this structure without the hydrogen bonds and van der Waals interactions formed with neighbouring β-strands (Baker and Hubbard, 1984). The six α-helices create a helical handshake which forms the interaction between the two monomer subunits that maintains the dimer structure and allows the β-strands to interact in the antiparallel formation. This helical handshake is formed through the binding of α-helix two of each subunit by all three α-helices of the other subunit. In effect the three α-helices of both subunits create a pocket into which α-helix two of the other strand is held on three sides (Figure 106).

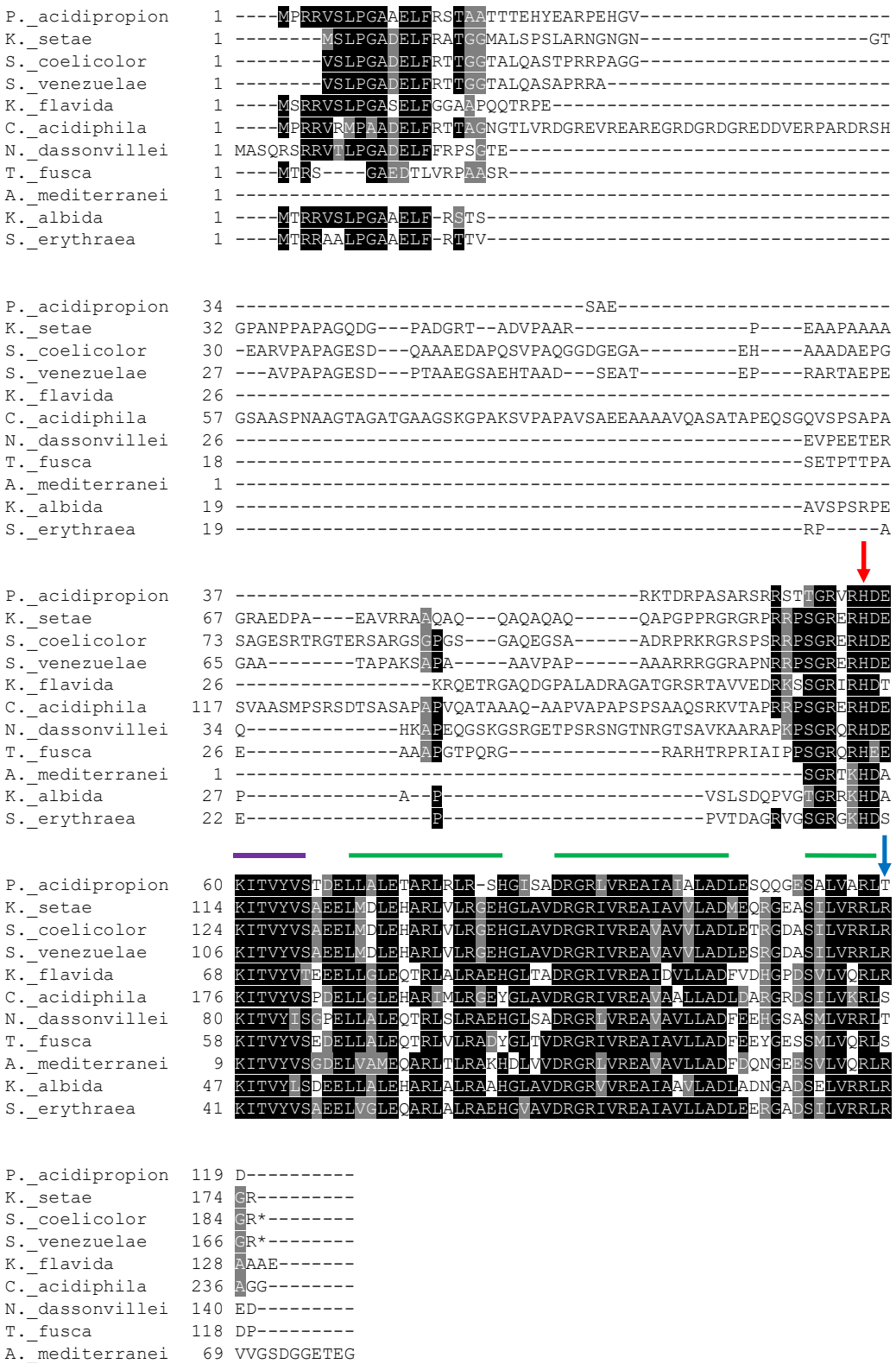

Figure 104: Sequence alignment of Hyp homologues.

The motifs from the Hyp structure are indicated with lines above the sequence with purple corresponding to the β-strand and green corresponding to the α-helices. The beginning of the solved structure is marked by a red arrow, while the end is marked by a blue arrow.

Figure 105: Ribbon diagram of C-terminal domain of Hyp.

The structure of the C-terminal domain of Hyp, represented as a ribbon diagram, reveals four subunits, each consisting of a β-strand followed by three α-helices. The third α-helix is much smaller than the first two. The disordered N-terminal domain underwent proteolysis during crystallisation trials allowing the crystallisation of the C-terminal domain. Each monomer chain is shown in a different colour.

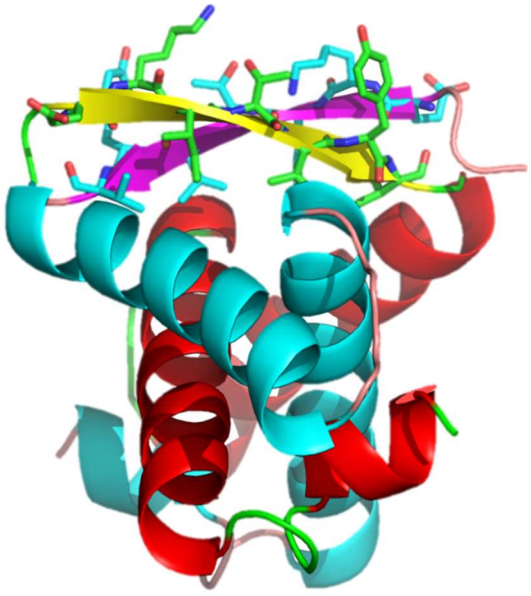

Figure 106: Ribbon diagram of C-terminal Hyp dimer.

The dimers of the C-terminal domain of Hyp, represented as a ribbon diagram, form a helical handshake from the α-helices in which α-helix two of each strand is bound on three sides by the α-helices of the other strand. The β-strands of each chain form an antiparallel dimer that sits in top of the α-helices.

The β-strand consists of a highly conserved EKITVYV motif, between Glutamate 123 (E) and Valine 129 (V). This sits at the top of the helix structure with the residues Lysine 124 (K), Threonine 126 (T) and Tyrosine 128 (Y) facing out from the protein, while the remaining residues, Isoleucine 125 (I) and Valine 127 (V) remain buried in the protein structure (Figure 107). The residues that point out from the protein structure have complete conservation across Hyp homologues while there is slight variation in the other residues (Figure 104).

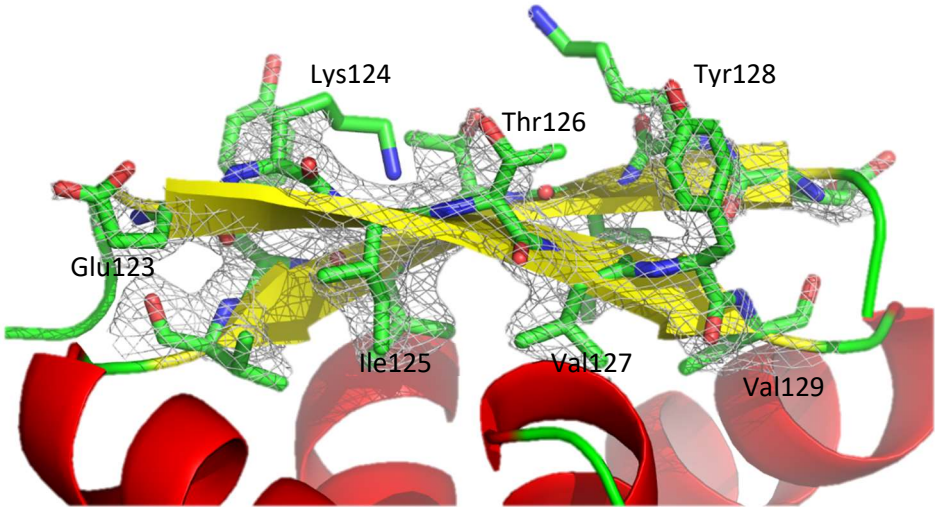

Figure 107: The DNA binding ribbon of the C-terminal domain.
The ribbon forms an antiparallel dimer between the two chains, which sits atop of the helices. It consists of an EKITVYV motif in which the residues Lysine 124, Threonine 126 and Tyrosine 128 face out and bind DNA. The remaining ribbon residues are buried within the protein structure.

6.3 Purification of the two Hyp domains

From the solved structure it is not easy to determine whether the two dimers are held together by interactions formed between the C-terminal dimers, or whether tetramerisation occurs in the N-terminal part of the protein. We therefore set out to separately purify both domains using the heterologous host *E. coli*. In order to purify HypN and HypC using nickel affinity chromatography the two gene domains were cloned into pET28a in order to create pET28a-HypN (Figure

108) and pET28a-HypC (Figure 109). The *hypN* gene domain (Met 1 to Asp 122) was amplified from *S. coelicolor* using the primers 'Hyp XbaI NdeI FRW' and 'HypN Eco UTC REV' before being digested with *Nde*I and *Eco*RI and cloned into pET28a. While the *hypC* gene domain (Arg 120 to Arg 180) was amplified from *S. coelicolor* using the primers 'HypC XbaI NdeI FRW' and 'Hyp Eco UTC REV' before also being digested with *Nde*I and *Eco*RI and cloned into pET28a. The forward primers add *Nde*I sites which allows for in frame translation of the tagged proteins. Plasmid pET28a-HypN generates His-HypN protein, which has an approximate molecular weight of 14.2 kDa with a theoretical PI of 6.71 and is not visible by UV spectrophotometry due to the lack of any Tryptophan, Tyrosine or Cysteine residues. Plasmid pET28a-HypC generates His-HypC protein, which has an

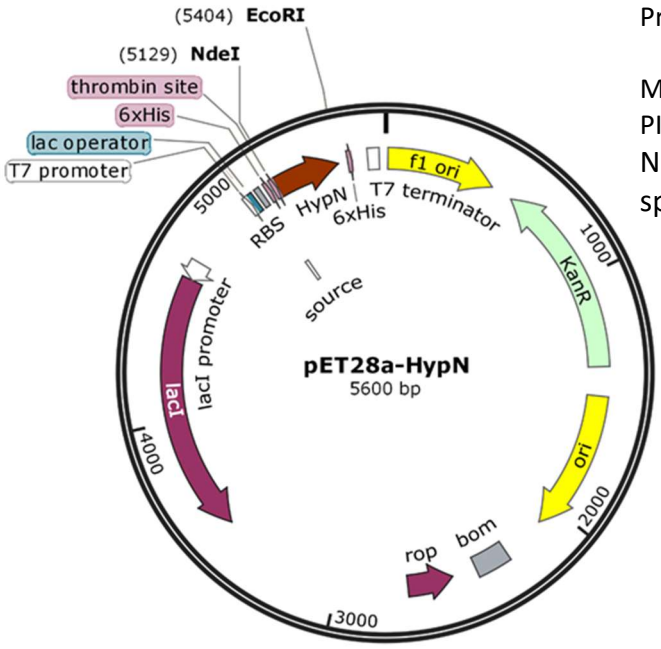

Properties of His-HypN:

Molecular Weight 14.2 kDa
PI 6.71
Not visible by UV spectrophotometry

MGSSHHHHHHSSGLVPRGSHMSLPGADELFRTTGGTALQASTPRRPAGGEARVPAPAGESDQAAAEDAP
QSVPAQGGDGEGAEHAAADAEPGSAGESRTRGTERSARGSGPGSGAQEGSAADRPRKRGRSPSRRPSGRE
RHD

Figure 108: Plasmid map of pET28a-HypN.

The plasmid pET28a-HypN is a derivative of pET28a with the *hypN* gene domain (Met 1 to Asp 122) cloned using the restriction sites *Nde*I and *Eco*RI. When induced with IPTG it produces His-HypN, which has an approximate molecular weight of 14.2 kDa and a theoretical PI of 6.71. The protein is not visible by UV spectrophotometry.
The amino acid sequence of His-HypN produced by pET28a-HypN is shown. The His-tag is labelled in red while the individual His residues are underlined.

approximate molecular weight of 9.6 kDa with a theoretical PI of 7.15 and an extinction coefficient of 1490 $M^{-1}cm^{-1}$.

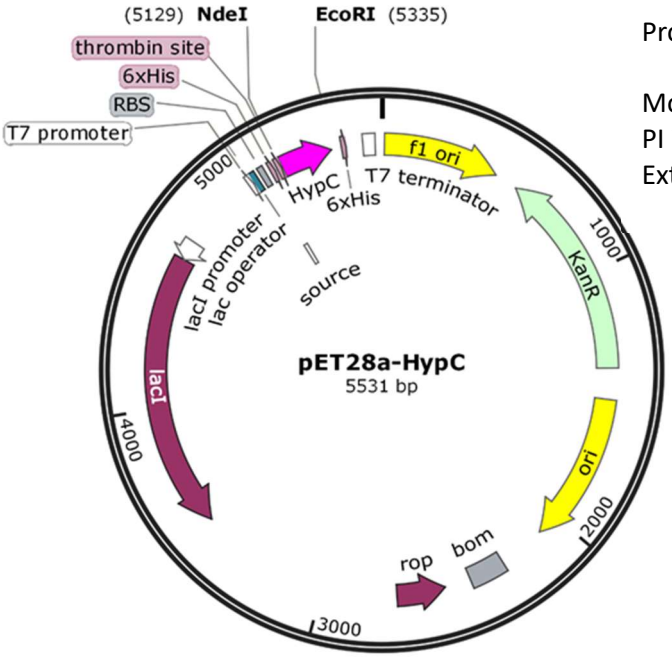

Properties of His-HypC:

Molecular Weight 9.6 kDa
PI 7.15
Extinction Coefficient 1490 $M^{-1}cm^{-1}$

MGSSHHHHHHSSGLVPRGSHMRHDEKITVYVSAEELMDLEHARLVLRGEHGLAVDRGRIVREAVAVVLADL
ETRGDASILVRRLRGR

Figure 109: Plasmid map of pET28a-HypC.

The plasmid pET28a-HypC is a derivative of pET28a with the *hypC* gene domain (Arg 120 to Arg 180) cloned using the restriction sites *Nde*I and *Eco*RI. When induced with IPTG it produces His-HypC, which has an approximate molecular weight of 9.6 kDa and a theoretical PI of 7.15. The protein has an extinction coefficient of approximately 1490 $M^{-1}cm^{-1}$.
The amino acid sequence of His-HypC produced by pET28a-HypC is shown. The His-tag is labelled in red while the individual His residues are underlined.

To determine the optimal purification method for each protein we once again undertook expression trials as before. To summarise, BL21(DE3)pLysS cells carrying either pET28a-HypN or pET28a-HypC were sub cultured from an overnight culture and grown at 37°C for 4 hours in 10ml LB containing kanamycin before induction with 1 mM IPTG. Expression was tested at 37°C, 25°C and 15°C, with 1 ml samples collected by centrifugation including pre induction, and then four hours and twenty hours after induction. The cells were re-suspended in Tris-magnesium buffer (20 mM Tris-HCl, 10 mM $MgCl_2$, pH8) and were lysed on ice using five 15 second bursts of sonication with 30 second intervals. The lysate was centrifuged

resulting in pellet and supernatant fractions which were then visualised using 15% SDS-PAGE (Figures 110 and 111). His-HypN was found to be best expressed when incubated for 20 hours after induction at 37°C. Under these conditions we see large band at the expected size of 14.2 kDa in the supernatant fraction indicating that most of the protein is soluble. We decided to use these conditions for the production of His-ParH in order to purify the protein.

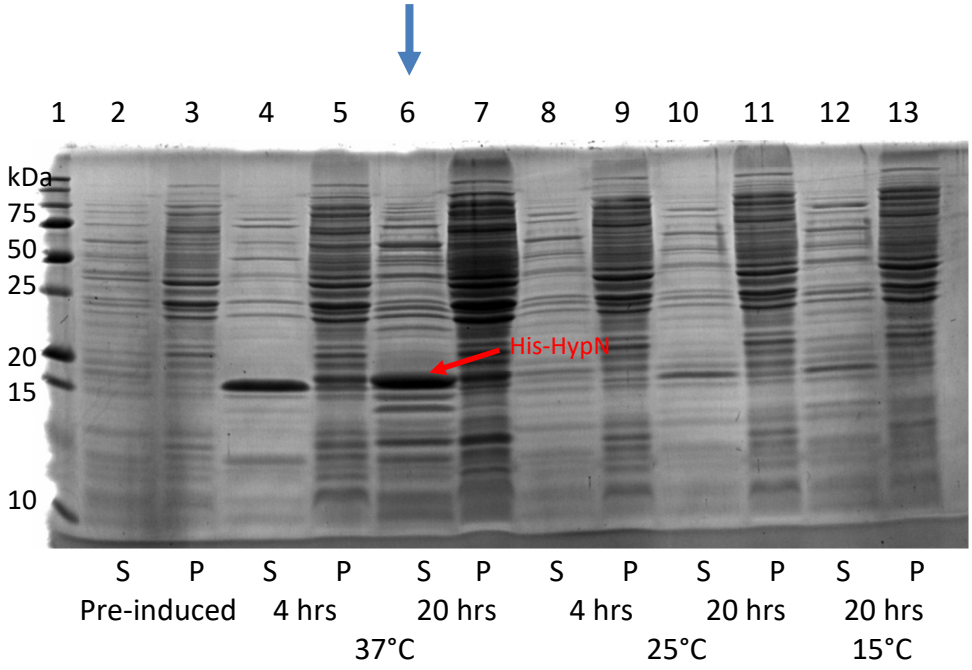

Figure 110: His-HypN expression trial.

Supernatant and pellet fractions from the His-HypN (14.2 kDa) expression trial in *E.coli* were analysed using 15% SDS-PAGE. Supernatant fractions were loaded into even lane numbers, while odd lane numbers contain pellet fractions. The samples were loaded as follows; pre-induced (2 and 3), four hours induction 37°C (4 and 5), twenty hours induction 37°C (6 and 7), four hours induction 25°C (8 and 9), twenty hours induction 25°C (10 and 11), and twenty hours induction 15°C (12 and 13). The blue arrow indicates the lane containing the fraction corresponding to the conditions used to purify His-HypN. 5 µl of Precision Plus Protein™ All Blue Standards from Bio-Rad was loaded into lane one (Molecular weight of marker proteins shown in kDa).

His-HypC was found to be best expressed when incubated for 4 hours after induction at 37°C. Under these conditions we see large band at the expected size of 9.6 kDa in the pellet fraction. We also see bands corresponding to the expected size of His-HypC in other conditions in pellet fractions indicating that the protein is

insoluble. We therefore decided to purify His-HypC using denaturing conditions, with protein production being carried out at 37°C for 4 hours.

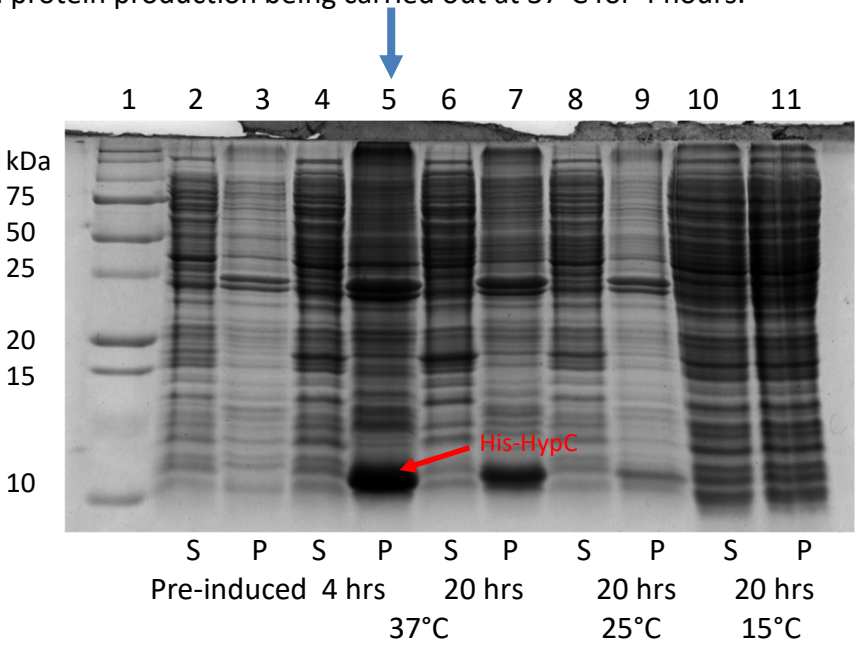

Figure 111: His-HypC expression trial.

Supernatant and pellet fractions from the His-HypC (9.6 kDa) expression trial in *E.coli* were analysed using 15% SDS-PAGE. Supernatant fractions were loaded into even lane numbers, while odd lane numbers contain pellet fractions. The samples were loaded as follows; pre-induced (2 and 3), four hours induction 37°C (4 and 5), twenty hours induction 37°C (6 and 7), twenty hours induction 25°C (8 and 9), and twenty hours induction 15°C (10 and 11). The blue arrow indicates the lane containing the fraction corresponding to the conditions used to purify His-HypN. 5 µl of Precision Plus Protein™ All Blue Standards from Bio-Rad was loaded into lane one (Molecular weight of marker proteins shown in kDa). Visualised by Coomassie staining.

Production of His-HypN protein was carried out in *E. coli* BL21(DE3)pLysS carrying pET28a-HypN. Protein expression was induced in 500 ml LB according to the optimal conditions for the production of His-HypN (Figure 110). The cells were collected by centrifugation and re-suspended in Tris binding buffer (50 mM Tris-HCl, 300 mM NaCl, 20 mM $MgCl_2$, 10 mM imidazole pH8). The cells were lysed using a Mitsubishi Electric E1061 cell disruptor set to a pressure of 30 Kpsi. Purification was achieved using an Amersham AKTA FRC FPLC machine with a 5ml HisTrap HP nickel column (GE Healthcare). Purification was performed at a rate of 1 ml/min throughout all steps of purification, which otherwise followed the protocol established in the purification of His-ParH (Chapter 4). Elution was carried out using a gradient increase in imidazole

concentration. Fractions were analysed on 15% SDS-PAGE to determine those containing His-Hyp. As His-Hyp is not visible UV spectrophotometry there was no indication from the chromatogram as to where His-HypN eluted, so it is not shown.

His-HypN was successfully purified through nickel affinity chromatography (Figure 112). While the protein completely appeared to completely bind to the column during loading, significant amounts of His-HypN were observable in the wash fraction suggesting that it was only weakly bound to the column. In addition more His-HypN was released from the column during the elution phase of purification. During purification a contaminant of a slightly larger size co-purified with His-HypN. These fractions were not kept. Fractions from lanes 3 and 4 were combined giving a total volume of 2 ml His-HypN. This was dialysed against a Tris arginine buffer (20 mM Tris, 150 mM NaCl, 10 mM $MgCl_2$, 200 mM arginine pH 8). After dialysis approximately 2 ml solution of His-HypN was recovered at a concentration of 1 mg/ml. We successfully purified and dialysed approximately 2 mg of His-HypN protein from a 500 ml cell culture.

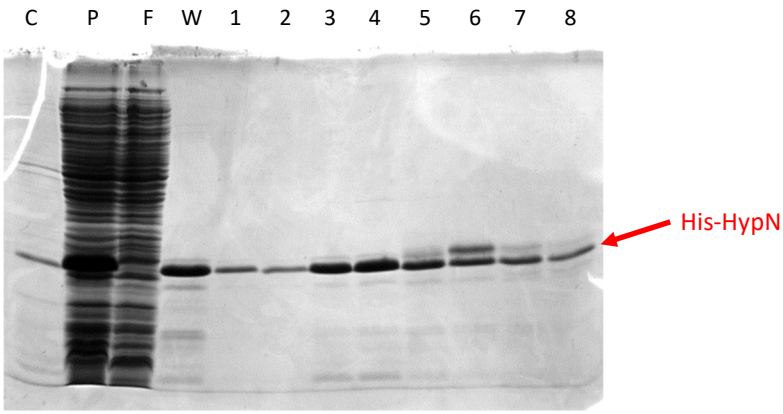

Figure 112: Purification of His-HypN

Fractions from FPLC nickel purification of His-HypN were run on 15% SDS-PAGE. Flow through (F), wash (W) and elution fractions (Lanes 1 to 8) were run along with a control containing His-HypN protein (C, Lane 6 from figure 109) and the pre-load (P). Fractions were analysed using 15% SDS-PAGE and visualised by Coomassie staining.

Production of His-HypC, in order to achieve large scale purification, was carried out in a 500 ml LB culture using the optimal conditions derived from the expression test. Cell lyses was initially carried out under native conditions using the

same method utilised in purification of His-HypN. After lysis the supernatant was discarded and the pellet re-suspended in denaturing loading buffer (8 M urea-HCl, 0.1 M NaH2PO4, 0.01 M Tris pH 8). Purification was carried out using the denaturing purification protocol using a gravity flow column from Novogen which contained approximately 2 ml Nickel Sepharose. The flow through and wash were collected as single fractions while the elution was collected in 1 ml aliquots. Fractions were analysed using 15% SDS-PAGE (Figure 113). Fractions from lanes 7, 8 and 9 were combined giving a total volume of 3 ml His-HypC. This was dialysed against a Tris arginine buffer (20 mM Tris, 150 mM NaCl, 10 mM $MgCl_2$, 200 mM arginine pH 8). After dialysis approximately 3 ml solution of His-HypN was recovered at a concentration of 0.2 mg/ml. We successfully purified and dialysed approximately 0.6 mg of His-HypC protein from a 500 ml cell culture.

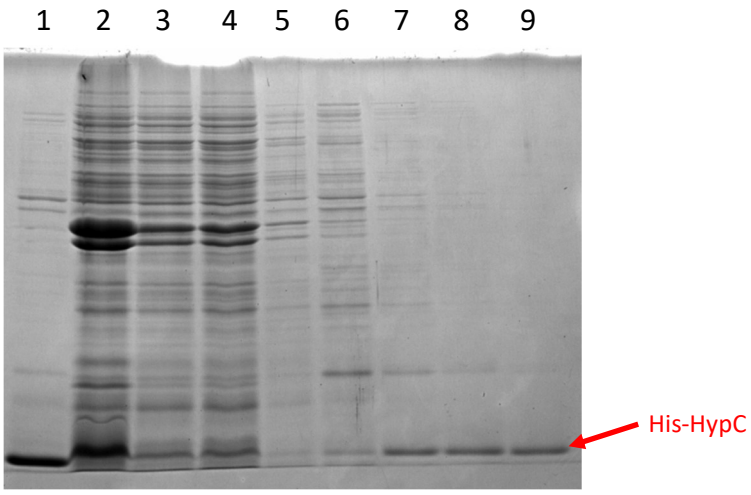

Figure 113: Purification of His-HypC under denaturing conditions.

Fractions from the purification of His-HypC were analysed on 15% SDS-PAGE. Pre-load (2), Flow through (3), Wash (4) and Elution fractions (5-11) were analysed alongside a control containing His-HypC protein (C, Lane 5 from figure 110). Visualised by Coomassie staining.

6.4 The N-terminal domain of Hyp forms a tetramer

After dialysis, both His-HypN and His-HypC proteins were analysed by analytical gel filtration to determine their oligomeric state. A Superdex 200 10/300 GL column was used, with the calibration curve generated in chapter 4 used to

estimate protein weight. Approximately 500 µg of His-HypN applied to the column at 0.5 ml/min. As previously discussed, His-HypN has an extinction coefficient of zero, meaning that no absorption of UV would take place. Therefore, the elution was collected in 250 µl fractions for analysis on SDS-PAGE. The expected elution volume for each theoretical oligomer was calculated (Table 12), and based on this appropriate fractions that cover the range of oligomers, from monomer to tetramer were analysed using 15% SDS-PAGE (Figure 114).

Table 12: Table showing calculation of theoretical elution volumes from Superdex 200 10/300 GL column of His-HypN oligomers.

HypN oligomer	**MW (kDa)**	**Log(MW)**	**K_{av}**	**Theoretical elution volume (ml)**
Monomer	14.20	1.15	0.62	17.66
Dimer	28.40	1.45	0.52	16.02
Trimer	42.60	1.63	0.46	15.07
Tetramer	56.80	1.75	0.42	14.39

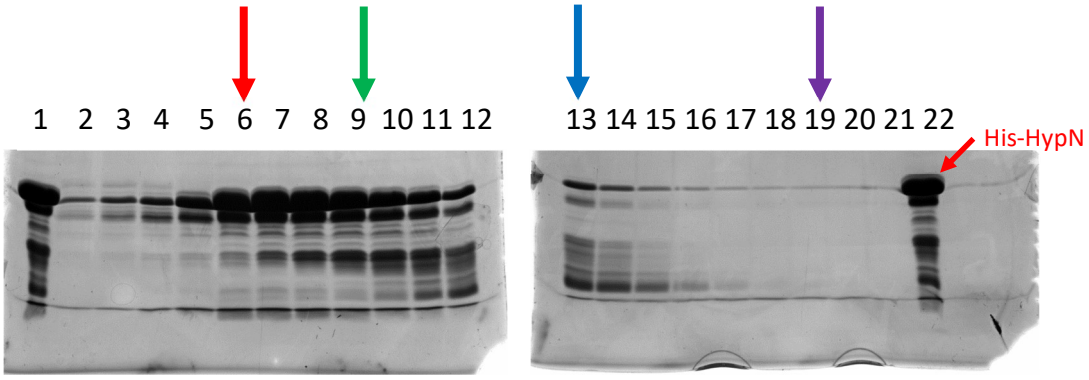

Figure 114: Fractions of His-HypN collected during elution from Analytical Gel Filtration.

Purified His-HypN protein was loaded onto the Superdex 200 10/300 GL analytical gel filtration column and the elution fractions collected in 250 µl aliquots. Fractions were analysed using 15% SDS-PAGE to determine the elution profile of His-HypN. The expected elution volume for the tetramer (red), trimer (green), dimer (blue) and monomer (purple) are indicated above the gel. Lanes 1 and 22 contains purified His-HypN protein as a control. Every fraction was loaded from an elution volume of 13.25 ml (lane 2) until 18 ml (lane 21).

The elution profile of His-HypN from the analytical gel filtration column suggests that the N-terminal domain of Hyp forms a tetramer. The majority of the protein eluted between 14 ml and 15.25 ml after loading. A tetramer His-HypN would elute at around 14.39 ml, while the trimer would elute at 15.07 ml. Even though some of the protein eluted at a volume suggestive of a trimer, it is more likely that a tetramer is formed as the protein clearly begins to elute long before the expected volume corresponding to the trimer. In addition, we can also observe some additional smaller weight proteins in the lanes containing His-HypN. This is important in explaining the long tail to the elution profile. As noted when we solved the structure, the N-terminal domain of Hyp proteolysed during the crystallisation process allowing for the crystallisation of the structured C-terminal domain. The presence of smaller proteins that eluted in the same lanes as His-HypN could be degradation products of His-HypN. If this is the case then some of the His-HypN tetramers would be smaller in size compared to the expected size of a tetramer containing four full His-HypN subunits. This would be due to tetramers that are formed of a mixture of full products and degradation products, resulting in larger than expected elution volumes. In fact, as you get to later elution fractions we start to see more and varied smaller protein products which could correspond to this observation.

After showing that the N-terminal domain of Hyp forms a tetramer we wished to see if the C-terminal domain of Hyp could form the same oligomer. AS such His-HypC was concentrated to 0.5 mg/ml from which a 500 µl (250 µg) aliquot was applied to the Superdex 200 10/300 GL column. While His-Hyp has a detectable extinction coefficient (1490 $M^{-1}cm^{-1}$), due to the relatively low amount of His-HypC (250 µg) that was applied to the column we decided to determine the elution volume by SDS-PAGE. Thus expected elution volume for each theoretical oligomer of His-HypC was calculated (Table 13), and based on this appropriate fractions that cover the range of oligomers, from monomer to tetramer, were analysed using 15% SDS-PAGE (Figure 115).

Table 13: Table showing calculation of theoretical elution volumes from Superdex 200 10/300 GL column of His-HypC oligomers.

HypC oligomer	MW (kDa)	Log(MW)	K_{av}	Theoretical elution volume (ml)
Monomer	9.60	0.98	0.67	18.58
Dimer	19.20	1.28	0.57	16.95
Trimer	28.80	1.46	0.52	15.99
Tetramer	38.40	1.58	0.48	15.31

This shows that His-Hyp is a monomer in the absence of the N-terminal domain of Hyp. We see feint His-HypC bands in fractions eluted around 18.5 ml after loading, which is consistent with the expected elution volume of the monomer (18.58 ml). In addition, fractions associated with the observable UV absorbance profile of the elution there are clearly small contaminant proteins. While this data supports the notion that tetramerisation of Hyp is achieved through interactions within an N-terminal domain of the protein, we must consider that because His-HypC was purified under denaturing conditions it is possible that re-folding of the protein was unsuccessful during dialysis. In order to determine whether the C-terminal domain of Hyp is able to oligomerise in the absence of the N-terminal domain of Hyp we need to determine conditions in which His-HypC can be purified from solution.

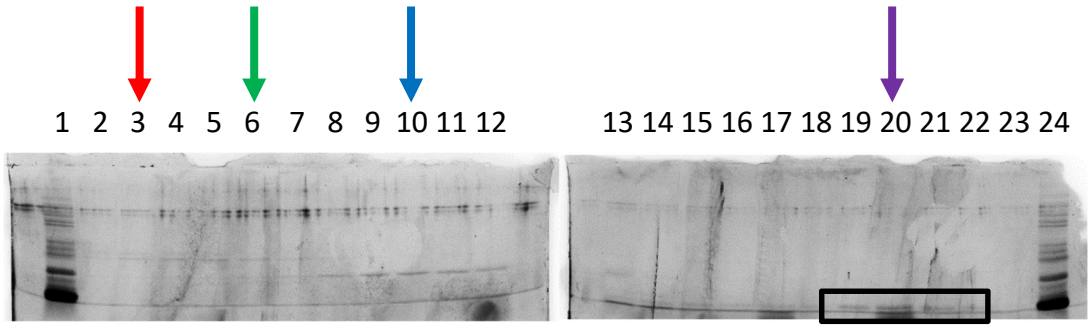

Figure 115: Fractions of His-HypC collected during elution from Analytical Gel Filtration.

Purified His-HypC protein was loaded onto the Superdex 200 10/300 GL analytical gel filtration column and the elution fractions collected in 250 µl aliquots. Fractions were analysed using 15% SDS-PAGE to determine the elution profile of His-HypC. The expected elution volume for the tetramer (red), trimer (green), dimer (blue) and monomer (purple) are indicated above the gel. Lanes 1 and 24 contains pre-load His-HypC as a control. Every fraction was loaded from an elution volume of 15 ml (lane 2) until 19.5 ml (lane 23). Black box encloses eluted His-HypC fractions.

6.5 Hyp has a ribbon-helix-helix domain

A search for structural homologues of hyp using Dali reveals that Hyp has a ribbon-helix-helix (RHH) domain in the C-terminus. The ribbon is formed by the anti-parallel interaction of the β-strands which form a β-sheet (Figure 116). This is followed by two α-helices that make up the domain. As discussed, Hyp has a third small α-helix after this domain which is not part of RHH domains.

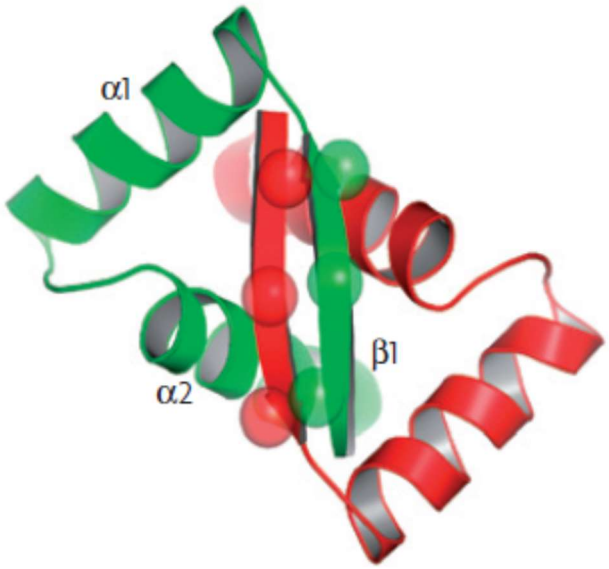

Figure 116: A representation of the ribbon-helix-helix domain.

Ribbon-helix-helix DNA binding domains have been implicated in a variety of functions in bacteria. In all proteins with RHH domains the ribbon confers specificity to the DNA target sequence. This is achieved through residues 2, 4 and 6 in the ribbon, all of which face out from the protein.

Historically protein-DNA interaction in prokaryotes was thought to be exclusively facilitated by the Helix-Turn-Helix (HTH) motif that is found across a variety of proteins including ParB. DNA interaction in these class of proteins occurs between an α-helix and the major groove of a specific target sequence of DNA

(Wintjens and Rooman, 1996). However, this is not the case with the discovery of a large group of DNA binding proteins that exhibit the RHH DNA binding domain. The first such protein identified MetJ, an *E. coli* methionine repressor, was first crystallised in 1989 and although it had an RHH domain, protein-DNA interaction was modelled on the assumption that interaction occurred between one of the α-helix and DNA, as seen with HTH proteins (Rafferty et al., 1989). Later extended data based on further crystallisation of MetJ in the presence of its target DNA sequence revealed that in fact interaction occurs between the antiparallel β-sheet, generated by MetJ dimerisation, and the cognate operator DNA rather than via α-helix (Somers and Phillips, 1992). Since the discovery of the RHH domain in MetJ, more and more proteins with this functional domain have been found across a range of bacteria. These proteins have been implicated in a wide variety of roles including: Arc and Mnt from Bacteriophage P22, involved in of the bacteriophage lytic cycle (Breg et al., 1990; Knight et al., 1989; Knight and Sauer, 1989); the antitoxin FitA from *Neisseria gonorrhoeae* (Buts et al., 2005; Mattison et al., 2006); the protein Nikr that is found across a range of bacteria including *E. coli* where it is a Ni^{2+}-dependent repressor of nickel uptake (Schreiter et al., 2006) and *Heliobacter pylori* where it is an inductor of urease (van Vliet et al., 2004); Omega and CopG which control plasmid copy number in Gram-positive bacteria (Costa et al., 2001; Misselwitz et al., 2001; Murayama et al., 2001); CcdA and ParD which are antitoxins (Madl et al., 2006; Oberer et al., 1999); AlgZ, a DNA binding protein from *Pseudomonas aeruginosa* involved in the regulation of alginate biosynthesis and motility (Baynham et al., 1999); TrwA, TraY and TraM which are responsible for the regulation of bacterial conjugation (Di Laurenzio et al., 1992; Moncalian and de la Cruz, 2004; Schildbach et al., 1998); the *E. coli* protein PutA, which regulates proline-utilisation genes through oxidation of proline to glutamate (Becker and Thomas, 2001); VirC2, which enhances T-DNA transfer and virulence in *Agrobacterium tumefaciens* (Lu et al., 2009); and plasmid partitioning such as ParG which is found on the multidrug resistance plasmid TP228 from *Salmonella newport* (Golovanov et al., 2003).

In addition to the common RHH domain that defines this group of proteins, they also often contain a second functional domain that varies across the proteins (Figure 117). Previously we were able to demonstrate that the N-terminal domain of

Hyp is probably responsible for tetramerisation of the protein. This is similar to domains found in the aforementioned Mnt protein from bacteriophage and TrwA, a protein involved in the regulation of bacterial conjugation of plasmid R388 (Moncalian and de la Cruz, 2004). In addition, there are also domains involved in Ni^{2+} binding, protein-protein interaction, and a proline dehydrogenase domain, demonstrating the wide adaptation of this class of protein. Comparing the domains of these bacterial RHH proteins shows that the RHH domain of Hyp, at 49 amino acids, is slightly longer than most of these RHH domains for which structural data exists. These RHH domains all fall between 30 and 40 amino acids in length and could be correlated to the spacer length between the cognate DNA sequences.

We previously discussed the sequence homology of Hyp proteins, which were identified by blast search, and in particular the highly conserved β-strand that forms the ribbon when it forms a dimer with another subunit. Comparisons of the amino acid residues that form the ribbon across bacterial RHH proteins shows the conservation of specific amino acid groups found at distinct positions of the ribbon (Figure 118). In positions 2, 4 and 6, positions which correspond to residues that face out from the structure and are responsible for contact with DNA are filled by amino acids with a positive charge, neutral and positive charge respectively. With regards to Hyp this is also true for the amino acids in position 2 and 4, however, Hyp has an aromatic amino acid (Tyrosine) at position 6. If we look at the amino acids in more depth, then we find some preferred residues at specific positions. In position 2 for example, there is a propensity for an Arginine (33%), while in position 4 there is a high chance of a Threonine (50%) which is seen in the Hyp ribbon. At position 6 we again see a propensity for an Arginine residue (38%). Positions 3, 5 and 7, which are buried have a very high propensity for hydrophobic residues with 46 out of the 54 residues being hydrophobic. Overall there are no particular surprises in the residues found in the ribbon of Hyp, with conformity when compared to the existing data. Studies on these other proteins, show that where investigated these ribbons have unique and specific DNA target sequences to which they bind, reinforcing the idea that Hyp in fact has a specific binding sequence.

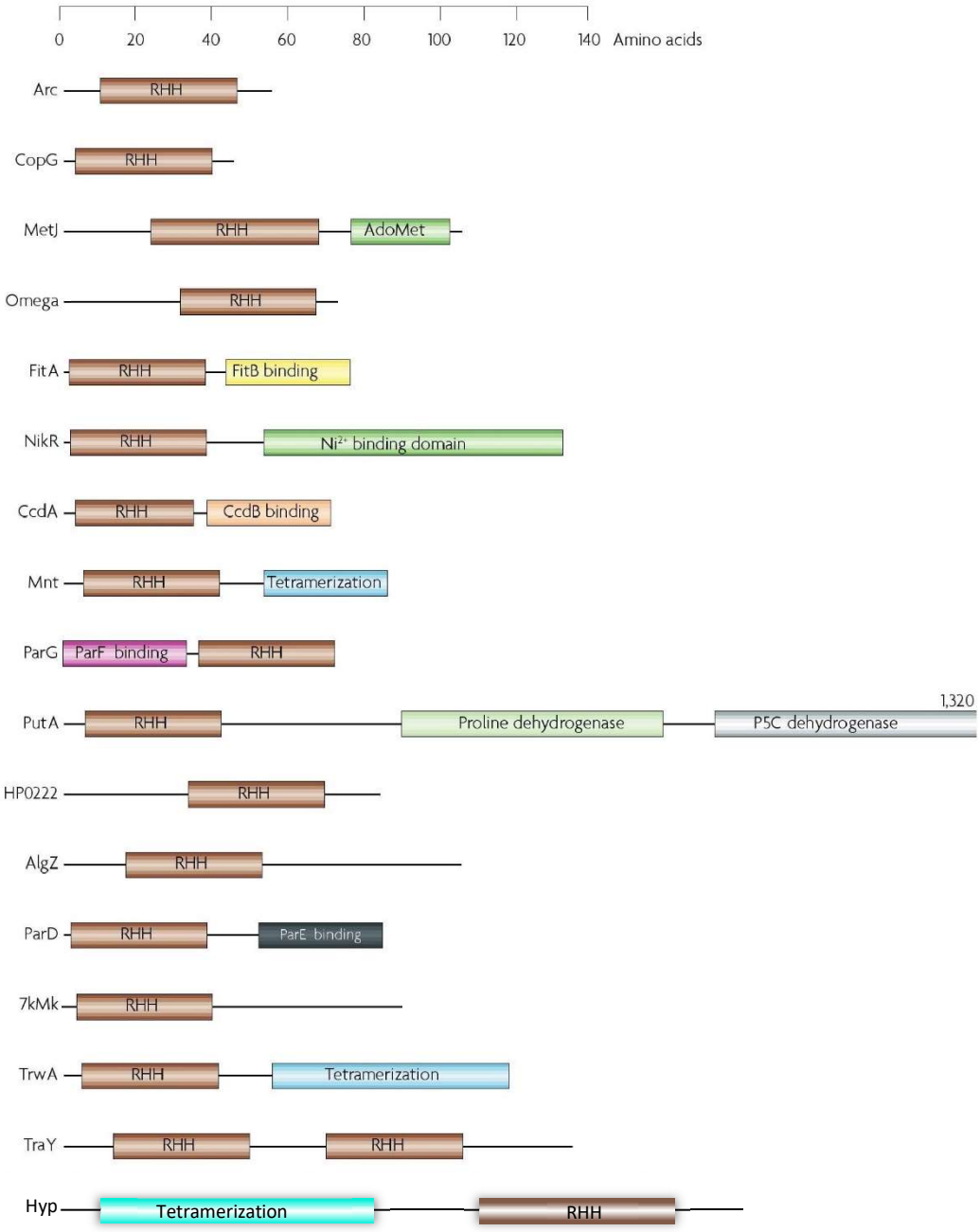

Figure 117: Domain alignment of bacterial RHH proteins

Domains of bacterial RHH domains have been aligned relative to their position and size. There is a wide variety of functional domains associated with RHH proteins including: protein-protein binding domains, tetramerisation domains and a Nickel binding domains. These domains can either be before or after the RHH domain. As shown, Hyp has a tetramerisation domain, which is situated upstream of its RHH domain. Figure adapted from (Schreiter and Drennan, 2007).

Investigations into the specific target sequence of different ribbon sequences has demonstrated the specificity with which they bind. MetJ (ribbon: -KKITVSI-) for instance binds the 8 bp palindromic so called 'met-box' with the optimal sequence 5'-AGACGTCT-3' (He et al., 1996). CopG (ribbon: -KRLTITL-) on the other hand recognises a 13 bp pseudosymmetric sequence that contains two 5'-TGCA-3' motifs (Gomis-Ruth et al., 1998; Hernandez-Arriaga et al., 2009). Finally ParG (ribbon: -KRVNVP-), recognises two 5'-ACTC-3' boxes that are separated by 4 bp AT-rich spacers (Wu et al., 2011; Zampini et al., 2009). Interestingly, creating chimeric recognition sites by swapping the ribbon of one protein with for the ribbon of another changes the cognate target sequence specific to the sequence which is targeted by the amino acid residues of the ribbon (Zampini and Hayes, 2012). This suggests that the target sequence is determined solely by the ribbon and not the α-helices.

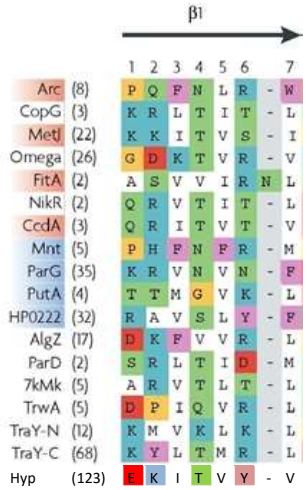

Figure 118: Ribbon comparison of bacterial RHH proteins

The ribbon sequence of bacterial RHH proteins have been aligned and colour coded based on the property of the amino acid: cyan, positive charge; red, negative charge; white, hydrophobic; green, neutral; purple, aromatic; orange, glycine or proline; yellow, cysteine. The number above the column refers to the C_α positions used for alignment. Figure adapted from (Schreiter and Drennan, 2007).

6.6 Summary

In this chapter we sort to solve the structure of Hyp. In the previous chapter, we demonstrated that hyp is a DNA binding protein. As there were no homologues of known function and structure, we sort to determine if Hyp had a novel DNA binding domain. We therefore undertook X-ray crystallography of Hyp. During crystallisation, the disordered N-terminal domain of the protein underwent proteolysis, leaving the C-terminal domain to form a crystal. From this we were able to ascertain the structure of this domain. This revealed that the C-terminal domain of Hyp had a β-strand followed by three α-helices that form a tetramer consisting of a dimer of dimers. We then sort to determine which domain of Hyp is responsible of tetramerisation. Therefore, we purified both domains in the heterologous host *E. coli*. While we were able to purify the N-terminal domain from solution, the C-terminal domain was found to be insoluble. We therefore purified this domain under denaturing conditions. Using analytical gel filtration, we were able to show that the N-terminal domain of Hyp is able to form a tetramer while the C-terminal domain was monomeric. While this demonstrates that the N-terminal domain is responsible for tetramerisation it does not rule out the possibility that the C-terminal domain could form a dimer of a tetramer in the absence of the N-terminal domain. We can only confirm this by trying to optimise production of the C-terminal domain in order to purify it from solution.

We undertook a search for structural homologues of Hyp, which revealed that the C-terminal domain consisted of a ribbon-helix-helix DNA binding domain. These proteins are widely spread in prokaryotes and have been implicated in diverse functions such as anti-toxicity, controlling plasmid copy numbers, repression of nickel uptake, methionine repression and regulation of bacterial conjugation. While this did not ultimately lead to a revelation about the function of Hyp it has given an indication of how it might function. A key feature of RHH domains is the specificity to the DNA target that the ribbon motif provides. Across RHH domains the residues in positions 2, 4 and 6 of the ribbon all provide a specific interaction to DNA bases. Domain swapping experiments have demonstrated that target sequences of the donor of the

ribbon motif is conferred to the recipient protein. All of this suggests that Hyp should bind to a specific target sequence in the *S. coelicolor* genome.

7 Discussion

Cell division in *Streptomyces* is still a poorly understood process. Considering that during sporulation, *Streptomyces* is required to segregate and compartmentalise many copies of the chromosome in each sporogenic hyphae, one would imagine that a vast network of regulation would govern the interplay between different components of this process. While we can point to understanding some aspects of growth with the characterisation of the TIPOC, a polar assembly of proteins that act as a scaffold to control growth (Holmes et al., 2013), we still do not know, for instance, how the establishment of the TIPOC initiates growth at new branch points and how the external environment is relayed back to the protein complex in order to affect changes in growth and branching. We understand about chromosome segregation during sporulation, the impact that the ParAB machinery has on chromosome organisation (Jakimowicz et al., 2007), but we have no idea how ParA localisation translates into chromosome positioning and precisely how the distance between chromosomes obtained. In vegetative hyphae we still do not understand the extent of chromosome organisation and how this impacts upon replication. While we know that, like in all bacteria, septum formation is dependent on FtsZ polymerisation and unique positive regulators of ring formation have been characterised (Willemse et al., 2011), but we have little understanding of exactly how septum site placement is determined during sporulation. We also have no understanding of how vegetative crosswalls are positioned and why they fail to complete division and undergo cell-cell separation. Most importantly, until relatively recently we had no understanding of how these processes are coordinated, instead, our understanding of these mechanisms were in relative isolation from one and other. Recent work has begun to link these individual systems starting with the findings that the TIPOC is able to inhibit chromosome segregation during growth by sequestering ParA to the tip (Figure 119)(Ditkowski et al., 2013; Holmes et al., 2013). Conversely, after aerial hyphae have formed, increased ParA production, causes ParA to polymerise and in turn depolymerise Scy which both curtails growth and begins

chromosome segregation. In spite of linking growth with chromosome segregation, we have no mechanism that links septum placement to these processes.

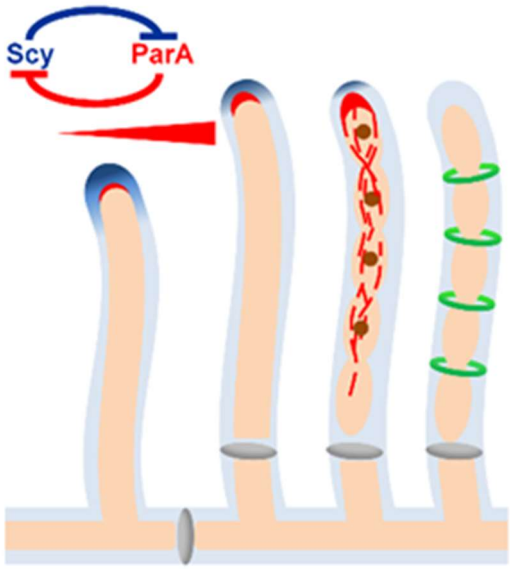

Figure 119: The interplay between ParA and Scy.

During growth ParA is sequestered to the tip where the polymerisation of ParA is inhibited by Scy. This prevents chromosome segregation from proceeding during growth. After the growth of aerial hyphal, increased levels of ParA overcomes inhibition of polymerisation by Scy and chromosome segregation begins. Increased ParA levels in turn cause depolymerisation of growth and thus curtailing growth. Taken from (Kelemen, 2017)

As we have discussed before ParA and MinD proteins play a crucial role in both chromosome segregation, through ParA proteins, and septum site placement, through MinD proteins (Lutkenhaus, 2012). Across bacteria we find that the process of chromosome segregation is very often linked to septum site placement, whether this is through the ParA/MinD superfamily or not. In both *E. coli* and *B. subtilis* this link is made by the nucleoid occlusion proteins SlmA and Noc respectively that are localised by the chromosomes that are being segregated (Lutkenhaus, 2012). The nucleoid occlusion proteins in turn prevent the septum from forming over the chromosomes so that a mid-cell location is found (Wu and Errington, 2004). In *C. crescentus* however, these process are linked directly through members of the

ParA/MinD superfamily. In this system it is the recruitment of MipZ to the chromosomes by the ParAB machinery that directly links chromosome segregation with septum site positioning (Kiekebusch et al., 2012; Thanbichler and Shapiro, 2006).

Therefore, in this project we have set out to identify novel ParA-like proteins in *Streptomyces* so that we may gain more a better mechanistic understanding into the interplay between these processes. Through bioinformatics analysis we identified a possible ParA-like protein, SCO1772, containing domain and sequence similarity with ParA proteins, which we have designated parH. By analysing the genes surrounding *parH* we were able to identify homologues of ParH across *Actinobacteria*. The *parH* gene is translationally coupled to the downstream gene, suggesting that the two encoded proteins are functionally linked. Initial investigation into the protein encoded by the downstream gene did not reveal any similarity to any proteins of known function, hence we have given the protein the working name Hyp. The gene locus has provided some thought-provoking insights into the possible function of the ParH and Hyp. Interestingly, upstream of *parH* in many *Actinobacteria*, although not *Streptomyces*, is *xerD* a gene that encodes a protein involved in the resolution of circular chromosomes after replication. As *Streptomyces* possess linear chromosomes it is not particularly surprising that this gene is absent from these species. In addition, downstream of *parH* and *hyp* we find genes encoding the proteins ScpA and ScpB. These proteins are associated with SMC with which they have been implicated in chromosome organisation in many bacteria. They are important for aligning chromosomes after replication when they are loaded onto the chromosome, in a manner similar to eukaryotic condensin, ensuring that the chromosomes adhere to the correct orientation (Le et al., 2013).

The gene locus could suggest that the function of ParH might be linked to the function of these proteins and by extension chromosome organisation. This would be in keeping with ParA-like proteins which are encoded on chromosomes and plasmids in the regions upon which they act. The ParABS system for example, is encoded around the *oriC* region of the chromosome, this region is also where ParB binds in order to segregate the chromosome (Gruber and Errington, 2009; Jakimowicz et al., 2002; Sullivan et al., 2009). This is true for both ParAB systems

found on chromosomes and those found on plasmids which suggests that an important mechanism of maintaining and transferring these mechanisms between organisms is through locating the DNA binding sites near the genes encoding the proteins. Any DNA binding activity of ParH and Hyp could therefore be likely to occur near their genes especially if either protein has a specific target sequence.

After identifying these genes we proceeded to create *S. coelicolor* mutant strains of *parH*, *hyp* and *parH-hyp*. Analysis of the *parH* strain, macroscopically showed that it exhibited a delay in sporulation after developing vegetative and aerial hyphae in the same time as the wild-type. Further microscopic inspection of the *parH* mutant revealed that unlike the wild-type it had irregular septum, produced fewer viable spores and exhibited branched aerial hyphae. Although we were unable to determine whether there was an effect on branching in vegetative hyphae we did find that the colonies produced by the *parH* mutant strain were smaller than those of the wild-type. This would indicate that perhaps there is a branching phenotype in vegetative hyphae which is leading to a reduced spread of the colony. The branching phenotype and smaller colony size, suggests that ParH is having an effect on the TIPOC and that it is disturbed in the *parH* mutant leading to growth defects. Given the previously established link between ParA and Scy, it would suggest that ParH also exhibits a similar interaction with Scy. The defect in septum placement both in timing, with a delay in appearance, and in placement, with irregular placement, suggests that ParH could function to regulate septum placement. This would be consistent with the function of ParA/MinD proteins which, as previously discussed, have been implicated in this process.

The *hyp* mutant strain resembled the wild-type strain under the conditions tested, so we were unable to derive any possible function from phenotypic studies. Given the previously stated translational coupling of Hyp and ParH, which suggests related function then it is possible that Hyp also has a role in septum placement. As expected, given the lack of a phenotype for the *hyp* mutant strain under these conditions, the *parH-hyp* double mutant strain resembled the parH mutant strain in its phenotype.

We then moved on to understand more about the biochemical properties of both Hyp and ParH. Given the discussed phenotype, we also set out to explore

interaction of ParH to both Scy, to determine a link between ParH and the TIPOC, and to ParB, in order to link the function of ParH with the chromosome segregation machinery. As such we undertook to purify all four proteins from the heterologous host *E. coli*, using nickel affinity chromatography. We generated overexpression constructs containing genes encoding ParH, Hyp and ParB proteins using pET28a as the *E. coli* expression vector, as well as a previously generated pET28a vector containing the gene encoding Scy. After determining the optimal conditions for the production of these proteins using expression trials we developed optimal purification procedures for the large scale purification of these proteins. ParH, Hyp and ParB were all purified from solution in their native form. However, we were only able to purify ParB under denaturing conditions using urea before trying to refold the protein by exchanging the denaturing buffer for a solution using dialysis. After purification the proteins were dialysed against different buffers to assess their biochemical properties. During dialysis we found that Hyp only remained soluble at high concentrations (above 0.2 mg/ml) in the presence of arginine.

A key aspect of ParA/MinD proteins is their oligomeric state and how that is regulated. The basic subunit of these proteins is a monomeric form upon which higher order assemblies can occur. Upon binding to ATP the proteins dimerise and this is a common feature of both ParA and MinD proteins from *E. coli*, *C. crescentus*, *B. subtilis* and *S. coelicolor* (Gerdes et al., 2010; Hester and Lutkenhaus, 2007; Jakimowicz et al., 2007; Ptacin et al., 2010). In some cases, such as Soj in *B. subtilis* and MinD proteins in *E. coli* and *B. subtilis*, these dimers do not associate into higher-order assemblies. But in the case of ParA from *S. coelicolor* and ParA encoded by the *E. coli* plasmid pB171, these dimers form the basis for filamentation (Gerdes et al., 2010; Jakimowicz et al., 2007). One thing is clear, that ATP seems to be essential for the formation of ParA dimers and by extension oligomerisation. Regulation of this state is therefore built upon regulation of ATP binding. The low ATPase activity of the proteins allow for stable ATP interactions to form and forms the basis upon which a regulatory mechanism can act. Most of these proteins have a partner protein, whether MinE in the case of MinD in *E. coli*, or ParB in the case of ParA in *S. coelicolor* and *C. crescentus*, which up regulate the ATPase activity of the respective ParA/MinD protein (Hu and Lutkenhaus, 2001; Jakimowicz et al., 2007). This tilts the balance of

the protein from one in which ATP binding occurs faster than ATP hydrolysis to one in which ATP hydrolysis occurs faster than ATP binding. This creates two scenarios, one where the ParA/MinD protein is in the absence of its partner protein and ATP bound, and thus undergoing oligomerisation; and a second where the ParA/MinD protein is interacting with its partner protein, hydrolysing ATP and thus pushed towards a monomeric state. The bacteria can then couple this two state mechanism to drive a division process. In *E. coli* for instance, MinD in its ATP bound form interacts with MinC, which is an inhibitor of FtsZ polymerisation, while MinD in its monomeric form does not interact with MinC (Dajkovic et al., 2008). By ensuring that MinD dimers are only present at the poles, MinC localisation is also polarly located which in turn helps to ensure mid-cell localisation of the FtsZ ring. With ParA proteins in both *S. coelicolor* and *C. crescentus*, this regulation is used to pull chromosomes during segregation with the retracting ParA filament or dimer cloud, pulling the ParB bound chromosome to the desired location in the cell (Ptacin et al., 2014; Ptacin et al., 2010).

We therefore set out to first determine the oligomerisation of ParH and then the nature of its association with Hyp, Scy and ParB. In determining the oligomerisation of ParH we utilised both analytical gel filtration, native-PAGE and crosslinking experiments to demonstrate that ParH forms a dynamic equilibrium of multi oligomeric states. The analytical gel filtration showed multiple elution peaks of ParH indicating that a mixed population existed. From this we were able to deduce the presence of both monomers and dimers in addition to higher oligomers. This was further confirmed in native-PAGE with the appearance of many ParH bands that had a 'ladder-like' formation, with a regular spacing which indicated a common subunit. By chemical crosslinking and observations on SDS-PAGE and using a Ferguson plot we deduced that these oligomers are built on a common monomer subunit with an n+ monomer progression. By separating the monomer oligomer from the rest using gel filtration, we were able to show that all the oligomers of ParH are able to reform. Most importantly, we were able to demonstrate that ParH oligomerisation occurs independently of ATP. This means that unlike other ParA/MinD proteins, dimerisation and oligomerisation under these conditions are not dependent on ATP. In addition to ParH oligomerisation we were also able, through the same techniques,

to show that Hyp forms a homo-tetramer and is able to interact with higher oligomers of ParH, demonstrating interaction between the proteins.

Next we began to investigate protein:protein interactions of ParH in order to search for partner proteins. For this we wished to observe interaction with Hyp, Scy and ParB. Interaction between ParH and Hyp was already demonstrated when we investigated the oligomerisation of ParH. We therefore wished to confirm this interaction both *in vivo* through bacterial two-hybrid assay in the heterologous host *E. coli*, and *in vitro* using pelleting assay. We were unable to show interaction between ParH and Hyp using bacterial two-hybrid. However, the limitations of this technique does not preclude interaction from occurring. Moreover, interaction was observed using the pelleting assay which confirmed the interaction observed by native-PAGE. ATP does not appear to play a role in ParH-Hyp interaction. Given that the two proteins interact and are translationally coupled suggests that they have a shared function in the cell and probably indicates that Hyp has a role in septum placement.

The link between ParA and Scy had already been established and so it is possible that given the similarity between ParH and ParA, we would be able to show a similar interaction between Scy and ParH. In addition, given the unusual branching of aerial hyphae in the *parH* mutant strain together with the smaller colony size, we surmised that there might have been an effect on the TIPOC from the absence of ParH. Using the same techniques we used to demonstrate interaction between ParH and Hyp, we were also able to show interaction between ParH and Scy. This interaction was confirmed both *in vivo* using the bacterial two-hybrid assay and *in vitro* using pelleting assay. We found that the ParH-Scy interaction is similar to the ParA-Scy interaction where, in the presence of ATP and a high molar ratio (8:1) of ParH to Scy appears to cause Scy to disassemble. This would indicate that ParH does have an effect on the oligomerisation of Scy and this is likely to explain the defect in growth of the *parH* mutant strain. It is also the first instance where we see an effect on ParH from the presence of ATP. Although ATP does not appear to be necessary for ParH-Scy interaction there does appear to be a regulation of that interaction through ParH ATP binding.

We next sort to investigate a possible link between ParH and ParB. Again given the similarity between ParA and ParH, we thought it possible that the two proteins could interact. In addition, we wished to explore whether there was any cross talk between the ParAB system and the ParH-Hyp system. We again used the same techniques used to demonstrate interaction between ParH and Scy and between ParH and Hyp. We were able to confirm interaction though bacterial two-hybrid assay indicating that there is indeed crosstalk between the systems. The *in vitro*, pelleting assay however indicated an interesting mechanism. In the absence of ATP, pelleting was observed for both of the proteins suggesting a complex was formed. Although this confirmed the interaction seen with bacterial two-hybrid assay, it does indicate that ATP is not a requirement for interaction. This is unlike ParA-ParB interaction which always requires the ability of ParA to bind ATP, or at least dimerisation of ParA. The real significance however, is that interaction appears to be abolished in the presence of ATP, although pelleting of ParH remains. This would indicate that a conformational, or oligomerisation of ParH is occurring through binding ATP in the presence of ParB.

As discussed regulation of the ATPase activity of ParA/MinD proteins are important for function, we therefore set out to monitor the ATPase activity of ParH and determine whether any of the partner proteins increase the activity. The base rate of ParH ATPase activity is comparable with the established rate of ParA-like proteins. We were able to detect a base rate whereby approximately one molecule of ParH hydrolyses one molecule of ATP every two hours. Reported rates of ParA-like proteins such as Soj in *B. subtilis*, and ParA from *S. coelicolor* and *T. thermophiles* suggest a rate of around one molecule of ParA hydrolysing one molecule of ATP (Jakimowicz et al., 2007; Leonard et al., 2004; Murray and Errington, 2008). When upregulated by a partner protein these rates can increase although are not consistent increases across proteins. The addition of Spo0J and DNA to the reaction causes an 82 fold increase in ATPase activity of Soj, while the addition of ParB and DNA containing *parS* sites doubles the ATPase activity of ParA from *S. coelicolor* (Jakimowicz et al., 2007; Leonard et al., 2004; Murray and Errington, 2008). We were unable to show an increase in the ATPase activity of ParH with the addition of either

Hyp or ParB to the reaction suggesting that under the conditions we tested they are not the regulator for ParH ATPase activity.

We then proceeded to investigate possible DNA interactions of ParH and Hyp. While Hyp is not a homologue of ParB, we hypothesised that it may be a DNA binding protein. Moreover, many ParA and MinD proteins have shown affinity to DNA, especially in the presence of ATP, so we thought it a possibility that ParH also would have affinity to DNA. Using electrophoretic mobility shift assays and pelleting assays we were able to show strong Hyp-DNA interaction. This interaction appeared to be non-specific with increasing shifts in the DNA upon the addition of increasing amounts of Hyp protein. We were also able to show ParH-DNA interaction in a pelleting assay but were unable to see this using the electrophoretic mobility shift assay. The lack of a shift with ParH is probably due to the disruption of any ParH-DNA complexes due to the effects of electrophoresis. This indicates that this ParH:DNA interaction is weak. Once again ATP had no effect on this interaction, which is unusual when compared to other ParA/MinD proteins where ATP is essential for DNA binding.

After confirming that Hyp is a DNA binding with no homology to ParB as well as any proteins of known function, we wished to elucidate the structure of Hyp to understand more about its DNA binding properties. We were only successful in crystallising the C-terminus of the protein. It is likely that the disordered N-terminus underwent proteolysis during crystallisation trials allowing the C-terminal domain to crystallise. The solved structure of the C-terminal domain of Hyp showed that it has a ribbon-helix-helix motif. This structure, while tetrameric, consisted of a dimer of dimers so we sort to investigate which domain of Hyp was responsible for oligomerisation. As such we purified both the N-terminal and the C-terminal domains of Hyp. Using analytical gel filtration, we were able to show that the N-terminus of Hyp is responsible for tetramerisation, while the C-terminus on its own is unable to oligomerise. Searching for structural homologues of Hyp demonstrated that structurally it belonged to the bacterial ribbon-helix-helix family of DNA binding proteins. These proteins are involved in a wide range of functions across bacteria including roles in anti-toxicity, controlling plasmid copy numbers, repression of nickel uptake, methionine repression and regulation of bacterial conjugation. The most interesting structural homologue however, is the ParG protein found on the multi-

drug resistant plasmid TP288 in *Salmonella newport, where it is involved in* plasmid segregation.

Could ParH-Hyp have a similar function to ParFG?

The most interesting structural homologue of Hyp that has been solved is the previously mentioned ParG protein (Figure 120). This is a plasmid encoded gene which forms part of the plasmid partitioning system for the plasmid TP228, a multi-drug resistance plasmid found in *S. newport* (Barilla and Hayes, 2003). Given that this protein is involved in plasmid segregation it is perhaps unsurprising to find that it is associated with a ParA-like ATPase, designated ParF. The existence of a ParA-like ATPase that is associated with a protein, structurally homologous to Hyp opens up the possibility that they could have a similar function.

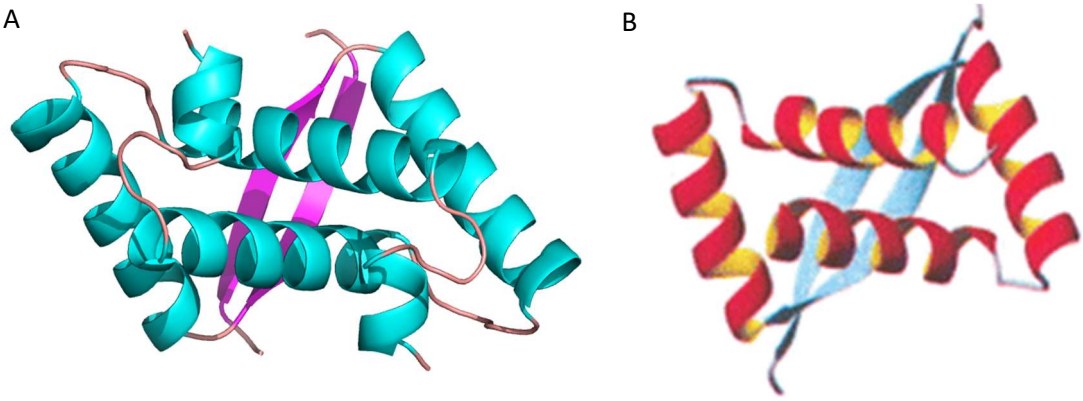

Figure 120: Structure comparison of Hyp and ParG.

Hyp (A) is structurally homologous to ParG (B), a plasmid partitioning protein found on *S. newport* multi-drug resistant plasmid TP228. ParG, like Hyp, is associated with a ParA-like ATPase designated ParF (Golovanov et al., 2003).

Interestingly homologues of the ParFG system are all encoded on plasmids associated with Gram-negative bacteria. This is the first instance of a ribbon-helix-helix protein that is associate with a ParA-like protein, being encoded on a chromosome rather than a plasmid. If functional similarity between the systems exist, this would mean either that ParH and Hyp are involved in chromosome segregation or, we have plasmid segregation machinery encoded on a chromosome.

The strain S. coelicolor A3(2), does contain two plasmids, Scp1 and Scp2, therefore we cannot rule out the possibility that ParH and Hyp are a plasmid segregating machinery encoded on a chromosome.

The proposed model of plasmid segregation through the ParFG system is either through bidirectional pulling or bidirectional pushing (Barilla et al., 2005). In both models ParG dimers bind the replicated plasmid TP228, attaching via the *parH* sequence, and interact with a ParF dimer to create two distinct segrosomes, one on each plasmid (Figure 121). ATP interaction with ParF causes a conformational change inducing ParF polymerisation. In the pushing model the polymerisation of ParF causes the two plasmids to be pushed to the opposing poles of the cell through

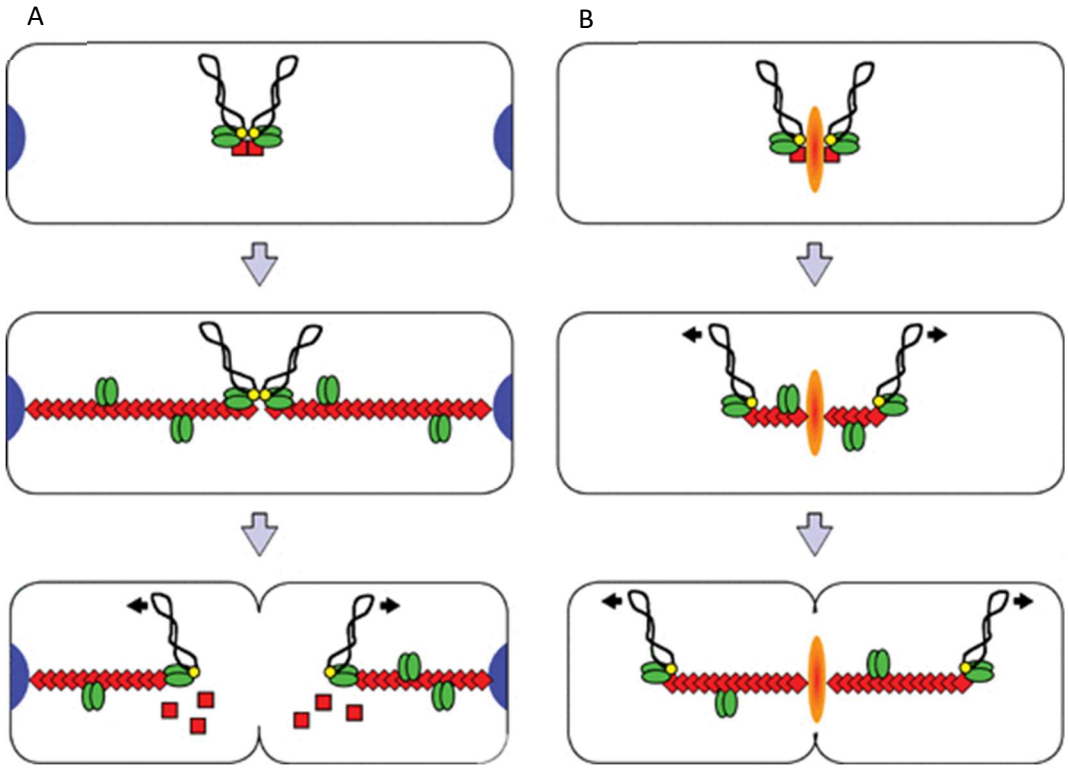

Figure 121: Model of the two possible modes of ParFG plasmid segregation

There are two possible models, bidirectional pulling and bidirectional pushing, for the mode of action of the ParFG plasmid portioning system. In both models a segrosome forms on each plasmid consisting of a ParG dimer (green), a ParF dimer (red) and the partition sites (yellow). Bidirectional pulling involves the ATP dependent polymerisation of ParF which stretches to each pole and attaches to an unknown tether protein (blue) that is bound to the pole. Upregulation of the ParF ATPase activity by the plasmid bound ParG dimer causes disassembly of the ParF polymer causing it to contract towards the pole and thus pulling the plasmids to opposite poles ready for division. Bidirectional pushing would require ParF to bind to a tethered mid cell position (orange) against which ParF polymerisation would push the plasmids to opposite poles. Model taken from (Barilla et al., 2005)

extension of ParF from a tethered mid cell position. In the pulling model, ParF polymerisation stretches out from the mid cell located plasmids to the poles where it attaches to an as of yet unknown pole tethering protein. Upregulation of the ParF ATPase activity by the plasmid bound ParG dimer causes disassembly of the ParF polymer causing it to contract towards the pole and thus pulling the plasmids to opposite poles ready for division.

Like the *parS* sites that are targeted by ParB, ParG binds to a specific sequence, designated *parH* site, which is located immediately upstream of the *parF* gene (Wu et al., 2011). The *parH* site consists of two 5'-ACTC-3' boxes that are separated by 4 bp AT-rich spacers (Wu et al., 2011; Zampini et al., 2009). Interestingly the incremental deletion of the N-terminal domain of ParG increased its affinity to the *parH* site. However the same progressive deletion caused loss of interaction between ParG and ParF meaning that ParF was less likely to bind to the complex and create the ParFGH segrosome (Wu et al., 2011). Unlike Hyp, which we have established is a tetramer, ParG is a homodimer in which the RHH domain forms the dimer while the N-terminal domain forms two disordered tails (Golovanov et al., 2003). The protein then forms a tetramer, or a dimer of dimers when bound to DNA and at even higher protein concentrations the tetramers start to associate into even higher order assemblies (Carmelo et al., 2005). In addition to its role in plasmid segregation, it is thought that ParG DNA binding functions as a transcriptional repressor of the ParFG operon, although the biological significance of this is not understood (Carmelo et al., 2005). Like ParH, ParF is able to form higher order assemblies as assessed by chemical crosslinking experiments and although this occurs to a small extent in the absence of ATP, polymerisation is certainly enhanced in the presence of ATP (Barilla et al., 2005). It has also been demonstrated that this polymerisation is based on an initial ATP mediated dimerisation of ParF creating subunits upon which higher order assemblies can form (Dobruk-Serkowska et al., 2012; Schumacher et al., 2012).

One of the key experiments that was used to investigate polymerisation of ParF and the effect of ATP on that process was the pelleting assay (Figure 122). What was demonstrated was that in the presence of ATP and, in a more pronounced manner, ATPγS (a non-hydrolysable ATP analogue) ParF pelleted when subjected to

centrifugation (Barilla et al., 2005). This was in contrast to the fractions containing just ParF or with the addition of ADP where ParF was observed in the supernatant fraction. This data suggested that ParF polymerised or at least the nature of the polymerisation changed as a result of ATP binding rather than the protein merely exhibiting self-assembly. There were a couple of differences in the pelleting conditions utilised to determine ParF polymerisation and the experimental conditions we followed. Firstly, they used a slightly different buffer system at a pH7.5

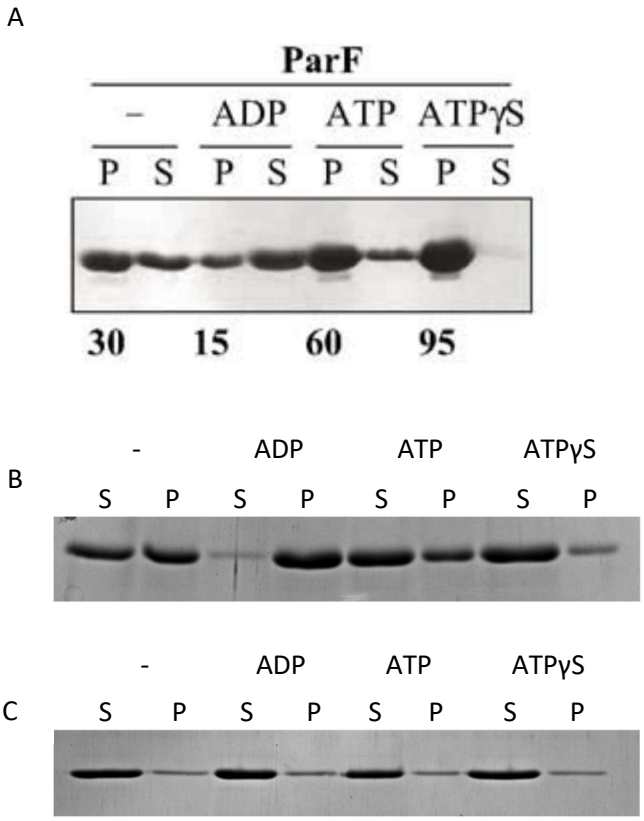

Figure 122: Pelleting assay of His-ParH in the presence of ADP, ATP, ATPγS.

(A) Pelleting assay showing ParF pelleting in the presence of ATP and ATPγS.
ParH (6 µM) was incubated both separately and in the presence of 2 mM of either ADP, ATP or ATPγS. After a 30 minutes incubation at room temperature in either (A) Tris buffer (30 mM Tris-HCl, 100 mM KCl, 5 mM MgCl2, 2 mM DTT pH7.5) or (B) Hepes buffer (30 mM Hepes-KOH, 100 mM KCl, 5 mM MgCl2, 2 mM DTT pH7.5) the samples were centrifuged for 30 minutes at 14,000 rpm at 4°C generating both supernatant and pellet fractions. In Tris buffer His-ParH was found mainly in the supernatant fractions except for in the presence of ADP, where it was found exclusively in the pellet fraction. In Hepes buffer all conditions lead to fractions in which His-ParH was predominantly found in the supernatant fraction. Samples were analysed using 10% SDS PAGE. Image (A) taken from (Barilla et al., 2005)

(30 mM Tris-HCl, 100 mM KCl, 5 mM $MgCl_2$, 2 mM DTT pH7.5) and secondly they centrifuged at 16,000 g instead of 464,452 g as we had done (Barilla et al., 2005).

To test whether the different conditions affected ParH polymerisation we decided to repeat this experiment with ParH to determine whether we could make the same observation and determine whether two systems are in fact similar. To investigate this 6 µM of purified His-ParH protein was incubated for 10 minutes at room temperature both separately and with 2 mM of either ADP, ATP or ATPγS in a Tris buffer (30 mM-HCl Tris, 100 mM KCl, 5 mM $MgCl_2$, 2 mM DTT pH7.5). After incubation the samples were centrifuged at 16,000 g at 4°C for 30 minutes after which the supernatant was collected and the pellet fraction re-suspended. All fractions were then analysed using SDS-PAGE (Figure 122). In agreement with our previous findings we observed no effect on either the extent of polymerisation of ParH or its confirmation in the presence of either ATP or its non-hydrolysable analogue ATPγS. Surprisingly we did find parH exclusively in the pellet fraction in the presence of ADP. This result was reproducible and clear protein precipitation was observable in the tube prior to centrifugation. This suggested that the pelleting was not a result of an effect on the polymerisation of ParH but more as a result of the protein falling out of solution. We wished to observe whether this effect could be seen in other buffers and so repeated the experiment in a Hepes buffer system (30 mM Tris, 100 mM KCl, 5 mM $MgCl_2$, 2 mM DTT pH7.5). In this buffer all conditions resulted in His-ParH being found mainly in the supernatant suggesting that the ADP effect on His-ParH was artificial and probably not biologically significant.

We therefore conclude that while ParG and Hyp share structural homology, and that we cannot completely rule out a similar function, they probably have different functions. While ParG is able to upregulate the ATPase activity of ParF which provides a mechanistic basis for plasmid segregation we are not able to show the same mechanism between ParH and Hyp. In addition, ParH does not appear, in the conditions tested, to show the same ATP dependent polymerisation that wold be suggestive of a plasmid or chromosome segregation system. It would however, be useful to rule out plasmid segregation as a function for Hyp. Therefore

experiments investigating the retention of S. coelicolor A3(2) plasmids Scp1 and Scp2 in the Hyp knockout strain would be useful.

What is the role of ParH?

From the phenotype of the ParH knockout strain, it is clear that ParH has a effect on septum positioning during sporulation. Not only are the septum placed irregularly in the aerial hyphae, there positioning is also delayed and the synchronicity of sporulation between the hyphae is lost. This suggests that the hyphae are unable to efficiently place septa during sporulation. However we still need to establish whether this is due to a direct effect on septum placement or a result of a chromosome segregation defect. The key to establishing this will be through localisation studies of ParH and ParB. We have already demonstrated interaction between the proteins so the question that remains is does ParH localise ParB or does ParB localise ParH. If ParH localises ParB then that would indicate that ParH is part of the chromosome segregation machinery, however if the alternative is true then that would indicate that ParH is involved in determining septum site placement.

If it were found that ParH was involved in chromosome segregation then it would be important to establish an interaction with ParA in order to determine whether ParH is part of the ParAB chromosome machinery or whether it acts independently on ParB either as an alternative to ParA or in a modified role. If it were to be in an alternative pathway to ParA, then that opens up the possibility that ParH functions with SMC and ScpAB as part of the chromosome organising pathway. Given the proximity of the genes encoding ParH and ScpA and ScpB it is possible that there is some kind of shared function between the proteins.

Given the low number of anucleate spores in the ParH knockout compared to the knockouts of ParA and ParB, it would suggest that ParB localisation is unaffected in the ParH knockout strain. This suggests that ParB is localising ParH during sporulation. Therefore it would be important to establish a mechanism by which ParH acts. The obvious mechanism for this would be a direct interaction with FtsZ. It would be important to first establish if ParH has an effect on FtsZ polymerisation. This could

be done in vitro by assessing FtsZ polymerisation dynamics in the presence of ParH using transmission electron microscopy and pelleting assays. This would establish if ParH has an effect on FtsZ polymerisation. If there is an effect it would also indicate whether ParH is a positive or negative regulator of FtsZ. Should no direct link be found then it would be important to establish if there is an intermediary protein.

The interaction between ParH and ParB produced an interesting dynamic when investigated *in vitro* using pelleting assay. This suggested that ParH interaction is independent of ParH ATP binding. This should be confirmed using bacterial two-hybrid assay with a non ATP binding ParH mutant. If confirmed this would show a very different mode of interaction when compared to ParA-ParB interaction which is ATP dependent. In the same experiment we also showed that interaction between ParH and ParB is abolished in the presence of ATP. Moreover, it appears that there was either a conformational or oligomerisation change in ParH. This could indicate that ParB is an activator of ATP bound ParH. This should be explored further to determine first of all whether this is caused by increased ParH affinity for ATP, and thus promoting ATP binding, or whether it is an oligomerisation change, and then to explore what effect this has on other properties of ParH, such as DNA binding or protein interaction. If this is confirmed then we may be able to search for regulators of ParH ATPase activity which could occur after activation of ParH by ParB.

Given the phenotype of the ParH knockout strain and the sequence homology to ParA, it was not surprising that we were able to detect ParH interaction with Scy. We also demonstrated a similar interplay between ParH and Scy as has previously been shown between ParA and Scy. ParA interaction with Scy serves two purposes, to localise ParA to the tip and to inhibit the polymerisation of ParA so that the chromosome segregation machinery is switched off. Localisation of ParA to the tip also plays a role in anchoring the tip associated chromosome to the TIPOC. Our data would indicate that ParH should also be localised to the tip during growth through its interaction with Scy. This should be confirmed using localisation studies of ParH and tested in a *scy* mutant background. Should this be shown to be true, then it suggests that perhaps that Scy is inhibiting the action of ParH during growth, which as ParH is likely involved in division would be consistent with the Scy interaction with ParA. However, given that the *parH* mutant is affected in growth could indicate that ParH

is having an effect on the TIPOC. Therefore, it would be important to assess whether ParH is having an effect on the assembly dynamics of Scy. Through transmission electron microscopy it may be possible to determine whether Scy assemblies are altered by the presence of ParH *in vitro*. If this is not the case, then perhaps ParH is also involved in the anchoring of the tip associated chromosome. Given we have already demonstrated that ParH interacts with ParB, and in a manner suggestive of an ATP independent interaction, the possibility that the anchoring of the chromosome through a Scy-ParH-ParB complex should be explored.

We were unable to determine a possible function for Hyp, based upon the phenotype observed for the *hyp* mutant strain. However, given that the gene encoding Hyp is translationally coupled to ParH and the interaction we observed *in vitro* using both native-PAGE and pelleting assay, it is likely that the function of Hyp is related to the function of ParH. Which would indicate that Hyp plays a role in septum positioning as well. Given that we have demonstrated that Hyp is a DNA binding protein, the possibility that it is a nucleoid occlusion type protein should be explored. More investigation should be carried out into whether Hyp acts as the ATPase regulator of ParH. While our investigations could not show this, given the gene organisation of the genes encoding ParH and Hyp, coupled with the studies described on other ParA-like proteins, Hyp remains the prime candidate to regulate the ParH ATPase. We determined that Hyp has a ribbon-helix-helix C-terminal domain with structural homologue to other DNA binding domains with the same motif. A key feature of these proteins is that they bind specific target sequences of DNA. It would be important to establish the DNA target sequence to which Hyp binds. This could be achieved through chromatin immunoprecipitation sequencing (ChIP-Seq). Determining the target sequence would perhaps lead to insights as to the nature of the function of Hyp and the regions of the chromosome upon which it acts. Another feature of bacterial ribbon-helix-helix proteins is there role as transcriptional repressors. Therefore it is not inconceivable that Hyp could act as a transcriptional repressor and is something that should be investigated.

Based upon the observations made in this study and the established literature, we propose a new model for division (Figure 123). In this model division as before after overcoming polymerisation inhibition by Scy, ParA forms filaments

along the length of the aerial hyphae. These filaments position ParB which is bound to the *parS* sites of each chromosome. This leads to the segregation of chromosomes prior to septation. ParH is then localised to the chromosome by ParB. This localisation then helps to coordinate the placement of septa either side of the chromosome in a manner yet to be determined.

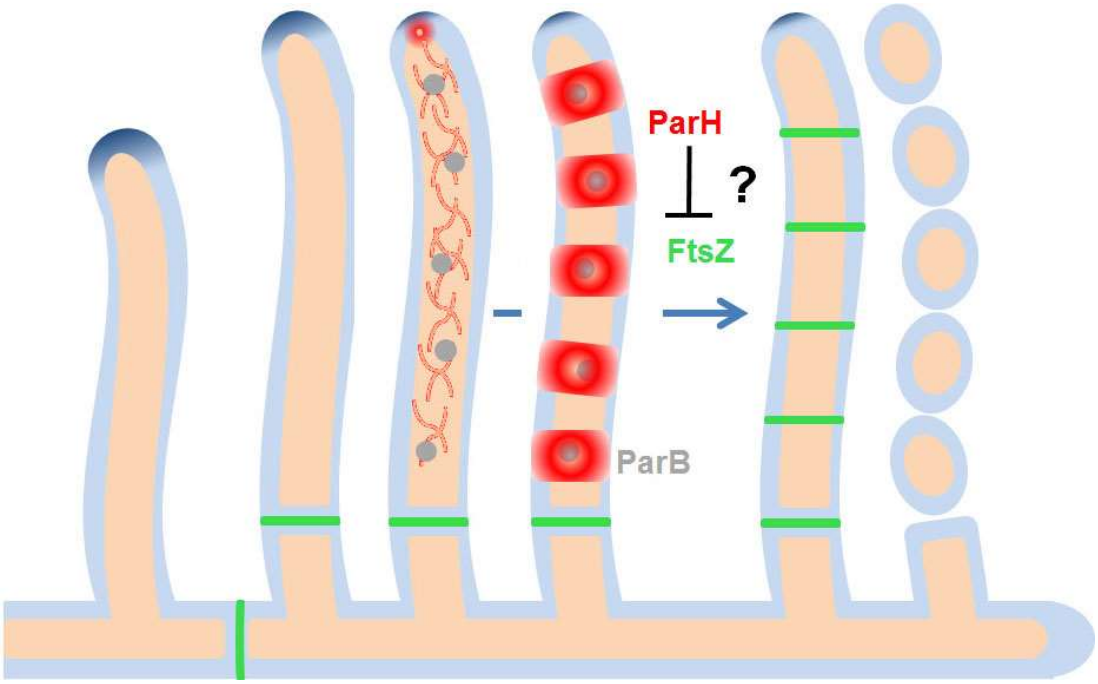

Figure 123: Suggested mode for the function of ParH.

The chromosomes are segregated through the previously established ParAB machinery. During segregation ParH is localised to the chromosomes by the chromosome bound ParB complexis. ParH influences septum placement such that each chromosome is enclosed be two septa.

References

Adams, D.W., Wu, L.J., and Errington, J. (2015). Nucleoid occlusion protein Noc recruits DNA to the bacterial cell membrane. EMBO J *34*, 491-501.

Adler, H.I., Fisher, W.D., Cohen, A., and Hardigree, A.A. (1967). Miniture *Escherichia coli* cells deficiant in DNA. Proc Natl Acad Sci U S A *57*, 321-326.

Aldridge, B.B., Fernandez-Suarez, M., Heller, D., Ambravaneswaran, V., Irimia, D., Toner, M., and Fortune, S.M. (2012). Asymmetry and aging of mycobacterial cells lead to variable growth and antibiotic susceptibility. Science *335*, 100-104.

Allan, I., and Pearce, J.H. (1983). Differential amino acid utilization by Chlamydia psittaci (strain guinea pig inclusion conjunctivitis) and its regulatory effect on chlamydial growth. J Gen Microbiol *129*, 1991-2000.

Allen, A.K., Neuberger, A., and Sharon, N. (1973). The purification, composition and specificity of wheat-germ agglutinin. Biochem J *131*, 155-162.

Arndt-Jovin, D.J., and Jovin, T.M. (1989). Fluorescence labeling and microscopy of DNA. Methods Cell Biol *30*, 417-448.

Ausmees, N., Kuhn, J.R., and Jacobs-Wagner, C. (2003). The bacterial cytoskeleton: an intermediate filament-like function in cell shape. Cell *115*, 705-713.

Aussel, L., Barre, F.X., Aroyo, M., Stasiak, A., Stasiak, A.Z., and Sherratt, D. (2002). FtsK Is a DNA motor protein that activates chromosome dimer resolution by switching the catalytic state of the XerC and XerD recombinases. Cell *108*, 195-205.

Bagchi, S., Tomenius, H., Belova, L.M., and Ausmees, N. (2008). Intermediate filament-like proteins in bacteria and a cytoskeletal function in Streptomyces. Mol Microbiol *70*, 1037-1050.

Baker, E.N., and Hubbard, R.E. (1984). Hydrogen bonding in globular proteins. Prog Biophys Mol Biol *44*, 97-179.

Ball Jr, A.R., and Yokomori, K. (2001). The structural maintenance of chromosomes (SMC) family of proteins in mammals. Chromosome Res *9*, 85-96.

Barilla, D., Carmelo, E., and Hayes, F. (2007). The tail of the ParG DNA segregation protein remodels ParF polymers and enhances ATP hydrolysis via an arginine finger-like motif. Proc Natl Acad Sci U S A *104*, 1811-1816.

Barilla, D., and Hayes, F. (2003). Architecture of the ParF*ParG protein complex involved in prokaryotic DNA segregation. Mol Microbiol *49*, 487-499.

Barilla, D., Rosenberg, M.F., Nobbmann, U., and Hayes, F. (2005). Bacterial DNA segregation dynamics mediated by the polymerizing protein ParF. EMBO J *24*, 1453-1464.

Baynham, P.J., Brown, A.L., Hall, L.L., and Wozniak, D.J. (1999). Pseudomonas aeruginosa AlgZ, a ribbon-helix-helix DNA-binding protein, is essential for alginate synthesis and algD transcriptional activation. Mol Microbiol *33*, 1069-1080.

Beall, B., and Lutkenhaus, J. (1992). Impaired cell division and sporulation of a Bacillus subtilis strain with the ftsA gene deleted. J Bacteriol *174*, 2398-2403.

Becker, D.F., and Thomas, E.A. (2001). Redox properties of the PutA protein from Escherichia coli and the influence of the flavin redox state on PutA-DNA interactions. Biochemistry *40*, 4714-4721.

Bentley, S.D., Chater, K.F., Cerdeno-Tarraga, A.M., Challis, G.L., Thomson, N.R., James, K.D., Harris, D.E., Quail, M.A., Kieser, H., Harper, D.*, et al.* (2002). Complete genome sequence of the model actinomycete Streptomyces coelicolor A3(2). Nature *417*, 141-147.

Benvenuti, M., and Mangani, S. (2007). Crystallization of soluble proteins in vapor diffusion for x-ray crystallography. Nat Protoc *2*, 1633-1651.

Bernhardt, T.G., and de Boer, P.A. (2005). SlmA, a nucleoid-associated, FtsZ binding protein required for blocking septal ring assembly over Chromosomes in E. coli. Mol Cell *18*, 555-564.

Bi, E.F., and Lutkenhaus, J. (1991). FtsZ ring structure associated with division in Escherichia coli. Nature *354*, 161-164.

Bigot, S., Corre, J., Louarn, J.M., Cornet, F., and Barre, F.X. (2004). FtsK activities in Xer recombination, DNA mobilization and cell division involve overlapping and separate domains of the protein. Mol Microbiol *54*, 876-886.

Bowman, G.R., Comolli, L.R., Zhu, J., Eckart, M., Koenig, M., Downing, K.H., Moerner, W.E., Earnest, T., and Shapiro, L. (2008). A polymeric protein anchors the chromosomal origin/ParB complex at a bacterial cell pole. Cell *134*, 945-955.

Breg, J.N., van Opheusden, J.H., Burgering, M.J., Boelens, R., and Kaptein, R. (1990). Structure of Arc repressor in solution: evidence for a family of beta-sheet DNA-binding proteins. Nature *346*, 586-589.

Breier, A.M., and Grossman, A.D. (2007). Whole-genome analysis of the chromosome partitioning and sporulation protein Spo0J (ParB) reveals spreading and origin-distal sites on the Bacillus subtilis chromosome. Mol Microbiol *64*, 703-718.

Britton, R.A., Lin, D.C., and Grossman, A.D. (1998). Characterization of a prokaryotic SMC protein involved in chromosome partitioning. Genes Dev *12*, 1254-1259.

Brown, P.J., de Pedro, M.A., Kysela, D.T., Van der Henst, C., Kim, J., De Bolle, X., Fuqua, C., and Brun, Y.V. (2012). Polar growth in the Alphaproteobacterial order Rhizobiales. Proc Natl Acad Sci U S A *109*, 1697-1701.

Buddelmeijer, N., and Beckwith, J. (2004). A complex of the Escherichia coli cell division proteins FtsL, FtsB and FtsQ forms independently of its localization to the septal region. Mol Microbiol *52*, 1315-1327.

Buts, L., Lah, J., Dao-Thi, M.H., Wyns, L., and Loris, R. (2005). Toxin-antitoxin modules as bacterial metabolic stress managers. Trends Biochem Sci *30*, 672-679.

Cabeen, M.T., and Jacobs-Wagner, C. (2005). Bacterial cell shape. Nat Rev Microbiol *3*, 601-610.

Cabre, E.J., Monterroso, B., Alfonso, C., Sanchez-Gorostiaga, A., Reija, B., Jimenez, M., Vicente, M., Zorrilla, S., and Rivas, G. (2015). The Nucleoid Occlusion SlmA Protein Accelerates the Disassembly of the FtsZ Protein Polymers without Affecting Their GTPase Activity. PLoS One *10*, e0126434.

Caddick, S.E., Harrison, C.J., Stavridou, I., Mitchell, J.L., Hemmings, A.M., and Brearley, C.A. (2008). A Solanum tuberosum inositol phosphate kinase (StITPK1) displaying inositol phosphate-inositol phosphate and inositol phosphate-ADP phosphotransferase activities. FEBS Lett *582*, 1731-1737.

Cagliero, C., Grand, R.S., Jones, M.B., Jin, D.J., and O'Sullivan, J.M. (2013). Genome conformation capture reveals that the Escherichia coli chromosome is organized by replication and transcription. Nucleic Acids Res *41*, 6058-6071.

Cameron, T.A., Zupan, J.R., and Zambryski, P.C. (2015). The essential features and modes of bacterial polar growth. Trends Microbiol *23*, 347-353.

Carballido-Lopez, R., and Errington, J. (2003). A dynamic bacterial cytoskeleton. Trends Cell Biol *13*, 577-583.

Carballido-Lopez, R., Formstone, A., Li, Y., Ehrlich, S.D., Noirot, P., and Errington, J. (2006). Actin homolog MreBH governs cell morphogenesis by localization of the cell wall hydrolase LytE. Dev Cell *11*, 399-409.

Carmelo, E., Barilla, D., Golovanov, A.P., Lian, L.Y., Derome, A., and Hayes, F. (2005). The unstructured N-terminal tail of ParG modulates assembly of a quaternary nucleoprotein complex in transcription repression. J Biol Chem *280*, 28683-28691.

Cha, J.H., and Stewart, G.C. (1997). The divIVA minicell locus of Bacillus subtilis. J Bacteriol *179*, 1671-1683.

Champoux, J.J. (2001). DNA topoisomerases: structure, function, and mechanism. Annu Rev Biochem *70*, 369-413.

Chater, K.F. (1993). Genetics of differentiation in Streptomyces. Annu Rev Microbiol *47*, 685-713.

Chauhan, A., Lofton, H., Maloney, E., Moore, J., Fol, M., Madiraju, M.V., and Rajagopalan, M. (2006). Interference of Mycobacterium tuberculosis cell division by Rv2719c, a cell wall hydrolase. Mol Microbiol *62*, 132-147.

Cho, H., McManus, H.R., Dove, S.L., and Bernhardt, T.G. (2011). Nucleoid occlusion factor SlmA is a DNA-activated FtsZ polymerization antagonist. Proc Natl Acad Sci U S A *108*, 3773-3778.

Costa, M., Sola, M., del Solar, G., Eritja, R., Hernandez-Arriaga, A.M., Espinosa, M., Gomis-Ruth, F.X., and Coll, M. (2001). Plasmid transcriptional repressor CopG oligomerises to render helical superstructures unbound and in complexes with oligonucleotides. J Mol Biol *310*, 403-417.

Dai, K., Xu, Y., and Lutkenhaus, J. (1993). Cloning and characterization of ftsN, an essential cell division gene in Escherichia coli isolated as a multicopy suppressor of ftsA12(Ts). J Bacteriol *175*, 3790-3797.

Dajkovic, A., Lan, G., Sun, S.X., Wirtz, D., and Lutkenhaus, J. (2008). MinC spatially controls bacterial cytokinesis by antagonizing the scaffolding function of FtsZ. Curr Biol *18*, 235-244.

Dalton, K.A., Thibessard, A., Hunter, J.I., and Kelemen, G.H. (2007). A novel compartment, the 'subapical stem' of the aerial hyphae, is the location of a sigN-dependent, developmentally distinct transcription in Streptomyces coelicolor. Mol Microbiol *64*, 719-737.

Daniel, R.A., and Errington, J. (2003). Control of cell morphogenesis in bacteria: two distinct ways to make a rod-shaped cell. Cell *113*, 767-776.

Danilova, O., Reyes-Lamothe, R., Pinskaya, M., Sherratt, D., and Possoz, C. (2007). MukB colocalizes with the oriC region and is required for organization of the two Escherichia coli chromosome arms into separate cell halves. Mol Microbiol *65*, 1485-1492.

Datsenko, K.A., and Wanner, B.L. (2000). One-step inactivation of chromosomal genes in Escherichia coli K-12 using PCR products. Proc Natl Acad Sci U S A *97*, 6640-6645.

Davis, M.A., Martin, K.A., and Austin, S.J. (1992). Biochemical activities of the parA partition protein of the P1 plasmid. Mol Microbiol *6*, 1141-1147.

Davis, N.K., and Chater, K.F. (1990). Spore colour in Streptomyces coelicolor A3(2) involves the developmentally regulated synthesis of a compound biosynthetically related to polyketide antibiotics. Mol Microbiol *4*, 1679-1691.

de Boer, P.A. (2010). Advances in understanding E. coli cell fission. Curr Opin Microbiol *13*, 730-737.

de Boer, P.A., Crossley, R.E., and Rothfield, L.I. (1992). Roles of MinC and MinD in the site-specific septation block mediated by the MinCDE system of Escherichia coli. J Bacteriol *174*, 63-70.

Defeu Soufo, H.J., and Graumann, P.L. (2006). Dynamic localization and interaction with other Bacillus subtilis actin-like proteins are important for the function of MreB. Mol Microbiol *62*, 1340-1356.

Desai, A., and Mitchison, T.J. (1997). Microtubule polymerization dynamics. Annu Rev Cell Dev Biol *13*, 83-117.

Di Laurenzio, L., Frost, L.S., and Paranchych, W. (1992). The TraM protein of the conjugative plasmid F binds to the origin of transfer of the F and ColE1 plasmids. Mol Microbiol *6*, 2951-2959.

Di Ventura, B., Knecht, B., Andreas, H., Godinez, W.J., Fritsche, M., Rohr, K., Nickel, W., Heermann, D.W., and Sourjik, V. (2013). Chromosome segregation by the Escherichia coli Min system. Mol Syst Biol *9*, 686.

Ditkowski, B., Holmes, N., Rydzak, J., Donczew, M., Bezulska, M., Ginda, K., Kedzierski, P., Zakrzewska-Czerwinska, J., Kelemen, G.H., and Jakimowicz, D. (2013). Dynamic interplay of ParA with the polarity protein, Scy, coordinates the growth with chromosome segregation in Streptomyces coelicolor. Open Biol *3*, 130006.

Ditkowski, B., Troc, P., Ginda, K., Donczew, M., Chater, K.F., Zakrzewska-Czerwinska, J., and Jakimowicz, D. (2010). The actinobacterial signature protein ParJ (SCO1662) regulates ParA polymerization and affects chromosome segregation and cell division during Streptomyces sporulation. Mol Microbiol *78*, 1403-1415.

Dobruk-Serkowska, A., Caccamo, M., Rodriguez-Castaneda, F., Wu, M., Bryce, K., Ng, I., Schumacher, M.A., Barilla, D., and Hayes, F. (2012). Uncoupling of nucleotide hydrolysis and polymerization in the ParA protein superfamily disrupts DNA segregation dynamics. J Biol Chem *287*, 42545-42553.

Doi, M., Wachi, M., Ishino, F., Tomioka, S., Ito, M., Sakagami, Y., Suzuki, A., and Matsuhashi, M. (1988). Determinations of the DNA sequence of the mreB gene and of the gene products of the mre region that function in formation of the rod shape of Escherichia coli cells. J Bacteriol *170*, 4619-4624.

Dominguez-Cuevas, P., Porcelli, I., Daniel, R.A., and Errington, J. (2013). Differentiated roles for MreB-actin isologues and autolytic enzymes in Bacillus subtilis morphogenesis. Mol Microbiol *89*, 1084-1098.

Dominguez-Escobar, J., Chastanet, A., Crevenna, A.H., Fromion, V., Wedlich-Soldner, R., and Carballido-Lopez, R. (2011). Processive movement of MreB-associated cell wall biosynthetic complexes in bacteria. Science *333*, 225-228.

Donczew, M., Mackiewicz, P., Wrobel, A., Flardh, K., Zakrzewska-Czerwinska, J., and Jakimowicz, D. (2016). ParA and ParB coordinate chromosome segregation with cell elongation and division during Streptomyces sporulation. Open Biol *6*, 150263.

Donovan, C., Schwaiger, A., Kramer, R., and Bramkamp, M. (2010). Subcellular localization and characterization of the ParAB system from Corynebacterium glutamicum. J Bacteriol *192*, 3441-3451.

Du, S., and Lutkenhaus, J. (2014). SlmA antagonism of FtsZ assembly employs a two-pronged mechanism like MinCD. PLoS Genet *10*, e1004460.

Dubendorff, J.W., and Studier, F.W. (1991). Controlling basal expression in an inducible T7 expression system by blocking the target T7 promoter with lac repressor. J Mol Biol *219*, 45-59.

Ebersbach, G., Briegel, A., Jensen, G.J., and Jacobs-Wagner, C. (2008). A self-associating protein critical for chromosome attachment, division, and polar organization in caulobacter. Cell *134*, 956-968.

Ebersbach, G., and Gerdes, K. (2001). The double par locus of virulence factor pB171: DNA segregation is correlated with oscillation of ParA. Proc Natl Acad Sci U S A *98*, 15078-15083.

Ebersbach, G., and Gerdes, K. (2004). Bacterial mitosis: partitioning protein ParA oscillates in spiral-shaped structures and positions plasmids at mid-cell. Mol Microbiol *52*, 385-398.

Ebersbach, G., Ringgaard, S., Moller-Jensen, J., Wang, Q., Sherratt, D.J., and Gerdes, K. (2006). Regular cellular distribution of plasmids by oscillating and filament-forming ParA ATPase of plasmid pB171. Mol Microbiol *61*, 1428-1442.

Erickson, H.P. (1998). Atomic structures of tubulin and FtsZ. Trends Cell Biol *8*, 133-137.

Erickson, H.P. (2007). Evolution of the cytoskeleton. Bioessays *29*, 668-677.

Errington, J. (2003). Regulation of endospore formation in Bacillus subtilis. Nat Rev Microbiol *1*, 117-126.

Errington, J. (2015). Bacterial morphogenesis and the enigmatic MreB helix. Nat Rev Microbiol *13*, 241-248.

Errington, J., Daniel, R.A., and Scheffers, D.J. (2003). Cytokinesis in bacteria. Microbiol Mol Biol Rev *67*, 52-65, table of contents.

Eswaramoorthy, P., Erb, M.L., Gregory, J.A., Silverman, J., Pogliano, K., Pogliano, J., and Ramamurthi, K.S. (2011). Cellular architecture mediates DivIVA ultrastructure and regulates min activity in Bacillus subtilis. MBio *2*.

Ezaki, B., Ogura, T., Mori, H., Niki, H., and Hiraga, S. (1989). Involvement of DnaK protein in mini-F plasmid replication: temperature-sensitive seg mutations are located in the dnaK gene. Mol Gen Genet *218*, 183-189.

Flardh, K. (2003). Essential role of DivIVA in polar growth and morphogenesis in Streptomyces coelicolor A3(2). Mol Microbiol *49*, 1523-1536.

Flardh, K. (2003). Growth polarity and cell division in Streptomyces. Curr Opin Microbiol *6*, 564-571.

Flardh, K., and Buttner, M.J. (2009). Streptomyces morphogenetics: dissecting differentiation in a filamentous bacterium. Nat Rev Microbiol *7*, 36-49.

Flardh, K., Leibovitz, E., Buttner, M.J., and Chater, K.F. (2000). Generation of a non-sporulating strain of Streptomyces coelicolor A3(2) by the manipulation of a developmentally controlled ftsZ promoter. Mol Microbiol *38*, 737-749.

Flardh, K., Richards, D.M., Hempel, A.M., Howard, M., and Buttner, M.J. (2012). Regulation of apical growth and hyphal branching in Streptomyces. Curr Opin Microbiol *15*, 737-743.

Fuchino, K., Bagchi, S., Cantlay, S., Sandblad, L., Wu, D., Bergman, J., Kamali-Moghaddam, M., Flardh, K., and Ausmees, N. (2013). Dynamic gradients of an intermediate filament-like cytoskeleton are recruited by a polarity landmark during apical growth. Proc Natl Acad Sci U S A *110*, E1889-1897.

Fuchino, K., Flardh, K., Dyson, P., and Ausmees, N. (2017). Cell-Biological Studies of Osmotic Shock Response in Streptomyces spp. J Bacteriol *199*.

Fung, E., Bouet, J.Y., and Funnell, B.E. (2001). Probing the ATP-binding site of P1 ParA: partition and repression have different requirements for ATP binding and hydrolysis. EMBO J *20*, 4901-4911.

Garner, E.C., Bernard, R., Wang, W., Zhuang, X., Rudner, D.Z., and Mitchison, T. (2011). Coupled, circumferential motions of the cell wall synthesis machinery and MreB filaments in B. subtilis. Science *333*, 222-225.

Gerdes, K., Howard, M., and Szardenings, F. (2010). Pushing and pulling in prokaryotic DNA segregation. Cell *141*, 927-942.

Gerding, M.A., Liu, B., Bendezu, F.O., Hale, C.A., Bernhardt, T.G., and de Boer, P.A. (2009). Self-enhanced accumulation of FtsN at Division Sites and Roles for Other Proteins with a SPOR domain (DamX, DedD, and RlpA) in Escherichia coli cell constriction. J Bacteriol *191*, 7383-7401.

Goffin, C., and Ghuysen, J.M. (1998). Multimodular penicillin-binding proteins: an enigmatic family of orthologs and paralogs. Microbiol Mol Biol Rev *62*, 1079-1093.

Goley, E.D., Yeh, Y.C., Hong, S.H., Fero, M.J., Abeliuk, E., McAdams, H.H., and Shapiro, L. (2011). Assembly of the Caulobacter cell division machine. Mol Microbiol *80*, 1680-1698.

Golovanov, A.P., Barilla, D., Golovanova, M., Hayes, F., and Lian, L.Y. (2003). ParG, a protein required for active partition of bacterial plasmids, has a dimeric ribbon-helix-helix structure. Mol Microbiol *50*, 1141-1153.

Golovanov, A.P., Hautbergue, G.M., Wilson, S.A., and Lian, L.Y. (2004). A simple method for improving protein solubility and long-term stability. J Am Chem Soc *126*, 8933-8939.

Gomis-Ruth, F.X., Sola, M., Acebo, P., Parraga, A., Guasch, A., Eritja, R., Gonzalez, A., Espinosa, M., del Solar, G., and Coll, M. (1998). The structure of plasmid-encoded transcriptional repressor CopG unliganded and bound to its operator. EMBO J *17*, 7404-7415.

Goodson, H.V., and Hawse, W.F. (2002). Molecular evolution of the actin family. J Cell Sci *115*, 2619-2622.

Grantcharova, N., Lustig, U., and Flardh, K. (2005). Dynamics of FtsZ assembly during sporulation in Streptomyces coelicolor A3(2). J Bacteriol *187*, 3227-3237.

Gregory, M.A., Till, R., and Smith, M.C. (2003). Integration site for Streptomyces phage phiBT1 and development of site-specific integrating vectors. J Bacteriol *185*, 5320-5323.

Gruber, S., and Errington, J. (2009). Recruitment of condensin to replication origin regions by ParB/SpoOJ promotes chromosome segregation in B. subtilis. Cell *137*, 685-696.

Gundogdu, M.E., Kawai, Y., Pavlendova, N., Ogasawara, N., Errington, J., Scheffers, D.J., and Hamoen, L.W. (2011). Large ring polymers align FtsZ polymers for normal septum formation. EMBO J *30*, 617-626.

Gust, B., Challis, G.L., Fowler, K., Kieser, T., and Chater, K.F. (2003). PCR-targeted Streptomyces gene replacement identifies a protein domain needed for biosynthesis of the sesquiterpene soil odor geosmin. Proc Natl Acad Sci U S A *100*, 1541-1546.

Gust, B., Challis, G.L., Fowler, K., Kieser, T., and Chater, K.F. (2003). PCR-targeted Streptomyces gene replacement identifies a protein domain needed for biosynthesis of the sesquiterpene soil odor geosmin. Proc Natl Acad Sci U S A *100*, 1541-1546.

Haeusser, D.P., and Margolin, W. (2016). Splitsville: structural and functional insights into the dynamic bacterial Z ring. Nat Rev Microbiol *14*, 305-319.

Hajduk, I.V., Rodrigues, C.D., and Harry, E.J. (2016). Connecting the dots of the bacterial cell cycle: Coordinating chromosome replication and segregation with cell division. Semin Cell Dev Biol *53*, 2-9.

Hale, C.A., and de Boer, P.A. (1999). Recruitment of ZipA to the septal ring of Escherichia coli is dependent on FtsZ and independent of FtsA. J Bacteriol *181*, 167-176.

Hamoen, L.W., Meile, J.C., de Jong, W., Noirot, P., and Errington, J. (2006). SepF, a novel FtsZ-interacting protein required for a late step in cell division. Mol Microbiol *59*, 989-999.

Hanahan, D. (1983). Studies on transformation of Escherichia coli with plasmids. J Mol Biol *166*, 557-580.

Hand, E.S., and Jencks, W.P. (1962). Mechanism of the reaction of imidoesters with amines. J Am Chem Soc *84*, 9.

Harry, E., Monahan, L., and Thompson, L. (2006). Bacterial cell division: the mechanism and its precison. Int Rev Cytol *253*, 27-94.

He, Y.Y., Stockley, P.G., and Gold, L. (1996). In vitro evolution of the DNA binding sites of Escherichia coli methionine repressor, MetJ. J Mol Biol *255*, 55-66.

Hempel, A.M., Cantlay, S., Molle, V., Wang, S.B., Naldrett, M.J., Parker, J.L., Richards, D.M., Jung, Y.G., Buttner, M.J., and Flardh, K. (2012). The Ser/Thr protein kinase AfsK regulates polar growth and hyphal branching in the filamentous bacteria Streptomyces. Proc Natl Acad Sci U S A *109*, E2371-2379.

Hempel, A.M., Wang, S.B., Letek, M., Gil, J.A., and Flardh, K. (2008). Assemblies of DivIVA mark sites for hyphal branching and can establish new zones of cell wall growth in Streptomyces coelicolor. J Bacteriol *190*, 7579-7583.

Hernandez-Arriaga, A.M., Rubio-Lepe, T.S., Espinosa, M., and del Solar, G. (2009). Repressor CopG prevents access of RNA polymerase to promoter and actively dissociates open complexes. Nucleic Acids Res *37*, 4799-4811.

Hester, C.M., and Lutkenhaus, J. (2007). Soj (ParA) DNA binding is mediated by conserved arginines and is essential for plasmid segregation. Proc Natl Acad Sci U S A *104*, 20326-20331.

Holmes, N.A., Walshaw, J., Leggett, R.M., Thibessard, A., Dalton, K.A., Gillespie, M.D., Hemmings, A.M., Gust, B., and Kelemen, G.H. (2013). Coiled-coil protein Scy is a key component of a multiprotein assembly controlling polarized growth in Streptomyces. Proc Natl Acad Sci U S A *110*, E397-406.

Hopwood, D.A., Bibb, M., Chater, K., Bruton, C.J., Kieser, H., Lydiate, D.J., Smith, C.P., Ward, J.M., and Schrempf, H. (1985). Genetic Manipulation of *Streptomyces*. A Laboratory Manual. John Innes Foundation, Norwich.

Hsu, Y.H., Chung, M.W., and Li, T.K. (2006). Distribution of gyrase and topoisomerase IV on bacterial nucleoid: implications for nucleoid organization. Nucleic Acids Res *34*, 3128-3138.

Hu, Z., Gogol, E.P., and Lutkenhaus, J. (2002). Dynamic assembly of MinD on phospholipid vesicles regulated by ATP and MinE. Proc Natl Acad Sci U S A *99*, 6761-6766.

Hu, Z., and Lutkenhaus, J. (2001). Topological regulation of cell division in E. coli. spatiotemporal oscillation of MinD requires stimulation of its ATPase by MinE and phospholipid. Mol Cell *7*, 1337-1343.

Hu, Z., Saez, C., and Lutkenhaus, J. (2003). Recruitment of MinC, an inhibitor of Z-ring formation, to the membrane in Escherichia coli: role of MinD and MinE. J Bacteriol *185*, 196-203.

Huang, K.H., Durand-Heredia, J., and Janakiraman, A. (2013). FtsZ ring stability: of bundles, tubules, crosslinks, and curves. J Bacteriol *195*, 1859-1868.

Huitema, E., Pritchard, S., Matteson, D., Radhakrishnan, S.K., and Viollier, P.H. (2006). Bacterial birth scar proteins mark future flagellum assembly site. Cell *124*, 1025-1037.

Ireton, K., Gunther, N.W.t., and Grossman, A.D. (1994). spo0J is required for normal chromosome segregation as well as the initiation of sporulation in Bacillus subtilis. J Bacteriol *176*, 5320-5329.

Ishikawa, S., Kawai, Y., Hiramatsu, K., Kuwano, M., and Ogasawara, N. (2006). A new FtsZ-interacting protein, YlmF, complements the activity of FtsA during progression of cell division in Bacillus subtilis. Mol Microbiol *60*, 1364-1380.

Jacob, F., and Brenner, S. (1963). [On the regulation of DNA synthesis in bacteria: the hypothesis of the replicon]. C R Hebd Seances Acad Sci *256*, 298-300.

Jakimowicz, D., Chater, K., and Zakrzewska-Czerwinska, J. (2002). The ParB protein of Streptomyces coelicolor A3(2) recognizes a cluster of parS sequences within the origin-proximal region of the linear chromosome. Mol Microbiol *45*, 1365-1377.

Jakimowicz, D., Gust, B., Zakrzewska-Czerwinska, J., and Chater, K.F. (2005). Developmental-stage-specific assembly of ParB complexes in Streptomyces coelicolor hyphae. J Bacteriol *187*, 3572-3580.

Jakimowicz, D., Zydek, P., Kois, A., Zakrzewska-Czerwinska, J., and Chater, K.F. (2007). Alignment of multiple chromosomes along helical ParA scaffolding in sporulating Streptomyces hyphae. Mol Microbiol *65*, 625-641.

Jensen, R.B., and Shapiro, L. (1999). The Caulobacter crescentus smc gene is required for cell cycle progression and chromosome segregation. Proc Natl Acad Sci U S A *96*, 10661-10666.

Jimenez, M., Martos, A., Vicente, M., and Rivas, G. (2011). Reconstitution and organization of Escherichia coli proto-ring elements (FtsZ and FtsA) inside giant unilamellar vesicles obtained from bacterial inner membranes. J Biol Chem *286*, 11236-11241.

Jones, L.J., Carballido-Lopez, R., and Errington, J. (2001). Control of cell shape in bacteria: helical, actin-like filaments in Bacillus subtilis. Cell *104*, 913-922.

Jyothikumar, V., Tilley, E.J., Wali, R., and Herron, P.R. (2008). Time-lapse microscopy of Streptomyces coelicolor growth and sporulation. Appl Environ Microbiol *74*, 6774-6781.

Kang, C.M., Nyayapathy, S., Lee, J.Y., Suh, J.W., and Husson, R.N. (2008). Wag31, a homologue of the cell division protein DivIVA, regulates growth, morphology and polar cell wall synthesis in mycobacteria. Microbiology *154*, 725-735.

Karimova, G., Ullmann, A., and Ladant, D. (2000). A bacterial two-hybrid system that exploits a cAMP signaling cascade in Escherichia coli. Methods Enzymol *328*, 59-73.

Karoui, M.E., and Errington, J. (2001). Isolation and characterization of topological specificity mutants of minD in Bacillus subtilis. Mol Microbiol *42*, 1211-1221.

Katis, V.L., Wake, R.G., and Harry, E.J. (2000). Septal localization of the membrane-bound division proteins of Bacillus subtilis DivIB and DivIC is codependent only at high temperatures and requires FtsZ. J Bacteriol *182*, 3607-3611.

Kawai, Y., Asai, K., and Errington, J. (2009). Partial functional redundancy of MreB isoforms, MreB, Mbl and MreBH, in cell morphogenesis of Bacillus subtilis. Mol Microbiol *73*, 719-731.

Kawai, Y., and Ogasawara, N. (2006). Bacillus subtilis EzrA and FtsL synergistically regulate FtsZ ring dynamics during cell division. Microbiology *152*, 1129-1141.

Keijser, B.J., Noens, E.E., Kraal, B., Koerten, H.K., and van Wezel, G.P. (2003). The Streptomyces coelicolor ssgB gene is required for early stages of sporulation. FEMS Microbiol Lett *225*, 59-67.

Kelemen, G.H. (2017). Intermediate filaments supporting cell shape and growth in bacteria.

Kelemen, G.H., Brian, P., Flardh, K., Chamberlin, L., Chater, K.F., and Buttner, M.J. (1998). Developmental regulation of transcription of whiE, a locus specifying the polyketide spore pigment in Streptomyces coelicolor A3 (2). J Bacteriol *180*, 2515-2521.

Kelemen, G.H., and Buttner, M.J. (1998). Initiation of aerial mycelium formation in Streptomyces. Curr Opin Microbiol *1*, 656-662.

Kiekebusch, D., Michie, K.A., Essen, L.O., Lowe, J., and Thanbichler, M. (2012). Localized dimerization and nucleoid binding drive gradient formation by the bacterial cell division inhibitor MipZ. Mol Cell *46*, 245-259.

Kieser, T., Bibb, M., Buttner, M.J., Chater, K., and Hopwood, D.A. (2000). Practical *Streptomyces* Genetics. The John Innes Foundation.

Kim, H.J., Calcutt, M.J., Schmidt, F.J., and Chater, K.F. (2000). Partitioning of the linear chromosome during sporulation of Streptomyces coelicolor A3(2) involves an oriC-linked parAB locus. J Bacteriol *182*, 1313-1320.

Knight, K.L., Bowie, J.U., Vershon, A.K., Kelley, R.D., and Sauer, R.T. (1989). The Arc and Mnt repressors. A new class of sequence-specific DNA-binding protein. J Biol Chem *264*, 3639-3642.

Knight, K.L., and Sauer, R.T. (1989). DNA binding specificity of the Arc and Mnt repressors is determined by a short region of N-terminal residues. Proc Natl Acad Sci U S A *86*, 797-801.

Kois-Ostrowska, A., Strzalka, A., Lipietta, N., Tilley, E., Zakrzewska-Czerwinska, J., Herron, P., and Jakimowicz, D. (2016). Unique Function of the Bacterial Chromosome Segregation Machinery in Apically Growing Streptomyces - Targeting the Chromosome to New Hyphal Tubes and its Anchorage at the Tips. PLoS Genet *12*, e1006488.

Koonin, E.V. (1993). A superfamily of ATPases with diverse functions containing either classical or deviant ATP-binding motif. J Mol Biol *229*, 1165-1174.

Kruse, T., Bork-Jensen, J., and Gerdes, K. (2005). The morphogenetic MreBCD proteins of Escherichia coli form an essential membrane-bound complex. Mol Microbiol *55*, 78-89.

Kwak, J., Dharmatilake, A.J., Jiang, H., and Kendrick, K.E. (2001). Differential regulation of ftsZ transcription during septation of Streptomyces griseus. J Bacteriol *183*, 5092-5101.

Lackner, L.L., Raskin, D.M., and de Boer, P.A. (2003). ATP-dependent interactions between Escherichia coli Min proteins and the phospholipid membrane in vitro. J Bacteriol *185*, 735-749.

Laloux, G., and Jacobs-Wagner, C. (2014). How do bacteria localize proteins to the cell pole? J Cell Sci *127*, 11-19.

Le, T.B., Imakaev, M.V., Mirny, L.A., and Laub, M.T. (2013). High-resolution mapping of the spatial organization of a bacterial chromosome. Science *342*, 731-734.

Lenz, P., and Sogaard-Andersen, L. (2011). Temporal and spatial oscillations in bacteria. Nat Rev Microbiol *9*, 565-577.

Leonard, T.A., Butler, P.J., and Lowe, J. (2004). Structural analysis of the chromosome segregation protein Spo0J from Thermus thermophilus. Mol Microbiol *53*, 419-432.

Leonard, T.A., Butler, P.J., and Lowe, J. (2005). Bacterial chromosome segregation: structure and DNA binding of the Soj dimer--a conserved biological switch. EMBO J *24*, 270-282.

Letek, M., Ordonez, E., Vaquera, J., Margolin, W., Flardh, K., Mateos, L.M., and Gil, J.A. (2008). DivIVA is required for polar growth in the MreB-lacking rod-shaped actinomycete Corynebacterium glutamicum. J Bacteriol *190*, 3283-3292.

Levin, P.A., and Losick, R. (1994). Characterization of a cell division gene from Bacillus subtilis that is required for vegetative and sporulation septum formation. J Bacteriol *176*, 1451-1459.

Levin, P.A., Margolis, P.S., Setlow, P., Losick, R., and Sun, D. (1992). Identification of Bacillus subtilis genes for septum placement and shape determination. J Bacteriol *174*, 6717-6728.

Lin, D.C., and Grossman, A.D. (1998). Identification and characterization of a bacterial chromosome partitioning site. Cell *92*, 675-685.

Lin, Y.S., Kieser, H.M., Hopwood, D.A., and Chen, C.W. (1993). The chromosomal DNA of Streptomyces lividans 66 is linear. Mol Microbiol *10*, 923-933.

Lindow, J.C., Kuwano, M., Moriya, S., and Grossman, A.D. (2002). Subcellular localization of the Bacillus subtilis structural maintenance of chromosomes (SMC) protein. Mol Microbiol *46*, 997-1009.

Livny, J., Yamaichi, Y., and Waldor, M.K. (2007). Distribution of centromere-like parS sites in bacteria: insights from comparative genomics. J Bacteriol *189*, 8693-8703.

Lowe, J., and Amos, L.A. (1998). Crystal structure of the bacterial cell-division protein FtsZ. Nature *391*, 203-206.

Lu, J., den Dulk-Ras, A., Hooykaas, P.J., and Glover, J.N. (2009). Agrobacterium tumefaciens VirC2 enhances T-DNA transfer and virulence through its C-terminal ribbon-helix-helix DNA-binding fold. Proc Natl Acad Sci U S A *106*, 9643-9648.

Lutkenhaus, J. (2012). The ParA/MinD family puts things in their place. Trends Microbiol *20*, 411-418.

Lutkenhaus, J., and Sundaramoorthy, M. (2003). MinD and role of the deviant Walker A motif, dimerization and membrane binding in oscillation. Mol Microbiol *48*, 295-303.

MacNeil, D.J., Gewain, K.M., Ruby, C.L., Dezeny, G., Gibbons, P.H., and MacNeil, T. (1992). Analysis of Streptomyces avermitilis genes required for avermectin biosynthesis utilizing a novel integration vector. Gene *111*, 61-68.

Madl, T., Van Melderen, L., Mine, N., Respondek, M., Oberer, M., Keller, W., Khatai, L., and Zangger, K. (2006). Structural basis for nucleic acid and toxin recognition of the bacterial antitoxin CcdA. J Mol Biol *364*, 170-185.

Margolin, W. (2000). Organelle division: Self-assembling GTPase caught in the middle. Curr Biol *10*, R328-330.

Margolin, W. (2001). Bacterial cell division: a moving MinE sweeper boggles the MinD. Curr Biol *11*, R395-398.

Margolin, W. (2005). FtsZ and the division of prokaryotic cells and organelles. Nat Rev Mol Cell Biol *6*, 862-871.

Marston, A.L., and Errington, J. (1999). Selection of the midcell division site in Bacillus subtilis through MinD-dependent polar localization and activation of MinC. Mol Microbiol *33*, 84-96.

Marston, A.L., Thomaides, H.B., Edwards, D.H., Sharpe, M.E., and Errington, J. (1998). Polar localization of the MinD protein of Bacillus subtilis and its role in selection of the mid-cell division site. Genes Dev *12*, 3419-3430.

Mason, J.M., and Arndt, K.M. (2004). Coiled coil domains: stability, specificity, and biological implications. Chembiochem *5*, 170-176.

Mattison, K., Wilbur, J.S., So, M., and Brennan, R.G. (2006). Structure of FitAB from Neisseria gonorrhoeae bound to DNA reveals a tetramer of toxin-antitoxin heterodimers containing pin domains and ribbon-helix-helix motifs. J Biol Chem *281*, 37942-37951.

McCormick, J.R., and Losick, R. (1996). Cell division gene ftsQ is required for efficient sporulation but not growth and viability in Streptomyces coelicolor A3(2). J Bacteriol *178*, 5295-5301.

McCormick, J.R., Su, E.P., Driks, A., and Losick, R. (1994). Growth and viability of Streptomyces coelicolor mutant for the cell division gene ftsZ. Mol Microbiol *14*, 243-254.

Melby, T.E., Ciampaglio, C.N., Briscoe, G., and Erickson, H.P. (1998). The symmetrical structure of structural maintenance of chromosomes (SMC) and MukB proteins: long, antiparallel coiled coils, folded at a flexible hinge. J Cell Biol *142*, 1595-1604.

Meniche, X., Otten, R., Siegrist, M.S., Baer, C.E., Murphy, K.C., Bertozzi, C.R., and Sassetti, C.M. (2014). Subpolar addition of new cell wall is directed by DivIVA in mycobacteria. Proc Natl Acad Sci U S A *111*, E3243-3251.

Misselwitz, R., de la Hoz, A.B., Ayora, S., Welfle, K., Behlke, J., Murayama, K., Saenger, W., Alonso, J.C., and Welfle, H. (2001). Stability and DNA-binding properties of the omega regulator protein from the broad-host range Streptococcus pyogenes plasmid pSM19035. FEBS Lett *505*, 436-440.

Moffatt, B.A., and Studier, F.W. (1987). T7 lysozyme inhibits transcription by T7 RNA polymerase. Cell *49*, 221-227.

Mohammadi, T., van Dam, V., Sijbrandi, R., Vernet, T., Zapun, A., Bouhss, A., Diepeveen-de Bruin, M., Nguyen-Disteche, M., de Kruijff, B., and Breukink, E. (2011). Identification of FtsW as a transporter of lipid-linked cell wall precursors across the membrane. EMBO J *30*, 1425-1432.

Moncalian, G., and de la Cruz, F. (2004). DNA binding properties of protein TrwA, a possible structural variant of the Arc repressor superfamily. Biochim Biophys Acta *1701*, 15-23.

Motallebi-Veshareh, M., Rouch, D.A., and Thomas, C.M. (1990). A family of ATPases involved in active partitioning of diverse bacterial plasmids. Mol Microbiol *4*, 1455-1463.

Mukherjee, P., Sureka, K., Datta, P., Hossain, T., Barik, S., Das, K.P., Kundu, M., and Basu, J. (2009). Novel role of Wag31 in protection of mycobacteria under oxidative stress. Mol Microbiol *73*, 103-119.

Muller, P., Ewers, C., Bertsche, U., Anstett, M., Kallis, T., Breukink, E., Fraipont, C., Terrak, M., Nguyen-Disteche, M., and Vollmer, W. (2007). The essential cell division protein FtsN interacts with the murein (peptidoglycan) synthase PBP1B in Escherichia coli. J Biol Chem *282*, 36394-36402.

Murayama, K., Orth, P., de la Hoz, A.B., Alonso, J.C., and Saenger, W. (2001). Crystal structure of omega transcriptional repressor encoded by Streptococcus pyogenes plasmid pSM19035 at 1.5 A resolution. J Mol Biol *314*, 789-796.

Murray, H., and Errington, J. (2008). Dynamic control of the DNA replication initiation protein DnaA by Soj/ParA. Cell *135*, 74-84.

Nanninga, N. (1998). Morphogenesis of Escherichia coli. Microbiol Mol Biol Rev *62*, 110-129.

Nguyen, L., Scherr, N., Gatfield, J., Walburger, A., Pieters, J., and Thompson, C.J. (2007). Antigen 84, an effector of pleiomorphism in Mycobacterium smegmatis. J Bacteriol *189*, 7896-7910.

Nielsen, H.J., Ottesen, J.R., Youngren, B., Austin, S.J., and Hansen, F.G. (2006). The Escherichia coli chromosome is organized with the left and right chromosome arms in separate cell halves. Mol Microbiol *62*, 331-338.

Nogales, E., Downing, K.H., Amos, L.A., and Lowe, J. (1998). Tubulin and FtsZ form a distinct family of GTPases. Nat Struct Biol *5*, 451-458.

Oberer, M., Lindner, H., Glatter, O., Kratky, C., and Keller, W. (1999). Thermodynamic properties and DNA binding of the ParD protein from the broad host-range plasmid RK2/RP4 killing system. Biol Chem *380*, 1413-1420.

Ohashi, T., Hale, C.A., de Boer, P.A., and Erickson, H.P. (2002). Structural evidence that the P/Q domain of ZipA is an unstructured, flexible tether between the membrane and the C-terminal FtsZ-binding domain. J Bacteriol *184*, 4313-4315.

Oliva, M.A., Halbedel, S., Freund, S.M., Dutow, P., Leonard, T.A., Veprintsev, D.B., Hamoen, L.W., and Lowe, J. (2010). Features critical for membrane binding revealed by DivIVA crystal structure. EMBO J *29*, 1988-2001.

Olshausen, P.V., Defeu Soufo, H.J., Wicker, K., Heintzmann, R., Graumann, P.L., and Rohrbach, A. (2013). Superresolution imaging of dynamic MreB filaments in B. subtilis--a multiple-motor-driven transport? Biophys J *105*, 1171-1181.

Osawa, M., Anderson, D.E., and Erickson, H.P. (2008). Reconstitution of contractile FtsZ rings in liposomes. Science *320*, 792-794.

Pace, C.N., Vajdos, F., Fee, L., Grimsley, G., and Gray, T. (1995). How to measure and predict the molar absorption coefficient of a protein. Protein Sci *4*, 2411-2423.

Palumbo, V., Pellacani, C., Heesom, K.J., Rogala, K.B., Deane, C.M., Mottier-Pavie, V., Gatti, M., Bonaccorsi, S., and Wakefield, J.G. (2015). Misato Controls Mitotic Microtubule Generation by Stabilizing the TCP-1 Tubulin Chaperone Complex [corrected]. Curr Biol *25*, 1777-1783.

Park, K.T., Wu, W., Battaile, K.P., Lovell, S., Holyoak, T., and Lutkenhaus, J. (2011). The Min oscillator uses MinD-dependent conformational changes in MinE to spatially regulate cytokinesis. Cell *146*, 396-407.

Park, K.T., Wu, W., Lovell, S., and Lutkenhaus, J. (2012). Mechanism of the asymmetric activation of the MinD ATPase by MinE. Mol Microbiol *85*, 271-281.

Patrick, J.E., and Kearns, D.B. (2008). MinJ (YvjD) is a topological determinant of cell division in Bacillus subtilis. Mol Microbiol *70*, 1166-1179.

Perry, S.E., and Edwards, D.H. (2006). The Bacillus subtilis DivIVA protein has a sporulation-specific proximity to Spo0J. J Bacteriol *188*, 6039-6043.

Pichoff, S., and Lutkenhaus, J. (2002). Unique and overlapping roles for ZipA and FtsA in septal ring assembly in Escherichia coli. EMBO J *21*, 685-693.

Pichoff, S., Shen, B., Sullivan, B., and Lutkenhaus, J. (2012). FtsA mutants impaired for self-interaction bypass ZipA suggesting a model in which FtsA's self-interaction competes with its ability to recruit downstream division proteins. Mol Microbiol *83*, 151-167.

Pogliano, K., Hofmeister, A.E., and Losick, R. (1997). Disappearance of the sigma E transcription factor from the forespore and the SpoIIE phosphatase from the mother cell contributes to establishment of cell-specific gene expression during sporulation in Bacillus subtilis. J Bacteriol *179*, 3331-3341.

Ptacin, J.L., Gahlmann, A., Bowman, G.R., Perez, A.M., von Diezmann, A.R., Eckart, M.R., Moerner, W.E., and Shapiro, L. (2014). Bacterial scaffold directs pole-specific centromere segregation. Proc Natl Acad Sci U S A *111*, E2046-2055.

Ptacin, J.L., Lee, S.F., Garner, E.C., Toro, E., Eckart, M., Comolli, L.R., Moerner, W.E., and Shapiro, L. (2010). A spindle-like apparatus guides bacterial chromosome segregation. Nat Cell Biol *12*, 791-798.

Rafferty, J.B., Somers, W.S., Saint-Girons, I., and Phillips, S.E. (1989). Three-dimensional crystal structures of Escherichia coli met repressor with and without corepressor. Nature *341*, 705-710.

Ramamurthi, K.S., and Losick, R. (2009). Negative membrane curvature as a cue for subcellular localization of a bacterial protein. Proc Natl Acad Sci U S A *106*, 13541-13545.

Ramos, A., Honrubia, M.P., Valbuena, N., Vaquera, J., Mateos, L.M., and Gil, J.A. (2003). Involvement of DivIVA in the morphology of the rod-shaped actinomycete Brevibacterium lactofermentum. Microbiology *149*, 3531-3542.

Raskin, D.M., and de Boer, P.A. (1999). Rapid pole-to-pole oscillation of a protein required for directing division to the middle of Escherichia coli. Proc Natl Acad Sci U S A *96*, 4971-4976.

Redenbach, M., Kieser, H.M., Denapaite, D., Eichner, A., Cullum, J., Kinashi, H., and Hopwood, D.A. (1996). A set of ordered cosmids and a detailed genetic and physical map for the 8 Mb Streptomyces coelicolor A3(2) chromosome. Mol Microbiol *21*, 77-96.

Reimold, C., Defeu Soufo, H.J., Dempwolff, F., and Graumann, P.L. (2013). Motion of variable-length MreB filaments at the bacterial cell membrane influences cell morphology. Mol Biol Cell *24*, 2340-2349.

Richards, D.M., Hempel, A.M., Flardh, K., Buttner, M.J., and Howard, M. (2012). Mechanistic basis of branch-site selection in filamentous bacteria. PLoS Comput Biol *8*, e1002423.

Ringgaard, S., Ebersbach, G., Borch, J., and Gerdes, K. (2007). Regulatory cross-talk in the double par locus of plasmid pB171. J Biol Chem *282*, 3134-3145.

Ringgaard, S., van Zon, J., Howard, M., and Gerdes, K. (2009). Movement and equipositioning of plasmids by ParA filament disassembly. Proc Natl Acad Sci U S A *106*, 19369-19374.

Saalbach, G., Hempel, A.M., Vigouroux, M., Flardh, K., Buttner, M.J., and Naldrett, M.J. (2013). Determination of phosphorylation sites in the DivIVA cytoskeletal protein of Streptomyces coelicolor by targeted LC-MS/MS. J Proteome Res *12*, 4187-4192.

Salje, J., van den Ent, F., de Boer, P., and Lowe, J. (2011). Direct membrane binding by bacterial actin MreB. Mol Cell *43*, 478-487.

Saludjian, P., Prange, T., Navaza, J., Menez, R., Guilloteau, J.P., Ries-Kautt, M., and Ducruix, A. (1992). Structure determination of a dimeric form of erabutoxin-b, crystallized from a thiocyanate solution. Acta Crystallogr B *48 (Pt 4)*, 520-531.

Schildbach, J.F., Robinson, C.R., and Sauer, R.T. (1998). Biophysical characterization of the TraY protein of Escherichia coli F factor. J Biol Chem *273*, 1329-1333.

Scholefield, G., Whiting, R., Errington, J., and Murray, H. (2011). Spo0J regulates the oligomeric state of Soj to trigger its switch from an activator to an inhibitor of DNA replication initiation. Mol Microbiol *79*, 1089-1100.

Schreiter, E.R., and Drennan, C.L. (2007). Ribbon-helix-helix transcription factors: variations on a theme. Nat Rev Microbiol *5*, 710-720.

Schreiter, E.R., Wang, S.C., Zamble, D.B., and Drennan, C.L. (2006). NikR-operator complex structure and the mechanism of repressor activation by metal ions. Proc Natl Acad Sci U S A *103*, 13676-13681.

Schumacher, M.A., Ye, Q., Barge, M.T., Zampini, M., Barilla, D., and Hayes, F. (2012). Structural mechanism of ATP-induced polymerization of the partition factor ParF: implications for DNA segregation. J Biol Chem *287*, 26146-26154.

Schwedock, J., McCormick, J.R., Angert, E.R., Nodwell, J.R., and Losick, R. (1997). Assembly of the cell division protein FtsZ into ladder-like structures in the aerial hyphae of Streptomyces coelicolor. Mol Microbiol *25*, 847-858.

Sharp, M.D., and Pogliano, K. (2003). The membrane domain of SpoIIIE is required for membrane fusion during Bacillus subtilis sporulation. J Bacteriol *185*, 2005-2008.

Sharpe, M.E., and Errington, J. (1996). The Bacillus subtilis soj-spo0J locus is required for a centromere-like function involved in prespore chromosome partitioning. Mol Microbiol *21*, 501-509.

Shen, B., and Lutkenhaus, J. (2009). The conserved C-terminal tail of FtsZ is required for the septal localization and division inhibitory activity of MinC(C)/MinD. Mol Microbiol *72*, 410-424.

Shih, Y.L., and Rothfield, L. (2006). The bacterial cytoskeleton. Microbiol Mol Biol Rev *70*, 729-754.

Shukla, D., and Trout, B.L. (2011). Understanding the synergistic effect of arginine and glutamic acid mixtures on protein solubility. J Phys Chem B *115*, 11831-11839.

Sieger, B., Schubert, K., Donovan, C., and Bramkamp, M. (2013). The lipid II flippase RodA determines morphology and growth in Corynebacterium glutamicum. Mol Microbiol *90*, 966-982.

Sievers, J., Raether, B., Perego, M., and Errington, J. (2002). Characterization of the parB-like yyaA gene of Bacillus subtilis. J Bacteriol *184*, 1102-1111.

Somers, W.S., and Phillips, S.E. (1992). Crystal structure of the met repressor-operator complex at 2.8 A resolution reveals DNA recognition by beta-strands. Nature *359*, 387-393.

Soppa, J. (2001). Prokaryotic structural maintenance of chromosomes (SMC) proteins: distribution, phylogeny, and comparison with MukBs and additional prokaryotic and eukaryotic coiled-coil proteins. Gene *278*, 253-264.

Steinert, P.M., and Roop, D.R. (1988). Molecular and cellular biology of intermediate filaments. Annu Rev Biochem *57*, 593-625.

Storts, D.R., Aparicio, O.M., Schoemaker, J.M., and Markovitz, A. (1989). Overproduction and identification of the ftsQ gene product, an essential cell division protein in Escherichia coli K-12. J Bacteriol *171*, 4290-4297.

Strunnikov, A.V., and Jessberger, R. (1999). Structural maintenance of chromosomes (SMC) proteins: conserved molecular properties for multiple biological functions. Eur J Biochem *263*, 6-13.

Studier, F.W. (1991). Use of bacteriophage T7 lysozyme to improve an inducible T7 expression system. J Mol Biol *219*, 37-44.

Studier, F.W., and Moffatt, B.A. (1986). Use of bacteriophage T7 RNA polymerase to direct selective high-level expression of cloned genes. J Mol Biol *189*, 113-130.

Studier, F.W., Rosenberg, A.H., Dunn, J.J., and Dubendorff, J.W. (1990). Use of T7 RNA polymerase to direct expression of cloned genes. Methods Enzymol *185*, 60-89.

Sullivan, N.L., Marquis, K.A., and Rudner, D.Z. (2009). Recruitment of SMC by ParB-parS organizes the origin region and promotes efficient chromosome segregation. Cell *137*, 697-707.

Swulius, M.T., Chen, S., Jane Ding, H., Li, Z., Briegel, A., Pilhofer, M., Tocheva, E.I., Lybarger, S.R., Johnson, T.L., Sandkvist, M.*, et al.* (2011). Long helical filaments are not seen encircling cells in electron cryotomograms of rod-shaped bacteria. Biochem Biophys Res Commun *407*, 650-655.

Szafran, M., Skut, P., Ditkowski, B., Ginda, K., Chandra, G., Zakrzewska-Czerwinska, J., and Jakimowicz, D. (2013). Topoisomerase I (TopA) is recruited to ParB complexes and is required for proper chromosome organization during Streptomyces coelicolor sporulation. J Bacteriol *195*, 4445-4455.

Szwedziak, P., Wang, Q., Freund, S.M., and Lowe, J. (2012). FtsA forms actin-like protofilaments. EMBO J *31*, 2249-2260.

Tadesse, S., and Graumann, P.L. (2006). Differential and dynamic localization of topoisomerases in Bacillus subtilis. J Bacteriol *188*, 3002-3011.

Thanbichler, M., and Shapiro, L. (2006). MipZ, a spatial regulator coordinating chromosome segregation with cell division in Caulobacter. Cell *126*, 147-162.

Tonthat, N.K., Milam, S.L., Chinnam, N., Whitfill, T., Margolin, W., and Schumacher, M.A. (2013). SlmA forms a higher-order structure on DNA that inhibits cytokinetic Z-ring formation over the nucleoid. Proc Natl Acad Sci U S A *110*, 10586-10591.

Touzain, F., Petit, M.A., Schbath, S., and El Karoui, M. (2011). DNA motifs that sculpt the bacterial chromosome. Nat Rev Microbiol *9*, 15-26.

Uhlmann, F. (2016). SMC complexes: from DNA to chromosomes. Nat Rev Mol Cell Biol *17*, 399-412.

Ursinus, A., van den Ent, F., Brechtel, S., de Pedro, M., Holtje, J.V., Lowe, J., and Vollmer, W. (2004). Murein (peptidoglycan) binding property of the essential cell division protein FtsN from Escherichia coli. J Bacteriol *186*, 6728-6737.

van den Ent, F., Amos, L., and Lowe, J. (2001). Bacterial ancestry of actin and tubulin. Curr Opin Microbiol *4*, 634-638.

van den Ent, F., Amos, L.A., and Lowe, J. (2001). Prokaryotic origin of the actin cytoskeleton. Nature *413*, 39-44.

van den Ent, F., Izore, T., Bharat, T.A., Johnson, C.M., and Lowe, J. (2014). Bacterial actin MreB forms antiparallel double filaments. Elife *3*, e02634.

van Teeffelen, S., Wang, S., Furchtgott, L., Huang, K.C., Wingreen, N.S., Shaevitz, J.W., and Gitai, Z. (2011). The bacterial actin MreB rotates, and rotation depends on cell-wall assembly. Proc Natl Acad Sci U S A *108*, 15822-15827.

van Vliet, A.H., Ernst, F.D., and Kusters, J.G. (2004). NikR-mediated regulation of Helicobacter pylori acid adaptation. Trends Microbiol *12*, 489-494.

van Wezel, G.P., van der Meulen, J., Kawamoto, S., Luiten, R.G., Koerten, H.K., and Kraal, B. (2000). ssgA is essential for sporulation of Streptomyces coelicolor A3(2) and affects hyphal development by stimulating septum formation. J Bacteriol *182*, 5653-5662.

Varley, A.W., and Stewart, G.C. (1992). The divIVB region of the Bacillus subtilis chromosome encodes homologs of Escherichia coli septum placement (minCD) and cell shape (mreBCD) determinants. J Bacteriol *174*, 6729-6742.

Viollier, P.H., Thanbichler, M., McGrath, P.T., West, L., Meewan, M., McAdams, H.H., and Shapiro, L. (2004). Rapid and sequential movement of individual chromosomal loci to specific subcellular locations during bacterial DNA replication. Proc Natl Acad Sci U S A *101*, 9257-9262.

Vollmer, W., Blanot, D., and de Pedro, M.A. (2008). Peptidoglycan structure and architecture. FEMS Microbiol Rev *32*, 149-167.

Wachi, M., Doi, M., Tamaki, S., Park, W., Nakajima-Iijima, S., and Matsuhashi, M. (1987). Mutant isolation and molecular cloning of mre genes, which determine cell shape, sensitivity to

mecillinam, and amount of penicillin-binding proteins in Escherichia coli. J Bacteriol *169*, 4935-4940.

Walshaw, J., Gillespie, M.D., and Kelemen, G.H. (2010). A novel coiled-coil repeat variant in a class of bacterial cytoskeletal proteins. J Struct Biol *170*, 202-215.

Walter, S., Wellmann, E., and Schrempf, H. (1998). The cell wall-anchored Streptomyces reticuli avicel-binding protein (AbpS) and its gene. J Bacteriol *180*, 1647-1654.

Wang, X., Liu, X., Possoz, C., and Sherratt, D.J. (2006). The two Escherichia coli chromosome arms locate to separate cell halves. Genes Dev *20*, 1727-1731.

Wang, X., and Lutkenhaus, J. (1996). FtsZ ring: the eubacterial division apparatus conserved in archaebacteria. Mol Microbiol *21*, 313-319.

Wang, X., Montero Llopis, P., and Rudner, D.Z. (2014). Bacillus subtilis chromosome organization oscillates between two distinct patterns. Proc Natl Acad Sci U S A *111*, 12877-12882.

Wang, X., and Rudner, D.Z. (2014). Spatial organization of bacterial chromosomes. Curr Opin Microbiol *22*, 66-72.

Waring, M.J. (1965). Complex formation between ethidium bromide and nucleic acids. J Mol Biol *13*, 269-282.

Watanabe, E., Inamoto, S., Lee, M.H., Kim, S.U., Ogua, T., Mori, H., Hiraga, S., Yamasaki, M., and Nagai, K. (1989). Purification and characterization of the sopB gene product which is responsible for stable maintenance of mini-F plasmid. Mol Gen Genet *218*, 431-436.

Weiss, D.S. (2004). Bacterial cell division and the septal ring. Mol Microbiol *54*, 588-597.

Weng, X., and Xiao, J. (2014). Spatial organization of transcription in bacterial cells. Trends Genet *30*, 287-297.

Willemse, J., Borst, J.W., de Waal, E., Bisseling, T., and van Wezel, G.P. (2011). Positive control of cell division: FtsZ is recruited by SsgB during sporulation of Streptomyces. Genes Dev *25*, 89-99.

Wintjens, R., and Rooman, M. (1996). Structural classification of HTH DNA-binding domains and protein-DNA interaction modes. J Mol Biol *262*, 294-313.

Wright, C.S. (1984). Structural comparison of the two distinct sugar binding sites in wheat germ agglutinin isolectin II. J Mol Biol *178*, 91-104.

Wu, L.J., and Errington, J. (2004). Coordination of cell division and chromosome segregation by a nucleoid occlusion protein in Bacillus subtilis. Cell *117*, 915-925.

Wu, L.J., Ishikawa, S., Kawai, Y., Oshima, T., Ogasawara, N., and Errington, J. (2009). Noc protein binds to specific DNA sequences to coordinate cell division with chromosome segregation. EMBO J *28*, 1940-1952.

Wu, M., Zampini, M., Bussiek, M., Hoischen, C., Diekmann, S., and Hayes, F. (2011). Segrosome assembly at the pliable parH centromere. Nucleic Acids Res *39*, 5082-5097.

Yamaichi, Y., and Niki, H. (2004). migS, a cis-acting site that affects bipolar positioning of oriC on the Escherichia coli chromosome. EMBO J *23*, 221-233.

Yamanaka, K., Mitani, T., Feng, J., Ogura, T., Niki, H., and Hiraga, S. (1994). Two mutant alleles of mukB, a gene essential for chromosome partition in Escherichia coli. FEMS Microbiol Lett *123*, 27-31.

Youngren, B., Nielsen, H.J., Jun, S., and Austin, S. (2014). The multifork Escherichia coli chromosome is a self-duplicating and self-segregating thermodynamic ring polymer. Genes Dev *28*, 71-84.

Zampini, M., Derome, A., Bailey, S.E., Barilla, D., and Hayes, F. (2009). Recruitment of the ParG segregation protein to different affinity DNA sites. J Bacteriol *191*, 3832-3841.

Zampini, M., and Hayes, F. (2012). Combinatorial targeting of ribbon-helix-helix artificial transcription factors to chimeric recognition sites. Nucleic Acids Res *40*, 6673-6682.